

Green Energy and Technology

Mayken Espinoza-Andaluz ·  
Martin Andersson · Tingshuai Li ·  
Jordy Santana Villamar ·  
Ángel Encalada Dávila ·  
Ester Melo Vargas *Editors*



# Congress on Research, Development and Innovation in Renewable Energies

Selected Papers from CIDiER 2021

 Springer

# **Green Energy and Technology**

Climate change, environmental impact and the limited natural resources urge scientific research and novel technical solutions. The monograph series Green Energy and Technology serves as a publishing platform for scientific and technological approaches to “green”—i.e. environmentally friendly and sustainable—technologies. While a focus lies on energy and power supply, it also covers "green" solutions in industrial engineering and engineering design. Green Energy and Technology addresses researchers, advanced students, technical consultants as well as decision makers in industries and politics. Hence, the level of presentation spans from instructional to highly technical.

**\*\*Indexed in Scopus\*\*.**

**\*\*Indexed in Ei Compendex\*\*.**

More information about this series at <https://link.springer.com/bookseries/8059>


Mayken Espinoza-Andaluz • Martin Andersson  
Tingshuai Li • Jordy Santana Villamar  
Ángel Encalada Dávila • Ester Melo Vargas  
Editors


# Congress on Research, Development and Innovation in Renewable Energies

Selected Papers from CIDiER 2021


 Springer


### *Editors*


Mayken Espinoza-Andaluz   
Faculty of Mechanical Engineering and  
Production Science  
Escuela Superior Politecnica del Litoral  
Guayaquil, Ecuador

Martin Andersson   
Energy Sciences  
Lund University  
Lund, Sweden

Tingshuai Li  
School of Materials and Energy  
University of Electronic Science and  
Science and Technology of China  
Chengdu, Sichuan, China

Jordy Santana Villamar   
Faculty of Mechanical Engineering and  
Production Science  
Escuela Superior Politecnica del Litoral  
Guayaquil, Ecuador

Ángel Encalada Dávila   
Faculty of Mechanical Engineering and  
Production Science  
Escuela Superior Politecnica del Litoral  
Guayaquil, Ecuador

Ester Melo Vargas   
Faculty of Social and Humanistic Science  
Escuela Superior Politecnica del Litoral  
Guayaquil, Ecuador

ISSN 1865-3529

ISSN 1865-3537 (electronic)

Green Energy and Technology

ISBN 978-3-030-97861-7

ISBN 978-3-030-97862-4 (eBook)

<https://doi.org/10.1007/978-3-030-97862-4>

© The Editor(s) (if applicable) and The Author(s), under exclusive license to Springer Nature Switzerland AG 2022

This work is subject to copyright. All rights are solely and exclusively licensed by the Publisher, whether the whole or part of the material is concerned, specifically the rights of translation, reprinting, reuse of illustrations, recitation, broadcasting, reproduction on microfilms or in any other physical way, and transmission or information storage and retrieval, electronic adaptation, computer software, or by similar or dissimilar methodology now known or hereafter developed.

The use of general descriptive names, registered names, trademarks, service marks, etc. in this publication does not imply, even in the absence of a specific statement, that such names are exempt from the relevant protective laws and regulations and therefore free for general use.

The publisher, the authors and the editors are safe to assume that the advice and information in this book are believed to be true and accurate at the date of publication. Neither the publisher nor the authors or the editors give a warranty, expressed or implied, with respect to the material contained herein or for any errors or omissions that may have been made. The publisher remains neutral with regard to jurisdictional claims in published maps and institutional affiliations.

This Springer imprint is published by the registered company Springer Nature Switzerland AG  
The registered company address is: Gewerbestrasse 11, 6330 Cham, Switzerland

# Preface

Figuring out solutions to face global warming is one of the key topics around the globe that has demanded great attention in the last decades. The acceleration of global warming, promoted mainly by the use of fossil fuels, produces hazardous effects and consequences on human well-being as well as economic and technological development of nations. These effects are evidenced in drastic changes to the environment such as glacial melting and natural disasters, which, in turn, put ecosystems in danger. On the other hand, the large emissions of polluting gases produced by fossil fuels, which are not renewable, make this resource not sustainable over time.

Due to this, international alliances, for instance, the European Green Deal, have arisen to face the challenges toward changing to a sustainable, clean, and economically viable energy matrix. In addition, one of the main concerns of the General Assembly of the United Nations regarding the 2030 Agenda is to promote sustainable initiatives related to developing renewable energies, such as SDG 7: Affordable and Clean Energy and SDG 13: Climate Action. On the other hand, Latin America also has a great interest in developing technologies that position renewable energies as the primary energy resource. However, strong cooperation synergies between countries that involve government, industry, and academia are missing to reach the common goals. Based on this, Congress on Research, Development, and Innovation in Renewable Energies (CIDiER 2021, acronyms from Spanish) had the objective put together teachers, students, researchers, engineers, and scientists from different disciplines and countries, mainly from Latin America, to present their latest studies and results.

This book consists of five key sections focused on solar, biomass, hydrogen, wind, and general renewable energy topics. Articles correspond to selected manuscripts from the Congress on Research, Development, and Innovation in Renewable Energies (CIDiER) 2021, held in Guayaquil, Ecuador (virtual mode), on September 20 and 21, 2021. This conference aimed to spread theoretical and experimental studies results and applications related to relevant topics in renewable energies and generate a space of multidisciplinary interaction to strengthen and establish new

contact networks in the academic and research community. Participants from all disciplines related to renewable energy and several Latin-American countries contributed to this important event.

This edited book meets some major topics related to renewable energies, such as developing and studying new materials, process design and simulation, computational modeling, energy efficiency, and chemical and mechanical analysis, among others. Finally, the editors of this book would like to thank the Springer editorial team and all contributing authors for their commitment and collaborative effort that have realized this book.

Guayaquil, Ecuador  
Lund, Sweden  
Chendgu, China

Mayken Espinoza-Andaluz  
Martin Andersson  
Tingshuai Li  
Jordy Santana Villamar  
Ángel Encalada Dávila  
Ester Melo Vargas

# Contents

## Part I Solar Energy

<b>Proposal of a Colombian Refrigeration Potential Map Based on Solar Powered Absorption Cooling Systems . . . . .</b>	<b>3</b>
--	----------

Jhojan Stiven Zea Fernández, Mario Luna-delRisco, Valeria Berrocal, Nildia Yamileth Mejias Brizuela, Carlos Arrieta González, Laura Paniagua, Sebastian Villegas Moncada, and Carlos A. Arredondo Orozco

<b>Evaluation of Univariate Time-Series Models for Short-Term Solar Energy Forecasting . . . . .</b>	<b>13</b>
--	-----------

Luis F. Martínez-Soto, Omar Rodríguez-Zalapa, José Alberto López-Fernández, José Joaquín Castellanos-Galindo, and José Horacio Tovar-Hernández

<b>Carbon-Based Perovskite Solar Cells: The Future Photovoltaic Technology . . . . .</b>	<b>33</b>
--	-----------

Israel Barrutia, Renzo Seminario-Córdova, and Vanessa Martinez-Rojas

## Part II Biomass Energy

<b>Design and Instrumentation of a Batch-Type Bioreactor for the Organic Fraction Fermentation of Urban Solid Waste . . . . .</b>	<b>47</b>
---	-----------

Remedios M. Bombela-Chávez, Belén Torres-Ramírez, Danay Carrillo-Nieves, and Oscar Aguilar-Juárez

<b>Design of Combustion Equipment for Residual Biomass at Laboratory Scale . . . . .</b>	<b>61</b>
--	-----------

Emerita Delgado-Plaza, William Avila, Gustavo Serrano, Carlos Rendon, and Anthony Arevalo



### **Part III Hydrogen Energy**

<b>Toward the Hydrogen Economy in Paraguay: End-Uses of Green Hydrogen Potential</b> . . . . .	77
--	----

Fausto Posso, Michel Galeano, César Baranda, David Franco, Ángel Rincón, and Juan Zambrano

### **Part IV Wind Energy**

<b>Analysis of Two-Dimensional Airfoil Models as Harvesters of Energy</b> . . . . .	91
---	----

Luis Gonzaga-Bermeo and Carlos A. Cuenca

### **Part V General Renewable Energy**

<b>Environmental and Ecotoxicological Impact of Alternative Energies: An Improvement Opportunity for Latin America</b> . . . . .	109
--	-----

Juan Carlos Valdelamar-Villegas and Julio Roman Maza-Villegas

<b>Design and Implementation of a Web-Based Residential Energy Assessment Platform: A Case Study in Cuenca, Ecuador</b> . . . . .	121
---	-----

Willian Carrión-Chamba, Wilson Murillo-Torres, Christian Naranjo-Ulloa, Katy Valdivieso-García, Andrés Montero-Izquierdo, and Iván Acosta-Pazmiño

<b>Analysis and Evaluation of Energy Efficiency in Buildings Based on Building Information Modeling</b> . . . . .	137
---	-----

Vicente Macas-Espinosa, Landie Vera-Rodríguez, and Julio Barzola-Monteses

<b>Strategies to Reduce Energy Curtailment in a Power System with High Penetration of Renewable Energy: Case Study of San Cristobal, Galapagos</b> . . . . .	151
--	-----

Jimmy Cordova, Manuel S. Alvarez-Alvarado, Ivan Endara, Edison Azuero, and Jose Diaz

<b>Energy and Economical Study of Different Renewable Energy Technologies for Domestic Hot Water Production Under the Climatic Conditions of the Main Cities in Ecuador</b> . . . . .	163
---	-----

Carlos Naranjo-Mendoza, Jesús López-Villada, Patricia Otero, and Sebastián Casco

<b>Impact of the Biodiesel Blend (B20) Strategy “Club de Biotanqueo” (Biofueling Club) on the Socioeconomic and Environmental Aspects in Medellín, Colombia</b> . . . . .	175
---	-----

Mónica Andrea Sánchez Anchiraico, Lily Margarita León Sánchez, Jhojan Stiven Zea Fernández, Mario Luna-delRisco, Carlos Arrieta Gonzalez, Erika Viviana Díaz Becerra, and Liliana González Palacio

<b>Index</b> . . . . .	187
------------------------	-----

## About the Editors

**Martin Andersson** PhD, is an associate professor at Lund University. He earned his doctoral degree from the Division of Heat Transfer, Department of Energy Sciences, Lund University. Dr. Andersson was awarded the title of Docent in 2014, and in 2015 he was granted a Marie Curie Fellowship, one of Europe's most competitive and prestigious awards to foster interdisciplinary research and international collaborations. His primary areas of research include analysis of heat and mass transfer and other transport phenomena in solid oxide fuel cells (SOFC) and polymer electrolyte fuel cells (PEFC). His current research interests are focused on a comprehensive understanding of chemical reactions and nano-/micro-structured porous material effects on various transport processes in various components of fuel cell systems. He has been a reviewer for a number of international journals, including the *International Journal of Hydrogen Energy*, *International Journal of Energy Research, Energy and Fuels*, *Journal of Power Sources*, and *Journal of Porous Media*.

**Ángel Encalada Dávila** received his bachelor's degree in mechatronics engineering in 2021 from Escuela Superior Politécnica del Litoral (ESPOL). He is currently working as a data scientist in an international data analytics company. He has also a solid experience in software industry for ATMs. Furthermore, he collaborates as a data scientist at the Control, Modeling, Identification, and Applications Research Group (CoDALab) at the Universitat Politècnica de Catalunya (UPC), Barcelona, Spain. His research interests include structural health monitoring (SHM) and fault prognosis applied to wind turbines and computer modeling applied to fuel cells. In addition, Mr. Encalada is author and co-author of several scientific articles that have been published in the journals like *Sensors*, *Energies*, and *Processes*. He recently worked as an organizer of the Congress of Research, Development, and Innovation in Renewable Energies (CIDiER), Guayaquil, Ecuador.

**Mayken Espinoza-Andaluz** PhD, is a full professor at Escuela Superior Politécnica del Litoral (ESPOL) and co-supervisor of PhD students in heat transfer

and energy systems at Lund University. He earned his PhD in heat transfer from the Department of Energy Sciences at Lund University. His areas of research include renewable energy, fuel cells, proton-exchange membrane fuel cells (PEMFC), solid oxide fuel cells (SOFC), physical and chemical phenomena, energy efficiency, Lattice Boltzmann methods (LBM), and computational modeling. He is a reviewer for a number of international journals, including the *International Journal of Energy Research*, *International Journal of Hydrogen Energy*, and *Computers and Mathematics with Applications*.

**Tingshuai Li** PhD, is a professor at the University of Electronic Science and Technology of China (UESTC). He earned his PhD degree in materials chemistry and physics from Ningbo Institute of Materials Technology and Engineering, Chinese Academy of Sciences. Dr. Li carried out postdoctoral research at Nanyang Technological University and the University of South Carolina. He has published numerous scientific papers, applied for more than 10 patents, participated in the writing of 2 monographs, and presided over the Natural Science Foundation of China and key research and development projects in Sichuan Province. His primary areas of research include materials design for fuel cells and electrochemical synthesis of various fuels. He has been a reviewer for the *International Journal of Hydrogen Energy*, *Journal of Materials Chemistry A*, and *ACS Applied Materials & Interfaces*.

**Ester Melo Vargas** received her bachelor's degree in audit and management control in 2021 from the Escuela Superior Politécnica del Litoral (ESPOL), obtaining an honors diploma and an award for her thesis project related to the management of medical supplies in Ecuador during the Covid-19 pandemic. From 2019 to the present, she has served as a research assistant at the same institution. Her interest in research, technology, and gender inclusion in STEM have motivated her to participate in different technological innovation competitions, as well as in STEM projects sponsored by the US Embassy in Ecuador. This experience gave her the opportunity to do an internship in project engineering at Huawei Technologies (Guayaquil, Ecuador) in 2020. Her research interests include data analysis and fault detection applied to fuel cells and quality analysis and lean manufacturing applied to productivity management. In addition, Ms. Melo is the author and co-author of scientific articles that have been presented at congresses, conferences, and scientific dissemination meetings.








**Jordy Santana Villamar** received his bachelor's degree in mechanical engineering from Escuela Superior Politécnica del Litoral (ESPOL) in 2020, obtaining a diploma of distinction in research. He was a teaching assistant at the early stage of his undergraduate studies on subjects such as calculus, electromagnetics physics, and statistics. Then, he got a position as research assistant during his last four semester. Currently, he is a junior researcher at the Center of Renewable and Alternative Energy at ESPOL. His area of research is electrochemical tests to evaluate the performance in fuel cells and redox flow batteries applying EIS technique, sweep

current, and linear and circular sweep voltammetry; expanded graphite-resin composite materials development with secondary fillers for bipolar plates; and modeling on transport phenomena. In addition, he has published several scientific papers in leading journals including the *International Journal of Hydrogen Energy*, *Journal of Electrochemical Society*, and *Energies*. He has also participated in congresses, international conferences, and meetings to spread his research work. He recently worked as an organizer of the Congress of Research, Development, and Innovation in Renewable Energies (CIDiER), Guayaquil, Ecuador.

**Part I**  
**Solar Energy**

# Proposal of a Colombian Refrigeration Potential Map Based on Solar Powered Absorption Cooling Systems



Jhojan Stiven Zea Fernández , Mario Luna-delRisco ,  
Valeria Berrocal , Nildia Yamileth Mejias Brizuela,  
Carlos Arrieta González , Laura Paniagua ,  
Sebastian Villegas Moncada , and Carlos A. Arredondo Orozco 

## 1 Introduction

The growing concern about the effects of global warming, as well as the uncertainty due to finite reserves of fossil fuels, have turned the world's attention to nonconventional renewable energy sources as the way to a clean and environmentally friendly energy transition [2]. Colombia has pledged to take part in this transition through international agreements such as the Paris agreement [3]; however, the country is still lagging in the development of renewable energy sources in the national territory.

By 2021, less than 1% of the electricity generated in the country comes from nonrenewable energy sources such as biomass, solar, and wind energy, a very low percentage compared to more developed countries such as the United States, where 12% of the energy consumed comes from these sources [4]. According to the accelerated growth of renewable energy for the next decade, Colombia has set itself the goal of reaching 15% share of renewables by 2030, with emphasis on the north coast of the country [5], where there is great potential for solar and wind energy [6].

In view of the accelerated growth expected for renewable energy in the next decade, emphasis must be placed on how these new technologies can help

---

J. S. Zea Fernández · M. Luna-delRisco (✉) · V. Berrocal · C. Arrieta González  
S. Villegas Moncada · C. A. Arredondo Orozco  
Universidad de Medellín, Medellín, Colombia  
e-mail: [mluna@udemedellin.edu.co](mailto:mluna@udemedellin.edu.co)

N. Y. Mejias Brizuela  
Universidad Politécnica de Sinaloa, Mazatlán, México

L. Paniagua  
Benemerita Universidad Autónoma de Puebla, Puebla, México

low-income people with no access to electrical energy. In Colombia, approximately 52% of the national territory is not connected to the electrical grid; this means that almost 2 million people who live in these places get sporadic and low-quality access to electricity or no access at all [1]. Since a large part of the people who live in non-interconnected areas engage in productive activities such as livestock, fishing, and agriculture, it is to be expected that part of the production is lost because they cannot cool their products.

The implementation of absorption cooling cycles that can use solar energy as a heat source means that large cooling centers could be available to residents of non-interconnected areas as a way of storing their products for later sale [7], thereby increasing the economic development and life quality [8]. However, not all areas of the country are suitable for the installation of these systems, since there are a wide variety of climates and weather conditions [9].

The objective of this chapter is to present a map of the absorption cooling potential for the Colombian territory. Maximum cooling volume capacity was determined based on data of solar radiation and temperature (mean values). Those variables were also used for the calculation of the system's efficiency allowing the geolocation of non-interconnected areas where the industrial facilities might be placed.

## 2 System Description

The system consists of a condenser, an evaporator, an absorber, a generator, a pump, expansion valves, a heat exchanger, and a solar collector, as shown in Fig. 1.

The cycle is possible because of the ability of certain substances to perform absorption and desorption reactions. In this case, water absorbs ammonia vapor in the absorber and creates a solution with a weak water concentration; the solution has its pressure increased by means of a pump and is sent to the generator, in which the heat coming from the solar collector heats the solution and causes most of the ammonia vapor to be desorbed.

The high-pressure ammonia vapor shifts to liquid phase in the condenser and is expanded to a low pressure with an expansion valve; the low-pressure liquid is then converted into ammonia vapor in the evaporator and is sent to the absorber to restart the cycle. The solution that is left on the generator, now with a strong water concentration, exchanges heat with the refrigerant flow exiting the pump to increase the system's efficiency and is expanded, using an expansion valve to go once again into the absorber [10].

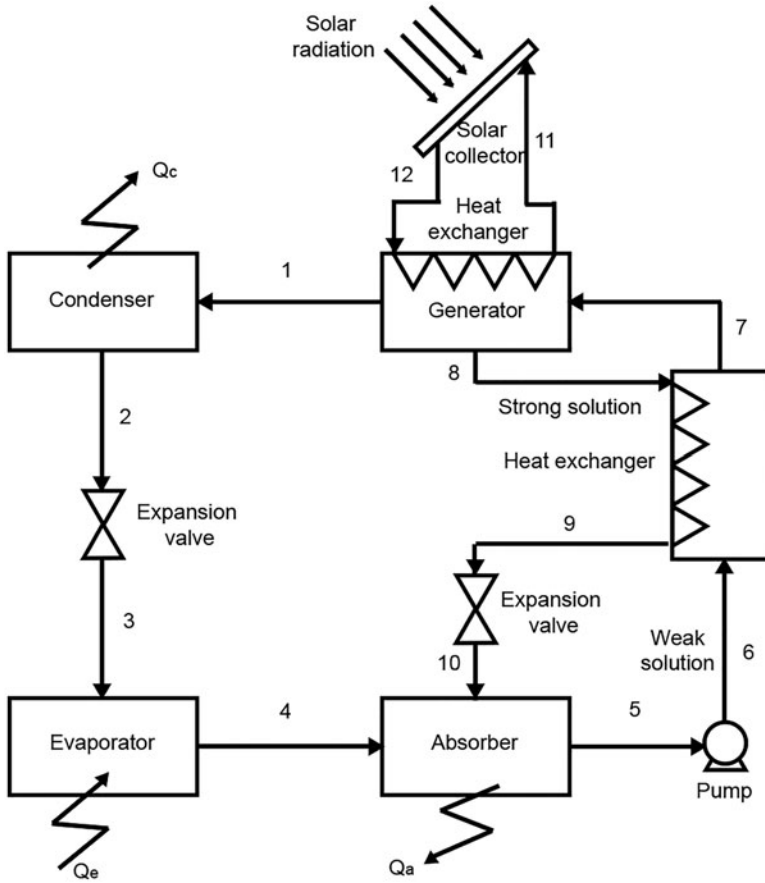


Fig. 1 System schematic

### 3 Modeling and Methodology

#### 3.1 Symbols and Subscripts

Symbols

COP

= Coefficient of performance

E = Efficiency

f = Mass flow ratio

h = Enthalpy [kJ/kg]

P = Pressure [kPa]

$\dot{m}$  = Mass flow [kg/s]



$q$  = Heat per unit mass [kJ/kg]

$Q$  = Heat [kJ]

$\dot{Q}$  = Heat rate [kW]

$T$  = Temperature [ $^{\circ}\text{C}$ ]

$\dot{W}$  = Power [kW]

$x$  = Concentration [kg/kg]

$G_{\text{stc}}$

= Global irradiance on standard test conditions [1000 W/m<sup>2</sup>]

Subscripts

a = Absorber

b = Pump

c = Condenser

e = Evaporator

l = Liquid

g = Generator

sc = Solar collector

ref = Refrigerant

sf = Strong solution

sd = Weak solution

v = Vapor

### 3.2 *Thermodynamic Model*

A simple steady-state model was considered for this particular study. There was no need for a thermal energy storage system. The model assumes heat and pressure losses on all the piping and units to be negligible and the refrigerant to be 100% ammonia (NH<sub>3</sub>) [11]. The mass balances are presented in Eqs. 1, 2, 3, 4, 5, 6, 7, 8, 9, 10 and 11 [11]:

$$\dot{m}_1 = \dot{m}_2 \quad (1)$$

$$\dot{m}_2 = \dot{m}_3 = \dot{m}_{\text{ref}} \quad (2)$$

$$\dot{m}_3 = \dot{m}_4 = \dot{m}_{\text{ref}} \quad (3)$$

$$\dot{m}_4 + \dot{m}_{10} = \dot{m}_5 \quad (4)$$

$$\dot{m}_9 = \dot{m}_{10} \quad (5)$$

$$\dot{m}_5 = \dot{m}_6 \quad (6)$$

$$\dot{m}_7 = \dot{m}_1 + \dot{m}_8 \quad (7)$$

$$\dot{m}_8 + \dot{m}_6 = \dot{m}_7 + \dot{m}_9 \quad (8)$$

$$\dot{m}_4 + \dot{m}_{10} = \dot{m}_5 \quad (9)$$

$$\dot{m}_9 = \dot{m}_8 \quad (10)$$

$$\dot{m}_{11} = \dot{m}_{12} \quad (11)$$

The generator is possible to perform an  $\text{NH}_3$  balance, as seen in Eq. 12 [11]:

$$\dot{m}_7 x_7 = \dot{m}_1 x_1 + \dot{m}_8 x_8 \quad (12)$$

Equations 13 and 14, which are expressions for the strong solution mass flow rates, can be obtained from Eqs. 12 and 7 [11]:

$$\dot{m}_8 = \frac{x_7 - x_1}{x_8 - x_7} \dot{m}_1 \quad (13)$$

$$\dot{m}_7 = \frac{x_8 - x_1}{x_8 - x_7} \dot{m}_1 \quad (14)$$

From Eq. 13, the circulation ratio can be formulated as [11]:

$$f = \frac{\dot{m}_7}{\dot{m}_1} = \frac{x_8 - x_1}{x_8 - x_7} \quad (15)$$

The energy balances are performed as follows in Eqs. 16, 17, 18, 19, 20, 21, 22, 23, 24 and 25 [11]:

$$\dot{Q}_c = \dot{m}_{ref}(h_1 - h_2) \quad (16)$$

$$h_2 = h_3 \quad (17)$$

$$\dot{Q}_e = \dot{m}_{ref}(h_4 - h_3) \quad (18)$$

$$\dot{Q}_a = \dot{m}_4 h_4 + \dot{m}_{10} h_{10} - \dot{m}_5 h_5 \quad (19)$$

$$\dot{W}_b = \dot{m}_5 (h_6 - h_5) \quad (20)$$

$$h_7 = h_6 + \frac{\dot{m}_8}{\dot{m}_6} (h_8 - h_9) \quad (21)$$

$$h_9 = h_{10} \quad (22)$$

$$\dot{m}_{12}(h_{12} - h_{11}) = \dot{m}_1 h_1 + \dot{m}_8 h_8 - \dot{m}_7 h_7 \quad (23)$$

$$\dot{m}_{12}(h_{12} - h_{11}) = G_{stc} A_{sc} E_{sc} \quad (24)$$

$$COP = \left[ \frac{\dot{Q}_e}{G_{stc} A_{sc} E_{sc} + \dot{W}_b} \right] \quad (25)$$

The authors express Eq. 18 in terms of the circulation ratio when dividing the whole expression by  $\dot{m}_4$  as presented in Eq. 26 [11]:

$$q_a = (h_5 - h_{10}) + f(h_{10} - h_5) \quad (26)$$

### 3.3 Methodology

The previous equations present an ideal absorption cooling system with no thermal energy storage system, assuming reference conditions for variables such as pressures and temperatures [12]. The model calculates the heat extracted by the heat pump ( $\dot{Q}_e$ ) based on the solar irradiance and ambient temperature of a particular location.

A MATLAB script identifies the color of each pixel on the average ambient temperature and average peak sun hours (PSH) maps that the Institute of Hydrology, Meteorology and Environmental Studies (IDEAM) provides [13] [14] and translates it into usable data. The script then calculates the amount of daily cooling each pixel of the map can generate and the efficiency of the system (expressed by the COP on each pixel).

The thermodynamic properties for the  $\text{NH}_3\text{-H}_2\text{O}$  mixture are calculated with the equations proposed by Sun [15]. Then, in each pixel, the system is simulated by setting  $T_c$  to the mean ambient temperature of each pixel. In this simulation, the solar collector receives a constant solar irradiance of  $1000 \text{ W/m}^2$ . The cycle works for the equivalent time to PSH of the pixel by calculating the daily amount of cooling and the system efficiency depending on the ambient temperature.

The result is a map of the country in which each pixel has a value for maximum amount of cooling produced with  $1 \text{ m}^2$  of solar collector and the system's efficiency, detailing the potential for the solar absorption system in every location of the region. The reference conditions considered were as follows:

$$\begin{aligned} T_g &= 80 \text{ }^\circ\text{C} \\ T_a &= 25 \text{ }^\circ\text{C} \\ T_c &= -5 \text{ }^\circ\text{C} \\ \dot{m} &= 1 \text{ kg/s} \\ E_{sc} &= 90\% \\ A_{sc} &= 1 \text{ m}^2 \end{aligned}$$

## 4 Results

The generated maps for daily cooling potential and system efficiency are presented in Figs. 2 and 3.

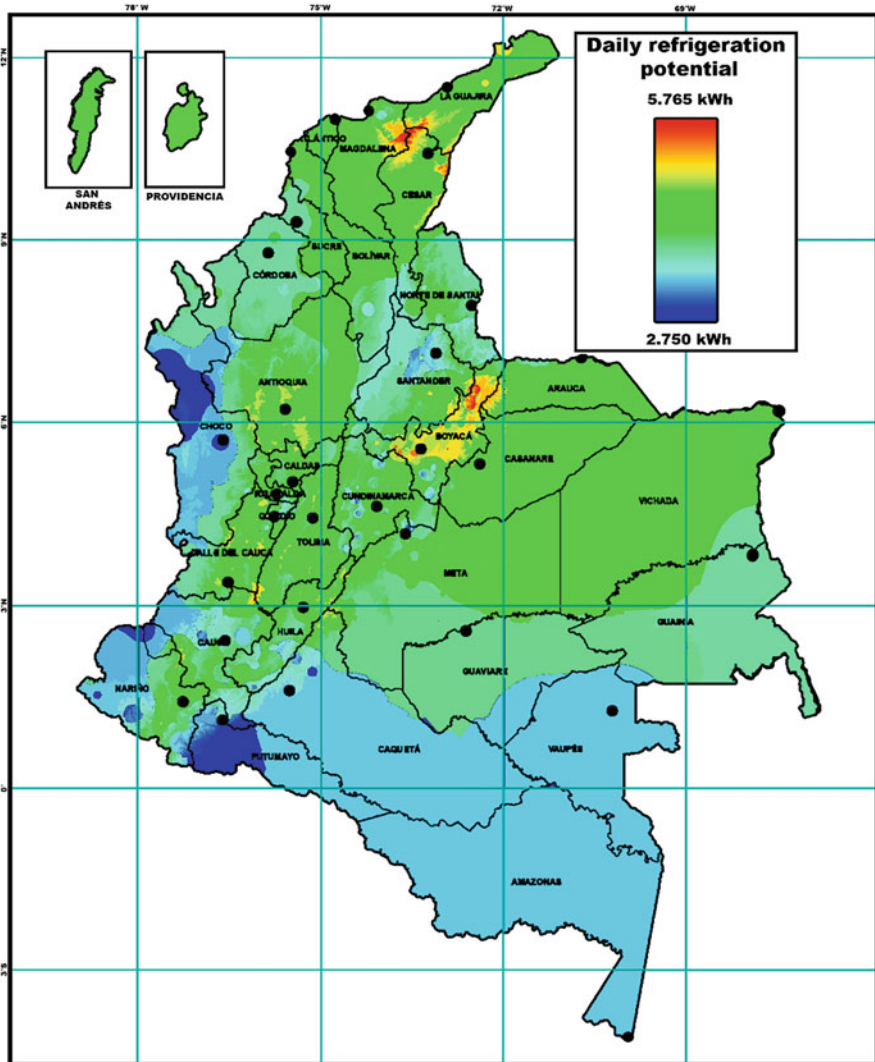


Fig. 2 Daily refrigeration potential map

## 5 Discussion

Since Colombia is a tropical country, there are no significant climatic variabilities due to the lack of seasons. Temperature conditions in any given location depend highly on the altitude. With this in mind, it can be determined that Fig. 3, which presents the system's efficiency, follows the contour of the relief in the national territory. There are higher COPs (1.10–1.22) in places such as the Andes Mountain

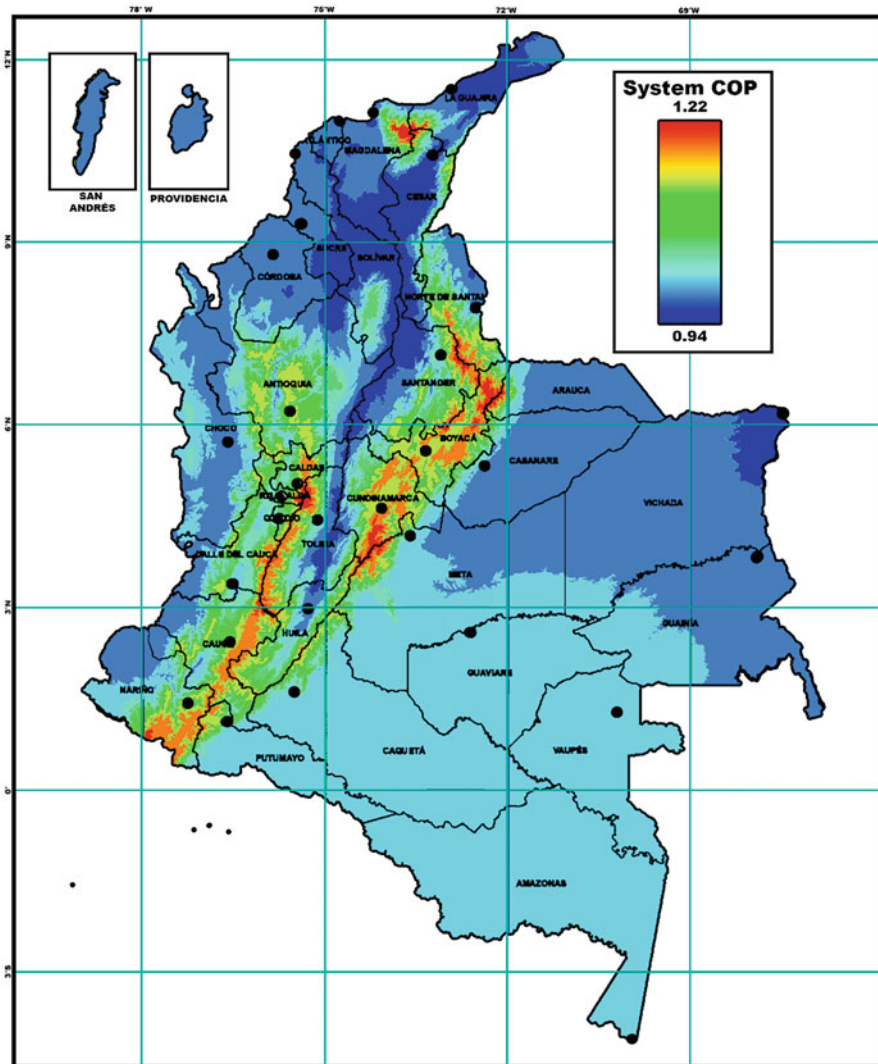


Fig. 3 System COP map

range or the snowy Sierra of Santa Marta. Moderate COPs (1–1.12) are in the Amazon area of the country, the high plains, and the pacific coast, whereas low performances (COP= 0.94–1) are in the Atlantic coast and the High Guajira.

The highest amount of cooling potential (5.4–5.765 kWh) was found in areas with low temperatures and high irradiations, such as the high mountains of Boyacá and the snowy Sierra of Santa Marta. All three branches of the Andes Mountain range across the country present high refrigeration potential (5.0–5.5 kWh) because of the low temperatures. The East Plains, the Atlantic Coast, and the San Andres and

Providencia Islands offer good potentials despite high temperatures (4.25–5.1 kWh). This phenomenon can be explained because these regions are the ones with the highest irradiation in the country.

The departments of Cordoba, Guainía, and Guaviare present moderate cooling potentials (3.5–4.33 kWh) because of high temperatures and low irradiation. The Pacific Coast and Amazon regions of the country are the ones that offer the lowest potentials (2.750–3.45 kWh). This can be explained because of the hot temperatures and low irradiances due to the high levels of cloudiness and rainfall that characterize these regions.

The northern part of the Guajira and the insular regions are the non-interconnected zones that would be the most attractive for the implementation of solar powered absorption cooling systems because of high potentials and the economic activities in which the lifestyle in these regions is based. The locals live mostly from fishing, livestock, and tourism [1], and the electricity is generated from fossil fuels. Fuel supply for this territory is inconsistent and unreliable. Construction of massive cooling systems that are solar powered can improve the quality of life of the inhabitants of these places by offering them a way to store their products and cool their hotels and inns without relying on fossil fuels. Additionally, this technology also offers a high potential for mitigating CO<sub>2</sub> emissions.

As for the Amazon and Pacific Coast, the other two identified non-interconnected regions presented a low potential for these cooling systems.

The results of this research are limited by a number of factors such as the use of multi-annual average ambient temperature and solar radiation, the lack of consideration of energy losses due to the non-ideality of real systems, and the steady nature of the equations used.

## 6 Conclusions

The outcome maps of this study suggest that solar powered absorption systems are a good and viable method for cooling generation in non-interconnected areas of Colombia such as the High Guajira, San Andres, and Providencia Islands, where locals live mainly from fishing, livestock, and tourism. This system will lead to an increase of the quality of life without CO<sub>2</sub> emissions. The Pacific Coast and Amazon region of the country present the lowest potential of any non-interconnected zone in Colombia. In these places, the implementation of these systems would be more costly because of the increased area of solar collection that is needed to meet the demands of the inhabitants.

This map uses multi-annual average radiation and temperature data, and because of the equatorial location of the country, the climate can change significantly from one day to the other in any given place, and this means that the system efficiency and performance can be diminished or enhanced due to the environmental conditions, but even if the maps do not exactly predict the daily behavior of the system, they are a good tool to estimate the mean amount of refrigeration a system can produce on

any part of the country. Also it can be used to calculate the solar collection area needed to achieve a certain amount of cooling power since the maps are based on a  $1 \text{ m}^2$  solar collector.



Future studies that can be done to further increase the understanding of the applicability of solar powered absorption systems on the Colombian territory include a transient simulation for the operation of the system on a whole day, with real data from minute-to-minute measurements rather than average solar radiation and ambient temperature. Additionally, including entropy and exergy analyses to the energy and mass balances to account for losses and the irreversibility of the system will make the results more exact and useful.

## References

1. Superintendencia de Industria y Comercio, “ZONAS NO INTERCONECTADAS - ZNI Diagnóstico de la prestación del servicio de energía eléctrica 2017 Superintendencia Delegada para Energía y Gas Combustible,” no. 1, p. 74, 2017.
2. Gielen, D., Boshell, F., Saygin, D., Bazilian, M. D., Wagner, N., & Gorini, R. (2019). The role of renewable energy in the global energy transformation. *Energy Strategy Reviews*, 24-(January), 38–50.
3. Ministerio de Ambiente. (2009) *El Acuerdo de Paris, así actuará Colombia frente al Cambio Climático*.
4. U. E. I. Administration, “Energy outlook 2021,” vol. 2021, no. January, pp. 1–22, 2021.
5. UPME, “Plan Energético Nacional 2021–2051,” p. 2015, 2021.
6. Ojeda, C. E., Candelo, B. J. E., & Silva, O. J. I. (2017). Caracterización de los potenciales de Energía Solar y Eólica para la integración de Proyectos sostenibles en Comunidades Indígenas en La Guajira Colombia. *Espacios*, 38(37), 11.
7. Al-Hamed, K. H. M., & Dincer, I. (2019). Investigation of a concentrated solar-geothermal integrated system with a combined ejector-absorption refrigeration cycle for a small community. *International Journal of Refrigeration*, 106, 407–426.
8. Aguilar-Jiménez, J. A., et al. (2020). Optimum operational strategies for a solar absorption cooling system in an isolated school of Mexico. *International Journal of Refrigeration*, 112, 1–13.
9. IDEAM. (2018). Características Climatológicas De Ciudades Principales Y Municipios Turísticos. *Inst. Hidrol. Meteorol. y Estud. Ambient.*, 48.
10. Nikbakhti, R., Wang, X., Hussein, A. K., & Iranmanesh, A. (2020). Absorption cooling systems – Review of various techniques for energy performance enhancement. *Alexandria Engineering Journal*, 59(2), 707–738.
11. A. J. Bula, D. L. Herrera, L. F. Navarro, and L. A. Corredor, “Thermodynamic Simulation of a Solar Absorption Refrigeration System Generator – Heat Exchanger,” *AMSE* no. 2000, 2000.
12. Wang, J., Qi, X., Ren, F., Zhang, G., & Wang, J. (2021). Optimal design of hybrid combined cooling, heating and power systems considering the uncertainties of load demands and renewable energy sources. *Journal of Cleaner Production*, 281, 125357.
13. IDEAM. (2014). “Distribución de la temperatura media anual (°C). Promedio multianual 1981–2010.,” p. 1.
14. Francisco, A. R. L. (2013). Atlas climatológico, radiación y viento en Colombia. *Journal of Chemical Information and Modeling*, 53(9), 1689–1699.
15. Taylor, P., Sun, D., & Sun, D. (2007). Computer simulation and optimization of ammonia-water absorption refrigeration systems. *Energy Sources*, 2013, 37–41.

# Evaluation of Univariate Time-Series Models for Short-Term Solar Energy Forecasting



Luis F. Martínez-Soto , Omar Rodríguez-Zalapa ,  
José Alberto López-Fernández, José Joaquín Castellanos-Galindo,  
and José Horacio Tovar-Hernández

## 1 Introduction

### 1.1 Background

The energy transition that most countries are currently experiencing toward renewable energies is part of the strategies to mitigate the effects of climate change and comply with the Paris Agreement and the Sustainable Development Goals [1], intending to limit the global temperature rise in this century below 2 °C. Among the technologies that favor this transition are those that operate on the side of the electric power user, such as distributed generation, microgrids, and demand management. These allow increasing the efficiency of electrical systems by avoiding energy losses in the transmission and distribution stages. Besides, the correct operation of these new technologies requires energy control strategies that allow the electrical systems to continue to operate reliably and safely in the face of this new paradigm, in which energy management systems are increasing their relevance [2].

Energy management systems make it possible to cope with the intermittency and natural variability of renewable energies related to local climatic conditions, the constant increase in demand, and the complexity of the electricity consumption

---

L. F. Martínez-Soto (✉)

Centro de Ingeniería y Desarrollo Industrial (CIDESI), Querétaro, México

TecNM-Campus Querétaro, Querétaro, México

e-mail: [lmartinez@cidesi.edu.mx](mailto:lmartinez@cidesi.edu.mx)

O. Rodríguez-Zalapa · J. A. López-Fernández · J. J. Castellanos-Galindo

TecNM-Campus Querétaro, Querétaro, México

J. H. Tovar-Hernández

TecNM-Campus Morelia, Morelia, México



habits of users. However, to achieve proper energy management, it is essential to adequately know the current and future energy production and consumption behavior and even estimate the batteries' state of charge in storage systems. This is possible by applying forecasting techniques, which can be done in various ways, whether from environmental forecast data, sky images, or data obtained with on-site measurements. The technique used depends on the objective of the forecast to be made, which in turn determines the required forecast horizon, that is, the time in advance in which the predictions are made. In the case of user-side applications involving distributed renewable generation sources, such as photovoltaic (PV) systems, the appropriate forecast horizon is usually short-term or one day in advance [3].

On the other hand, it is also necessary to use well-established and robust baseline forecasting techniques to evaluate the performance of new forecasting methodologies and algorithms. However, there are no generalized conclusions in the literature on which models are suitable in different circumstances [4], so it is necessary to previously analyze and implement reference models of forecasting to have a common reference in the evaluation of new methodologies or algorithms.

## ***1.2 Forecast of Solar Energy in Microgrids***

One of the biggest problems in forecasting PV power is its variability. For example, partly cloudy conditions can reduce solar radiation by up to 80% in one second, which, depending on the degree of penetration, represents a great challenge for power system operators. It is common to use classical or statistical forecasting techniques based on time-series to predict solar energy in microgrid applications. Still, the application of supervised machine learning algorithms is becoming increasingly relevant. There are deep learning models based on recurrent neural networks (RNN), such as gated recurrent units (GRU) [5, 6], long short-term memory (LSTM) [7, 8], and combined models or ensemble [9, 10]. Some combine multiple algorithms to achieve better prediction results than those obtained with individual algorithms [11].

The machine learning and statistical forecasting models can work adequately in intra-hour temporal resolutions (less than one hour) and intra-day (up to 72 h) and with spatial resolutions mainly at the microscale level, that is, up to 1 km [12]. This spatial resolution mainly favors the application of these forecasting techniques in microgrids and photovoltaic solar plants in areas of up to 100 ha.

There are also forecasting applications in the state of the art that use models composed of sub-processes for different time scales, known as multi-horizon [13, 14] (e.g., 5 min to 1 h, 1 to 6 h, 6 to 48 h, and greater). Each subprocess can use different datasets as inputs and even different granularity in the data for each time scale. This implies working with different data storage intervals for each prediction subprocess. Consequently, the initial and most crucial step in data analytical process applications is preparing or preprocessing the data [15]. It is also possible to forecast photovoltaic generation using fuzzy prediction interval (FPI)

models [16, 17], as was done in projects developed in the experimental microgrid of Huatocondo, Chile (24 kW), and the Goldwind microgrid in China (two PV systems: 200 and 250 kW). In the first case, better results were obtained with FPI than those obtained with linear regression algorithms for horizons of 15 min and 24 h in advance. In the second case, in combination with a particle swarm optimization (PSO) algorithm, superior performance was obtained, compared to the application of other optimization algorithms, for horizons of 10 min and 24 h in advance.

Besides, combinations of artificial intelligence techniques with PSO-type optimization algorithms have also been used. For example, in [18], the PSO is combined with an adaptive neuro-fuzzy inference system (ANFIS) to forecast the photovoltaic power of 3 photovoltaic generation units of 100 kW each. The algorithm results were evaluated in terms of RMSE, mean absolute error (MAE), and nMAE (normalized MAE), obtaining superior results for a forecast horizon of one hour in advance. Results are based on algorithms based on backpropagation artificial neural networks (ANN) and the persistence method. As part of the design of a centralized controller for energy management of a microgrid, in [19], two forecasting algorithms of the photovoltaic generation are applied: autoregressive moving average (ARMA) using the final prediction error (FPE) and a model based on multilayer perceptron nonlinear autoregressive (NAR). The neural network could predict sudden changes better, while the ARMA algorithm could only follow trends.

The potential for improving the prediction models of photovoltaic power when applying rolling forecasting is shown in [20]. This technique makes it possible to enhance the values predicted by the forecasting model, simultaneously extending and correcting the time-series model using real-time measurements. The results of this strategy were combined with a hybrid forecasting model based on support vector regression (SVR) sub-elements or sub-SVRs and an ARIMA algorithm to forecast instantaneous PV power. The precision of the model was evaluated with the RMSE and mean absolute percentage error (MAPE), and the results were better for sunny days than those obtained in the presence of clouds.

Combining two ANFIS algorithms has proven to be effective in applying Sugeno-type inference systems [21] to perform forecasting in microgrids in a 10 kW PV system. The analysis was conducted via simulation, using monitoring datasets from a PV system in Targoviste, Romania. The results were evaluated using MAE and the RMSE, observing that the error increases as the forecast horizon increases. Improvements in predictions were obtained by increasing the number of membership functions for each variable (increment from 2 to 3).

On the other hand, a method of forecasting PV power applicable to community microgrids has been proposed, based on deep learning [22], using deep recurrent neural networks (DRNN) with an LSTM forecasting algorithm with a short-term horizon. The algorithm was tested on a residential microgrid in Austin, Texas, consisting of a 100 kW PV system. The results were evaluated in terms of RMSE, MAE, MAPE, and Pearson's correlation coefficient and were compared with support vector machine (SVM)-based prediction algorithms and a multilayer perceptron ANN. The forecast results showed the best performance for the DRNN algorithm,

followed by the multilayer perceptron (MLP) and finally the SVM. The DRNN model practically outperformed the SVM algorithm by 2 to 1.

Statistical linear models are the time-series prediction methods most traditionally used as an alternative to numerical weather prediction (NWP) techniques. They are based on a physical approach where atmospheric models describe the variability of meteorological processes. Descriptions are given at the mesoscale level or global datasets of meteorological measurements [23]. On the other hand, time-series statistical models are based on historical data, as a sequence of observations, measured at certain moments in time. They are ordered chronologically and evenly spaced, which makes the data dependent on each other in most cases to develop a descriptive relationship between various magnitudes to obtain an estimate of the future of a certain magnitude [24, 25]. In such a model, the dependent or output variable depends only on its past values [26].

There are also forecasting applications for solar energy and other energy fields using time-series, such as SARIMA models, to forecast hydroelectric production in Ecuador [27, 28]. It was shown that the proposed models are suitable for forecasting time-series with seasonal components, which can also be improved with the use of exogenous variables, such as precipitation, to predict monthly hydroelectric production in forecasting horizons up to a year in advance. On the other hand, triple exponential smoothing or Holt-Winters models have also been used to forecast solar irradiance in PV-distributed generation facilities for intra-hour prediction horizons in a PV system located on the roof of the University of Utrecht, Netherlands [29]. The implemented model was suitable for forecasting the time-series, including its seasonal component, with a high degree of accuracy, in terms of the MAE, compared to other forecasting methods, such as the persistence and the average methods.

To evaluate forecasting models based on univariate time-series, which can later be applied as forecasting benchmarks to assess the performance of other more advanced multivariate forecasting techniques, a comparison between the Box-Jenkins and exponential smoothing approaches has been conducted. A general methodology proposal for forecasting in a univariate time-series model, applied and validated in this study, is also revealed.

## 2 Methods

### 2.1 *Time-Series Decomposition*

A decomposition of the PV power time-series was applied, which consists of a statistical analysis that allows separating the time-series into different components or sub-series of time, each representing one of the characteristics of the original time-series: trend, seasonality, and residuals [30]. This makes it possible to analyze each of the components separately, allowing to complement the determination of stationarity of the time-series, that is, if its mean and variance are constant over

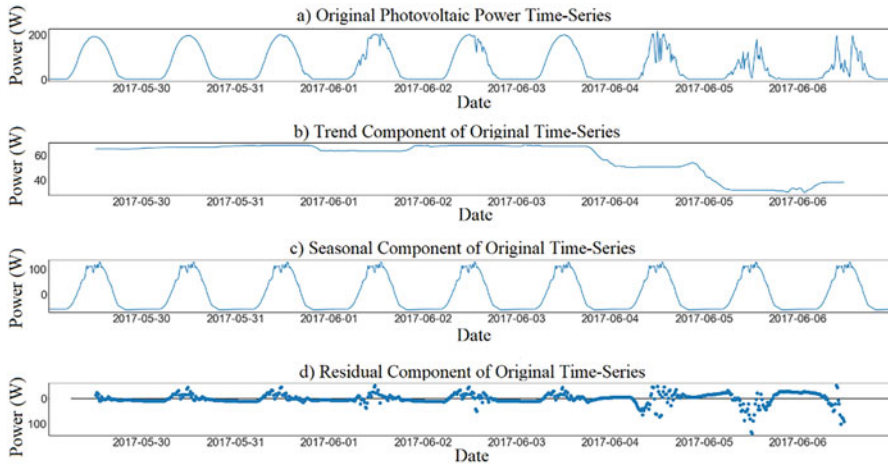


**Fig. 1** Time-series decomposition of photovoltaic power

time. In addition, it will enable us to analyze how dominant the seasonal component of the time-series is, determining whether there is periodicity in the seasonal variation of the time-series, which can be annual, monthly, daily, or on another time scale [31]. Therefore, determine if the forecasting model should contain components to predict those dominant characteristics.

In general, there are two methods to perform time-series decomposition, the multiplicative and the additive [32]. In this case, the additive method has been used using the Python *statsmodels* package. The result is shown in Fig. 1, where it is observed that the time-series has a small trend component, with a value of up to 60 W, when there are variations in photovoltaic power, unrelated to the daily cyclical behavior of irradiance (e.g., shadows). In the case of seasonality, it is the dominant component of the time-series, reflecting the daily cycles of photovoltaic power. Finally, the residual component is shown as the weakest, with maximum values coinciding with the reductions in photovoltaic power caused by shadows.

## 2.2 Exponential Smoothing Forecasting Model

The exponential smoothing forecasting techniques, or error, trend, and seasonality (ETS), are state-space models widely used to forecast time-series in other areas of knowledge [33, 34], despite being proposed between 1957 and 1960 [35]. In issues related to electrical energy forecasting, they are applied, either individually or in combination with other techniques, in applications such as wind power forecasting [36] and photovoltaic solar power [37] in forecast horizons from short-term to long-term. This forecasting method uses weighted combinations of past observations from the time-series, giving the most recent observations more weight than the oldest

ones. The weight given to old observations exponentially decreases as they get older, so this method is called exponential smoothing. These forecasting techniques are divided into three: simple exponential smoothing, used to predict time-series that do not have seasonality or trend; Holt's linear smoothing, applicable to trend time-series; and finally, Holt-Winters smoothing method, useful for forecasting time-series that include seasonality and trend. Eqs. (1, 2, 3 and 4) describe a Holt-Winters forecasting model [38]:

$$S_t = \alpha \left( \frac{X_t}{I_{t-s}} \right) + (1 - \alpha)(S_{t-1} + T_{t-1}) \quad (1)$$

$$T_t = \gamma(S_t - S_{t-1}) + (1 - \gamma)T_{t-1} \quad (2)$$

$$I_t = \delta \left( \frac{X_t}{S_t} \right) + (1 - \delta)I_{t-s} \quad (3)$$

$$\widehat{X}_{t+h} = (S_t + hT_t)I_{t-s+h} \quad (4)$$

where  $S_t$  and  $T_t$  are the equations of the level of the time-series (average value) and the additive trend, with smoothing parameters  $\alpha$  and  $\gamma$ .  $I_t$  is the index of the seasonal length of the time-series, with smoothing parameters  $\delta$ .  $X_t$  represents the observed data, while  $\widehat{X}_{t+h}$  is the forecasting equation for  $h$  instants of time in advance.

### 2.3 Box-Jenkins Methodology

On the other hand, the Box-Jenkins methodology of ARIMA models has dominated for almost 50 years in the field of time-series forecasting [39]. It is widely used to forecast photovoltaic production and solar irradiance, either as a reference model for validating new forecasting techniques [40] or as a functional forecasting technique [41]. This approach indicates that a non-seasonal time-series can be modeled as a combination of the values and past errors, which is denoted as ARIMA (p, q, d), which can be expressed according to Eq. (5):

$$x_t = \sum_{i=1}^p \varphi_i x_{t-i} + \sum_{i=1}^q \theta_i \varepsilon_{t-i} + k + \varepsilon_t \quad (5)$$

where  $x_t$  is the predicted parameter at each instant  $t$ ,  $\varphi$  represents the autoregression (AR) coefficients,  $\theta$  represents the moving average (MA) coefficients,  $k$  is a constant, and  $\varepsilon_t$  models the white noise. For their part,  $p$  and  $q$  are the orders of the AR and MA models, respectively, while  $d$  represents the order of differentiation of the model. Similarly, a time-series that contains seasonality can be expressed with a seasonal ARIMA model. It is also known as SARIMA or ARIMA (p, d, q) (P, D, Q), where P, D, and Q represent the seasonal order of autoregression, differentiation, and moving average, respectively.

## 2.4 Forecasting Errors

To evaluate the performance of forecasting techniques, several indices allow measuring the performance of prediction algorithms by comparing the predicted values against actual or observed values. The most common indices are the MAE, the MAPE, the mean square error (MSE), and RMSE. Each of these indices has its particular characteristics, so selecting the most suitable index depends on the approach of the case of application [42]. However, it has been observed in the state of the art that, for the operation of microgrids and short-term forecasting, the most widely used indices are the RMSE, the MAE, and the MSE, which is why they are the ones used in this work. These indices are calculated according to Eqs. (6, 7 and 8):

$$RMSE = \sqrt{\frac{1}{N} \sum_{i=1}^N (\hat{y}_i - y_i)^2} \quad (6)$$

$$MSE = \frac{1}{N} \sum_{i=1}^N (\hat{y}_i - y_i)^2 \quad (7)$$

$$MAE = \frac{1}{N} \sum_{i=1}^N |\hat{y}_i - y_i| \quad (8)$$

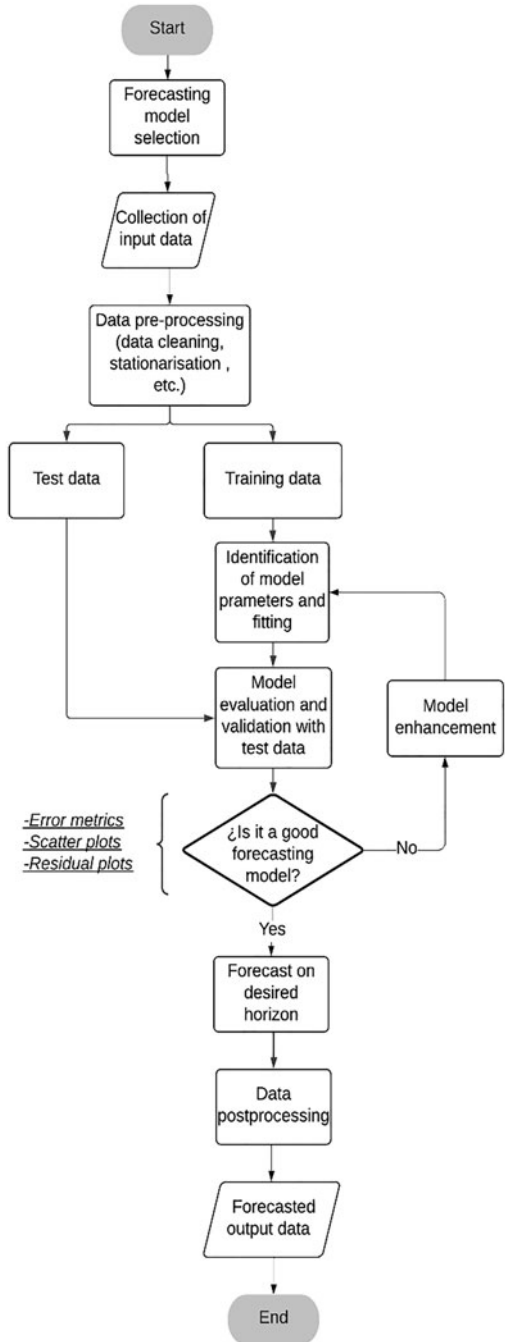
where  $y_i$  is the real value or observed at the time  $i$ ,  $\hat{y}_i$  is the predicted value at the time  $i$ , and  $N$  represents the number of data samples used to make the forecast and therefore represents the forecast horizon. Additionally, it is possible to evaluate the forecast results using scatter plots and histograms of the frequency of errors, among other indicators [43, 44]. The prediction model results are evaluated by comparing the predicted data with the test or actual data in all cases.

## 2.5 Proposed Forecasting Approach

By comparing the process of identification of parameters, training, and testing of the prediction algorithms used for one-variable or univariate time-series, a methodology has been identified, proposed, and implemented for its general application in these cases, which has been reflected in the flow diagram of Fig. 2. As an initial stage, three substages are included: (1) collection of input data, (2) selection of forecasting model, and (3) data preprocessing. The forecasting model selection stage allows the methodology to be generalized and applicable to any univariate time-series forecasting technique applicable to PV power or solar irradiance.

On the other hand, data collection can be done in various ways, either with data obtained from measurements, or using state-of-the-art datasets, as was done in this work. The preprocessing data stage is of great relevance, and its characteristics will depend on the forecasting technique to be used. For example, if ARMA models are used, the stationarity of the data should be evaluated to determine if a prediction

**Fig. 2** Proposed forecasting methodology for univariate time-series models



model is adequate. Data resolution change and cleaning can also be performed at this stage. The methodology considers error indicators and dispersion and residual graphs to compare the predicted values against the real values of the PV power or solar irradiance.

This methodology has been implemented using Python programming language and its Auto ARIMA function and the statsmodels package for the ARIMA and exponential smoothing models, respectively, to determine the coefficients and adjust the prediction models. The forecast horizon used is short-term, 24 h in advance, applicable to demand-side installations, such as microgrids.

## 2.6 *Experimental Design and Characteristics of Datasets*

Like other research on forecasting applications of other energy fields [45], an empirical comparative evaluation of forecasting techniques has been carried out. This was done with two methods based on time-series, ARIMA and exponential smoothing. The research was conducted with historical data to predict solar energy on a short-term forecasting horizon of 24 h ahead and to evaluate both forecasting methods as possible benchmarks for future stages of this research.

The validation of both forecasting methods was done with two different datasets. The first predicts solar irradiance using a dataset collected over one and a half years and 1 s time resolution. It was obtained from a 29.25 kW PV system installed in Queretaro, Mexico, where the project is developed. This PV system consists of 90 polycrystalline photovoltaic modules of 325 W each one, an inclination angle of 20°, and an azimuth orientation of 18°. Currently, the measurement system does not include data on PV power. Therefore, only the irradiance forecast is considered in this case. Another purpose with this dataset was to evaluate the forecast accuracy changing the data resolution from 1 min to 15 min.

Irradiance and PV power data are relevant to test the forecasting algorithms as indicative variables of the available solar energy due to the high Pearson correlation. It varies between 0.89 and 0.99, depending on the season of the year and the presence or absence of clouds [46–48]. Therefore, the study is performed with a dataset available on IEEE DataPort [49] to forecast PV power tests. This dataset includes six magnitudes corresponding to 2017, with a time resolution of 1 min, obtained from a PV installation located at the Polytechnic of Milan. The dataset contains information on photovoltaic power (W), ambient temperature (°C), global horizontal irradiance (GHI, W/m<sup>2</sup>), the plane of photovoltaic array irradiance (POA, W/m<sup>2</sup>), wind speed (m/s), and wind direction (°).

The PV installation of Polytechnic of Milan consists of a PV module with a peak power of 285 W, made of monocrystalline silicon, and installed with an inclination angle of 30° and an azimuth orientation 6° 30'. This dataset has been already referenced in other PV power forecasting research work based on ANN [50], which will allow in the future to compare the obtained forecast results with those already reported. A relevant characteristic of this dataset is the presence of snowfall



days, a meteorological condition never available locally in México, where the project is currently being carried out. The main reason and motivation to use this dataset is the possibility of assessing the proposed forecast methods with that kind of meteorological condition. It ensures a good generality of application for different places and weather conditions.

Two general conditions were considered with the second dataset: sunny days in winter and cloudy days in spring. As a subcase for sunny days, it was considered a variation in the number of training data days, with variations in PV power caused by clouds, to assess its impact on the accuracy of forecasting models.

### 3 Results

#### 3.1 Solar Irradiance Forecast

Initially, a Holt-Winters model with additive error component (A), additive trend component (A), and additive seasonal component (A) or (A, A, A), to forecast a solar irradiance time-series of 7 days, with sampling per minute is performed. The model adjusted to the time-series and made an adequate forecast, as shown in Fig. 3. The curves reflect minor variations, which can be observed when using a sampling per minute. Despite the variations, the Holt-Winters model (blue curve) manages to

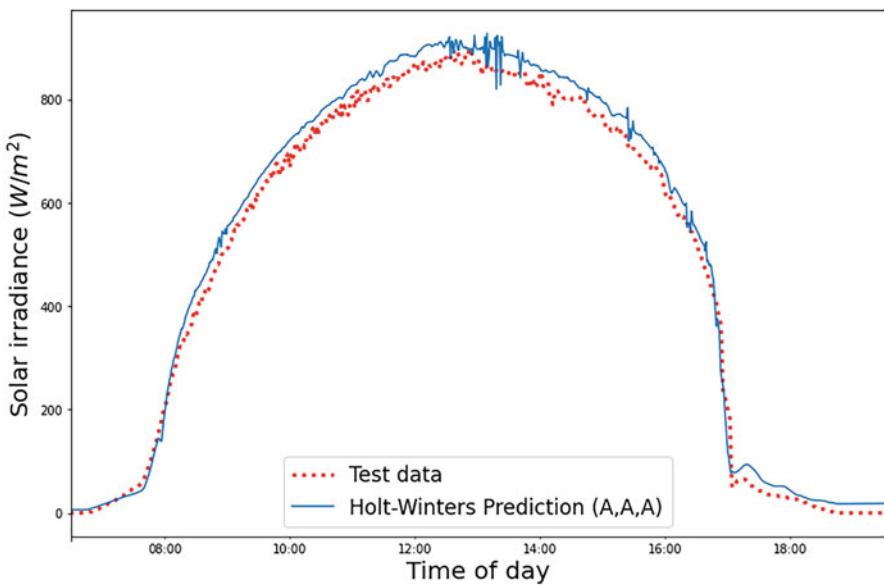


**Fig. 3** Irradiance data and predicted data, using a Holt-Winters model, with data sampling per minute

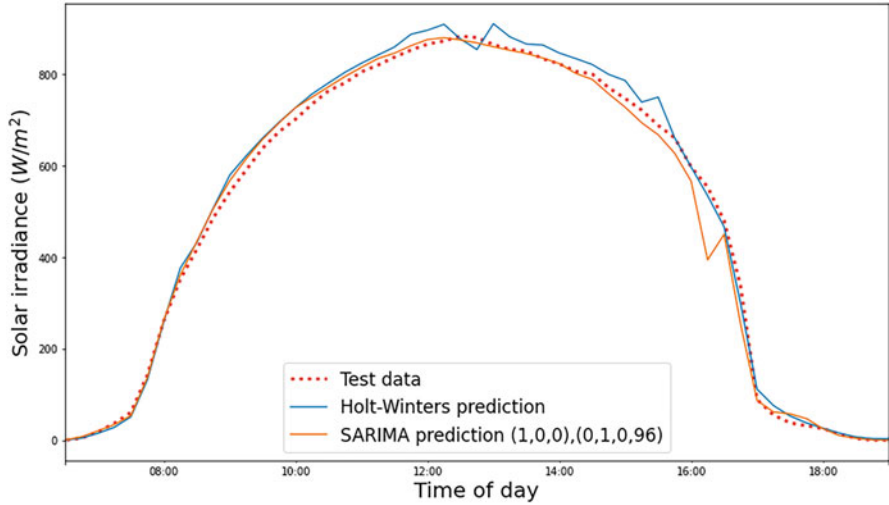


**Fig. 4** Irradiance data and predicted data, using a Holt-Winters model, with a sampling interval of 15 min

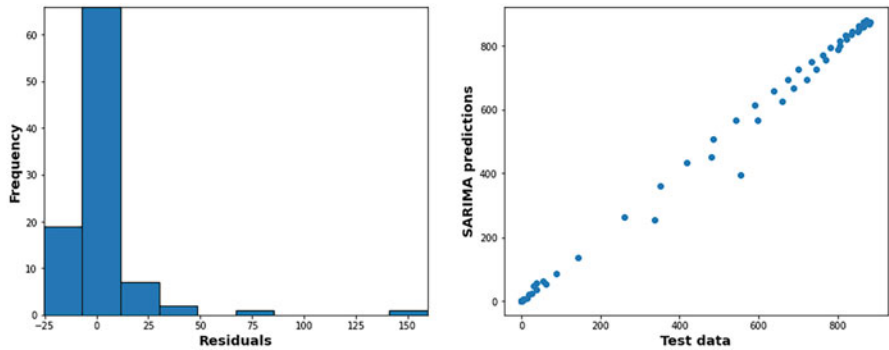


**Fig. 5** Residual and dispersion plots of SARIMA model forecasting results for irradiance, with a sampling interval of 15 min

follow the general trajectory of the measured irradiance curve (red color). The RMSE obtained was  $23.95 W / m^2$  (Fig. 4).

Subsequently, the same model was applied to the same time-series with an adjusted sampling to 15 min to analyze the impact of data preprocessing on forecasting results. In this case, the RMSE was lower, with a value of  $17.15 W / m^2$ . A second model was identified and trained as a SARIMA  $(1, 0, 0) \times (0, 1, 0)$  [96], showing a similar graphical performance but with a bigger RMSE of  $21.13 W / m^2$ . These results are confirmed with residuals and scatter plots of Figs. 5 and 6, showing most of the residuals or differences between the actual and predicted values are close to zero with the Holt-Winters model. In contrast, its scatter plot resembles a linear regression.

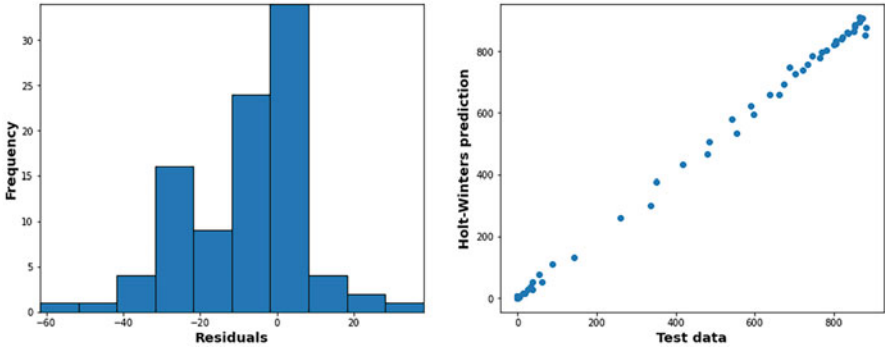


**Fig. 6** Residual and dispersion plots of Holt-Winters model forecasting results for irradiance, with

**Table 1** Summary of irradiance forecast results

Conditions	Dataset resolution	Number of training data days/ test data days	Model	RMSE (W/m <sup>2</sup> )
Sunny	1 min	6/1	Holt-winters (A, A, A)	1.89
Sunny	15 min	6/1	Holt-winters (A, A, A)	37.19
Sunny	15 min	6/1	SARIMA (1,0,0) × (0,1,0) [96]	21.13

a sampling interval of 15 min

A summary of obtained irradiance forecasts results is shown in Table 1, indicating the general weather conditions in each case, the data resolution, the number of training and test data days used, the characteristics of the fitted model, and the RMSE obtained.

## 4 Photovoltaic Power Forecast

### 4.1 Forecast for the Winter Season: First Case

In all cases of PV power forecasting, the dataset has been preprocessed to a resolution of 15 min.

The first analysis case of PV power forecasting considers a time-series of 9 days, from January 13 to 21, considering eight days as training data and the ninth as test data. Two forecasting models were identified and trained, the first SARIMA (5, 0, 4) × (0, 1, 0) [96] and the second from Holt-Winters. The SARIMA model yielded an RMSE of 1.89 W, while the Holt-Winters model had an RMSE of 37.19 W. The

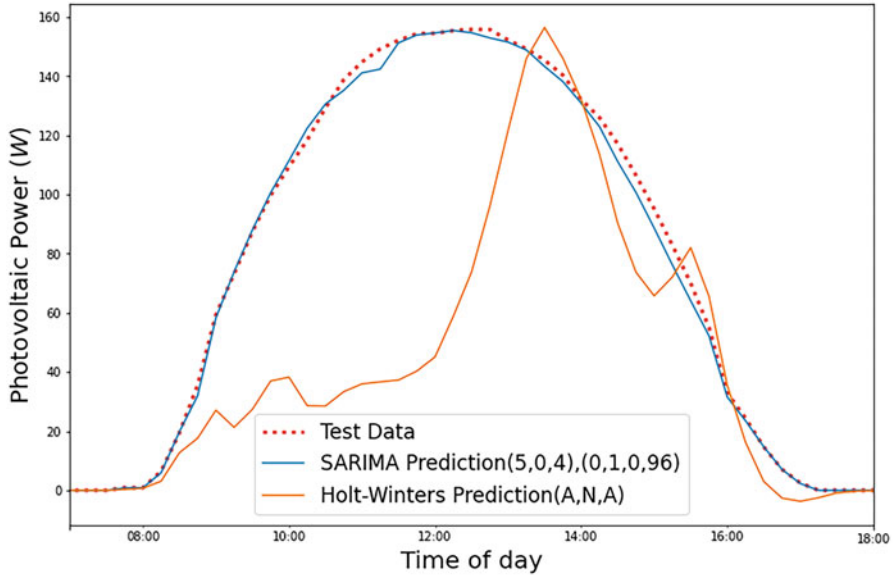


Fig. 7 PV power test data and predicted data, using both models, case 1

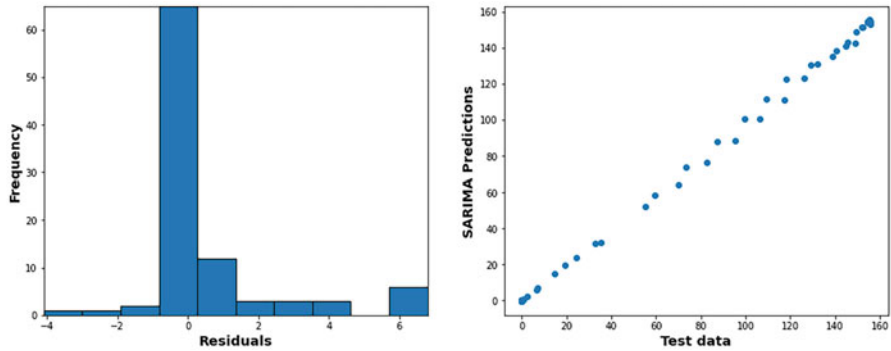


Fig. 8 Residual and dispersion plots of SARIMA model forecasting results, case 1

comparison of the forecast results is shown in Fig. 7 with a significant similarity between the test data and the SARIMA prediction. It is confirmed in the results of the residuals and scatter plots (Fig. 8) since most of the residuals or differences between the actual and predicted values are close to zero. In contrast, the scatter plot strongly resembles a linear regression. On the other hand, the Holt-Winters prediction model shown in Fig. 7 with orange color could not accurately predict the PV power. It was confirmed in the results of residuals and dispersion (Fig. 9), with residuals far from zero and a marked dispersion between the test or actual data and the predictions.

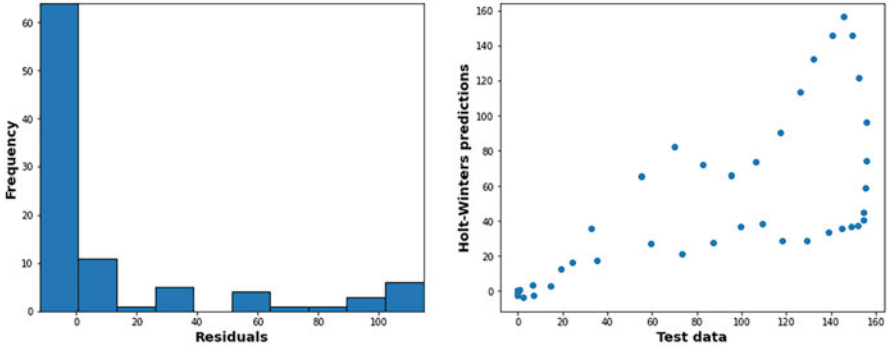


Fig. 9 Residual and scatter plots of Holt-Winters model forecasting results, case 1

## 4.2 Forecast for the Winter Season: Second Case

The second case also considers the PV power forecast of January 22. In this case, a 7-day time-series is used, eliminating the two first days (January 13 and 14) with the presence of clouds, to evaluate the potential improvement of the Holt-Winters model. In this way, the training data is reduced from 8 to 6 days. The test data is the same (January 21). The models identified and fitted to the training data are a SARIMA  $(4, 0, 0) \times (0, 1, 0)$  [96] model and the second Holt-Winters model. The SARIMA model yielded an RMSE of 1.93 W, very similar to the previous case, while the Holt-Winters model obtained an RMSE of 10.31 W, 20 W lower than the previous case. The comparison of the test data with the results of both forecasting models is shown in Fig. 10. The similarity between the SARIMA curve model and test data is confirmed, unlike with the Holt-Winters model. However, the behavior of the latter is improved in comparison to the previous case.

## 4.3 Forecast for the Spring Season

The third case evaluated is a time-series of nine days of photovoltaic power, from May 29 to June 6, 2017, using eight days as training data and the ninth day as test data. In this case, the primary purpose was to evaluate the behavior of the models to forecast cloudy days. Two forecasting models were identified and trained, the first SARIMA  $(5, 0, 1) \times (0, 1, 0)$  [96] and the second from Holt-Winters. The SARIMA model yielded an RMSE of 37.74 W, while the Holt-Winters model had an RMSE of 54.45 W. In both cases, the errors are considerably high, considering that the maximum value of the photovoltaic power during that period is around 200 W. A

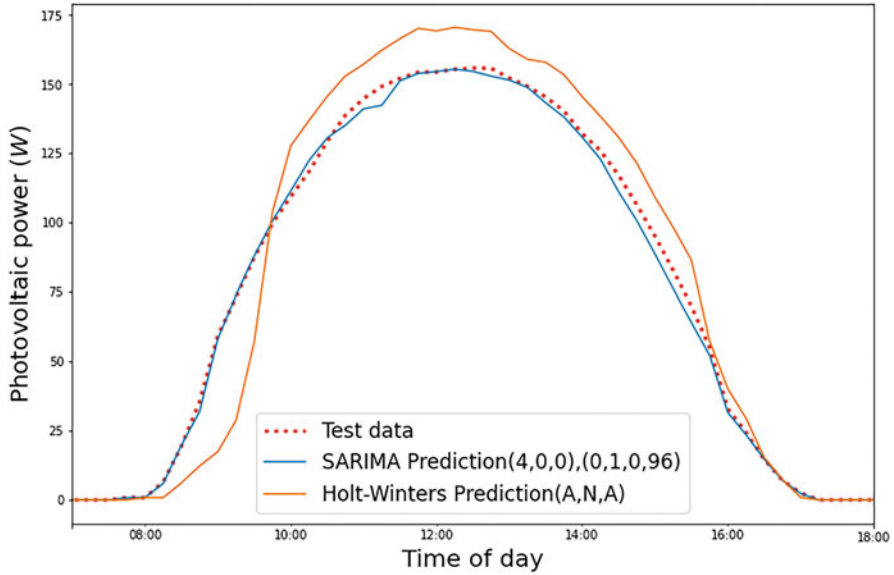


Fig. 10 PV power test data and predicted data using both models, case 2

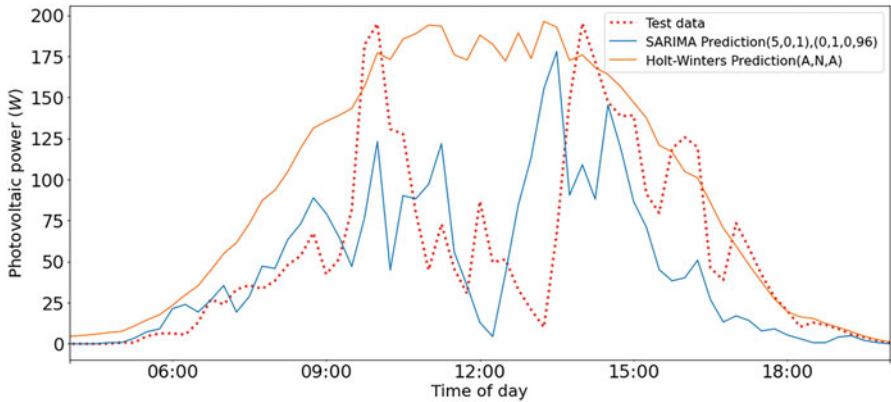


Fig. 11 PV power test data and predicted data using both models, case 3

graphical comparison of the real PV power curve concerning the prediction result of both models is shown in Fig. 11. The SARIMA model presents typical day variations with a high incidence of clouds, although it does not follow the general trajectory of the curve of real values. On the other hand, the Holt-Winters model shows only some slight variations close to the peak of the photovoltaic production curve.

**Table 2** Summary of PV power forecast results

Conditions	Number of training data days/test data days	Model	RMSE (W/m <sup>2</sup> )
Winter, sunny	8/1	SARIMA (5,0,4) × (0,1,0) [96]	1.89
Winter, sunny	8/1	Holt-Winters (A, N, A)	37.19
Winter, sunny	6/1	SARIMA (4,0,0) × (0,1,0) [96]	1.93
Winter, sunny	6/1	Holt-Winters (A, N, A)	10.31
Spring, cloudy	8/1	SARIMA (5,0,1) × (0,1,0) [96]	37.74
Spring, cloudy	8/1	Holt-Winters (A, N, A)	54.45

Finally, a summary of obtained PV power forecasts is shown in Table 2. General weather conditions are presented in each case, such as sunny or cloudy days and the year's season. The number of training and test data days used, the characteristics of the fitted model, and the RMSE obtained are also shown. In all cases, the dataset had a resolution of 15 min.

## 5 Discussion

Both scenarios of irradiance forecasting during sunny days show a similar predicted irradiance profile compared to the measured values, as can be seen in Figs. 3 and 4. Nevertheless, when reducing the data resolution from 1 min to 15 min, the irradiance profile shows fewer variations in the general trend due to data resampling. When forecasting with 1 min data resolution, the Holt-Winters method lets us predict the fast variation of the general trend of irradiance. This could be useful to forecast irradiance in PV systems with high accuracy, Class A, monitoring systems, suggested by the standard IEC 61724-1:2017 [51], for applications of fault location, electric network interaction assessment, PV technology assessment, and precise PV system degradation measurement.

In the first case analyzed of PV power forecasting, the Holt-Winters prediction model (Fig. 7), in orange color, presents a significant distortion, apparently caused by the effect of cloudy days existing in the training data. This was confirmed when two cloudy days were removed in training data, as seen in Fig. 10 from the second case of PV power forecasting. Therefore, for nonhomogeneous datasets, where the training data include variations due to cloud cover, the SARIMA model is more suitable for predicting photovoltaic power.

The second case of irradiance forecasting shown in Fig. 4 and the first case of PV power forecasting during the winter season depicted in Fig. 10, showed that, when there are fewer fast variations in the magnitude of solar energy caused by clouds, the SARIMA model can eliminate its moving average (MA) component. Again, this can be considered a result of the presence of prevailing homogeneous datasets.

As a relevant finding in the implementation and analysis of these two univariate forecasting techniques of solar energy, it was found that, unlike cases reported in the state of the art [19], the ARIMA forecasting models are not enough to forecast solar energy accurately if they do not include the seasonal component, as the SARIMA model does. For the same reason, the Holt-Winters model predicts solar energy with acceptable results by including a third equation to handle the time-series seasonality. The application of the proposed forecasting methodology has allowed validating the applicability of the exponential smoothing and Box-Jenkins forecasting methods, allowing us to identify and verify which weather conditions are adequate to predict solar irradiance and photovoltaic power. In addition, the use of this general methodology to evaluate forecasting techniques in the field of solar energy for microgrids was validated.

## 6 Conclusions

Based on the obtained results, the SARIMA model yields better results in all the cases analyzed in terms of the RMSE index and the dispersion of the results. Specifically, it could adequately represent the characteristics of trend, seasonality, and average values of the time-series of photovoltaic power or solar irradiance. However, in cases with minimum or no cloud incidence, expressly with predominantly homogeneous data, the Holt-Winters exponential smoothing model is also an alternative to fit the time-series training data to represent the dominant component of the seasonality of this type of time-series. As a general conclusion, it was confirmed that they are not the most suitable for representing variations in highly nonlinear time-series, as is the case of rapid variations in the magnitude of the photovoltaic power caused by the incidence of clouds. Moreover, it was possible to identify, propose, and implement a forecasting methodology applicable to forecast univariate time-series of solar energy in microgrids, which can be generalized and applied to state-of-the-art forecasting algorithms. Therefore, as future work, forecasting models of solar energy in microgrids, capable of predicting nonlinearities and sudden changes in the time-series, will be implemented, with a multivariable approach, such as machine learning and deep learning techniques.



## References

1. Dzebo, A., Janetschek, H., Brandi, C., & Iacobuta, G. (2019) *Connections between the Paris agreement and the 2030 agenda. The case for policy coherence*, p. 38.
2. Van Der Meer, D., Mouli, G. R. C., Mouli, G. M. E., Elizondo, L. R., & Bauer, P. (2018). *Energy management system with PV power forecast to optimally charge EVs at the workplace*. IEEE Transactions on Industrial Informatics.
3. A. Ahmad, N. Javaid, A. Mateen, M. Awais, and Z. A. Khan, "Short-term load forecasting in smart grids: An intelligent modular approach," *Energies*, vol. 12, no. 1, p. 164, Jan. 2019.
4. Salamanis, A. I., et al. (2020). Benchmark comparison of analytical, data-based and hybrid models for multi-step short-term photovoltaic power generation forecasting. *Energies*, 13(22). <https://doi.org/10.3390/en13225978>
5. Wang, Y., Liao, W., & Chang, Y. (2018). Gated recurrent unit network-based short-term photovoltaic forecasting. *Energies*, 11, 2163.
6. Gao, B., Huang, X., Shi, J., Tai, Y., & Xiao, R. (2019). Predicting day-ahead solar irradiance through gated recurrent unit using weather forecasting data. *Journal of Renewable and Sustainable Energy*, 11.
7. Harrou, F., Kadri, F., & Sun, Y. (2020). Forecasting of photovoltaic solar power production using LSTM approach. In *Advanced statistical modeling, forecasting, and fault detection in renewable energy systems*. IntechOpen.
8. Ge, Y., Nan, Y., & Bai, L. (2019). A hybrid prediction model for solar radiation based on long short-term memory, empirical mode decomposition, and solar profiles for energy harvesting wireless sensor networks. *Energies*, 12, 4762.
9. Liu, D., & Sun, K. (2019). Random forest solar power forecast based on classification optimization. *Energy*, 187, 115940.
10. M. W. Ahmad, M. Mourshed, and Y. Rezgui, "Tree-based ensemble methods for predicting PV power generation and their comparison with support vector regression," *Energy*, vol. 164, pp. 465–474, Dec. 2018.
11. Martínez, C. G. (2018). *Árboles de decisión y métodos de ensemble*. RPubS.
12. Ahmad, T., Zhang, H., & Yan, B. (2020). *A review on renewable energy and electricity requirement forecasting models for smart grid and buildings* (Sustainable cities and society) (Vol. 55, p. 102052). Elsevier Ltd.
13. Mishra, S., & Palanisamy, P. (2018). Multi-time-horizon solar forecasting using recurrent neural network. In *2018 IEEE energy conversion congress and exposition*. ECCE.
14. Fan, C. et al. (2019). Multi-horizon time-series forecasting with temporal attention learning. In *Proceedings of the ACM SIGKDD international conference on knowledge discovery and data mining*.
15. Huang, Q. (2018). *Application of machine learning in power systems: Part I – An overview*. IEEE Smart Grid.
16. Sáez, D., Ávila, F., Olivares, D., Cañizares, C., & Marín, L. (2015). Fuzzy prediction interval models for forecasting renewable resources and loads in microgrids. *IEEE Transactions on Smart Grid*, 6(2), 548–556.
17. Rafique, F., Jianhua, Z., Rafique, R., Guo, J., & Jamil, I. (2018). Renewable generation (wind/solar) and load modeling through modified fuzzy prediction interval. *International Journal of Photoenergy*, 2018, 1–14.
18. Semero, Y. K., Zheng, D., & Zhang, J. (2018). A PSO-ANFIS based hybrid approach for short term PV power prediction in microgrids. *Electric Power Components and Systems*, 46.
19. Hernández-Hernández, C., Rodríguez, F., Moreno, J. C., Da Costa Mendes, P. R., Normey-Rico, J. E., & Guzmán, J. L. (2017). The comparison study of short-term prediction methods to enhance the model predictive controller applied to microgrid energy management. *Energies*, 10(7), 35.
20. Mei, F., Pan, Y., Zhu, K., & Zheng, J. (2018). A hybrid online forecasting model for ultrashort-term photovoltaic power generation. *Sustainability*, 10(3), 1–17.

21. Dragomir, O. E., Dragomir, F., Stefan, V., & Minca, E. (2015). Adaptive neuro-fuzzy inference systems as a strategy for predicting and controlling the energy produced from renewable sources. *Energies*, 8(11), 13047–13061.
22. Wen, L., Zhou, K., Yang, S., & Lu, X. (2019). Optimal load dispatch of community microgrid with deep learning based solar power and load forecasting. *Energy*, 171, 1053–1065.
23. Ma, J., & Ma, X. (2018). A review of forecasting algorithms and energy management strategies for microgrids. *Systems Science & Control Engineering*, 6(1), 237–248.
24. Villavicencio, P. J. (2010). Introducción a Series de Tiempo. *Man. Metodol. Ser. tiempo*, 33.
25. Ssekulima, E. B., Anwar, M. B., Al Hinai, A., & El Moursi, M. S. (2016). Wind speed and solar irradiance forecasting techniques for enhanced renewable energy integration with the grid: A review. *IET Renewable Power Generation*, 10(7), 885–898.
26. Atique, S., Noreen, S., Roy, V., Subburaj, V., Bayne, S., & MacFie, J. (2019). Forecasting of total daily solar energy generation using ARIMA: A case study. In *2019 IEEE 9th Annual Computing and Communication Workshop and Conference* (pp. 114–119). CCWC.
27. Mite-León, M., & Barzola-Monteses, J. (2018). Statistical model for the forecast of hydropower production in Ecuador. *International Journal of Renewable Energy Research*, 10(2), 1130–1137. 1309-0127.
28. Barzola-Monteses, J., Mite-León, M., Espinoza-Andaluz, M., Gómez-Romero, J., & Fajardo, W. (2019). Time series analysis for predicting hydroelectric power production : The Ecuador case. *Sustainability*, 11(6539), 1–19. <https://doi.org/10.3390/su11236539>
29. Dev, S., Alskaf, T., Hossari, M., Godina, R., Louwen, A., & Van Sark, W. (2018). Solar irradiance forecasting using triple exponential smoothing. In *International conference on smart energy systems and technology*. SEST. <https://doi.org/10.1109/SEST.2018.8495816>
30. Yang, D., Sharma, V., Ye, Z., Lim, L. I., Zhao, L., & Aryaputera, A. W. (2015). Forecasting of global horizontal irradiance by exponential smoothing, using decompositions. *Energy*, 81.
31. Prema, V., & Rao, K. U. (2015). Time-series decomposition model for accurate wind speed forecast. *Renewables: Wind, Water, and Solar*, 2.
32. Tran Anh, D., Duc Dang, T., & Pham Van, S. (2019). Improved rainfall prediction using combined pre-processing methods and feed-forward neural networks. *J*, 2.
33. Farias, R. L., Puig, V., Rangel, H. R., & Flores, J. J. (2018). Multi-model prediction for demand forecast in water distribution networks. *Energies*, 11.
34. Liu, L., & Wu, L. (2020). Predicting housing prices in China based on modified Holt's exponential smoothing incorporating whale optimization algorithm. *Socio-Economic Planning Sciences*, 72.
35. Hyndman, R. J., & Athanasopoulos, G. (2018). *Forecasting: Principles and practice*.
36. Ferreira, M., Santos, A., & Lucio, P. (2019). Short-term forecast of wind speed through mathematical models. *Energy Reports*, 5.
37. Sánchez-Durán, R., Barbancho, J., & Luque, J. (2019). Solar energy production for a decarbonization Scenario in Spain. *Sustainability*, 11(24).
38. Trull, Ó., García-Díaz, J. C., & Troncoso, A. (2020). Stability of multiple seasonal holt-winters models applied to hourly electricity demand in Spain. *Applied Sciences*.
39. Box, G. E. P., Jenkins, G. M., & Reinsel, G. C. (2013). *Time-series analysis: Forecasting and control* (4th ed.). Wiley.
40. Suresh, V., Janik, P., Rezmer, J., & Leonowicz, Z. (2020). Forecasting solar PV output using convolutional neural networks with a sliding window algorithm. *Energies*, 13, 723.
41. David, M., Ramahatana, F., Trombe, P. J., & Lauret, P. (2016). Probabilistic forecasting of the solar irradiance with recursive ARMA and GARCH models. *Solar Energy*.
42. Xu, Z., Hu, Z., Zhao, J., Song, Y., Lin, J., & Wan, C. (2016). Photovoltaic and solar power forecasting for smart grid energy management. *CSEE Journal Power Energy System*, 1(4), 38–46.
43. Sharafi, M., Ghaem, H., Tabatabaee, H. R., & Faramarzi, H. (2017). Forecasting the number of zoonotic cutaneous leishmaniasis cases in south of Fars province, Iran using seasonal ARIMA time-series method. *Asian Pacific Journal of Tropical Medicine*, 10(1), 79–86.

44. Sabir, E. C., & Batuk, E. (2013). Demand forecasting withof using time-series models in textile dyeing-finishing mills. *Tekst. ve Konfeksiyon*, 23(2), 143–151.
45. Divina, F., Torres, M. G., Vela, F. A. G., & Noguera, J. L. V. (2019). A comparative study of time series forecasting methods for short term electric energy consumption prediction in smart buildings. *Energies*, 12(10). <https://doi.org/10.3390/en12101934>
46. Yadav, H. K., Pal, Y., & Tripathi, M. M. (2020). Parameter optimization using PSO for neural network-based short-term PV power forecasting in Indian electricity market. *Lecture Notes in Electrical Engineering*, 597, 331–348.
47. Zhu, H., Li, X., Sun, Q., Nie, L., Yao, J., & Zhao, G. (2015). A power prediction method for photovoltaic power plant based on wavelet decomposition and artificial neural networks. *Energies*, 9(1), 11.
48. Li, L.-L., Cheng, P., Lin, H.-C., & Dong, H. (2017). Short-term output power forecasting of photovoltaic systems based on the deep belief net. *Advances in Mechanical Engineering*, 9(9), 168781401771598.
49. Leva, E., Sonia, P., & Silvia, O. (2020). *Photovoltaic power and weather parameters* | *IEEE DataPort*. IEEE DataPort.
50. Nespoli, A., et al. (2019). Day-ahead photovoltaic forecasting: A comparison of the most effective techniques. *Energies*, 12. <https://doi.org/10.3390/en12091621>
51. IEC. (2017). *IEC 61724-1:2017 photovoltaic system performance - part 1: Monitoring*. IEC.

# Carbon-Based Perovskite Solar Cells: The Future Photovoltaic Technology



Israel Barrutia, Renzo Seminario-Córdova, and Vanessa Martinez-Rojas

## 1 Introduction

The **behavior** of energy consumption is closely **related** to the increase of the world population, as well as the economic and social development, which **as a consequence** has dramatically increased the demand for energy services, and this demand is expected to continue to increase [1]. However, overuse of fossil fuels has irreversible consequences on the planet, which has caused people and governments **in** the world to look for ways to generate energy while minimizing greenhouse gas emissions and other environmental impacts [2].

**Due to its remarkable progress in recent years and their simple manufacturing methods, PSC have become a promising photovoltaic technology**, as a consequence so in a near future PSC-based photovoltaic technologies will generate the terawatt-scale power output to generate a low carbon economy reshaping our society energetic future. Besides, its low weight, semitransparency, and flexibility along with the possibility of integrating it into a wide range of shapes make PSC an ideal energy source for application in self-powered devices required for the future.

This chapter **displays some** power conversion efficiency (PCE) of PSC with carbon-based electrode, which is used as a strategy to replace unstable hole transport materials or improve moisture stability by utilizing semiconducting oxides as transport layers or scaffolds.

---

I. Barrutia (✉) · R. Seminario-Córdova  
Innova Scientific, San Miguel, Perú

V. Martinez-Rojas  
Universidad Tecnológica del Perú, Lima, Perú

## 1.1 Perovskite Solar Cells

The photovoltaic performance of PSC, especially organic-inorganic hybrid perovskite materials, is attributed to its intrinsic properties, which include high absorption coefficient [3], tunable bandgap [4], large carrier diffusion length [5], ambipolar carrier transport ability [6], and carrier mobility [7].

Usually, PSC consists of a light-absorbing layer, which is perovskite that is inserted between electron transport material (ETM) and hole transport material (HTM). Figure 1 presents the sequence of reactions that occur in a PSC; the perovskite absorbs light and  $e^-/h^+$  pairs are created in the material. This charge separation can occur through two possible primary reactions: (1) injection of photogenerated electrons to the ETM, which is, in this setting,  $\text{TiO}_2$  or (2) injection of holes to the HTM. **Undesired** processes are a recombination of photogenerated charges (3), charge transfer at the two interfaces of  $\text{TiO}_2$  with perovskite (4) and the HTM with perovskite (5), **finally between  $\text{TiO}_2$**  and the HTM (6), for example, in the presence of nanoparticles or holes [8].

Kojima et al. in 2009 first reported on the application of PSC. The device consisted of a liquid electrolyte-based dye-sensitized solar cell configuration. The adsorption of methylammonium lead halide perovskite ( $\text{CH}_3\text{NH}_3\text{PbI}_3$ ) on a nanocrystalline  $\text{TiO}_2$  surface produced a photocurrent with a power conversion efficiency (PCE) of 3.80% [9].

As of this report, research in this **arena** started to intensify; especially since 2013, when the PSC reached 14% of PCE, which continued to increase drastically and currently the record PCE is 25.50% [10], **which attracted more attention** of numerous research groups and **even from** companies in the photovoltaic business.

Figure 2 shows the PSC configurations that have been developed since 2009, which include an electrolyte-based mesoscopic cell with the perovskite  $\text{CH}_3\text{NH}_3\text{PbBr}_3$ , followed by a solid-state cell, using Spiro OMeTAD as HTM, from 2012; then a planar heterojunction cell, with Spiro OMeTAD; and finally, a mesoporous cell using Spiro OMeTAD from 2016 [6].

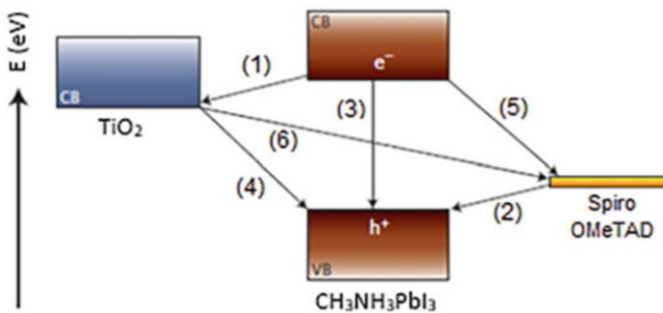


**Fig. 1** Schematic diagram of the energy levels and electron transfer process in an HTM perovskite  $\text{TiO}_2$  structure cell. The numbers correspond to the reactions mentioned above [8]

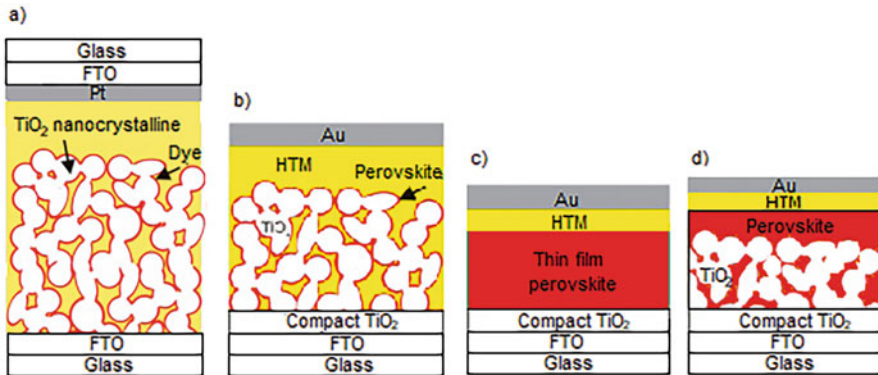


**Fig. 2** Scheme of PSC configurations. (a) Electrolyte-based mesoscopic cell, (b) solid-state cell, (c) planar heterojunction cell, and (d) mesoporous cell. (Adapted from [6])

A brief review of the literature related to perovskite solar cells (PSC) was carried out to present concepts of their operation, and in the next section some outstanding research results of carbon-based perovskite solar cells (C-PSC) since their invention will be presented.

## 2 Results

Year-wise reports on the values of C-PSC and materials used are summarized elaborately in Table 1. Finally, the findings show the feasibility of the commercialization of C-PSC.

### 2.1 Carbon-Based Perovskite Solar Cell

Carbon is an abundant and low-cost material and has a work function of  $-5$  eV which is higher compared to that of gold, which is  $-5.1$  eV [11]. Also, its energy level is conveniently located to absorb the hole of perovskite materials, so the HTM layer which is often costly and unstable can be eliminated [12]. Due to its simple fabrication process using techniques such as screen printing which does not require vacuum evaporation as gold or silver does so, carbon can be used as a counter electrode. Therefore, carbon can replace gold and silver electrodes [13]. Figure. 3 shows the first scheme of this type of device.

In C-PSC, the production cost is reduced; moreover, due to the hydrophobic nature of the carbon top component, the presence of humidity and, therefore, the humidity-vulnerable perovskite is substantially protected [14, 15]. Furthermore, it is worth mentioning that, using screen printing or roll-to-roll methods in this type of

**Table 1** Carbon-based perovskite solar cells with their characteristic values

Year	ETM	Perovskite	HTM	V <sub>oc</sub> (V)	J <sub>sc</sub> (mA/cm <sup>2</sup> )	FF (%)	PCE (%)	Ref
2014	m-TiO <sub>2</sub>	MAFAPbI <sub>3</sub>	–	0.921	20.90	67.00	12.90	[13]
2015	m-TiO <sub>2</sub>	CH <sub>3</sub> NH <sub>3</sub> PbI <sub>3</sub>	TPDI	1.030	20.10	74.90	15.50	[22]
2016	m-TiO <sub>2</sub>	CH <sub>3</sub> NH <sub>3</sub> PbI <sub>3</sub>	CuPc	1.050	20.80	74.00	16.10	[23]
2016	m-TiO <sub>2</sub>	CH <sub>3</sub> NH <sub>3</sub> PbI <sub>3</sub>	–	0.927	20.20	77.00	14.50	[29]
2017	m-TiO <sub>2</sub>	CH <sub>3</sub> NH <sub>3</sub> PbI <sub>3</sub>	–	0.893	22.43	74.70	15.00	[30]
2017	m-TiO <sub>2</sub>	CsMAFAPb (IBr) <sub>3</sub>	Spiro O	1.030	22.00	63.00	15.00	[31]
2017	m-TiO <sub>2</sub>	CH <sub>3</sub> NH <sub>3</sub> PbI <sub>3</sub>	–	0.903	22.38	76.10	15.38	[32]
2017	TiO <sub>2</sub> /AlO <sub>3</sub> /NiO	CsMAFAPb (IBr) <sub>3</sub>	–	1.008	23.40	72.00	17.02	[24]
2018	m-TiO <sub>2</sub>	CH <sub>3</sub> NH <sub>3</sub> PbI <sub>3</sub>	–	0.930	23.30	71.00	14.90	[33]
2018	TiO <sub>2</sub> /SnO <sub>2</sub>	CsMAFAPb (IBr) <sub>3</sub>	CuPc	0.980	23.28	67.00	15.39	[34]
2018	TiO <sub>2</sub> :NiO	CsMAFAPb (IBr) <sub>3</sub>	CuPc	1.073	22.41	72.60	17.46	[25]
2018	m-TiO <sub>2</sub>	MAFAPb(IBr) <sub>3</sub>	Spiro O	1.080	23.33	76.20	19.20	[21]
2019	C <sub>60</sub> : HMB	CH <sub>3</sub> NH <sub>3</sub> PbI <sub>3</sub>	–	1.060	22.68	66.74	16.03	[35]
2019	m-TiO <sub>2</sub>	PbTiO <sub>3</sub>	–	0.930	23.47	75.00	16.37	[36]
2019	SnO <sub>2</sub> @TiO <sub>2</sub>	(NH <sub>4</sub> CH <sub>3</sub> NH <sub>3</sub> ) <sub>0.3</sub> (NH <sub>3</sub> CH <sub>3</sub> ) <sub>0.7</sub> PbI <sub>3</sub>	P3HT	1.060	22.30	74.00	18.10	[37]
2019	SnO <sub>2</sub>	CsMAFAPb (IBr) <sub>3</sub>	Spiro O	1.050	22.78	78.00	18.65	[26]
2020	m-TiO <sub>2</sub>	CsMAFAPb (IBr) <sub>3</sub>	–	0.940	23.51	68.00	15.09	[27]
2020	SnO <sub>2</sub>	MAFAPb(IBr) <sub>3</sub>	Spiro O	1.050	20.37	72.00	15.37	[38]
2020	SnO <sub>2</sub>	FAPbI <sub>3</sub>	CZTS	1.095	23.90	67.67	17.71	[39]
2020	SnO <sub>2</sub>	CsMAFAPb (IBr) <sub>3</sub>	Spiro O	1.117	21.11	79.00	18.56	[40]
2021	Cu <sub>2</sub> ZnSnS <sub>4</sub>	MAPbI <sub>3</sub>	–	0.997	22.74	71.01	16.10	[41]
2021	SnO <sub>2</sub>	MAPbI <sub>3</sub>	Spiro O	1.109	19.71	73.78	16.13	[28]
2021	m-TiO <sub>2</sub>	MAPbI <sub>3</sub>	–	1.023	22.25	76.70	17.47	[19]

m-TiO<sub>2</sub> = mesoporous TiO<sub>2</sub>, Spiro O = Spiro OMeTAD, CZTS = Cu<sub>2</sub>ZnSnS<sub>4</sub>, P3HT = Poly (3-hexylthiophene-2,5-diyl), J<sub>sc</sub> = current density, FF = fill factor

cells, acceptable efficiencies higher than 10% have been obtained [14, 15]; that is, comparable to commercial silicon photovoltaic cells, turning into a promising nominee for industrialization and substitution of organic or hybrid organic-inorganic solar cells.

The first report on solar cells using carbon as the electrode was in 1996. Kay and Grätzel designed a new type of monolithic liquid electrolyte-sensitized solar cell using black carbon/graphite as a composite counter electrode and obtained an

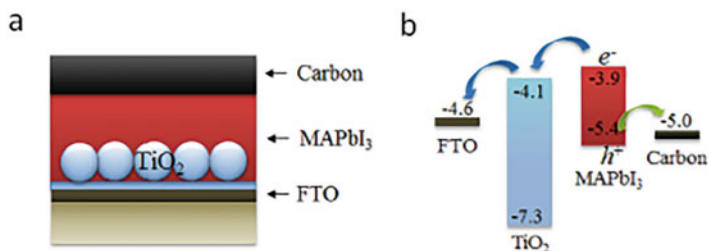


**Fig. 3** (a) Schematic drawing of a carbon-based perovskite solar cell. (b) Energy band diagram of the device. Energy levels of the conduction band edges of TiO<sub>2</sub>, and MAPbI<sub>3</sub> are at  $-4.1$ , and  $-3.9$  eV, respectively, whereas the valence band edge of the perovskite is at  $-5.4$  eV, and that of the Fermi level of carbon is at  $-5.0$  eV [12]

encouraging PCE of 6.70% [17]. Such a device was printed layer by layer on single fluorine-doped tin oxide (FTO) glass substrate by screen printing technique, which offered greater prospects for commercial production. However, it was not until 2013 that Ku et al. assembled a monolithic perovskite CH<sub>3</sub>NH<sub>3</sub>PbI<sub>3</sub>/TiO<sub>2</sub> solar cell using black carbon/graphite as counter electrode and screen-printing technique, obtaining 6.64% efficiency and 840 h dark stability [11].

After this result, several C-PSC investigations followed [12, 13, 18–20]. Nowadays, these devices call the attention and have reached the maximum PCE of 19.20% [21], a value not far from the current record of Au counter electrode PSC (Au-PSC) [10]. Hereafter, some representative results of C-PSC per year are outlined.

In 2014, Mei et al. manufactured the HTM-free printable C-PSC consisting of a double layer of TiO<sub>2</sub> and ZrO<sub>2</sub>; the second layer acted as a spacer. Perovskite, a solution of PbI<sub>2</sub>, methylammonium iodide (MA), and 5-ammonium valeric acid iodide (5-AVA) as an additive, was infiltrated into the device by the drop-casting method; the additive was key producing lower defect concentration and better pore filling, as well as full contact with the TiO<sub>2</sub> layer, resulting in longer exciton lifetime and higher quantum yield for photoinduced charge separation, compared to only CH<sub>3</sub>NH<sub>3</sub>PbI<sub>3</sub> (MAPbI<sub>3</sub>) (Fig. 4). C-PSC achieved a PCE of 12.80% [18] and remained stable for more than 1000 h exposed to the environment in full sunlight.

In 2014, fully printable C-PSC composed by methylammonium lead trihalide (MAPbI<sub>3</sub>) and formamidinium lead trihalide (FAPbI<sub>3</sub>) perovskites were reported with the sequential deposition method. By optimizing the mixing ratio of formamidinium and methylammonium cations to 3:2, an efficiency of 12.90% was achieved [13].

In 2015, a new HTM named TDPI (5,10,15-triphenyl-5Hdiindolo[3,2-a:30,20-c]carbazole) was synthesized. This material showed a good thermal stability, high hole mobility, and appropriate energy-level alignment with the perovskite CH<sub>3</sub>NH<sub>3</sub>PbI<sub>3</sub> (MAPbI<sub>3</sub>) and carbon. By interfacial engineering with the doped TPDI, the energy barrier at MAPbI<sub>3</sub>/carbon interface was efficiently removed, and a PCE of 15.50% was achieved [22].



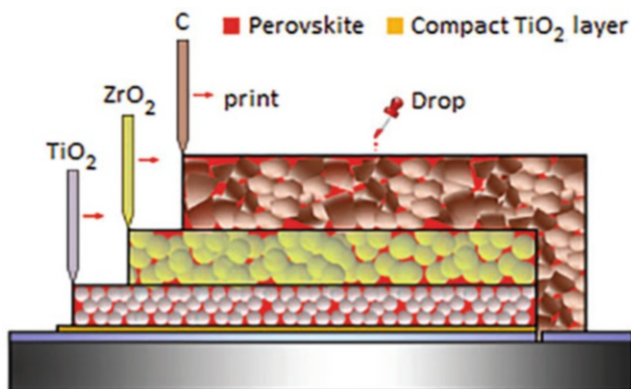


**Fig. 4** Schematic drawing showing the cross section of the triple-layer perovskite-based fully printable mesoscopic solar cell. Perovskite is infiltrated by drop-casting method [18]

In 2016, Zhang F. et al. designed printable C-PSC by applying interfacial engineering; by incorporating undoped copper phthalocyanine (CuPc) nanowires as HTM, they showed high ability to accelerate charge extraction and suppress charge recombination, and thus a PCE of 16.10% was obtained [23].

In 2017, the triple cation perovskite  $\text{Cs}_{0.05}(\text{FA}_{0.4}\text{MA}_{0.6})_{0.95}\text{PbI}_{2.8}\text{Br}_{0.2}$  was manufactured and introduced into a fully printable C-PSC of mesoporous  $\text{TiO}_2/\text{Al}_2\text{O}_3/\text{NiO}$  metal oxide-layered structure with carbon counter electrode. They proved that partial replacement of FA/MA by Cs could increase the bandgap and exciton binding energy of the perovskite  $\text{Cs}_x(\text{FA}_{0.4}\text{MA}_{0.6})_{1-x}\text{PbI}_{2.8}\text{Br}_{0.2}$ , obtaining an optimum efficiency of 17.02% [24]. It was revealed that the presence of Cs in perovskite composites can increase the lifetime charge carrier along with the diffusion length benefiting from charge transport in thick mesoscopic layers.

That same year (i.e., 2017), the work of Grancini et al. was also highlighted, which presented the PSC with the highest stability reported to date a one-year stable device by engineering the ultra-stable 2D/3D  $(\text{HOOC}(\text{CH}_2)_4\text{NH}_3)_2\text{PbI}_4/\text{CH}_3\text{NH}_3\text{PbI}_3$ . This multidimensional interface yielded 12.90% efficiency in a C-PSC. Furthermore, it fabricated  $10 \times 10 \text{ cm}^2$  solar modules using a fully printable industrial-scale process with a stable yield of 11.20% over 10,000 h without loss of performance, measured under controlled standard conditions [15].

In 2018, a C-PSC was performed by Liu et al.; Ni-doped rutile  $\text{TiO}_2$  as ETM, organometallic trihalide perovskite  $\text{CsMAFAPb}(\text{IBr})_3$  as light absorber, and CuPc as HTM were used. They found that Ni doping can shift the Fermi level of the ETM upward and enhance the charge mobility of the  $\text{TiO}_2$  film, thus improving the charge transport and extraction, achieving a 17.46% of PCE [25].

In the same year, 2018, Zhang H. et al. developed, as a counter electrode, a self-adhesive macroporous carbon film by a solvent exchange method at room temperature. Through the simple press transfer technique, the carbon film was able to form an excellent interface contact with the underlying gap transport layer, very beneficial

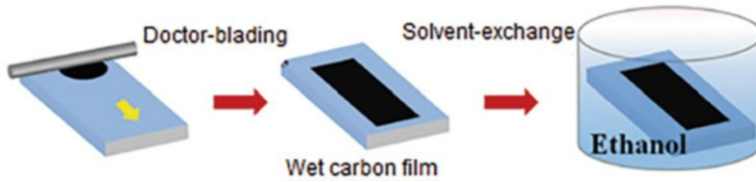


**Fig. 5** Schematic diagram of the room-temperature solvent-exchange preparation process of carbon film [21]

for interface charge transfer. Thus, a PCE of 19.20% was obtained [21]. A schematic of the carbon film preparation is shown in Fig. 5.

In 2019, an innovative modular C-PSC design was presented, and its strength and sheet thickness were greatly reduced by coating it with another pressure-applied carbon-coated FTO glass. In addition, a comparison was made between various commercial carbon sources (black smoke, graphite sheets, and graphene). Graphene showed the best overall performance, demonstrating the crucial importance of graphene as a charge collector; a PCE of 18.65% was achieved for graphene-based PSC (G-PSC). G-PSC showed significant structural flexibility and a prospect for easy repair and maintenance of PSC through modular interconnects [26].

In 2020, the systematic investigation of interfacial bridging carbon materials was performed to improve the interfacial contact. The result showed that the morphology of interfacial bridging carbon materials played a more important role than their energy band and conductivity, and carbon nanotubes (CN) showed a better interfacial bridging effect and energy level alignment than other carbon materials, achieving a PCE of 15.09% and a stability in HTM-free C-PSC due to optimal interfacial bridging carbon material [27].

This year, Liu et al. (2021) applied a technology used in Au-PSC, by manufacturing high-quality perovskite films under 70% relative humidity, with the preheating method at 120°C. The perovskite exhibited high-quality crystallinity, low charge transfer resistance at interfaces, high charge recombination rate, and efficiency of 16.13% [28]. In addition, it provides a fabrication method of C-PSC under high humidity atmosphere.

In the same way, Chen et al. implemented a post-treatment to C-PSC which used FAPbI<sub>3</sub> perovskite, which consisted on increasing the open circuit voltage ( $V_{OC}$ ) from 0.963 to 1.023 V after post-treatment, giving it a PCE of 17.47%, the highest value reported for printable HTM-free C-PSC. This strategy provides a simple method to tune the energy level alignment for mesoscopic perovskite based on optoelectronics [19]. Table 1 shows the ETM, HTM, and perovskite layer used in the C-PSC with outstanding results by year, in addition to their characteristic values.

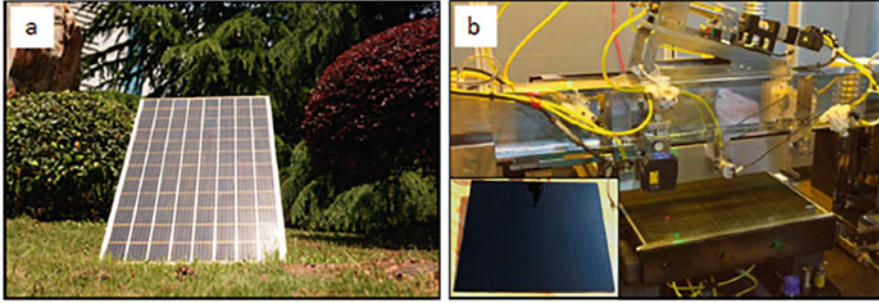


**Fig. 6** (a) Photograph of a meso C-PSC module from Han’s group and (b) photograph of the slot-die coating process of the hybrid perovskite thin film on a rigid substrate. The inset is a photograph of an HTM-free encapsulated planar C-PSC module (45 cm × 65 cm) based on the slot-die coating technology [16]

## 2.2 C-PSC Commercialization Outlook

For commercialization, efficient C-PSC modules need to be produced on a large scale. Some progress has been made by Prof. Han’s group, who has fabricated large-scale meso C-PSC modules using the drop-to-drop process to deposit perovskite. Also, Mhaisalkar’s group, in cooperation with Dyesol, manufactured a 70 cm<sup>2</sup> surface area monolithic meso C-PSC module by screen printing, deposition of mesoporous layers, and the perovskite by drop to drop, which achieved a PCE of 10.74%. In addition, Weihua-Solar Company used slot-die coating technology to produce large-scale perovskite for produce large-scale perovskite for C-PSC panels [16], as shown in Fig. 6.

## 3 Discussion

This chapter briefly describes C-PSC works that have achieved PCE yearly records and mentions some research works with results are close to that value. Unlike other reviews, this chapter covers different manufacturing methods and materials used by research groups dedicated to these devices, and it is not restricted to not using HTM in their configuration as Chen and Yang [42]. Besides, the literature review conducted shows that nowadays C-PSC has proven to be the most stable among all PSC [14, 15], although they still have to match or improve the efficiencies of Au-PSC, which currently hold the record in efficiency [10]. It is worth mentioning that C-PSC has benefited considerably from mechanisms dedicated to traditional PSC. Among them, advances in materials engineering [25], device configuration [26], and learning interfacial engineering applied to Au-PSC [15, 22, 23]. As a result, the efficiencies of HTM-free C-PSC have achieved 17% [24]. And C-PSCs using spiro-OMeTAD as HTM have reached 19% [21]. It is anticipated that these

efficiencies can be greatly improved and start a successful commercialization, which would make them the solar photovoltaic technology par excellence. Another great advantage is the electrode fabrication technologies for C-PSC lower cost, which is different from that of metal electrodes.

Electrodes of various carbon materials generally have been deposited on top of the prepared substrate by screen printing [18], doctor-blading [21], inkjet printing, press transferring [21], rolling transfer, and hot pressing by slot-die coating [16], while vacuum evaporation is usually employed for metallic electrodes. Although scale-up fabrication has been proven for perovskite layer deposition and C-PSC in general, the dare is to form consistently a uniform and high-purity perovskite layer at large scale, due to the difficulty in controlling the crystallization behavior, which affects the efficiency of the modules [42].

## 4 Conclusions

The most outstanding advances of C-PSC since their inception have been summarized and are presented in Table 1, highlighting the reported PCE values; these devices have achieved efficiencies comparable with metal electrode PSC. The highest PCE achieved by C-PSC is 19%; however, the goal is to improve their efficiency to maintain or improve their competitiveness. It is claimed that the main advantage of C-PSC, compared to metal electrode-based PSC, is their significantly higher stability; as proof of this, they currently hold the record for stability greater than one year under standard conditions. Intensive research is still in progress; therefore, it is expected that they will soon reach and surpass the current values of Au-PSC. On the other hand, since mesoporous layers of C-PSC can be deposited by scalable screen-printing techniques, large-scale meso C-PSC with high yields has been manufactured and reported. In addition, they have also benefited from flexible manufacturing technologies, such as slot-die coating, inkjet printing, among others, for large-scale fabrication. However, there is a need to develop and optimize these large-scale manufacturing technologies for perovskite layer deposition in order to produce efficient C-PSC modules and therefore promote their commercialization.

## References

1. IRENA: Rethinking energy: Towards a new power system. International Renewable Energy Agency (IRENA) (2014).
2. O'Neill, B. C., Oppenheimer, M., Warren, R., Hallegatte, S., Kopp, R. E., Pörtner, H. O., Scholes, R., Birkmann, J., Foden, W., Licker, R., Mach, K. J., Marbaix, P., Mastrandrea, M. D., Price, J., Takahashi, K., van Ypersele, J.-P., & Yohe, G. (2017). IPCC reasons for concern regarding climate change risks. *Nature Climate Change*, 7, 28–37.
3. Green, M., Ho-Baillie, A., & Snaith, H. (2014). The emergence of perovskite solar cells. *Nature Photonics*, 8, 506–514.

4. Hao, F., Stoumpos, C., Cao, D., Chang, R., & Kanatzidis, M. (2014). Lead-free solid-state organic-inorganic halide perovskite solar cells. *Nature Photonics*, *8*, 489–494.
5. Dong, Q., Fang, Y., Shao, Y., Mulligan, P., Qiu, J., Cao, L., & Huang, J. (2015). Electron-hole diffusion lengths > 175  $\mu\text{m}$  in solution-grown  $\text{CH}_3\text{NH}_3\text{PbI}_3$  single crystals. *Science*, *347*, 967–970.
6. Snaith, H. J. (2013). Perovskites: The emergence of a new era for low-cost, high-efficiency solar cells. *Journal of Physical Chemistry Letters*, *4*, 3623–3630.
7. Stranks, S. D., Eperon, G. E., Grancini, G., Menelaou, C., Alcocer, M. J. P., Leijtens, T., Herz, L. M., Petrozza, A., & Snaith, H. J. (2013). Electron-hole diffusion lengths exceeding 1  $\mu\text{m}$  in an organometal trihalide perovskite absorber. *Science*, *342*, 341–344.
8. Marchioro, A., Teuscher, J., Friedrich, D., Kunst, M., van de Krol, R., Moehl, T., Grätzel, M., & Moser, J.-E. (2014). Unravelling the mechanism of photoinduced charge transfer processes in lead iodide perovskite solar cells. *Nature Photonics*, *8*, 250–255.
9. Kojima, A., Teshima, K., Shirai, Y., & Miyasaka, T. (2009). Organometal halide perovskites as visible-light sensitizers for photovoltaic cells. *Journal of the American Chemical Society*, *131*, 6050–6051.
10. NREL: Best research-cell efficiency chart. <https://www.nrel.gov/pv/cell-efficiency.html>. Last accessed 2021/06/08.
11. Ku, Z., Rong, Y., Xu, M., Liu, T., & Han, H. (2013). Full printable processed mesoscopic  $\text{CH}_3\text{NH}_3\text{PbI}_3/\text{TiO}_2$  heterojunction solar cells with carbon counter electrode. *Scientific Reports*, *3*, 3132.
12. Chen, H., Wei, Z., He, H., Zheng, X., Wong, K. S., & Yang, S. (2016). Solvent engineering boosts the efficiency of paintable carbon-based perovskite solar cells to beyond 14%. *Advanced Energy Materials*, *6*, 1502087.
13. Hu, M., Liu, L., Mei, A., Yang, Y., Liu, T., & Han, H. (2014). Efficient hole-conductor-free, fully printable mesoscopic perovskite solar cells with a broad light harvester  $\text{NH}_2\text{CHNH}_2\text{PbI}_3$ . *Journal of Materials Chemistry A*, *2*, 17115–17121.
14. Raminafshar, C., Dracopoulos, V., Mohammadi, M. R., & Lianos, P. (2018). Carbon based perovskite solar cells constructed by screen-printed components. *Electrochimica Acta*, *276*, 261–267.
15. Grancini, G., Roldán-Carmona, C., Zimmermann, I., Mosconi, E., Lee, X., Martineau, D., Nabey, S., Oswald, F., De Angelis, F., Graetzel, M., & Nazeeruddin, M. K. (2017). One-year stable perovskite solar cells by 2D/3D interface engineering. *Nature Communications*, *8*, 15684.
16. Zhou, Y., & Zhu, K. (2016). Perovskite solar cells shine in the “Valley of the Sun.”. *ACS Energy Letters*, *1*, 64–67.
17. Kay, A., & Grätzel, M. (1996). Low cost photovoltaic modules based on dye sensitized nanocrystalline titanium dioxide and carbon powder. *Solar Energy Materials and Solar Cell*, *44*, 99–117.
18. Mei, A., Li, X., Liu, L., Ku, Z., Liu, T., Rong, Y., Xu, M., Hu, M., Chen, J., Yang, Y., Gratzel, M., & Han, H. (2014). A hole-conductor-free, fully printable mesoscopic perovskite solar cell with high stability. *Science*, *345*, 295–298.
19. Chen, X., Xia, Y., Huang, Q., Li, Z., Mei, A., Hu, Y., Wang, T., Cheacharoen, R., Rong, Y., & Han, H. (2021). Tailoring the dimensionality of hybrid perovskites in mesoporous carbon electrodes for type-II band alignment and enhanced performance of printable hole-conductor-free perovskite solar cells. *Advanced Energy Materials*, *11*, 2100292.
20. Martinez, V. (2019). Preparation of highly efficient carbon-based perovskite solar cells (C-based PSCs) by screen-printing. In *Organic, hybrid, and perovskite photovoltaics XX* (p. 110942L). International Society for Optics and Photonics.
21. Zhang, H., Xiao, J., Shi, J., Su, H., Luo, Y., Li, D., Wu, H., Cheng, Y., & Meng, Q. (2018). Self-adhesive macroporous carbon electrodes for efficient and stable perovskite solar cells. *Advanced Functional Materials*, *28*, 1802985.

22. Zhang, F., Yang, X., Cheng, M., Li, J., Wang, W., Wang, H., & Sun, L. (2015). Engineering of hole-selective contact for low temperature-processed carbon counter electrode-based perovskite solar cells. *Journal of Materials Chemistry A*, 3, 24272–24280.
23. Zhang, F., Yang, X., Cheng, M., Wang, W., & Sun, L. (2016). Boosting the efficiency and the stability of low cost perovskite solar cells by using CuPc nanorods as hole transport material and carbon as counter electrode. *Nano Energy*, 20, 108–116.
24. Liu, S., Huang, W., Liao, P., Pootrakulchote, N., Li, H., Lu, J., Li, J., Huang, F., Shai, X., & Zhao, X. (2017). 17% efficient printable mesoscopic PIN metal oxide framework perovskite solar cells using cesium-containing triple cation perovskite. *Journal of Materials Chemistry A*, 5, 22952–22958.
25. Liu, X., Liu, Z., Sun, B., Tan, X., Ye, H., Tu, Y., Shi, T., Tang, Z., & Liao, G. (2018). 17.46% efficient and highly stable carbon-based planar perovskite solar cells employing Ni-doped rutile TiO<sub>2</sub> as electron transport layer. *Nano Energy*, 50, 201–211.
26. Zhang, C., Wang, S., Zhang, H., Feng, Y., Tian, W., Yan, Y., Bian, J., Wang, Y., Jin, S., & Zakeeruddin, S. M. (2019). Efficient stable graphene-based perovskite solar cells with high flexibility in device assembling via modular architecture design. *Energy & Environmental Science*, 12, 3585–3594.
27. Gao, L., Hu, J., Meng, F., Zhou, Y., Li, Y., Wei, G., & Ma, T. (2020). Comparison of interfacial bridging carbon materials for effective carbon-based perovskite solar cells. *Journal of Colloid and Interface Science*, 579, 425–430.
28. Liu, B.-T., Yang, J.-H., & Huang, Y.-S. (2021). Highly efficient perovskite solar cells fabricated under a 70% relative humidity atmosphere. *Journal of Power Sources*, 500, 229985.
29. Sheng, Y., Hu, Y., Mei, A., Jiang, P., Hou, X., Duan, M., Hong, L., Guan, Y., Rong, Y., & Xiong, Y. (2016). Enhanced electronic properties in CH<sub>3</sub>NH<sub>3</sub>PbI<sub>3</sub> via LiCl mixing for hole-conductor-free printable perovskite solar cells. *Journal of Materials Chemistry A*, 4, 16731–16736.
30. Tsai, C.-M., Wu, G.-W., Narra, S., Chang, H.-M., Mohanta, N., Wu, H.-P., Wang, C.-L., & Diau, E. W.-G. (2017). Control of preferred orientation with slow crystallization for carbon-based mesoscopic perovskite solar cells attaining efficiency 15%. *Journal of Materials Chemistry A*, 5, 739–747.
31. Aitola, K., Domanski, K., Correa-Baena, J., Sveinbjörnsson, K., Saliba, M., Abate, A., Grätzel, M., Kauppinen, E., Johansson, E. M., & Tress, W. (2017). High temperature-stable perovskite solar cell based on low-cost carbon nanotube hole contact. *Advanced Materials*, 29, 1606398.
32. Yang, Y., Chen, H., Zheng, X., Meng, X., Zhang, T., Hu, C., Bai, Y., Xiao, S., & Yang, S. (2017). Ultrasound-spray deposition of multi-walled carbon nanotubes on NiO nanoparticles-embedded perovskite layers for high-performance carbon-based perovskite solar cells. *Nano Energy*, 42, 322–333.
33. Hu, Y., Zhang, Z., Mei, A., Jiang, Y., Hou, X., Wang, Q., Du, K., Rong, Y., Zhou, Y., & Xu, G. (2018). Improved performance of printable perovskite solar cells with bifunctional conjugated organic molecule. *Advanced Materials*, 30, 1705786.
34. Liu, Z., Sun, B., Liu, X., Han, J., Ye, H., Tu, Y., Chen, C., Shi, T., Tang, Z., & Liao, G. (2018). 15% efficient carbon based planar-heterojunction perovskite solar cells using a TiO<sub>2</sub>/SnO<sub>2</sub> bilayer as the electron transport layer. *Journal of Materials Chemistry A*, 6, 7409–7419.
35. Zhou, J., Hou, J., Tao, X., Meng, X., & Yang, S. (2019). Solution-processed electron transport layer of n-doped fullerene for efficient and stable all carbon based perovskite solar cells. *Journal of Materials Chemistry A*, 7, 7710–7716.
36. Yang, Y., Liu, Z., Ng, W. K., Zhang, L., Zhang, H., Meng, X., Bai, Y., Xiao, S., Zhang, T., & Hu, C. (2019). An ultrathin ferroelectric perovskite oxide layer for high-performance hole transport material free carbon based halide perovskite solar cells. *Advanced Functional Materials*, 29, 1806506.
37. Chu, Q.-Q., Ding, B., Peng, J., Shen, H., Li, X., Liu, Y., Li, C.-X., Li, C.-J., Yang, G.-J., & White, T. P. (2019). Highly stable carbon-based perovskite solar cell with a record efficiency of

- over 18% via hole transport engineering. *Journal of Materials Science & Technology*, 35, 987–993.
38. Peng, C., Su, H., Li, J., Duan, Q., Li, Q., Xiao, J., Ku, Z., Zhong, J., Li, W., & Peng, Y. (2021). Scalable, efficient and flexible perovskite solar cells with carbon film based electrode. *Solar Energy Materials and Solar Cells*, 230, 111226.
  39. Cao, Y., Li, W., Liu, Z., Zhao, Z., Xiao, Z., Zi, W., & Cheng, N. (2020). Ligand modification of  $\text{Cu}_2\text{ZnSnS}_4$  nanoparticles boosts the performance of low temperature paintable carbon electrode based perovskite solar cells to 17.71%. *Journal of Materials Chemistry A*, 8, 12080–12088.
  40. Su, H., Xiao, J., Li, Q., Peng, C., Zhang, X., Mao, C., Yao, Q., Lu, Y., Ku, Z., & Zhong, J. (2020). Carbon film electrode based square-centimeter scale planar perovskite solar cells exceeding 17% efficiency. *Materials Science in Semiconductor Processing*, 107, 104809.
  41. Liu, Z., Yu, Z., Li, W., Zhao, Z., Xiao, Z., Lei, B., Zi, W., Cheng, N., Liu, J., & Tu, Y. (2021). Scalable one-step heating up synthesis of  $\text{Cu}_2\text{ZnSnS}_4$  nanocrystals hole conducting materials for carbon electrode based perovskite solar cells. *Solar Energy*, 224, 51–57.
  42. Chen, H., & Yang, S. (2017). Carbon-based perovskite solar cells without hole transport materials: The front runner to the market? *Advanced Materials*, 29, 1603994.


# **Part II**

## **Biomass Energy**



# Design and Instrumentation of a Batch-Type Bioreactor for the Organic Fraction Fermentation of Urban Solid Waste



Remedios M. Bombela-Chávez, Belén Torres-Ramírez,  
Danay Carrillo-Nieves, and Oscar Aguilar-Juárez 

## 1 Introduction

The growing generation of municipal solid waste (MSW), mainly in large cities, is a cause for concern due to the serious health and environmental problems caused by its inefficient management [1]. However, the recovery (composting, vermiculture, anaerobic digestion, among other methods) of the organic fraction of MSW (OFMSW) can contribute to alleviate these problems, by reducing the amount of waste that is available and obtaining useful by-products from them, such as compost, vermicompost, biogas, and biosolids, which have positive impacts on both the environment and the economy [2]. The biological treatment of the organic fraction (MSW) with energy recovery from fuels derived from residues is finally an alternative to consider [3, 4].

In Mexico, it is difficult to achieve sustainable waste management when daily MSW production reached 1020 grams per capita in 2010. The main urban areas of the country generate waste that is counted in hundreds and thousands of tons per day. These enormous quantities of MSW present a complex problem for collection

---

R. M. Bombela-Chávez  
Universidad Politécnica de Pénjamo, Guanajuato, Mexico

B. Torres-Ramírez  
Universidad Politécnica de Puebla, Puebla, Mexico

D. Carrillo-Nieves  
Escuela de Ingeniería y Ciencias, Tecnológico de Monterrey, Zapopan, Mexico

O. Aguilar-Juárez (✉)  
Centro de Investigación y Asistencia en Tecnología y Diseño del Estado de Jalisco, Guadalajara, Mexico  
e-mail: [oaguilar@ciatej.mx](mailto:oaguilar@ciatej.mx)

coverage, for its use and especially in final disposal. As in many Mexican cities, waste management in the Guadalajara Metropolitan Zone (GMZ) in recent years has caused environmental deterioration that negatively affects water sources and air quality. Urban sprawl has caused the old dumps and landfills to be surrounded by residential areas. Even operating final landfills often have housing in the immediate vicinity. Although by regulation the final disposal sites are located (at the beginning of their operations) in places far from inhabited areas, after a few years the city grows, and the empty spaces are urbanized to give rise to new settlements. In this process, residents living near municipal landfills are affected by the contamination vectors generated by MSW burial sites. In the GMZ, several cases exemplify the problematic relationship between landfills and neighboring residents [5].

In this way, the management of urban solid waste is a problem that can be disaggregated, and the organic fraction can be energetically valued by anaerobic digestion [6], but several questions require an answer. The evaluation of particle size, density, particle surface, and inoculum and the evolution of different critical parameters and their effect on biogas production, etc., require tools that allow the simulation of representative cells of a complex system such as MSW.

The objective of this work is to present the design of a bioreactor, its design parameters, the manufacturing process, and its instrumentation and to determine the potential production of biogas from OFMSW obtained from the GMZ through anaerobic fermentation and to be a useful tool for future experiments.

## 2 Methods

Solid-state anaerobic digestion (SSAD) is the most suitable for OFMSW treatment due to its high solid concentration (> 15%) and better process performance [6]. Tools are needed that, with a minimum of unit operations, can simulate anaerobic digestion under these conditions. Next, it is necessary to determine the design parameters (which are the subject of this work), such as geometry, materials, instrumentation, and appropriate operating protocols.

### 2.1 Geometry

The bioreactor was designed for a capacity of 10 L, volume considered adequate to simulate an acceptable diversity of organic substrates on a real scale, and then the dimensions required to cover the process were calculated. Finally, the bioreactor will then have a diameter of 0.24 meters (m) and a height of 0.30 m.

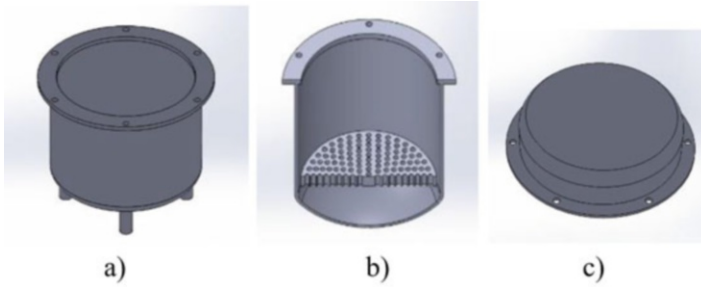


**Fig. 1** Bioreactor tank design: (a) exterior view, (b) tank with the false background placed, and (c) view of the reactor cover

### 2.1.1 Bioreactor Design

The design of the bioreactor was developed using SolidWorks software in such a way that it had a structure like that of a batch bioreactor tank, to which four support pieces approximately 10 centimeters (cm) high were added. In addition, a stopcock was placed at the bottom of the tank, which allows leachate to exit. Two perforations were added to the tank to place the pH and ORP sensors, and these perforations are placed in an inclined way in such that they help to obtain the reading of the leachate produced by the organic matter during the anaerobic fermentation. The tank has a heating jacket that works with hot water, and this allows to maintain the desired temperature for OFMSW fermentation (Fig. 1a).

Inside it, a false bottom was placed that serves as a deposit of the solid substrate, and it was made of acrylic whose thickness was 3 millimeters (mm) and has perforations that help to separate the solid part (organic matter) and the liquid part (leachate). The false bottom in place can be easily removed for proper cleaning of the bioreactor. To place the false bottom in the bioreactor tank, four internal tabs were placed as support (Fig. 1b).

And finally, a bioreactor lid was considered at a height of 6 cm by adding the concave part of this lid, and two perforations were made: one for the temperature sensor and the other that was added for the release of the gas produced by the fermentation. The designed cover closes with the help of screws placed around it to avoid leaks or particles that can affect the substrate (Fig. 1c).

### 2.1.2 Materials

It was decided to build the structure and covers with acrylic of various thicknesses (6 mm, 15 mm, and 21 mm), since acrylic is a noble material; easy to mold, manipulate, and access; quick to build; and low in cost. It has a transparency 5% higher than that of ordinary glass, good resistance to impact, with excellent tolerance to the rigors of the elements and ultraviolet radiation. Acrylic has physical properties that characterize it as:

- Weather resistance: Acrylic can be exposed to rain and sunlight without losing its physical properties.
- Clarity: It stays clear over time, unlike polycarbonate or acetates that turn yellow.
- Light weight: Only half the weight of glass and 43% of the weight of aluminum.
- Impact resistance: It is a much more rigid material than ordinary plastics, and its impact resistance offers you the security that glass does not give you.
- Light transmission: Acrylic is an excellent light transmitter; its light transmission is 92%.
- Insulating property: Acrylic has the particularity of isolating heat and noise. A 1/4-inches (inch)-thick acrylic sheet can isolate noise as much as a concrete wall.

One of the great advantages of acrylic is its recyclability, that is, when it is heated to a certain temperature, the material is depolymerized, and the monomer or raw material is generated again. This recycled material can be polymerized again, resulting in a lower quality product [7].

### 2.1.3 Instrumentation

For the installation of the bioreactor, first a flat place is selected, that is, the bioreactor is not inclined because it could alter the volume of the bioreactor or there could be spills; as a second point, the pH and ORP sensors were placed, as well as the false bottom is placed trying to ensure that it is completely horizontal. As a third step, the temperature sensor is placed on the lid, and then the lid is placed on the bioreactor tank and secured with the screws, trying to be careful when placing them so as not to damage the perforations in the lid and the tank. As the penultimate step, the hose is placed in the tube placed in the cap, and this step must be carried out carefully so as not to break the tube. Finally, all the sensors are connected to the LabQuest Mini to begin with their configuration and to be able to use them.

To use the control system for Vernier devices, software called Logger Lite was downloaded and installed on a computer for better monitoring. The first device to connect was the LabQuest Mini, which is a control system that has three inputs or channels for connecting sensors and has two control outputs for digital control units. In one of the digital control units, a small motor was connected that aims to supply the base or acid to the mixture inside the bioreactor, that is, it helps to maintain the pH during the fermentation of organic matter. Therefore, the pH, ORP, and temperature sensors were placed in the inputs; to activate the systems according to the signal from the sensors through the Logger Lite software, click on the “Experiment” section, then “Configuration Sensor,” and finally “LabQuest Mini 1” to find out how they are integrated. Having digitized sensors allows us to modify the parameters to be observed during the fermentation process of the bioreactor and thus makes recording through a computer more feasible. That is, the results obtained for pH, ORP, and temperature can be better stored in each time so that they can then be plotted and compared according to the needs or required modalities (Fig. 2).

**Fig. 2** Finished and instrumented bioreactor



### 3 Results

#### 3.1 Sample Characteristics

It is estimated that the State of Jalisco produces 7515 tons of urban solid waste per day, which means about 2743 million tons per year, that is, a per capita generation of 0.906 kilograms (kg)/inhabitant/day. 67.95% is produced in the central region where the GMZ is located and 32.05% in the rest of the eleven regions of the State [8].

Fig. 3 shows the OFMSW used for the development of the research. The final sample was obtained by mixing different domestic samples from the GMZ.

For the calculation of biogas production, the collection of about 4.4 kg of organic matter, which was stored for a period of 15 days at 4 °C before utilization, was taken as an example. In this work, physical and scale aspects such as mass in the reactor, waste diversity, standard particle size, among others were prioritized. The degree of urbanization [9], as well as the season of the year, significantly affect the composition of the OFMSW [10]. Therefore, despite being a fundamental parameter, in this case, it constitutes a representative sample of the organic fraction of the urban area in the GMZ during the spring of 2021, where the objective is to evaluate the performance of the bioreactor. Table 1 shows the composition of the organic matter used in the bioreactor.



**Fig. 3** Organic matter used for the filling of the bioreactor

**Table 1** Amount and percentage of organic matter used in the bioreactor

Constituent	Mass	Unit	Percentage
Salad	268.2	g	6%
Tomato	329.7	g	7%
Banana peel	592.9	g	13%
Papaya peel	639.7	g	14%
Chili	180.6	g	4%
Spinach	311.0	g	7%
Green tomatoes	244.7	g	6%
Cilantro	42.5	g	1%
Chayote squash	465.9	g	10%
Mango peel	705.9	g	16%
Cucumber	217.1	g	5%
Potato and carrot peel	196.7	g	4%
Inoculum	250.0	g	6%
TOTAL	4444.9	g	100%

**Fig. 4** Inoculum used in the fermentation of organic matter



The inoculum used for the fermentations was an anaerobic granular sludge from an anaerobic digester intended for the treatment of tequila vinasses obtained from a tequila house in Tequila, Jalisco, which received a pretreated drying with heat at 105 °C for 24 h and grinding to reduce its particle size to sizes less than 600  $\mu\text{m}$  (Fig. 4).

### ***3.2 Bioreactor Preparation and Monitoring***

The samples were weighed giving a total of 4195 kg and added to the reactor including 250 grams (g) of inoculum of anaerobic digester sludge from a tequila company; next, 2700 milliliters (mL) of water were used to cover the bottom of the bioreactor. The active volume of the reactor is 5850 mL, and the empty spaces were saturated with 1300 mL of water (i.e., the residue has a density of 976 g/L) (Fig. 5a). If the air volume of the lid is 2500 mL and 1300 mL of air in the pores of the active volume of the reactor, the gas phase inside the reactor is 3800 mL of a total of 11,050 mL, that is, 34% of the reactor is gas phase, 24.4% is liquid (leachate), and 41.2% the residues deposited in the humidity of origin (Fig. 5b).

Once brought to field capacity, the bioreactor was installed and monitored by the Logger Lite installed on a computer for better analysis and monitoring of the parameters involved in the OFMSW fermentation process.

### ***3.3 Biogas Production***

The main goal of the system is to evaluate the biogas production in a static system, where the control parameters are effectively stable and to be able to perform other evaluations such as the effect of the composition of the leachate and its recirculation.

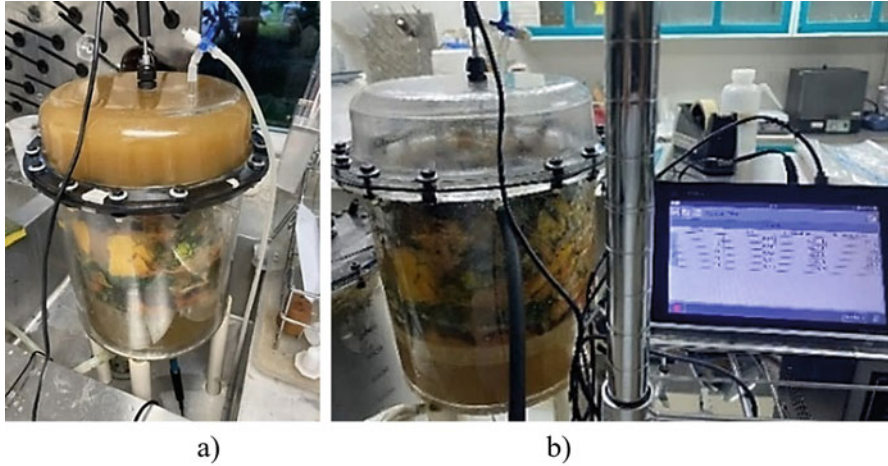


**Fig. 5** (a) Bioreactor brought to its field capacity and (b) bioreactor in operation

At this stage of the work, some of the parameters that could affect the metabolic activity of the microorganisms were evaluated.

The metabolic activity involved in the methane gas production process is affected by various factors [11]. Because each group of bacteria involved in the different stages of the process responds differentially to the influence of these factors, it is not possible to give qualitative values on the degree to which each of them affects the production of biogas precisely. Among the most important factors influencing production are the following [12]:

- Absence of oxygen
- Dry mass
- Volumetric organic load
- Volumetric hydraulic load
- Degree of biomass mixing
- Hydraulic retention time
- Addition of inoculants
- Substrate type
- Volatile mass
- Nutrients
- Carbon/nitrogen ratio
- Process temperature
- Acidity level (pH)
- Witness of process inhibitor compounds

According to the following graphs, we can observe the production of biogas in the fermentation experiment with respect to the amount of organic matter (OFMSW) and the relationship with the inoculum. In Figs. 6, 7, and 8), a comparison of biogas production with respect to pH, ORP, and temperature can be observed.



**Fig. 6** Volume of biogas with respect to pH

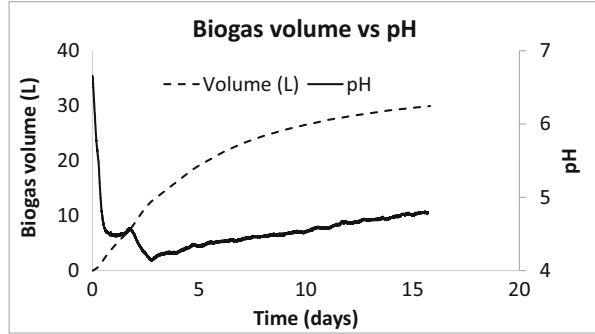


**Fig. 7** Volume of biogas with respect to ORP

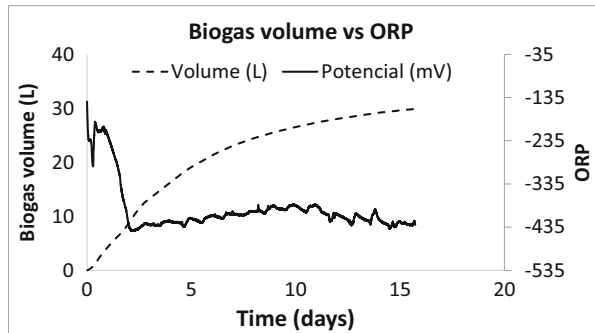
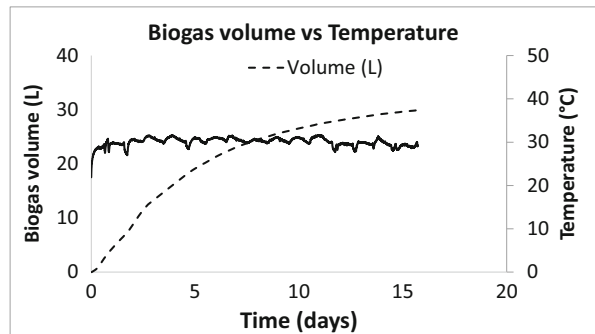


**Fig. 8** Volume of biogas with respect to temperature



According to the graphs obtained, it is observed that each biogas production factor studied presents a different behavior, that is, in Fig. 6, the behavior of biogas production concerning pH is affected when the pH begins to decrease (less than 4.5), since in each phase of the process, the microorganisms present a maximum activity in a differentiated pH range: hydrolytic, between 7.2 and 7.4; acetogenic, between 7 and 7.2; and methanogenic, between 6.5 and 7.5. The maintenance of pH is of vital importance [13]. In the case of biogas production with respect to the redox potential, in Fig. 7, we can observe that as the redox potential decreases, methane production increases; according to [13], this is because it must be low enough to ensure the

development of strict methanogenic populations. Methanogenic bacteria require oxidation-reduction potentials below  $-300$  mV. Therefore, in Fig. 8, it can be analyzed that, if a constant temperature is maintained, biogas production remains high, that is, with increasing temperature range, the rate of hydrolysis increases and the growth rate of bacteria increases and with it the rate of biogas production. The viscosity also decreases, which may allow lower energy consumption for pumping and agitation (in case of recirculation) [13].

Despite the factors involved in biogas production, a total production of 29.93 liters of biogas was obtained over a period of 15.81 days using microflow equipment that measures biogas volume and reports it under standard pressure and temperature conditions. It is possible to monitor significant parameters without acting on them and to perform uninterrupted monitoring for a reasonable period.

### 3.4 Gompertz Model Application

The adjustment of the data obtained to an adapted mathematical model allows to describe the cumulative progress of biogas during a fermentation in batch tests, for which the following equation was used:

$$B(t) = B_{\max} \times \exp \left\{ - \exp \left[ \frac{R_{\max} \times e}{B_{\max}} \times (\gamma - t) + 1 \right] \right\} \quad (1)$$

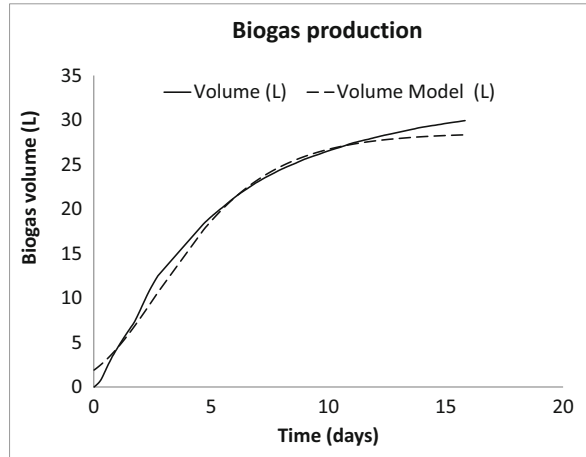
which corresponds to the modified Gompertz model, where  $B(t)$  is the cumulative biogas production with respect to time (mL);  $B_{\max}$  is the maximum production of biogas obtained during fermentation (mL),  $R_{\max}$  is the maximum flow rate (mL/h),  $\gamma$  is the lag phase that indicates the time it takes to start the production of biogas and Euler number ( $e$ ) with value 2.7182, and  $t$  is the time of fermentation [14].

The determination of the  $R_{\max}$  and  $\gamma$  parameters was carried out with the least square's method minimizing the error using the Excel "Solver" application. This command is based on the use of linear and nonlinear methods and algorithms to find a value (maximum, minimum, or specific) of a formula, and that value may be subject to constraints or limits. Table 2 shows the values of the model that best fits reality.

**Table 2** Parameters used in the Gompertz model

Parameter	Value
$B_{\max}$	28.56
$R_{\max}$	3.892
Lag	0
$R^2$	0.994

**Fig. 9** Volume of biogas obtained versus pH using the Gompertz model



In Fig. 9, it can be seen that initial growth accelerates followed by stabilization. When comparing both data it can be observed that both asymptotes approximate symmetrically, that is, the data obtained during the monitoring of the bioreactor are like those obtained using the Gompertz model.

The slowdown in methane production represents the depletion of nutrients during the fermentation process of MSW and the death of bacteria involved in anaerobic digestion. Initially, the rate of methane production stops increasing over time and then proceeds at a constant rate, producing exponential decay.

It is concluded that, for the analysis of methane production from municipal solid waste, the application of the Gompertz model is effective in estimating limits and maximum methane production. The maximum speed of biogas production was 253.6 mL/h and occurred at the beginning of the experiment at 0.52 days, that is, 13 h after starting the run and just when 2 L of biogas had accumulated.

## 4 Discussion

It has been demonstrated that it is possible to design, instrument, and operate an efficient, low-cost, and versatile bioreactor. The size of the reactor is considered adequate to evaluate the controlled physical parameters and phenomena (particle size, density, volatile solids content, humidity, temperature, etc.) and to be able to evaluate the behavior of the key response parameters (temperature evolution, redox potential, pH, leachate production, leachate composition, biogas volume and composition, etc.).

The prototype built has demonstrated that the use of low-cost materials can allow stable monitoring of key parameters, which will permit in the future to perform parallel studies with reactors under different conditions and to validate experimental designs that accept, for example, simulate a vertical profile of a landfill with

temperature conditions, moisture density, and other critical parameters that are likely to be present in landfills today and will be present in a solid-state anaerobic digestion (SSAD) for OFMSW or simulate conditions to establish a combination of substrates, densities, particle sizes, and other factors to maximize biogas production.

However, some improvements can be implemented, such as placing the temperature probe fully submerged in the solids, although the material used has withstood the operation in a reasonable time, its long-term behavior needs to be evaluated, and alternative materials such as glass will probably need to be sought. Also, the arrangement of the pH and redox potential sensors is operational, it is very vulnerable in case of need for maintenance or cleaning.

The reactor design aims to provide a tool to promote and evaluate the bioenergetic use of OFMSW as a treatment alternative [2, 4, 6, 11]; to minimize health risks [1], with fewer unit operations [3]; and to facilitate management according to urbanization [9] and time of year [10] for specific areas such as the GMZ.

## 5 Conclusions

The objectives have been achieved, and it has been possible to design and implement a batch bioreactor with the corresponding adaptations for the fermentation of the organic fraction of municipal solid waste in solid state. Accessories and equipment have been incorporated to the bioreactor that allow the control of the process variables and their recording through an interface channel, for example, pH, ORP, temperature, and biogas release. The bioreactor, already instrumented, has been put into operation with the organic solid waste fraction characterized during the retention time and considerations established to produce biogas from MSW fermentation.

A mathematical model for a time series known as the Gompertz model was fitted. It was shown how to use this model to apply it in the analysis of a fermentation process. The biogas production over a given period was determined. From this study, the biogas production showed that there are different regions of stability and that each of them leads to operating conditions with different specific characteristics. If these particularities are not considered or if the conditions and characteristics of both the OFMSW and the inoculum and the type of bioreactor and the measurement systems are not considered, low performance and productivity operating conditions can be reached.

**Acknowledgments** This research was supported by the State Council of Science and Technology of Jalisco (COECYTJAL) for the economic support it gave me during the process of preparing my thesis in project 8226: “Quality and quantity of biogas and digestate from the OFMSW of the GMZ, evaluation of scenarios” and CIATEJ. The first and second authors thank COECYTJAL for the scholarship awarded for the realization of the undergraduate thesis.

## References

1. Khoiron, K., Probandari, A. N., Setyaningsih, W., Kasjono, H. S., Setyobudi, R. H., & Anne, O. (2020). A review of environmental health impact from municipal solid waste (MSW) landfill. *Annals of Tropical Medicine and Public Health*, 23(3), 60–67.
2. Espinosa, Ma. C., López, M., Pellón, A., Mayarí, R., & Fernández, A. (2007). The organic fraction of municipal solid waste as a potential source of biogas production CENIC magazine. *Ciencias Biológicas, Centro Nacional de Investigaciones Científicas Ciudad de La Habana, Cuba.*, 38(1), 33–37.
3. Herva, M., & Roca, E. (2013). Ranking municipal solid waste treatment alternatives based on ecological footprint and multi-criteria analysis. *Ecological Indicators*, 25, 77–84.
4. Singh, R. P., Tyagi, V. V., Allen, T., Ibrahim, M. H., & Kothari, R. (2011). An overview for exploring the possibilities of energy generation from municipal solid waste (MSW) in Indian scenario. *Renewable and Sustainable Energy Reviews*, 15(9), 4797–4808.
5. Gran Castro, J. A., & Bernache, G. (2015–2016). Urban solid waste management, municipal government capacities and environmental rights. *Society and Environment*, 1(9), 73–101.
6. Zamri, M. F. M. A., Hasmady, S., Akhbar, A., Ideris, F., Shamsuddin, A. H., Mofijur, M., . . . Mahlia, T. M. I. (2021). A comprehensive review on anaerobic digestion of organic fraction of municipal solid waste. *Renewable and Sustainable Energy Reviews*, 137, 110637.
7. Naranjo, M. (2018). *Technical information: what is acrylic*. February 26, 2021, from Docplayer Website:<https://docplayer.es/14169409-Informacion-tecnica-que-es-el-acrilico.html>
8. Nava, C. C. (2017). *Waste diagnosis*. Retrieved September 8, 2018, by Cristina Cortinas.org: <http://cristinacortinas.org/sustainability/waste-diagnostics/>
9. Chen, Y. C. (2018). Effects of urbanization on municipal solid waste composition. *Waste Management*, 79, 828–836.
10. Denafas, G., Ruzgas, T., Martuzevičius, D., Shmarin, S., Hoffmann, M., Mykhaylenko, V., . . . Ludwig, C. (2014). Seasonal variation of municipal solid waste generation and composition in four east European cities. *Resources, Conservation and Recycling*, 89, 22–30.
11. Alibardi, L., & Cossu, R. (2015). Composition variability of the organic fraction of municipal solid waste and effects on hydrogen and methane production potentials. *Waste Management*, 36, 147–155.
12. Ortega Rodriguez Fernando. (2011). *Design and construction of a homemade biodigester*. Autonomous University of Guadalajara.
13. Campos, E., & Flotats, X. (2004). Biological processes: anaerobic digestion and composting.
14. Ladrillero, V. (2018). *Dark fermentation of whey for hydrogen production*. University of Guadalajara.

# Design of Combustion Equipment for Residual Biomass at Laboratory Scale



Emerita Delgado-Plaza , William Avila, Gustavo Serrano, Carlos Rendon, and Anthony Arevalo

## 1 Introduction

Currently, around 100 million tons of rice husk are produced annually worldwide [1]. In addition, one of the main characteristics of rice husk is the low level of biodegradation, which can last up to 5 years, accumulating it in the soil, generating large amounts of methane CH<sub>4</sub>—one of the leading causes of the greenhouse effect. It should also be said that rice husk is one of the greatest biomasses with the availability and possibility to generate energy. According to the Ministry of Agriculture, Livestock, Aquaculture, and Fisheries (MAGAP, acronym in Spanish), Ecuador produces around 1.71 tons per year, ranking fifth in Latin America as a rice producer. This occupies 15.34% of the area for planting and is considered a self-sustaining agricultural product, as it satisfies the national demand for consumption. Its production is focused on the provinces of Guayas and Los Ríos, with 60% and 34%, respectively, corresponding to approximately 94% of the planting that corresponds to the Costa region, according to the National Institute of Statistics and Censuses (INEC, acronym in Spanish).

In Ecuador, the large rice mill plants use husk as fuel for drying rice, being one of the processes that require the highest energy demand because the percentage of water associated with the product and the humidity of the surface must be extracted [2]. This industry sells the waste to cogeneration plants [3]. Analyzing the rice mill plants during the study, it is estimated that 50% of the husk is used as fuel, in exceptional cases 100% of it, but 35% of the husk is used in other production processes [4]. The technology of combustion furnaces coupled to dryers handles

---

E. Delgado-Plaza (✉) · W. Avila · G. Serrano · C. Rendon · A. Arevalo  
Escuela Superior Politécnica del Litoral, CDTS, FIMCP, Guayaquil, Ecuador  
e-mail: [eadelgad@espol.edu.ec](mailto:eadelgad@espol.edu.ec); [wavila@espol.edu.ec](mailto:wavila@espol.edu.ec); [guarserr@espol.edu.ec](mailto:guarserr@espol.edu.ec);  
[crendon@espol.edu.ec](mailto:crendon@espol.edu.ec); [afareval@espol.edu.ec](mailto:afareval@espol.edu.ec)

many failures in the combustion process, generating CO<sub>2</sub> emissions, unprocessed products (100% ash is not produced), silica in furnaces, and particulate matter. The amount of ash generated from combustion corresponds to 14–25% depending on the region's variety, climate, and soil [5]. It is composed of silica, potassium, carbon, calcium, phosphorus, and other elements [6]. Being considered harmful to the employee's health, it is essential to maintain controlled combustion of the system.

Concerning the medium-scale industry, few rice milling plants have changed their technology. Currently, industrial LPG is the primary source of fuel, not being competitive for the national market due to the cost of fuel for a drying time from 12 to 16 h. Other problems in the sector are thermal losses, flame temperature, flow, and temperature air of hot ranging between 35 °C and 80 °C, generating a problem in terms of the final quality of the product because of the range temperature that the dryer must reach is between 40 °C and 50 °C.

From the mentioned problems, to carry out the study of the combustion process of this biomass source, the design and construction of a controlled furnace at laboratory-scale are proposed, taking advantage of the energy value of biomass. Among the analysis, properties are flame temperature, flow and operating temperature, emission control, and ash control.

## 2 Methods

Several problems were detected from different studies using drying technology through biomass furnace: nonuniform drying air temperature, diesel fuel consumption for husk ignition, inadequate sizing of the air extractor, heat losses in the chamber, and smoke in the area. Based on the limitations found in the study area and the user's requirements, some essential parameters have been raised for the design of laboratory equipment [7].

- (a) *Type of biomass*: It is necessary to consider the chemical composition, calorific value, biomass combustion temperature, effects on the environment, and amount of ash.
- (b) *Operating conditions*: Requirements for the correct operation of the equipment, the dimensions of the feeder, combustion chamber, external temperature, humidity, radiation, and operating temperature were considered.
- (c) *Energy efficiency*: Relationship between the heat generated by the burner and the calorific value of the fuel so that the oven's percentage amount takes advantage of the chemical energy of the rice husk to convert into proper heat. The physicochemical decomposition of the husk occurs in three stages: desiccation, pyrolysis, and combustion. The final phase of combustion occurs at temperatures above 500 °C.
- (d) *Temperature control*: A temperature control inside the combustion chamber is necessary to control the complete incineration point of the rice husk.

- (e) *Market accessibility*: The components, materials, and equipment will be manufactured and can be purchased in the local market.
- (f) *Maintenance*: The equipment to be designed must be easy to operate and maintain.
- (g) *Accessibility of materials in the market*: The design requires to be built with materials available in the national market.
- (h) *Safety for operators*: The design must ensure safety for workers, preventing the flame from being outdoors.
- (i) *Costs*: Materials and parts for the construction of laboratory equipment are intended to be used as recycled or reusable material to lower the equipment cost.

## 2.1 Alternatives for Design Selection

There are several models of combustion furnaces, but for this process, the fluidized bed and grill-type models were analyzed. The method to make the selection consisted of a decision matrix where a range between 1 and 10 was established to give value to each design parameter, giving a percentage to the essential requirements so that the most viable alternative was obtained. Table 1 shows the decision matrix.

It was determined that the grill-type oven is the most viable option because it had a relatively low power range concerning the fluidized bed. The combustion of the rice husk produces high ash content; therefore, the grill must be tilted for better control of the feeding zone, combustion, and ash deposit [8].

To exchange heat between the hot gas from combustion and the heat transfer fluid that will enter the dryer, it is necessary to design a heat exchanger, which allows an easy cleaning from silica that can be formed by husk combustion. Safety, temperature control, and ease of construction need to be considered. Table 2 discusses the design criteria and models of exchangers.

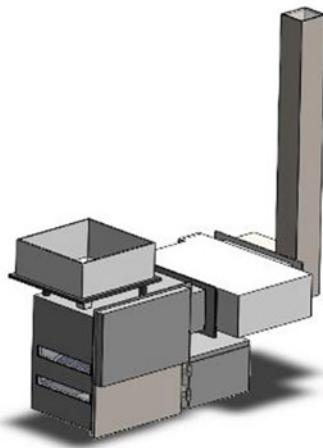
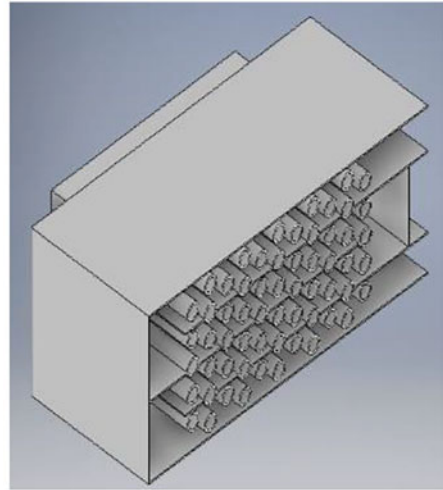
**Table 1** Decision matrix for oven type selection

Parameters	Weight	Furnaces	
		Fluidized bed	Grill type
Safety	10%	8	8
Type of biomass	5%	10	9
Cost	15%	5	10
Maintenance	10%	7	8
Ease of use	5%	8	7
Temperature control	20%	9	8
Ash extraction	15%	6	7
Energy efficiency	15%	7	9
Environmental conservation	5%	7	8
Total	100%	7.25	8.3



**Table 2** Decision matrix for heat exchanger selection

Criteria	Weight	Heat exchanger (one pass)	Heat exchanger (three pass)	Heat exchanger (four pass)
Easy to use	20%	8	6	9
Safety	15%	5	8	7
Production costs	30%	8	5	8
Maintenance	10%	5	6	8
Temperature control	25%	7	8	8
Total	100%	6.75%	6.5%	8.05%

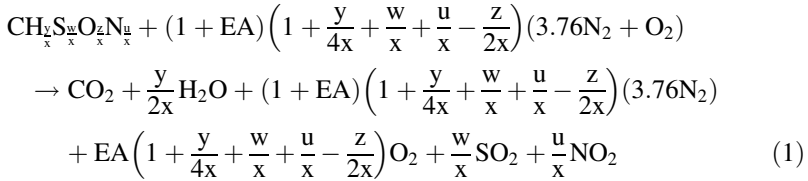
**a)****b)****Fig. 1** (a) Biomass furnace shape design. (b) Heat exchanger

As a result of this analysis, the viability of the four-step heat exchanger with the internal gas flow is determined. It is essential to mention that the biomass oven has the advantage that can use rice husk, pruning log residues, or mixtures with pellets as biomass sources which makes the process cheaper. In addition, as an initial process of ignition of the biomass, it will be intended to use an electrical resistance, considered less polluting than diesel. The heat exchanger will be coupled to one side of the combustion furnace. The flue gases will pass internally in the exchanger tubes to clean the unquenched material, and the airflow from a fan will pass through the outside of the tubes (Fig. 1).

## 2.2 Mathematical Analysis

**Combustion.** Fossil fuels have a high content of carbon (C), hydrogen (H), and oxygen (O), in addition to other elements in smaller proportions such as sulfur (S) and nitrogen (N).

The general formula for fossil fuels was expressed below (Eq. 1) [8] [9].



The relationships  $y/x$ ,  $w/x$ ,  $z/x$   $y$   $u/x$  represent the ratio of hydrogen, sulfur, oxygen, and nitrogen atoms to each carbon atom, respectively. EA is the air in excess.

There is the formula of fuel and air on the left side, with an excess of the latter, and on the right side are the combustion products [8] [7].

$$\frac{y}{x} = \frac{M_c * m_H}{M_H * m_c} \quad (2)$$

The subscript  $y/x$ ,  $w/x$ ,  $z/x$   $y$   $u/x$  is the ratio of the mass M of the elements and m their percentage present in the compound.

To determine the subscripts that correspond to each element, it is necessary to know the chemical composition of the fuel. The composition of the rice husk is shown with the percentages assigned to each element: C = 47,029%, H = 5.02%, N = 0.18%, O = 47.45%, and S = 0.05% [4].

**Theoretical Air-Fuel Ratio** It is expressed as the amount of air ( $m_{\text{aire}}$ ) by fuel quantity ( $m_{\text{combustible}}$ ). Eq. 3:

$$m_{\left(\frac{\text{a}}{\text{f}}\right),t} = \frac{m_{\text{aire}}}{m_{\text{combustible}}} \quad (3)$$

The mass was determined. Eq. 4:

$$m = n * M \quad (4)$$

Number of moles(n), molar mass M.

**Real Air-Fuel Ratio** For the determination of the value of the actual air-fuel ratio, it was necessary to consider the excess air needed and is determined by the following equation:

$$m_{(a)}_r = m_{(a)}_t * (1 + EA) \quad (5)$$

where EA represents the excess air and has a value of 20%.

**Rice Husk Flow for Continuous Combustion** To maintain continuous combustion, it was necessary to calculate the flow of the rice husk; from the simulation, the airflow was obtained, and with the total air-fuel ratio, it could be calculated from the expression:

$$\dot{m}_{CA} = \dot{m}_{aire} * m_{(a)}_{real} \quad (6)$$

**Flue Gas Flow** It was required to establish a mass balance between the mass flow of the air, the flue gases, and the ashes that were produced due to the combustion process, according to Eq. 7:

$$\sum \dot{m}_{entrada} = \sum \dot{m}_{salida} \\ \dot{m}_{CA} + \dot{m}_{aire-blower1} + \dot{m}_{aire-blower2} = \dot{m}_{combustion} + \dot{m}_{cenizas} \quad (7)$$

Therefore, the total heat of combustion is determined from the relation between the amount of mass flow of the rice husk entering the chamber and its corresponding calorific value; it was determined from the following equation:

$$Q_{CA} = \dot{m}_{CA} * P_c \quad (8)$$

where  $P_c$  = calorific power of the husk kJ/kg.

**Thermal Analysis of the Combustion Furnace** The furnace wall is considered a composite material; therefore, the heat stored in the steel and insulation was calculated separately. During the heat transfer process, a fraction is stored on the walls of the furnace and in the insulator, increasing the internal temperature; this amount was calculated from the following equation:

$$Q_{ac} = m_{ac} c_{p_{ac}} (T_{p_{int}} - T_{m_p}) \quad (9)$$

where  $m_{ac}$  is the total mass of steel [Kg],  $c_{p_{ac}}$  is the specific heat of steel  $\left[ \frac{J}{Kg \cdot K} \right]$ ,  $T_{p_{int}}$  is the internal wall temperature [K],  $T_{m_p}$  is the average wall temperature [K], and  $T_{p_{out}}$  is the external wall temperature [K].

During the combustion process, a fraction of the heat is used for the decomposition of the husk into ash; if 14% [10] of the total value of the mass of the rice husk is transformed into ash, the value is determined with the following expression:

$$Q_{cz} = m_{cz}c_{p_{cz}}(T_{cz} - T_{out}) \quad (10)$$

where  $m_{cz}$  is the mass of ash [Kg],  $c_{p_{cz}}$  is the specific heat of ash  $\left[\frac{J}{kg \cdot K}\right]$ ,  $T_{cz}$  is ash temperature [K], and  $T_{out}$  is the environmental temperature [K].

It is necessary to indicate that the furnace design was based on the API 560 standard, where the minimum requirements and recommendations for manufacturing a fuel burner furnace are established.

**Heat Exchanger Design Analysis** Input and output temperatures were defined for the exchanger design. The flow of air and flue gases entering the heat exchanger was determined. Flue gas inlet temperature [K]  $T_{hi}$  (250 °C); flue gas outlet temperature [K]  $T_{ho}$  (120 °C), inlet air temperature [K]  $T_{ci}$ : (27 °C) y the outlet air temperature [K]  $T_{co}$  (50 °C).

Subsequently, the system's energy balance is made to determine the flow of the combustion gases and the flow of hot air necessary to dry; for this, Eqs. 11 and 12 must be equalized:

$$q = \dot{m}_c * C_{pc} * (T_{ci} - T_{co}) \quad (11)$$

$$q = \dot{m}_h * C_{ph} * (T_{hi} - T_{ho}) \quad (12)$$

where  $\dot{m}_h$  is the mass flow of gases [Kg/s],  $\dot{m}_c$  is the air mass flow [Kg/s],  $C_{pc}$  is the specific heat of air [J/Kg. K], and  $C_{ph}$  is the specific heat of gases [J/Kg. K].

The total heat transfer heat between both fluids is determined through Eq. 13:

$$Q = U * \pi * Di * L * NT * \Delta T_{ml} \quad (13)$$

where  $U$  is the global heat transfer coefficient [ $W/m^2 \cdot K$ ],  $Di$  pipe is the inner diameter [m],  $L$  is the pipe length [m],  $Nt$  is the number of pipe, and  $\Delta T_{ml}$  is the difference in average logarithmic temperatures [K].

The overall heat transfer coefficient is determined through the internal convection coefficient  $hi$  and the external  $ho$ ; it depends on the Nusselt number,  $k$  the thermal conductivity [ $W/m^2 \cdot K$ ], and the pipe diameter [m] [10]. It was open to considering that the Nusselt number is a geometry function as well as the Reynolds number ( $Re$ ) and the Prandtl number ( $Pr$ ). Therefore, the equation used to determine the Reynolds number in internal flow is presented in Eq. 14, and the representative equation to determine the external Reynolds number is presented in Eq. 15:

$$\text{Re}_D = \frac{4\dot{m}_h}{\pi * D_i * \mu_{\text{gas}} * N_T} \quad (14)$$

$$\text{Re}_{D_{\text{max}}} = \frac{\rho_{\text{aire}} * V_{\text{max}} * D}{\mu_{\text{aire}}} \quad (15)$$

where  $\rho_{\text{aire}}$ , density of air [ $\text{Kg}/\text{m}^3$ ];  $\mu_{\text{aire}}$ , dynamic air viscosity [ $\text{N}\cdot\text{s}/\text{m}^2$ ]; and  $V_{\text{max}}$ , maximum speed on the tube bank [ $\text{m}/\text{s}$ ].

Finally, the drop pressure of the tube bank is determined where  $N_L$  represents the number of lines,  $x$  the correlation factor, and  $f$  the friction factor (Eq. 16):

$$\Delta p = N_L * x * \left( \frac{\rho * V_{\text{max}}^2}{2} \right) * f \quad (16)$$

## 3 Results

### 3.1 Theoretical Results

The corresponding mass flows at the input and outlet were determined for complete combustion of the rice husk, using the general equation for combustion (Eq. 1). The mass flow of the air was iterated until obtaining a temperature between 50 and 60 °C at the outlet of the exchanger. The blowers must have located at the bottom of the grill with an airflow of 70 CFM (cubic feet per minute), the top of the grill reaches the 30 CFM. With the data obtained, the mass flows of the husk and the combustion gases were calculated. The total heat of combustion of the rice husk was calculated considering a percentage of humidity of 10.33% [11]. The amount of heat that can be extracted for the established husk flow is determined to be 74.39 [kW].

In relation to the results of the analysis of the lost in the combustion chamber, the coefficient of conduction, radiation, and convection of the furnace was considered, assuming the grill as a homogeneous plate, isothermal, and with an inclination of 70° with respect to the Y-axis. In addition, free convection was assumed for the inner and outer surface of the furnace; for the calculation of the radiation coefficient, grilling was considered as a heat source with an emissivity of 0.8. The result was 1.46 [kW]. For the calculation of the heat stored in the steel walls and the insulator, the average temperature between the outside and inside of the furnace was determined, opening a loss of 2.64 [kW] as heat stored in the steel wall and 5.29 [kW] as heat stored in the insulator. For the calculation of heat transferred to ash, 14% of the total mass of rice husk that decomposes into ash was considered, and its result was 0.015 [kW], being a very small value concerning the other results obtained and can be disregarded without affecting the results. Finally, the total heat of combustion that is transferred

**Table 3** Results of the combustion furnace design

Equation	Nomenclature	Symbology	Unit	Result
3	Actual air-fuel ratio	$m_{(f)}r$	dimensionless	13.83
–	Air inlet flow	$\dot{m}_{aire-blower1}$	kg/h	138.13
		$\dot{m}_{aire-blower2}$	kg/h	59.19
		$\dot{m}_{aire-blower3}$	kg/h	138.13
6	Scale flow into the chamber	$\dot{m}_{CA}$	kg/h	15.18
7	Mass flow of combustion gases	$\dot{m}_{combustion}$	kg/h	209.80
8	Heat of combustion	$Q_{CA}$	[kW]	74.39
9	Heat stored in the walls	$Q_{ac}$	[kW]	2.64
–	Heat stored in insulation	$Q_{ais}$	[kW]	5.29
–	Heat given to the ashes	$Q_{cz}$	[kW]	0.015
	Total heat lost from the system	$Q_i$	[kW]	9.41

**Table 4** Theoretical results of heat exchanger analysis

Nomenclature	Unit	Result
Total heat transfer in the heat exchanger	W	2180.70
Global heat transfer coefficient	W/m <sup>2</sup> K	6.15
Internal convection coefficient	W/m <sup>2</sup> K	6.79
Maximum speed on the tube bank	m/s	4.8
Wind speed at dryer inlet (exchanger outlet)	m/s	2.1
Pressure drop in pipe bank	Pa	67.28

to the airflow was obtained considering the system's losses; its result was 64.98 [kW]. In Table 3, from the established equations, the results are shown.

In Table 4, the theoretical results of the heat exchanger obtained when using the proposed methodology are shown. Through simulation, these results were validated.

Therefore, the design of the heat exchanger will be 76 cm in length, 30 cm in height, and 50 cm in width, with four steps and 60 tubes distributed in a staggered way. For the analysis both fluids (hot combustion gas and air from a fan) were analyzed in perpendicular trajectories (crossflow). The materials selected were 1 inch diameter schedule 40 tubes and ASTM A36 steel plates for the housing.

### 3.2 Combustion Furnace Simulation

The materials used for the walls, roof, and base of the furnace structure were 6 mm thick ASTM A36 steel, coated with 100 mm of fiberglass insulation to prevent thermal losses. The material of the gates was ASTM A36 steel 3 mm thick with the difference that in the main gate it had a layer of 100 mm thick fiberglass insulation. The parts that made up the system were designed separately and joined in a single assembly and then used the SolidWorks "Flow Simulation" tool, which works with

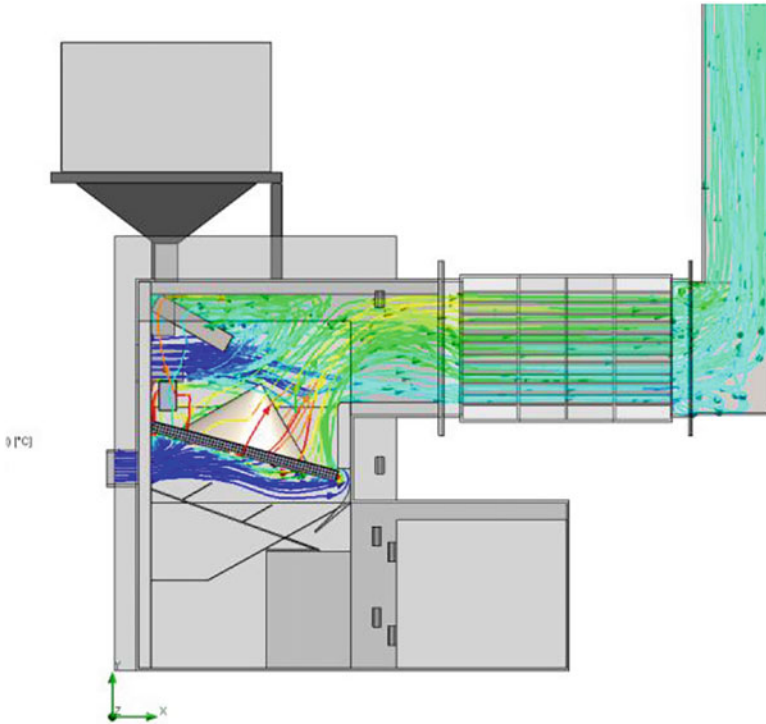


**Fig. 2** Flow lines inside the combustion chamber

computational fluid dynamics or CFD in which, through simulated iterations, allowed to validate the design before the construction of the prototype.

An iterative process of trial and error was followed, modifying the internal geometry of the combustion chamber with the initial conditions to obtain the best possible result. Alternatives were considered a change of flow direction by baffles and different air inlets to the chamber.

In Fig. 2, the results of the simulation of the final geometry are shown. The orientation of the grill was changed, and baffles were included under the hole where the air entered the combustion chamber, which served to redirect the flow, so it did not go to the ash collection chamber.

Below are the temperature profiles of the outer walls of the combustion chamber, which do not exceed  $90\text{ }^{\circ}\text{C}$ . This means that the system is safe for the operator and the constituted material is in the thermal operating range (Fig. 3a). Fig. 3b shows the flow inside the heat exchanger chamber, where it can be seen that the temperature at the outlet is  $60\text{ }^{\circ}\text{C}$ , ideal for drying the rice grain.

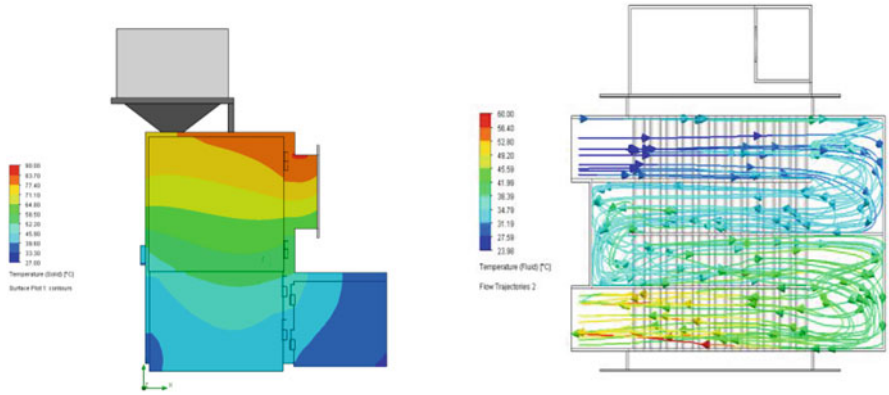


**Fig. 3** (a) External chamber temperature. (b) Flowlines inside the heat exchanger

**Fig. 4** Laboratory equipment prototype



### 3.3 Theoretical Results

Once the experimental equipment was built, the experimental tests were carried out using 180 kg of rice husk, with a duration of 4 hours [12]. Temperature measurements were made at various points in the furnace chamber, heat exchanger, and chimney, to determine the thermal efficiency of the equipment. Fig. 4 shows the laboratory-scale equipment designed for 136 kg of wet products such as rice, corn, coffee, and other cereals.

During the tests the proper functioning of the equipment was evidenced, with few heat losses, smoke through the doors and chimney, from the control of the air flow inlet to the chamber, and the temperature reached 230 °C, with a percentage of ash



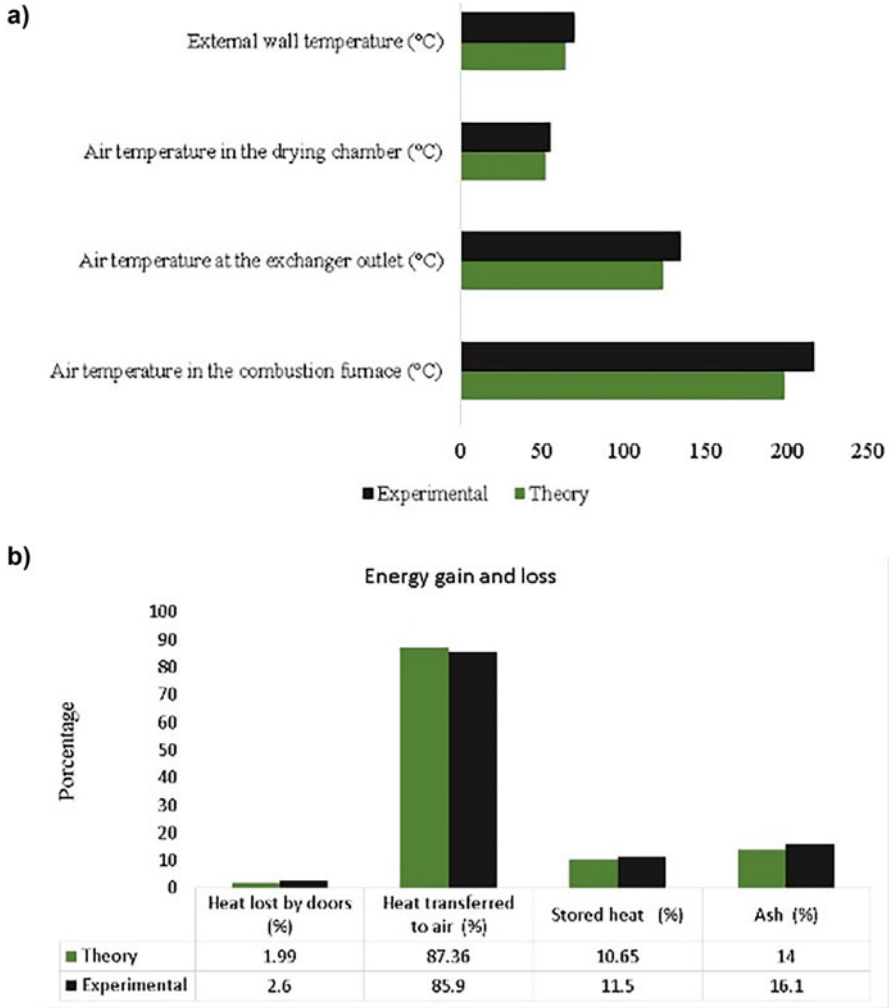


**Fig. 5** (a) Comparison of experimental and simulated tests (temperature). (b) Comparison of experimental and simulated tests (energy gain and loss)

around 16% about the total weight of the shell [3]. It became clear that pellet compaction of the biomass in the furnace in the form of pellets would have improved the combustion of the equipment and reached a higher temperature. For future tests, it is provided to make mixtures of various types of biomasses. Fig. 5a and b presents the comparison of the simulated theoretical results with the experimental results (90.95 kg of husks were used for the experiment).

## 4 Discussion

The areas of Ecuador with the highest rice production are the province of Guayas and Los Ríos, representing an approximate total of 95% of the production at the regional level, representing an excellent availability of rice husk that should be used for internal energy generation of rice processors.

Currently solid biomass such as husk is only used in large rice processing plants. It will be of interest at the local level to adapt existing technologies in small and medium production plants to these combustion chambers that allow taking advantage of the waste for heat generation; with this, the consumption of LPG that is used daily for the drying of rice is reduced. The proposed design to be laboratory equipment will not reflect the real consumption of biomass for large industrials, but a staggering of production, energy consumption, and failures due to the inadequate combustion of the rice husk with the possible environmental and maintenance problems of the equipment is determined.

## 5 Conclusions

The most suitable type of furnace for the combustion of rice husk was the grill type. This is because the equipment operates in a relatively low power range for the use of the fluidized bed and is designed for a husk supply of 90.95 kg. In addition, the project is intended for the drying of rice in sectors where production is from small to medium scale; thus, there is a low operating and investment cost.

The combustion chamber was optimized, relocating the grille to an angle of 70° with respect to the vertical, allowing a greater amount of airflow through the grill and is directed toward the inlet of the heat exchanger; in addition, baffles were in the main air inlet at an angle of 30° with respect to the horizontal, so they redirect the air flow upward and not toward the ash chamber preventing a lifting of particulate matter within the combustion chamber.

The outside temperature of the walls of the combustion chamber reached a range between 50 and 70 °C. This was achieved by increasing the thickness of the insulator to 100 mm, decreasing heat losses in the walls.

The baffles located for the redirection of the inlet airflow will also serve to direct the ash resulting from combustion to the bottom of the chamber, where it will be easier to handle. It is important that there is a correct arrangement of ash; it is considered a highly polluting material.

STM A36 Steel was selected as a material because the maximum temperature in the furnace is 650 °C ensuring that the equipment operates without modifying the mechanical properties. In addition, fiberglass was selected as an insulating material since it has a low thermal conductivity which makes heat conservation and can be transferred to air, and it is essential to mention that these materials are easily found in the national market.

## References

1. C. Martínez, G. Acevedo y G. Espinal, «La cadena del arroz en Colombia: Una mirada global de su estructura y dinámica, 1991–2005.» Ministerio de Agricultura y Desarrollo Rural, , 2005.
2. Delgado, «Tecnología de secado para los productos de arroz, maíz y cacao en las provincias del Guayas y los Ríos,» , 2018.
3. Delgado-Plaza, «Estimation of the energy consumption of the Rice and corn drying process in the equatorial zone» Applied Sciences,2020, vol. 10, n° 21, p. 7497, doi:<https://doi.org/10.3390/app10217497>.
4. Peláez-Samaniego, M., García-Peréz, M., Martí-Herrero, J., & Montero-Izquierdo, A.. (2015). Estado de uso de la biomasa para la producción de bioenergía, biocombustibles y bioproductos en Ecuador, p. 447.
5. Martínez, «Experimentos de combustión con cascarilla de arroz en lecho fluidizado para la producción de ceniza rica en sílice» , 2009.
6. A. F. Arévalo y W. A. Ávila, «Diseño de un horno –intercambiador de biomasa y gas para la generación de calor utilizada en el proceso de secado de arroz,» Escuela Superior Politécnica del Litoral, , 2018.
7. Aguirre, J. (2011). *Diseño e implementación de un horno automático de secado y envejecido de arroz para la procesadora PROYELEC*. Escuela Politécnica del ejército.
8. Jimbo, C., & Arboleda, F. (2016). *Diseño y construcción de un secador de cacao al vacío para medianos y grandes productores de la provincia de Manabí*. Escuela superior politécnica del litoral.
9. Miranda, G. (2011). *Evaluación del proceso de secado de granos de cacao fermentado, en un secador de bandejas con convección forzada de aire*. Universidad de Oriente.
10. Valverde, Sarria y Monteagudo, «Análisis comparativo de las características fisicoquímicas de la cascarilla de arroz» scientia et technica, pp. 255–260, 2007.
11. M. A. Echeverria, O. A. Lopez., Caracterización energética de la cascarilla de arroz para su aplicación en la generación de energía termoeléctrica. , 2010.
12. Arteaga, J. F. (2020). *Caracterización de cascarilla de arroz como biomasa residual para combustible térmico*. Universidad Internacional SEK.

**Part III**  
**Hydrogen Energy**

# Toward the Hydrogen Economy in Paraguay: End-Uses of Green Hydrogen Potential



Fausto Posso, Michel Galeano, César Baranda, David Franco, Ángel Rincón,  
and Juan Zambrano

## 1 Introduction

The hydrogen economy represents an innovative energy infrastructure with hydrogen destined to meet the energy needs of most sectors of society. Thus, hydrogen is obtained from renewable energy sources, stored, transported, and distributed in demand centers for its final conversion into useful energy [1]. Hydrogen generated in this way is known as green hydrogen and it is produced by water electrolysis, with the required electricity from renewable energy sources, and it is perceived as the best technical and economic prospects in the medium term [2]. Currently, the hydrogen economy has aroused exceptional interest to promote global and national economic recovery, energy decarbonization, and sustainable development in a post-SARS-CoV-2 (COVID-19) pandemic scenario [3].

Green hydrogen offers a diversity of potential uses. While direct electrification using renewable energy and energy efficiency is the most efficient path to reducing emissions in easier to abate sectors, green hydrogen can be an important option in the decarbonization of harder to abate sectors where direct renewable electrification is not technically feasible or would take too long time. The objective of this study was

---

F. Posso (✉)

Universidad de Santander, Facultad de Ingenierías y Tecnologías, Instituto de Investigación Xerira, Bucaramanga, Colombia

M. Galeano · C. Baranda · D. Franco

Universidad Nacional de Asunción, San Lorenzo, Paraguay

Á. Rincón

Consultora de Gestión Ambiental (CGA S.A.), Asunción, Paraguay

J. Zambrano

Universidad Nacional Experimental Táchira, San Cristóbal, Venezuela

© The Author(s), under exclusive license to Springer Nature Switzerland AG 2022

M. Espinoza-Andaluz et al. (eds.), *Congress on Research, Development and Innovation in Renewable Energies*, Green Energy and Technology,

[https://doi.org/10.1007/978-3-030-97862-4\\_6](https://doi.org/10.1007/978-3-030-97862-4_6)

to identify end-uses of green hydrogen production potential in Paraguay. To accomplish this objective, two sectors of the Paraguayan economy were analyzed: residential and transportation.

## 2 Methodology

Methodologically, considering the potential for hydrogen production from key renewable resources (solar PV, wind, and hydro) in Paraguay [4], end-uses are focused on two sectors already identified as potential niche opportunities: transportation and residential. In the first sector, it was proposed to replace gasoline and diesel with green hydrogen since the energy equivalence between these fuels. At present, Paraguay counts  $1.6 \times 10^6$  vehicles of which  $7.7 \times 10^5$  are light vehicles [5]. In the residential sector, it is intended to replace firewood and LPG with green hydrogen as a heat source for cooking. Firewood is an inefficient and polluting energy source for cooking, and LPG is totally imported from Bolivia and Argentina. Charcoal consumption was not considered in this study because in Paraguay this sector is quite informal, without reliable data and unwilling commercial consumers and industrial companies to share consumption and price data.

The calculation method is like that used by [6]. For example, it is considered the following hypothetical case:

Gasoline consumption in the transportation sector in department A: 100 t/year.  
 Diesel consumption in the transportation sector in department A: 100 t/year.  
 Firewood consumption in the residential sector in department A: 100 t/year.  
 LPG consumption in the residential sector in department A: 100 t/year.  
 Green hydrogen production potential in department A: 30 t/year.

Then:

Hydrogen consumption equivalent to gasoline consumption: 90 t/year.  
 Hydrogen consumption equivalent to diesel consumption: 87.6 t/year.  
 Hydrogen consumption equivalent to firewood consumption: 12.6 t/year.  
 Hydrogen consumption equivalent to LPG consumption: 42 t/year.

$$Substitution(\%) = \left( \frac{H_2 \text{ production potential}}{H_2 \text{ equivalent consumption}} \right) \times 100 \quad (1)$$

For gasoline:  $(30/90) \times 100 = 33.3\%$ .

For diesel:  $(30/87.6) \times 100 = 34.2\%$ .

For firewood:  $(30/12.6) \times 100 = 238\%$ .

For LPG:  $(30/42) \times 100 = 71\%$ .

### 3 Estimation Method of H<sub>2</sub> Consumption Equivalent to Gasoline and Diesel Consumption in Each Department

This study was conducted to estimate the amount of gasoline and diesel consumption that could potentially be displaced by green hydrogen in each department of Paraguay. In 2020, gasoline and diesel consumption in Paraguay was  $6.9 \times 10^5$  t and  $1.6 \times 10^9$  t, respectively [7]. Gasoline and diesel consumption data for 2018 were obtained from the Ministry of Industry and Commerce (MIC) as seen in Table 1.

As shown in Table 1, the most populated departments of Paraguay are Central, Alto Paraná, and Itapúa, present the highest gasoline and diesel consumptions.

The replacement is based on the energy equivalence between hydrogen, gasoline, and diesel and on gasoline and diesel consumption in each department. Thus, the lower heating value (LHV) the density for gasoline, diesel [8] and hydrogen are [10]:

Gasoline:

LHV: 9.04 kWh/L

Density = 814 kg/m<sup>3</sup>

Diesel:

**Table 1** Gasoline and diesel annual consumption in each department of Paraguay

Department	Gasoline consumption ( $\times 10^3$ m <sup>3</sup> /year)	Diesel consumption ( $\times 10^3$ m <sup>3</sup> /year)
Distrito Capital	49.5	57.6
Concepción	12.3	16.6
San Pedro	176	24.9
Cordillera	13.3	16.2
Guairá	8.8	9.2
Caaguazú	22.8	39.8
Caazapá	4.8	4.8
Itapúa	26.7	44.9
Misiones	7.2	6.0
Paraguarí	8.5	8.1
Alto Paraná	61.9	91.2
Central	143.6	179.9
Ñeembucú	2.9	3.2
Amambay	25.4	20.5
Canindeyú	19.9	35.5
Presidente Hayes	5.6	20.7
Boquerón	4.5	27.5
Alto Paraguay	1.2	6.8
Paraguay	436.4	613.7

Source: [8]

LHV = 10.07 kWh/L

Density = 884 kg/m<sup>3</sup>

Hydrogen:

LHV = 33.3 kWh/kg

Density at STP = 0.09 kg/m<sup>3</sup>

Then, the relation presented in Eq. 2 shows the equivalence between different fuels:

$$1 \text{ kg } H_2 = 3 \text{ kg Gasoline} = 2.92 \text{ kg Diesel} \quad (2)$$

### ***3.1 Estimation Method of H<sub>2</sub> Consumption Equivalent to Firewood and LPG Consumption in Each Department***

In the residential sector, it is proposed to replace firewood and LPG with green hydrogen as a heat source for cooking. At first, firewood and LPG residential consumption in each department was calculated. Then, energy equivalence between firewood, LPG, and electrolytic hydrogen, based on the LHV, was calculated in order to determine the electrolytic hydrogen amount required for each department of Paraguay. Several studies show a wide range in the consumption per capita of firewood in Paraguay. Firewood consumption in Paraguayan homes is  $2.86 \times 10^6$  t [11]. According to [12], this consumption was  $2.6 \times 10^6$  t in 2005. There are various values from different studies, which vary between 0.6 and 8.0 t/inhabitant/year, for different sites in the Eastern Region of Paraguay [13]. Regarding the mentioned data, “not all the information is officially registered in statistical sources, the real figure for firewood consumption should be a lot higher,” and total firewood production is approximately  $7.5 \times 10^6$  t that includes firewood for charcoal production. According to [13], 65% ( $4.875 \times 10^6$  t) is used for self-consumption. Firewood consumption in households is approximately 10–15 t/household/year [14]. This consumption is very high compared to other countries, but it is explained by the inefficient use of firewood: traditional cooking in the oven (Tatacua) and the permanent use of firewood in rural households. Consumption of firewood in rural households varies between 10 and 15 t/household/year [15]. Firewood consumption in households in Paraguay is approximately 1.8–2.7 t/inhabitant/year considering four members per household [9].

To calculate firewood consumption in Paraguayan households, it was used official statistical data [16]. In 2020, LPG consumption in Paraguay was  $8.7 \times 10^4$  t [7]. According to [17], Paraguay’s average LPG consumption is approximately  $7.5 \times 10^3$  t/month. In Paraguay, LPG is totally imported, 80% from Bolivia and 20% from Argentina. In July 2021, the importation cost was US\$ 0.54/



**Table 2** Considered values to estimate firewood and LPG consumption in households for cooking in Paraguay

Parameter	Value	Unit	Source
Household	4	Members	[8]
Average firewood consumption	12.5	t/household/year	[14]
Average LPG consumption	0.18	t/household/year	[16]

**Table 3** Firewood and LPG consumption by department, annual average from 2017 to 2019

Department	LPG ( $\times 10^3$ t/year)	Firewood ( $\times 10^3$ tn/year)
Distrito Capital	17.1	137.9
Concepción	4.3	330.1
San Pedro	4.6	770.9
Cordillera	6.1	351.7
Guairá	3.6	340.0
Caaguazú	9.0	702.2
Caazapá	2.6	379.5
Itapúa	14.1	703.8
Misiones	3.3	139.3
Paraguarí	3.8	523.3
Alto Paraná	28.9	348.6
Central	64.0	266.5
Ñeembucú	2.8	110.5
Amambay	6.5	37.2
Canindeyú	5.9	267.5
Presidente Hayes	2.7	78.9
Boquerón	n.d.a.	n.d.a.
Alto Paraguay	n.d.a.	n.d.a.
Paraguay	179.6	5216.6

Source: [17]

n.d.a. = no data available

kg LPG. Finally, Table 2 shows the values considered in this study to estimate firewood and LPG consumption in households for cooking in Paraguay.

Table 3 shows firewood and LPG consumption by department, annual average from 2017 to 2019.

As shown in Table 3, the highest demand for firewood corresponds to the rural residential sector. Currently, in Paraguay, firewood consumption is higher than production, and firewood sources are diminishing due to deforestation. Regarding the urban residential sector, it can be seen in Table 3 that LPG is the main fuel for cooking. According to [7], more than  $3.0 \times 10^4$  households do not use firewood for cooking anymore in 2020 compared to 2019.

The replacement is based on the energy equivalence between hydrogen, firewood, and LPG and on firewood and LPG consumption of each department of Paraguay.

Thus, the lower heating value and density for hydrogen [10] and for firewood and LPG [9] are:

Firewood (20% moisture):

LHV: 4187 kWh/t

Density: 768.8 kg/m<sup>3</sup>;

LPG:

LHV: 14 MWh/t

Density: 550 kg/m<sup>3</sup>

Hydrogen:

LHV: 33.3 kWh/kg

Density at STP: 0.09 kg/m<sup>3</sup>

The equivalence between fuels is presented in Eq. 3.

$$1 \text{ kg } H_2 = 2.38 \text{ kg } LPG = 7.95 \text{ kg } Firewood \quad (3)$$

## 4 Results

### 4.1 Renewable Hydrogen Potential Relative to Gasoline and Diesel Consumption by Department in Paraguay

Table 4 shows gasoline and diesel consumption that could potentially be displaced by green hydrogen in each department of Paraguay.

Considering the energy equivalence between gasoline, diesel, and hydrogen, it was verified that the Capital District and the Central department, the latter the most populated department of Paraguay, cannot produce enough hydrogen from renewable resources to completely displace their high gasoline and diesel consumption. However, they could rely on hydrogen from surrounding departments. In the Capital District and the Central department, renewable hydrogen could displace 3% and 52% of their gasoline and diesel consumption, respectively. According to Table 4, Fig. 1 shows renewable hydrogen production potential relative to gasoline and diesel consumption, by department in Paraguay.

According to Fig. 1, departments in the Western region, because of their relatively low gasoline and diesel consumption and high amounts of renewable solar and wind resources, have the potential to displace more than  $5 \times 10^3$  times their current gasoline demand. As mentioned above, only the Capital District and the Central department cannot produce enough renewable hydrogen to completely displace their high gasoline and diesel consumption.

**Table 4** Green hydrogen potential relative to gasoline and diesel consumption by department in Paraguay ( $\times 10^3$  t/year)

Department	Gasoline + diesel	Equivalent H <sub>2</sub> production	H <sub>2</sub> production potential	Substitution %
Distrito Capital	91.2	30.9	0.9	3
Concepción	24.7	8.4	3996.1	47,813
San Pedro	36.4	12.3	3373.1	27,343
Cordillera	25.1	8.5	456.4	5370
Guairá	15.3	5.2	356.8	6902
Caaguazú	53.8	18.2	1218.8	6682
Caazapá	8.1	2.7	1568.9	57,392
Itapúa	61.5	20.8	1931.9	9258
Misiones	11.2	3.8	1992.9	52,586
Paraguarí	14.1	4.8	1196.7	25,187
Alto Paraná	131.0	44.4	1494.3	3365
Central	275.9	93.5	48.9	52
Ñeembucú	5.2	1.7	3554.8	203,083
Amambay	38.8	13.1	2959.8	22,591
Canindeyú	47.5	16.1	3017.3	18,710
Presidente Hayes	22.9	7.8	52526.1	673,859
Boquerón	38.0	9.6	111750.8	1,169,046
Alto Paraguay	7.0	2.4	202723.8	8,486,890
Paraguay	897.8	304.2	394168.4	129,573

#### 4.2 Renewable Hydrogen Potential Relative to Firewood and LPG Consumption by Department in Paraguay

Table 5 shows firewood and LPG consumption that could potentially be displaced by renewable hydrogen potential in each department of Paraguay.

LPG is getting popular with its convenience and clean burning in use compared to firewood in urban areas. Firewood is mostly used as a cooking fuel in rural areas where people have no access to LPG. According to Table 5, Fig. 2 shows firewood and LPG consumption substitution percentage with renewable hydrogen for the residential sector in Paraguay. Fig. 2 shows renewable hydrogen production potential relative to firewood and LPG consumption, by department in Paraguay.

As shown in Fig. 2, it is possible to comprehensively satisfy firewood and LPG consumption in all departments of Paraguay with local renewable hydrogen production, except in Asuncion. The results of this analysis show that the Capital District and Central department cannot produce enough hydrogen from renewable resources to completely displace their high firewood and LPG consumption. However, they could, in most cases, rely on hydrogen from surrounding departments. Renewable hydrogen in the Capital District and Central department could displace

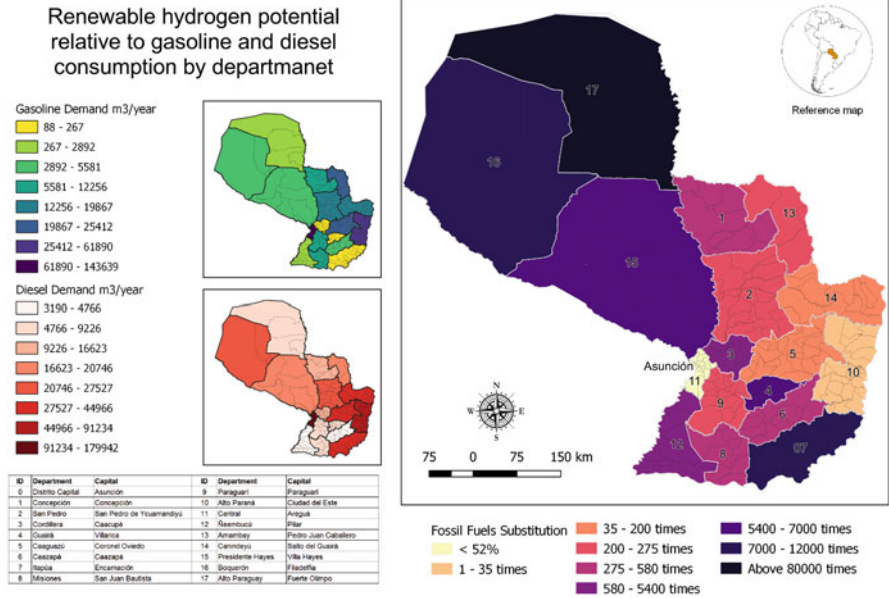


**Fig. 1** Renewable hydrogen production potential relative to gasoline and diesel consumption, by department in Paraguay

**Table 5** Renewable hydrogen potential relative to firewood and LPG consumption by department in Paraguay ( $\times 10^3$  t/year)

Department	Firewood + LPG	Equivalent H <sub>2</sub> production	H <sub>2</sub> production potential	Substitution %
Capital District	155.0	24.5	0.9	4
Concepción	334.4	43.3	3996.1	9226
San Pedro	775.5	98.9	3373.1	3410
Cordillera	357.7	46.8	456.4	976
Guairá	343.6	44.3	356.8	806
Caaguazú	711.2	92.1	1218.8	1323
Caazapá	382.1	48.8	1568.9	3213
Itapúa	718.9	94.5	1931.9	2045
Misiones	143.0	19.0	1992.9	10,506
Paraguarí	527.1	67.4	1196.7	1775
Alto Paraná	377.5	56.0	1494.3	2667
Central	330.5	60.4	48.9	81
Ñeembucú	113.3	15.1	3554.8	23,556
Amambay	79.7	11.9	2959.8	24,785
Canindeyú	273.4	36.1	3017.3	8352
Presidente Hayes	81.6	11.1	52526.1	474,839
Boquerón	n.d.a.	n.d.a.	111750.8	–
Alto Paraguay	n.d.a.	n.d.a.	202723.8	–
Paraguay	5703.7	770.3	394168.4	51,170

n.d.a. = no data available

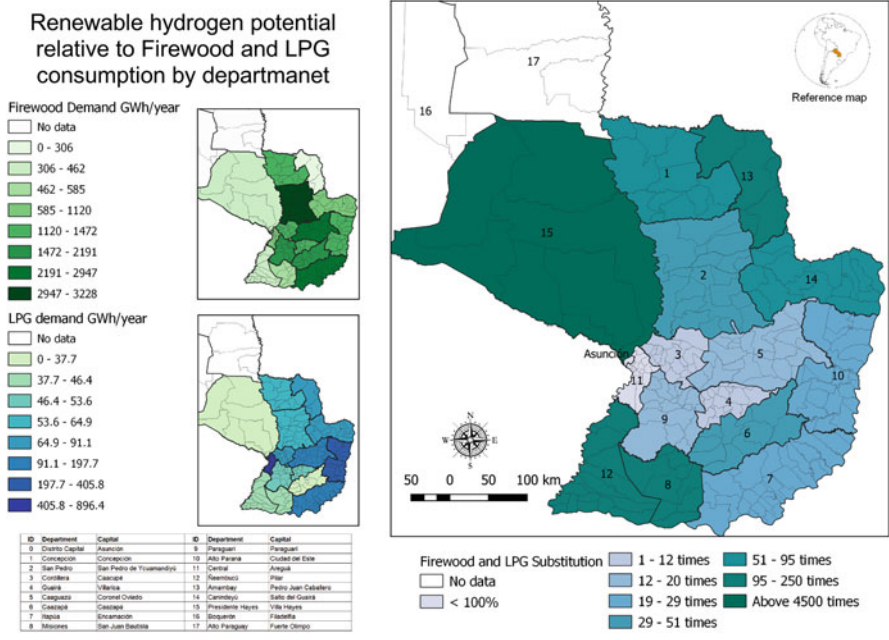


**Fig. 2** Renewable hydrogen production potential relative to firewood and LPG consumption, by department in Paraguay

approximately 4% and 81% of their firewood and LPG consumption, respectively. In contrast, the Boquerón department in the Western region, because of their relatively low firewood and LPG consumption and high amount of renewable solar and wind resources, have the potential to displace more than  $4.7 \times 10^3$  times their current firewood and LPG demand. The renewable hydrogen production surplus of each department can be used to generate electricity from PEMFC to supply  $1.4 \times 10^4$  households that do not have this basic service in Paraguay. For calculations, it was assumed an electricity consumption of 3 MWh/household/year [16], and a typical household is composed of four people [18]. To generate electricity, it was considered a proton exchange membrane fuel cell (PEMFC) with an average efficiency of 53% [19], higher than the efficiency of an internal combustion engine. Results demonstrate that the green hydrogen production surplus of each department would satisfy this requirement in the whole country. The end-use technologies of hydrogen are known and commercially available, especially fuel cell electricity generation on a small scale. However, its adoption for specific situations requires a detailed technical and economic analysis, which supports decision-making and whose development is beyond the scope and purpose of this study.

## 5 Discussion

At present, Paraguay's 100% need of petroleum products such as gasoline, diesel, and LPG (cooking gas) is imported by paying the hard currency. These imported fossil fuels can be completely replaced by electrolytic hydrogen produced from domestic renewable energy sources. Obtained results envisage an optimal scenario for a future hydrogen economy in Paraguay. This will require financial investment from both public and private sectors for sustainable energy project development and the suitable infrastructure implementation for using renewable hydrogen as an energy carrier in the transportation sector. Furthermore, renewable energy sources geospatial distribution in Paraguay also implies an important opportunity for distributed generation advancement in energy policies, meaning greater decentralization, redistribution, self-sufficiency, and democratization of the energy system, and, consequently, greater regionalization of production and economy.

## 6 Conclusion

The results conclude that the green hydrogen production potential of Paraguay can meet 367 times firewood, LPG, gasoline, and diesel consumption in 2021. At present, Paraguay's 100% need of petroleum products such as gasoline, diesel, and LPG (cooking gas) is imported by paying the hard currency. These fossil fuels can be completely replaced by electrolytic hydrogen produced from solar, wind, and hydro-power. Using green hydrogen as a fuel for vehicles not only saves money on import of fossil fuels but also reduces harmful emissions and carbon dioxide, improving the air quality significantly in most populated cities, for example, Asunción, Encarnación, and Ciudad del Este. According to the National Development Plan Paraguay 2030, Paraguay has proposed to reduce the consumption of fossil fuels by 20% and increase the consumption of renewable energy sources by 60% by 2030. This research demonstrates that hydrogen obtained from domestic renewable energy sources in Paraguay is a very attractive alternative to achieve mentioned national goals. Besides, green hydrogen could promote technological development and energy transition in Paraguay, not only in the transportation and residential sectors but also in industry and other sectors. Green hydrogen would be a 100% domestic fuel that would take advantage of large biomass, solar, wind, and hydro resources making a significant contribution to the value chain and the different productive sectors. Paraguay could take advantage of its strategic geographic location in the center of South America to become a logistics and green hydrogen hub.

**Acknowledgments** Financial support from CONACYT (Consejo Nacional de Ciencia y Tecnología del Paraguay) through the project "Electrolytic hydrogen production potential from renewable energy sources in Paraguay" (PINV18-41) is gratefully acknowledged.

## References

1. Falcone, P., Hiete, M., & Sapio, A. (2021). Hydrogen economy and sustainable development goals: Review and policy insights. *Current Opinion in Green and Sustainable Chemistry*, 31, 100506.
2. Kovač, A., Paranos, M., & Marciuš, D. (2021). Hydrogen in energy transition: A review. *International Journal of Hydrogen Energy*, 46(16), 10016–10035.
3. Mohideen, M., Ramakrishna, S., Prabu, S., & Liu, Y. (2021). Advancing green energy solution with the impetus of COVID-19 pandemic. *Journal of Energy Chemistry*, 59, 688–705.
4. Galeano, M., Baranda, C., Franco, D., Posso, F., & Zambrano, J. (2021). *Towards the hydrogen economy in Paraguay: Estimation of the green hydrogen production potential*. Paper presented at the XXI International Congress of the Hydrogen Mexican Society, Mérida, Yucatán (online), 20–24 September 2021.
5. Dirección Nacional del Registro de Automotores. (2021). Informe Estadístico. Disponible Online. <https://www.pj.gov.py/>. Accessed Aug 2021.
6. Posso, F., Sánchez, J. E., Espinoza, J. L., & Siguencia, J. (2016). Preliminary estimation of electrolytic hydrogen production potential from renewable energies in Ecuador. *International Journal of Hydrogen Energy*, 41, 2326–2344.
7. Viceministerio de Minas y Energía. (2020). Balance Energético Nacional 2019. En términos de energía final. Informe y resumen estadístico, Asunción. Accessed Aug 2020.
8. Ministerio de Industria y Comercio. (2021). Estadísticas de combustibles. <https://www.mic.gov.py/>. Accessed June 2021.
9. Viceministerio de Minas y Energía. (2019). Balance Energético Nacional 2018. En términos de energía final. Available Online. <http://ssme.gov.py>. Accessed Aug 2020.
10. International Energy Agency. (2019). The future of hydrogen: Seizing today's opportunities. In: OECD iLibrary. Available Online. <https://doi.org/10.1787/1e0514c4-en>. Accessed 2020.
11. Owen, R., & Larrobla, R. (2004). Estrategia para el desarrollo forestal en el Cono Sur. Estudios de caso: Paraguay y Uruguay. In: Programa de Cooperación FAO/Banco Mundial. Available Online. <http://www.fao.org/3/k1163s/k1163s00.htm>. Accessed 2020.
12. Bohn, E. (2011). Paraguay: Informe Final. Producto 1: Líneas base de las tecnologías energéticas. Producto 2: Estado del arte de las tecnologías energéticas (Casos de estudio). Organización Latinoamericana de Energía (OLADE), Organización de las Naciones Unidas (ONUDI). Available Online. <https://fdocuments.ec/reader/full/paraguay-product-paraguay-observatorio-de-energias-renovables-en-amrica-latina>. Accessed 2020.
13. Banco Internacional de Desarrollo. (2008). Herramientas para mejorar la efectividad del mercado de combustible de madera en la economía rural. Informe diagnóstico Paraguay. Available Online. <https://bit.ly/3DahcdO>. Accessed 2020.
14. Viceministerio de Minas y Energía. (2013). Balance Energético Nacional 2012. En términos de energía final. Available Online. <http://ssme.gov.py>. Accessed Aug 2020.
15. Pirelli, T., & Rossi, A. (2018). Sostenibilidad de la biomasa para energía y del etanol de maíz y caña de azúcar en Paraguay. In: Environment and Natural Resources Management – Working Paper 70. FAO - Organización de las Naciones Unidas para la Alimentación y la Agricultura. Available Online. <http://www.fao.org/documents/card/en/c/I9576ES/>. Accessed 2020.
16. Instituto Nacional de Estadística. (2021). Hogares por año, según departamento y tipo de combustible utilizado principalmente para cocinar 2017–2019. Available Online. <https://www.ine.gov.py/>. Accessed June 2021.
17. Ministerio de Industria y Comercio. (2021). Estadísticas de GLP. <http://www.mic.gov.py>. Accessed Aug 2021.
18. VMME, BID. (2019). Producción y consumo de biomasa forestal con fines energéticos en el Paraguay. Available Online. <https://www.ssme.gov.py>. Accessed 2021.
19. Contreras, A., Posso, F., & Guervos, E. (2010). Modelling and simulation of the utilization of a PEM fuel cell in the rural sector of Venezuela. *Applied Energy*, 87(4), 1376–1385.

**Part IV**  
**Wind Energy**



# Analysis of Two-Dimensional Airfoil Models as Harvesters of Energy



Luis Gonzaga-Bermeo  and Carlos A. Cuenca 

## 1 Introduction

The process of decarbonization of the industry in countries that signed the Paris Agreement of 2008 has promoted the study and development of renewable energy sources as a replacement for fossil fuels. One of the promising concepts is the use of airfoils that describe heave and pitching movements simultaneously [1]. In the present study, two airfoils, one symmetric (NACA0020) and the other asymmetric (NACA1412), are modeled in two dimensions (2D) with the purpose of comparing their efficiencies when these are working in power-extraction regime from an approaching fluid, in this case is water with velocity  $U_\infty$ .

Previous numerical simulations in 2D have been carried out with asymmetric airfoil [2], in laminar regime (100–1000) at different plunging motion profile (sinusoidal and induced), reaching in the best of the cases a maximum efficiency of 20%.

Around this theory of oscillatory airfoils, a hydrokinetic turbine with two airfoils disposed in tandem was tested experimentally in 2009 by Kinsey et al. [3], and the extracted energy compared with conventional rotor blades showed a maximum efficiency greater than 25%.

---

L. Gonzaga-Bermeo (✉)  
DINAVALE, Daule, Ecuador

University of Strathclyde, Naval Architecture, Ocean, & Marine Engineering, Glasgow, UK  
e-mail: [luis.gonzaga-bermeo.2020@uni.strath.ac.uk](mailto:luis.gonzaga-bermeo.2020@uni.strath.ac.uk)

C. A. Cuenca  
Facultad de Ingenieria Mecanica y Ciencias de la Produccion, Escuela Superior Politecnica del Litoral, ESPOL, Guayaquil, Ecuador

Department of Naval Architecture and Ocean Engineering, University of São Paulo, São Paulo, Brazil

This study aims to determine the optimal parameters regarding pitching angle, heaving amplitude, and frequency of oscillation when the airfoils are involved in steady laminar flow (Re 735, Re 1100). In addition, following the recommendation of [2], to ensure that airfoils are operating in power-extraction regime, the feather parameter  $\chi = \theta_0 / \arctan(\frac{H_0}{v_\infty}) > 1$  must be applied as necessary condition. This parameter qualifies the effect of the sinusoidal movement of airfoils on the flow regime, where  $\theta_0$  is the pitching amplitude,  $H_0$  is the heaving amplitude, and  $\gamma = 2\pi f$  which is the angular frequency. Hence, the range of values taken is between  $1 < \chi < 2.5$ , which represent pitching amplitude between  $43.32^\circ \leq \theta_0 < 90^\circ$ . In addition, the effects on varying parameters such as nondimensional frequency  $0.11 \leq f^* \leq 0.27$  and heaving amplitude  $0.5 \cdot \text{chord} \leq H_0 \leq 1 \cdot \text{chord}$  are investigated.

A mapping of efficiency in the parametric space: pitching amplitude versus nondimensional frequency ( $f^*, \theta_0$ ) is presented for each airfoil when  $Re = 735$ , heave amplitude ( $H_0 = 1 \cdot \text{chord}$ ), and pitching axis located at 33% of chord length (C.L.).

In this research, the Eulerian frame of reference is the method used to know the response of the wing when parameters vary. Furthermore, the use of dynamic mesh allowed the deformation of the domain, while the programming in the C language of a user-defined function (UDF) achieved the prescribed oscillatory movement for the airfoils.

Finally, the validation of results is made when contrasting numerical simulation from Kinsey and Dumas with our study at the same chord length of the airfoil (240 mm), symmetric airfoil, Reynolds number of 1100, nondimensional frequency,  $f^* = 0.14$ , and pitching amplitude of  $62.01^\circ < \theta_0 < 90^\circ$ .

## 2 Methods

The methodology applied for this study was simulation of the symmetric and asymmetric airfoils at different parameters like nondimensional frequency and amplitude of pitching angle, without considering the angle of attack in the equation of movement. After many simulations (see Table 1), the forces obtained were lifting

**Table 1** Range of parameters to evaluate for NACA 0020 and NACA 1412 when fluid velocity in  $x$  direction is 0.0030 m/s (Re = 735) and 0.0045 m/s (Re = 1100)

$f^* = \frac{fc}{U_\infty}$	$\omega = 2\pi f$	$U_\infty$	$\chi$	$\theta_0[\text{rad}]$	$\theta_0[\text{deg}]$
0.11	0.0086394	0.0030	$1 < \chi \leq 2.5$	$0.75 \leq \theta_0 < 1.57$	$43.32^\circ \leq \theta_0 < 90^\circ$
0.14	0.0109956	0.0045			
0.16	0.0125664				
0.20	0.0157080				
0.25	0.0196350				
0.27	0.0212058				

force and moment, where both results let us to compute the power efficiency and power extracted. In addition, the authors investigated the influence of the Re number and change of amplitude of heave over the efficiency and power extracted. A flow chart shows the general scheme in Fig. 6. To compare efficiencies when Re number varies, the same parameters in which Kinsey and Dumas found the maximum efficiency were selected.

### 2.1 Description of Movements

The movement of the airfoils are described as heaving and pitching, in which these movements are simultaneously done with a rotational axis  $x_p$  located at 33% chord from the leading edge, as shown in Fig. 1. Equations 1 and 2 describe mathematically the harmonic movements. For heaving, its movement is described with amplitude  $H_0$  which is defined as  $1 \cdot \text{chord} = 240 \text{ mm}$ . On another side, angular frequency omega is defined as  $\omega = 2\pi \cdot f$ , where  $f$  is the frequency of oscillation and depends on the operating regime (propulsion or extraction of energy). Finally, the phase angle, Phi, is considered in all simulations as  $\phi = 90^\circ$ :

$$h(t) = H_0 \sin(\omega t + \phi) \tag{1}$$

For pitching, its movement is around  $z$  axis, and the pitching amplitude  $\theta_0$  will be varying from  $40^\circ < \theta_0 < 90^\circ$ . In Eq. 2, the movement is described as a sin function without phase angle:

$$\theta(t) = \theta_0 \sin(\omega t) \tag{2}$$

To know the velocities in heaving and pitching, Eqs. 1 and 2 are derivative respect to time. Therefore, Eqs. 3 and 4 represent these velocities, respectively:

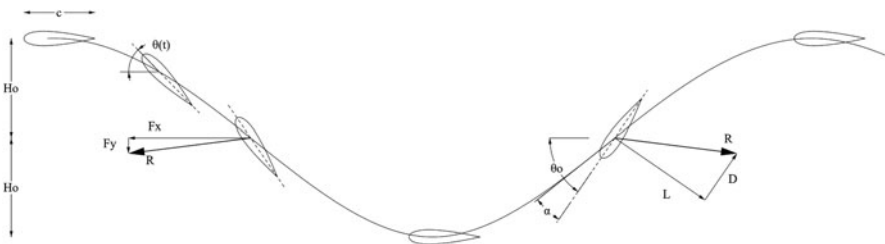


**Fig. 1** Representation of oscillatory movement of airfoil. The heave motion follows a sinusoidal function, while the pitching motion is out of phase by  $90^\circ$ . The oncoming water comes from left to right

$$\dot{h}(t) = H_0 \omega \cos(\omega t + \phi) \quad (3)$$

The pitching velocity is described in Eq. 4.

$$\dot{\theta}(t) = \theta_0 \omega \cos(\omega t) \quad (4)$$

## 2.2 Operating Regime for Power Extraction

Power extraction regime is reached when the forces acting on the airfoil, which has imposed movement and upstream flow conditions, such as lift and drag force, have a net force  $\vec{R}$  that once decomposed into  $\vec{F}_x$  and  $\vec{F}_y$ , the force acting on “y” direction is producing work when the airfoil is heaving while the force acting on “x” direction produces zero work due to angle between vectors  $\vec{F}_x$  and displacement of airfoil  $\vec{y}$  is  $90^\circ$ .

In this study, the feathering parameter,  $\chi$ , is applied as a necessary condition to assure that the airfoil is working in power-extraction regime [4]:

$$\chi = \frac{\theta_0}{\arctan\left(\frac{H_0\omega}{U_\infty}\right)} \quad (5)$$

That is when  $\chi > 1$  and the angle of attack which is constant is  $\alpha_{T/4} < 0$ . As consequence, using Equation 5, the pitching amplitude,  $\theta_0$ , is defined as:

$$\theta_0 = \chi \cdot \arctan\left(\frac{H_0\omega}{U_\infty}\right) \quad (6)$$

The range of pitching amplitude,  $\theta_0$ , when  $0.11 \leq f^* \leq 0.27$  is shown in Table 1.

## 2.3 Power and Efficiency

The power extracted per unit of depth is produced by vertical force,  $F_y(t)$  and velocity when heaving  $V_y(t)$ , also by the Torque,  $M(t)$ , about the axis  $x_p$  and angular velocity  $\dot{\theta}(t)$ :

$$P = P_y(t) + P_\theta(t) = F_y(t) V_y(t) + M(t) \dot{\theta}(t) \quad (7)$$

Then for calculation of efficiency, the total power available  $P_a$  from oncoming water flow through the extraction plane is calculated as follows:

$$P_a = \frac{1}{2} \rho U_\infty^3 d \tag{8}$$

where  $U_\infty$  is the velocity of flow,  $\rho$  is the water density (999 kg/m<sup>3</sup>), and “ $d$ ” is the overall extent of airfoil when it moves in  $y$  direction.

The efficiency is defined as the ratio of the cycle-average power extracted ( $\bar{P}$ ) to the total power available  $P_a$ :

$$\eta = \frac{P_y(t) + P_\theta(t)}{\frac{1}{2} \rho U_\infty^3 d s} \tag{9}$$

Usually, the power extraction efficiency maximum value is about 59% from the Betz analysis of a stationary inviscid stream tube around a power-extraction device [5].

### 2.4 Geometrical Model

The geometry of domain, as well as the symmetrical and nonsymmetrical airfoils, was modeled in rhinoceros, [6]. The airfoils have the same chord length of 240 mm, measured from leading edge to the trailing edge. The distance from leading edge to inlet is given in terms of chord length ( $10 \cdot \text{chord}$ ), the same with the distance from trailing edge to outlet ( $16 \cdot \text{chord}$ ), and finally, from top or bottom of airfoil to symmetry (see Fig. 2). The initial position of wing is at ( $7 \cdot \text{chord}$ ) from upper symmetry to top surface of airfoil, while the lowest position of airfoil is when it reaches ( $7 \cdot \text{chord}$ ) from bottom symmetry to bottom surface of airfoil, that is when  $t/T = 0.5$ . The airfoil is moving vertically in the range  $0.5 \leq \frac{H_0}{\text{chord}} \leq 1$ .

The dimension of the domain is given so that there is no interference between the movement of the folio and the control surface, in addition to guaranteeing the capture of the wake of the airfoil. This was verified by observing the velocity vectors in the near parts of the symmetry zones of some of the analyzed models, identifying that they remain parallel to said symmetry contours.

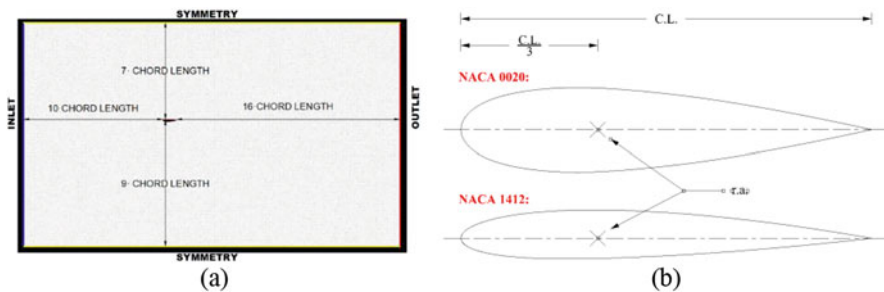


**Fig. 2** (a) Dimension of domain and (b) upper airfoil NACA 0020 and bottom NACA 1412 geometries with chord length (C.L.) 240 mm

## 2.5 Numerical Model

After modeling in rhinoceros, the domains and airfoils were exported into Ansys Fluent [7]. For NACA 0020, five types of meshes were used to guarantee independence of results, (see Table 2).

From this table, the coarse mesh has 21 k nodes, medium mesh has 61 K nodes, and fine mesh has 201 k nodes. The selection of the mesh followed the flow chart given at left side of Fig. 6.

### 2.5.1 Meshing and Mesh Independence Analysis

For each type of mesh considered, both the external limits and the edge of the profile analyzed have been refined, increasing the refinement in the area close to the border of the airfoil. In this way, elements of the linear triangular type have been used to discretize the area of interest. In addition, layers of quadrangular elements were used in the inflation option around the wall surface, as shown in Fig. 3. In all cases, it was ensured that the aspect ratio of the generated elements is not greater than three to avoid discontinuity errors. To achieve this, the height of the first element was calculated using the theory of  $Y^+$  for laminar flows, which allows to determine the appropriate size of element height in the area near the wall of the airfoil [8].

To verify the mesh size selected during the analysis, the value corresponding to the area obtained under the curve (area under the curve, AUC) which represents “Lift vs.  $t$ ” is used. This is achieved by verifying that the area under the selected curve does not change drastically when obtaining responses with different meshes as shown in Fig. 4, which is used due to these let us determine the efficiency of the airfoils.

This means that when the mesh is refined, in this case, with 201 K nodes, it does not produce a variation of results greater than 7% when the mesh has 21 K nodes as observed in Fig. 4c. Therefore, considering the difference in computational analysis shown in Table 2, it can be concluded that a numerical model with a mesh of approximately 21 K nodes allows obtaining a result as significant as a much more

**Table 2** Summary of meshing

Type of mesh	Number of nodes	Size of elements around the wall [mm]	Size of elements on domain [mm]	Time for processing [h]
Mesh 1	6000	4.00	200	4
Mesh 2	21,000	1.50	100	10
Mesh 3	43,000	1.50	50	12
Mesh 4	61,000	0.47	100	77
Mesh 5	201,000	1.00	12.5	168

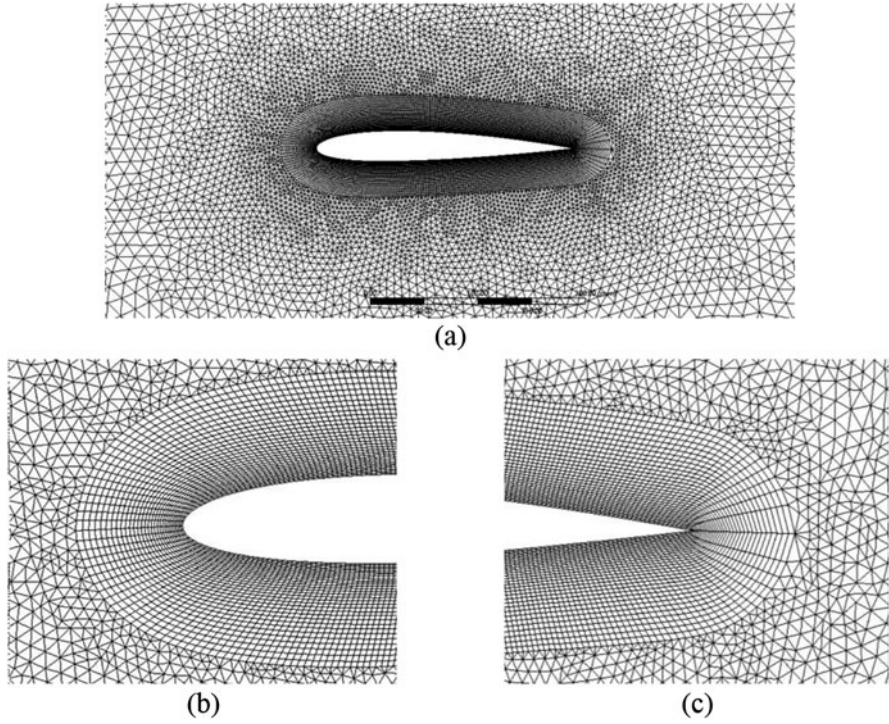


**Fig. 3** (a) Mesh around the airfoil, (b) mesh detail on leading edge, and (c) mesh detail on trailing edge

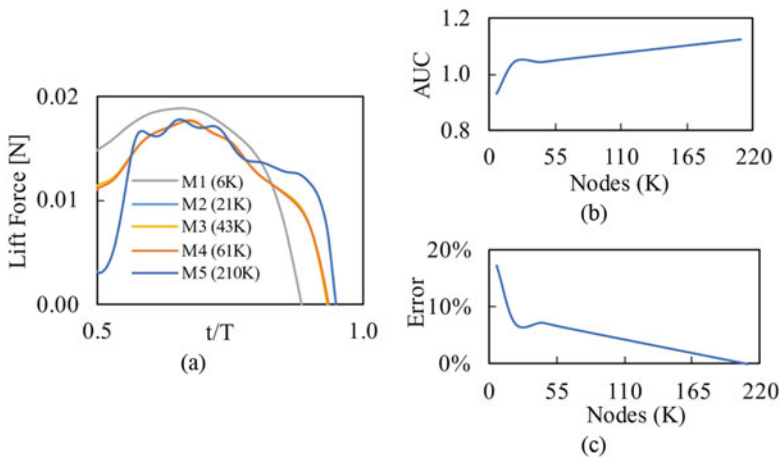


**Fig. 4** (a) Lift curves (RLC) per each mesh's quality, (b) area under the curve for each RLC per each mesh's quality, and (c) relative error of calculation of AUC for each lift curve measured between 0.5 and 1 T

refined mesh. Finally, according to the results obtained, the type of numerical discretization defined for mesh type 2 is selected for the models to be analyzed for both the symmetric and asymmetric airfoils.

### 2.5.2 Boundary Conditions and Loads

In this study, the fluid moves in laminar state from left to right at  $V_x = 0.003$ , ( $Re = 735$ ). The *Inlet BC* is located at the left side of airfoil leading edge at  $10 \cdot \text{chord} = 2400$  mm. On another hand, the *Outlet BC* is located at  $16 \cdot \text{chord} = 3840$  mm, measured from trailing edge to right side of domain. Its distance is far away from the airfoils in order to not affecting the developed state of flow [9, 10].

The exit pressure was defined as “*gauge pressure*” equal to zero. After that, the *wall BC* applied to airfoil profiles (solid wall) is no-slip condition ( $v_x = v_y = 0$ ); this is based on viscosity of boundary layer theory. Finally, but not less important, symmetry condition is applied to upper and bottom edge of domain based on there is no flow across these boundaries ( $\vec{v} \cdot \vec{n} = 0$ ).

### 2.5.3 Dynamic Mesh, User-Defined Function

The dynamic mesh selected method is diffusion-based smoothing which is recommended when there is large deformation of mesh and involves rotational movement. Although this method is computationally costly than spring-based smoothing, diffusion-based generates better quality meshes [11]. The formulation for the diffusion coefficient selected is boundary distance:  $\gamma = \frac{1}{d^2}$  where  $d$  is the normalized boundary (0.50 mm) and  $\xi$ , the diffusion parameter, is taken as 1.5, due to high values (0–2) preserve the mesh close the moving boundary. Thanks to the programming of a user-defined function (UDF), the symmetric and nonsymmetric airfoils can move in heaving and pitching following the equation of movements 1 and 2.

After many simulations, it was demonstrated that after the first period, the forces did not change, as shown in Fig. 5. As consequence, only two cycles were simulated, which permitted reduction of the computational process time. On another hand, the time step was defined using Courant-Friedrichs-Lewy condition  $CFL = \frac{U_x \Delta t}{\Delta h} \tilde{1}$ , where  $\Delta h$  is the size of the cell, measured horizontally around the airfoil, and  $\Delta t$  is the time step.

Table 3 shows the CFLs for the  $f^*$  that allow obtaining efficiencies greater than zero.



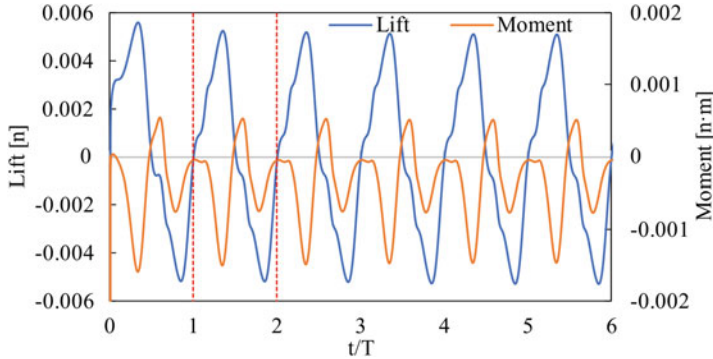


**Fig. 5** Stability of periodic response for lift force by moment

**Table 3** Summary of CFL, time step, period in one cycle, and number of time steps for two cycles

$f^*$	Frequency	CFL	$\Delta t$ [s]	T[s]	N° time steps in 2 T
0.11	0.00138	1.00	0.167	727.27	8731
0.14	0.00175	1.00	0.167	571.43	6860
0.16	0.00200	0.9996	0.167	500.00	6006

### 2.5.4 Solver and Residuals

The model to solve Navier–Stokes equation is laminar model [12], while the numerical solution was computed with finite volume method using the SIMPLE scheme. The time-stepping is second-order upwind scheme.

On another side, the effect of convergence of the value for the residual was analyzed, where it verified that residual of  $10^{-3}$  produced the same response as  $10^{-8}$ ; hence, this value was adopted for all simulations that allow the optimization of computational process time [13].

Finally, two airfoils were analyzed with two flow velocities of 0.003 m/s and 0.0045 m/s, at different values of  $f^*$  as shown in Table 1. The velocity 0.0045 m/s ( $Re = 1100$ ) is used to validate results with previous literature.

To summarize the methodology applied, the flow chart of Fig. 6 at the left side presents how the mesh was selected, while at the right side is showing what forces are calculated once parameters like  $Re$ , nondimensional frequency, and pitching amplitude were set. Then the results of efficiency are printed only when it is positive.

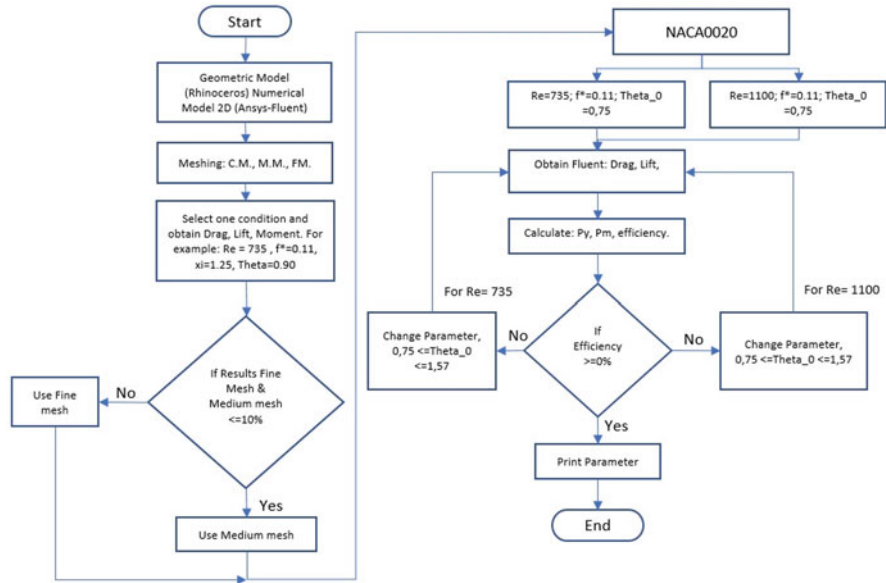


Fig. 6 Flowchart process

### 3 Results

#### 3.1 Forces Acting on NACA 0020 Versus NACA 1412

Lift force and moment were used to calculate the power where it was found that lift force contributed more than moment. On another hand, while the airfoil is extracting energy, the drag force is greater than zero. After calculating the extracted power using Eq. 7, the efficiency was calculated using the average power of one period. In Table 7, the summary of efficiencies for the airfoils NACA 0020 are NACA 1412 are shown.

#### 3.2 Extract of Energy and Efficiency on NACA 0020 Versus NACA 1412

The simulations were carried on for  $0.11 \leq f^* \leq 0.27$ , and for amplitude of pitching angles between  $43.32^\circ \leq \theta_0 < 90^\circ$ , the angle of attack was not considered on these simulations as a fixed parameter neither variable. Therefore, the results showed that maximum efficiencies for symmetric airfoil is reached when  $f^* = 0.14$  and  $\theta_0 = 62.01^\circ$ , while for  $f^* > 0.16$ , the values of efficiencies turn into negative showing that these parameters should be omitted when extracting power. In addition, when

**Table 7** Summary of efficiency with pitching angle  $43.32^\circ < \theta_0 < 90^\circ$  at  $Re = 735$

NACA	$\theta_0$	$f^* = 0.11$	$f^* = 0.14$	$f^* = 0.16$	$f^* = 0.20$	$f^* = 0.25$	$f^* = 0.27$
0020 (1412)	43.32	0.89% (3.92%)	0.79% (-4.80%)	-15.34% (-13.35%)	-42.42% (-38.66%)	-95.08% (-92.79%)	-118.39% (-119.08%)
0020 (1412)	51.98	4.04% (12.34%)	2.42% (5.36%)	-3.08% (-0.79%)	-20.71% (-17.78%)	-57.96% (-51.64%)	-76.14% (-70.26%)
0020 (1412)	62.01	10.29% (16.42%)	11.31% (13.66%)	7.30% (9.63%)	-11.90% (-2.67%)	-29.96% (-26.24%)	-42.06% (-38.26%)
0020 (1412)	72.34	6.56% (9.27%)	9.27% (10.55%)	6.38% (7.16%)	-3.10% (-1.17%)	-24.64% (-21.32%)	-35.63% (-32.04%)
0020 (1412)	77.97	0.10% (1.77%)	2.04% (2.93%)	-1.03% (-1.43%)	-12.68% (-11.63%)	-34.34% (-31.10%)	-46.78% (-42.11%)
0020 (1412)	84.90	-11.12 (-10.44%)	-11.40% (-12.67%)	-16.52% (-22.08%)	-34.32% (-36.79%)	-64.43% (-61.81%)	-80.28% (-74.20%)
0020 (1412)	90.00	-20.60% (-21.36%)	-25.88% (-28.22%)	-32.71% (-37.26%)	-59.82% (-63.54%)	-98.53% (-99.57%)	-119.11% (-116.44%)

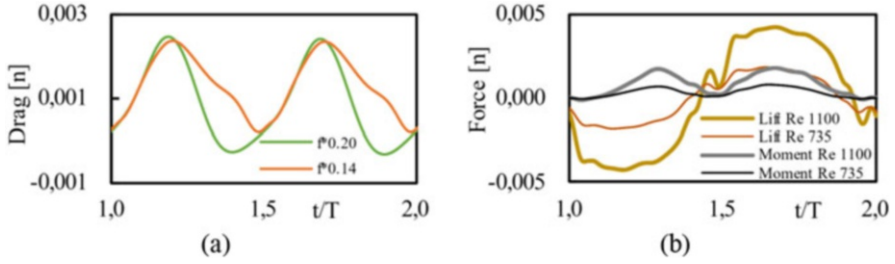


**Fig. 7** (a) Drag force for NACA 0020 at  $0.11 \leq f^* \leq 0.2$  at  $\theta_0 = 62.01^\circ$ . (b) Lift and moment responses for symmetric airfoil at  $\theta_0 = 62.01^\circ$

**Table 4** Efficiencies for symmetric and asymmetric airfoils at  $\theta_0 = 72^\circ$  and  $f^* = 0.16$

Airfoil	Re = 735	Re = 1100
Symmetric	26.08%	19.54%
Asymmetric	17.80%	22.90%

$f^* \leq 0.16$ , the amplitude pitching angle plays an important role due to when angle is less than  $60^\circ$  and greater than  $70^\circ$  the efficiencies are less than 10%.

For the asymmetric airfoil NACA 1412, the maximum efficiency is reached when  $f^* = 0.16$  with  $\theta_0 = 62.01^\circ$ . Furthermore, the efficiency values are positive when  $f^* \leq 0.16$  and amplitude of pitching angle  $62.01^\circ \leq \theta_0 \leq 72.34^\circ$ .

Another important characteristic that is shown in Table 7 is that after reaching the peak of efficiency, it decreases. Besides, Reynolds number also has influence on the efficiency due to it was found that at higher value, Re 1100, the efficiency grew up to 2.6% and nondimensional frequency decreases 0.03 which suggest that at higher  $Re$ , the efficiency improve when the angular frequency reduces. According to [1] at large flow, probably the  $Re$  reduces the effective thickness of the airfoil and increases the force generation, as shown in Fig. 7b.

In addition, when evaluating the efficiency when the ratio  $H_0/\text{chord} = 0.5$ , it is observed that the efficiency increases for asymmetric airfoil but not for symmetric one, as observed in Table 4. The main reason is because the authors assumed that by applying Kinsey and Dumas numerical simulation parameters ( $\theta_0 = 72^\circ$  and  $f^* = 0.16$ ), they would get maximum efficiencies which is not necessarily true.

On another hand, the average extracted power when Re 735, in one cycle, is calculated when the maximum efficiency is reached. For example, in the symmetric airfoil, the average power in one cycle is  $5.23E - 10$  [KWh] when  $f^* = 0.14$ ,  $\theta_0 = 62.01^\circ$ , while for Re 1100 the average power is  $3.13E - 9$  [KWh]. This, in turn, represents 598% of increment. For asymmetric airfoil, the average power is  $8.65E - 10$  [KWh],  $f^* = 0.11$ , and  $\theta_0 = 62.01^\circ$ , and for Re = 1100 the average

**Table 5** Efficiencies and extracted power for each NACA airfoil at different  $Re$  at  $\frac{H_0}{c} = 1$

Airfoil – $H_0/c = 1$	$Re = 735$	$Re = 1100$
NACA 0020	11.31% 5.23E-10 [KWh] ( $f^* = 0.14; \theta_0 = 62.01^\circ$ )	13.93% 3.13E-09 [KWh] ( $f^* = 0.11; \theta_0 = 62.01^\circ$ )
NACA 1412	16.42% 8.65E-10 [KWh] ( $f^* = 0.11; \theta_0 = 62.01^\circ$ )	17.14 4,74E-09 [KWh] ( $f^* = 0.11; \theta_0 = 62.01^\circ$ )

**Table 6** Efficiencies and extracted power for each NACA airfoil at different  $Re$  at  $\frac{H_0}{c} = 0.5$

Airfoil – $H_0/c = 0.5$	$Re = 735$	$Re = 1100$
NACA 0020	26.08% 1.39E-09 [KWh] ( $f^* = 0.14; \theta_0 = 62.01^\circ$ )	19.54% 3.08E-09 [KWh] ( $f^* = 0.11; \theta_0 = 62.01^\circ$ )
NACA 1412	17.80% 5.10E-10 [KWh] ( $f^* = 0.11; \theta_0 = 62.01^\circ$ )	22.90% 4.24E-09 [KWh] ( $f^* = 0.11; \theta_0 = 62.01^\circ$ )

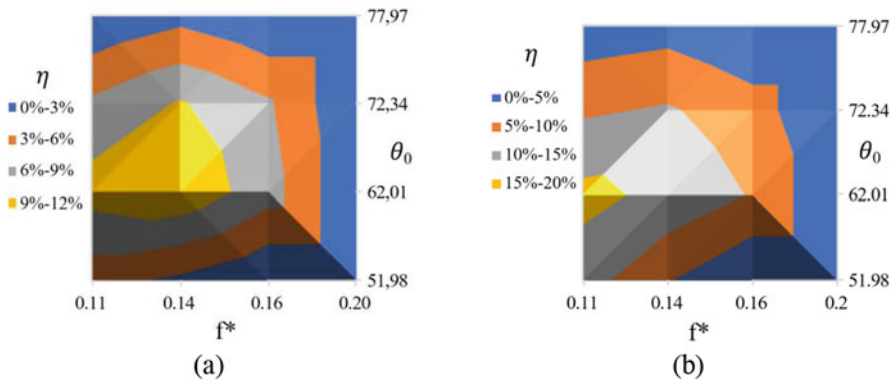


**Fig. 8** Efficiency at  $0.11 \leq f^* \leq 0.2$  at  $\theta_0 = 62.01^\circ$  for: (a) NACA 0020, (b) NACA 1412

power is  $4.74E - 09$  [KWh] same  $f^*$  and  $\theta_0$  what means 548% of increment. In Tables 5 and 6, the reader can observe the improvement of working at different  $Re$  number and reduced heave amplitude.

Figure 8 shows the maximum efficiency values for each airfoil analyzed in a mapping of efficiencies in the space  $(f^*, \theta_0)$ .

### 3.3 Validation of Results

The validation of results is done when the authors compare the trend of the results for the efficiencies and amplitude of pitching angle  $\theta_0$  with Kinsey-Dumas literature, [4], where higher efficiencies are reached when  $f^* < 0.18$  and  $60 < \theta_0 < 80^\circ$ .

## 4 Discussion

For the analyses carried out, computers whose computing capacity corresponds to Core i7 processor, 8 cores, and 16 GB of RAM with AMD Radeon HD 7000 graphics card were used in which the calculations could be performed in an average of 10 hours.

It was numerically verified that the results had minimum error when modifying parameters such as the number of nodes in the selected mesh. In addition, when the tolerance in the residuals is reduced, the computational processing time was improved.

It was analyzed that the results obtained did not vary for different mesh changes, obtaining that with models of 21 K nodes, the responses were less than 7% for the models of 210 K nodes. That confirmed that the responses are independent with the selected mesh.

## 5 Conclusions and Recommendations

From the results obtained, the following can be observed:

1. The geometry of the airfoils affects the efficiency obtained, where this value with the asymmetric type airfoil presents an efficiency 2.62% greater than that obtained with symmetric airfoil as stated in [1].
2. The calculations presented in the present investigation were carried out without considering an angle of attack in the rotational motion equation, that is,  $\alpha = 0$ . Likewise, the simulation was carried out for  $\Omega = 1100$ ,  $f^* = 0.12$ ,  $\theta_0 = 62^\circ$ , and  $\alpha = 23^\circ$  with which it was observed that there is an increase in efficiency, which shows the importance of including this value within the equation of motion to improve efficiency.
3. It was found that the efficiency of the two airfoils increases when the value of the  $H_0/chord$  ratio decreases from 1 to 0.5, as well as increases when the Re increases.
4. The power generation is very small. Consequently, changes must be implemented to the magnitudes of airfoil geometry, and thus, analyze if the efficiency increases. Besides, the 3D analysis of these must be carried out to identify any change in the results.

Recommendations for future work are the following:

1. To add the value of the angle of attack to increase the power and efficiency obtained for the airfoils.
2. To analyze the airfoils considering their three dimensions. In addition, the variations on the  $H_0$ /chord ratio and at different frequencies  $f^* < 0.20$  with  $\Delta f^* = 0.01$ , values of  $60^\circ \leq \theta_0 \leq 80^\circ$  with  $\Delta\theta = 2^\circ$ , to determine the response of these changes and generate a space of efficiencies,  $\eta(f^*, \theta_0)$ , more detailed.
3. To analyze the pressure coefficient along the chord and the effect of the leading-edge vortex shredding.

## References

1. Xiao, Q., & Zhu, Q. (2014, April). A review on flow energy harvesters based on flapping foils. *Journal of Fluids and Structures*, 46, 174–191. <https://doi.org/10.1016/j.jfluidstructs.2014.01.002>
2. Zhu, Q. (2011, May). Optimal frequency for flow energy harvesting of a flapping foil. *Journal of Fluid Mechanics*, 675, 495–517. <https://doi.org/10.1017/S0022112011000334>
3. Kinsey, T., et al. (2011, June). Prototype testing of a hydrokinetic turbine based on oscillating hydrofoils. *Renewable Energy*, 36(6), 1710–1718. <https://doi.org/10.1016/j.renene.2010.11.037>
4. Kinsey, T., & Dumas, G. (2008, June). Parametric study of an oscillating airfoil in a power-extraction regime. *AIAA Journal*, 46(6), 1318–1330. <https://doi.org/10.2514/1.26253>
5. Betz, A. (2013, August). The maximum of the theoretically possible exploitation of wind by means of a wind motor. *Wind Engineering*, 37(4), 441–446. <https://doi.org/10.1260/0309-524X.37.4.441>
6. McNeel, R., et al. (2010). *Rhinoceros 3D, Version 6.0*. Robert McNeel & Associates.
7. Swanson, J. (2020). *Ansys, 2020 R1*. NASDAQ. [Online]. Available: <https://www.ansys.com/academic/students>
8. Cadence. (2020). Compute Grid Spacing for a Given Y+. [pointwise.com](https://www.pointwise.com). <https://www.pointwise.com/yplus/index.html>. Accessed 23 July 2021.
9. Versteeg, H. K., & Malaladekera, W. (2007). *An introduction to computational fluid dynamics* (2nd ed.). Pearson Prentices Hall.
10. Blazek, J. (2015). *Computational fluid dynamics: Principles and applications* (3rd ed.). Elsevier.
11. Ansys Training. (2019). *Ansys fluent dynamic mesh modeling*. Virtual – WebEx. [Online]. Available: <https://www.ansys.com/training-center/course-catalog/fluids/ansys-fluent-dynamic-mesh-modeling>
12. ANSYS Inc. (2013). *Ansys fluent theory guide* (15th ed.). ANSYS.
13. ANSYS Inc. (2012). Monitoring residuals. In *ANSYS FLUENT 12.0 User's guide*. <https://www.afs.enea.it/project/neptunius/docs/fluent/html/ug/node812.htm>. Accessed 1 Sept 2021

**Part V**  
**General Renewable Energy**



# Environmental and Ecotoxicological Impact of Alternative Energies: An Improvement Opportunity for Latin America



Juan Carlos Valdelamar-Villegas and Julio Roman Maza-Villegas

## 1 Introduction

Development and implementation of alternative energy sources is the nowadays response to the unusual change in environmental conditions consequence of the indiscriminate use of fossil fuels. These alternatives are intended to significantly reduce greenhouse gas emissions, such as carbon dioxide (CO<sub>2</sub>), methane (CH<sub>4</sub>), or nitrous oxide (NO<sub>2</sub>) [1]. Therefore, the massive use of alternative energies constitutes a strategy to mitigate global climate change due to the significant reduction of CO<sub>2</sub> emissions while implementing these planet-friendly technologies. Similarly, the development of alternative energy projects catapults scientific development, a requirement for highly trained human capital, and the design and search for new materials with close-to-zero ecological and environmental toxicity.

Among the set of production systems for alternative energy sources, we highlight the use of (i) *water-driven forces* such as hydraulic dams or wave/tidal power [2], (ii) *wind-driven forces* such as the energy obtained from windmills and wind turbines, and (iii) *photovoltaic-driven forces*, based on solar light harvesting, catalyzing the excitation of the electronic states of molecules carefully arranged in panels or cells. These alternative energy production systems have shown great potential for large-scale implementation in countries from North America, Central Europe, and East Asia. Still, the implementation in South America has been late [3].

---

J. C. Valdelamar-Villegas (✉)

Facultad de Ingeniería, Fundación Universitaria Tecnológico Comfenalco, Cartagena, Colombia

e-mail: [jvaldelamar@tecnologicocomfenalco.edu.co](mailto:jvaldelamar@tecnologicocomfenalco.edu.co)

J. R. Maza-Villegas

Facultad de Ciencias Básicas, Universidad del Atlántico, Puerto Colombia, Atlántico, Colombia

© The Author(s), under exclusive license to Springer Nature Switzerland AG 2022

M. Espinoza-Andaluz et al. (eds.), *Congress on Research, Development and Innovation in Renewable Energies*, Green Energy and Technology,

[https://doi.org/10.1007/978-3-030-97862-4\\_8](https://doi.org/10.1007/978-3-030-97862-4_8)

109

There is no doubt in the altruistic philosophy behind the alternative energy production systems aimed to reduce greenhouse gas emissions. However, it is also undeniable that some processes, directly and indirectly, related to the development and implementation of these production systems create environmental effects that worsen the conditions of life harbored by ecosystems and the biodiversity present [4, 5].

This paper arises from the considerations outlined in the preceding paragraphs, is intended to provide the reader with a context about the ecotoxicological and environmental effects derived from the start-up, construction, and implementation of the above-regarded energy production systems, drawing the policies and project considerations of alternative energy implementations, especially in regions, such as Latin America, where the development of these clean-energy technologies is still incipient. Acknowledging the direct and/or indirect effects on the ecosystem of alternative sources of energy will be of great help to reduce the ecological and environmental footprint generated from its implementation that guarantees the sustainability of ecosystems in the medium and long term. The analysis presented in the present paper was intentionally biased to the three sources of energy mentioned above: water-driven, wind-driven, and photovoltaic-driven forces, since these three technologies currently represent between 2% and 5.6% of the global energy production. Furthermore, it is projected that these technologies will supply between 20% and 40% of the worldwide energy demand by 2050 [6, 7], excluding the hydraulic production systems, whose ecological and environmental impacts have been widely documented.

## 2 Methods

A systematic review of literature sources was carried out on the probable ecotoxicological and environmental impact of alternative energies, aiming for PubMed, Science Direct, and Scopus databases. The chosen language for the screened manuscripts was English, and spanning case studies, reviews, meta-analyses (Fig. 1), and query hits were filtered manually. The query was defined using the following word descriptors: wind energy, photovoltaic energy, wave energy, environmental, and ecotoxicological impact.

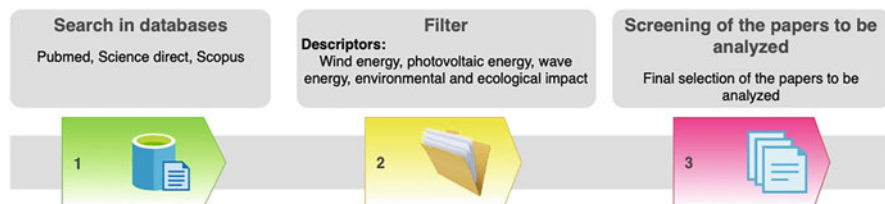


**Fig. 1** Methodology used for the search and analysis of the information

Subsequently, manuscripts that meet the query criteria and initial filter were selected for a thorough review, converging on articles that made a clear allusion to potential of alternative energies to generate ecotoxicological and environmental impacts, as well as the proposal for management strategies to reduce the impact, and manuscripts that did not include the ecotoxicological or environmental impact component were excluded from this review.

During the database screening process, the manuscripts were initially selected by the name of the published research (in which there were the four phrases descriptors: wind energy, photovoltaic energy, wave energy, environmental impact, and ecotoxicological impact), then by reviewing the abstracts, in which the established inclusion and exclusion criteria were taken into account, and finally, the selected publications that passed to the next filter were full-text read and analyzed thoroughly, synthesizing the material in a spreadsheet where the information on the ecotoxicological and environmental impacts was generated according to the type of technology and the advances in its management were included.

### **3 Results**

#### ***3.1 Selected Articles***

Results from the queries deployed in the search engines of the databases allowed us to identify more than 3000 documents, and by reviewing the title and abstract of these documents, 210 documents were selected. Finally, a thorough screening of the content of the documents allowed us to select 34 papers highly related to the topic of the ecotoxicological and environmental impact of alternative energies, uncovered below.

#### ***3.2 Alternative Energy Sources and their Impacts***

The alternative energy production systems include all those systems other than the generation of energy through the combustion of fossil fuels, spanning the use of biomass residues, dams, geothermal, wave-force, wind, and photovoltaic [8]. The implementation of these types of systems has been useful to solve energy problems in communities that have limited access to fossil fuels. More recently, the overwhelming environmental impact on the planet, such as global warming, due to indiscriminate fossil fuel uses has potentiated and extended the systems and technologies related to alternative sources of energy. Now, we describe issues and adverse effects related to the development of these systems.

### 3.3 Wave Power

The production of this type of energy is carried out from devices capable of converting the mechanical-oscillating energy from marine waves and tides to electrical energy [2]. Several technologies have been developed to achieve energy interconversion (Fig. 2), among which are oscillating water column equipment (OWCE), which is characterized by having an opening in the upper part, through which compressed air comes out due to the action of the waves, which activates power-generating turbines [9], the articulated semi-submerged cylindrical equipment (AsSCE) produces an oscillating movement when impacted by the waves, which induces an internal flow of oil at high pressure, activating hydraulic motors coupled to a series of electric generators, the wave collectors (WC) are devices attached to the seabed, emerging to the surface and capturing waves through a ramp, the inertia moment of the waves is transferred to turbines and electric generators [10]. Similarly, there are floating structures capturing water waves and filling tanks that once descend to the seabed, activate a series of hydroelectric turbines [11]. More details on the ecotoxicological and environmental impacts of wave energy production systems are shown in Table 1.

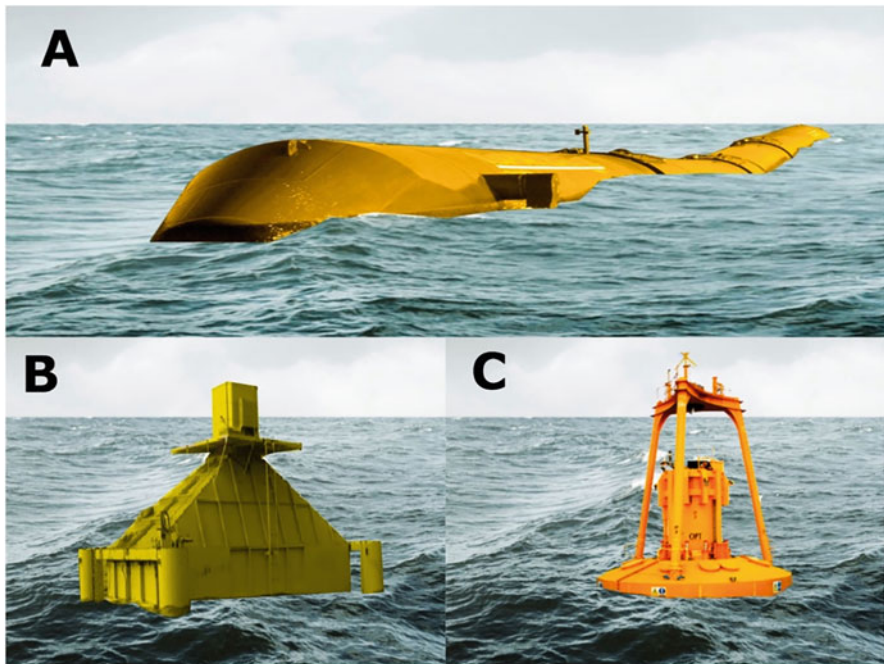


**Fig. 2** Technologies used to produce energy from waves. (a) Wave collectors [12], (b) oscillating water column equipment [13], and (c) articulated semi-submerged cylindrical equipment [14]

**Table 1** Ecotoxicological and environmental impacts caused by wave power energy

Ecotoxicological or environmental impact	Wave power technology implemented	References
Potential collision, entanglement, entrapment, habitat disruption, noise interfering with marine mammals that use sound to communicate, and electromagnetic fields interference with navigating, feeding, and evade predators	WC	[15, 16]
Biomass changes by alteration of deposition and migration habits of benthic organisms, decreasing the abundance of these organisms due to constant mix of seabed as consequence of the power of waves	OWCE, AsSCE	[17, 18]
Electromagnetic fields disrupting the orientation of cetaceans and elasmobranchs, which are sensitive to magnetic fields	AsSCE	[19]
Changes in the development of embryos and alterations in the development of cellular processes in sea urchins and some fish	WC, OWCE	[20]
New habitat creations, change in wave energy and physical damage to marine habitats during the installation, operation, and maintenance phases. Changes in the bio-availability of nutrients and ecological interactions	WC, OWCE, AsSCE	[21]
Wave power devices and associated cables could act as a potential source of cumulative stressors in aquatic ecosystems	WC, OWCE	[22]
Electromagnetic fields could also disrupt the migration patterns of fish, such as eels, by interfering with their ability to orient themselves relative to the geomagnetic field	AsSCE, OWCE	[23]

WC wave collectors, OWCE oscillating water column equipment, AsSCE articulated semi-submerged cylindrical equipment

### 3.4 Wind Power

The production of this type of energy occurs through the movement of turbines coupled to blades that are activated when wind circulates through in a propeller movement, the kinetic energy transferred from gas particles present in the air, driven by the wind currents to the mechanism of a windmill is transformed into electrical energy through magnetic induction in the generators [24]. Wind power production is considered one of the inexhaustible alternatives, with little space occupation, low operating cost, and null greenhouse gas production, with an energy production calculated over 500 gigawatts per year, among alternative energy systems [25]; this has propitiated the use of wind power in parts of the world where the probability of wind is geographically significant, such as in coastal areas where some adverse ecological and environmental impacts generated by this type of technological development have also been identified. Some examples of the ecological and environmental impact generated by wind energy are described in Table 2.

**Table 2** Ecotoxicological and environmental impacts caused by wind power energy

Ecotoxicological or environmental impact	References
Noise generated by wind turbines on the marine ecosystem impacts on the atmosphere either through direct changes in wind speed or turbulent heat flows	[26]
The noise caused by the operation of wind turbines on land and its visual impact, can cause symptoms of stress, sleep disturbances, headaches, and hearing problems in people living in areas near wind farms	[27]
High level of noise produced by the rotor blades, visual impacts, and the death of birds and bats by collision with the blades	[5, 28]
The construction and maintenance of wind power plants alter the structure of the vegetation through the clearing of forests, alteration, and possible soil erosion. As these factors, potentially, represent the greatest significant change through the fragmentation and loss of habitat of some species	[29]
Noise related to offshore wind farms has the potential to affect the physiology and behavior of harbor porpoises and seals at considerable distances, even affecting their hearing	[30, 31]
According to observations regarding to the vocalization of the squirrels (anti-predatory behavior), there are behavioral differences between the squirrels that live near the wind turbine and those in the control site, indicating that the noise of the wind turbines (when they are active) interfere with the wildlife underneath the wind farms	[32]

### 3.5 Photovoltaic Energy

Photovoltaic energy is produced through a molecular light harvesting process, which induces vertical transition excitation states to molecules, granting electron conduction properties by reducing the abortion bandgap level, allowing to store electric energy into batteries. The whole device is acknowledged as photovoltaic/solar panel or cell, with different constitution, being the monocrystalline ones, made of molten pure silicon, doped with boron, polycrystalline panels that have the same constitution, but in these the growth of silicon crystals is not controlled, allowing them to grow in different directions, thus facilitating the formation of groups of heterogeneous crystals joined together [33]. Another type of solar panel is the thin-film one, and this is produced in a different way than the previous ones, through a process in which a thin layer of amorphous silicon is deposited, or of cadmium, copper, indium, gallium, and selenium telluride, or in some cases of organic photovoltaic cells, on substrates made of plastic or glass.

The development of photovoltaic panels is not recent. However, it has heavily developed in the last 20 years, due to the discovery and implementation of new materials that have improved the efficiency of energy production and have also contributed to the reduction of costs associated with the production and commercialization of these devices [34, 35]. Despite the environmental advantages offered by the implementation and use of photovoltaic panels, there are direct and indirect negative impacts on ecosystems. Some effects generated during the development of photovoltaic systems are listed in Table 3.

**Table 3** Ecotoxicological and environmental impacts caused by photovoltaic energy

Ecotoxicological or environmental impact	References
Generation of electronic waste from solar panels since they have a useful life of 20–30 years. The toxic gases and heavy metals emitted during the processing of materials and the manufacture of solar cells are associated with the category of carcinogens, due to the extensive use of chemicals such as acids and dangerous solvents	[36–38]
Reduction of water sources in the assembly and building area due to excessive water consumption due to the manufacturing process of photovoltaic panels	[39]
Floating photovoltaic plants cause a reduction in the penetration of sunlight to bodies of water, which negatively affects the growth of animals and aquatic vegetation	[40]
Emissions of gases, particles, and liquid discharges. Consumption of resources, generation of waste and permanent impact on the biotic environment due to the construction of access roads and auxiliary buildings	[34, 39]
Because plants of photovoltaic systems are carried out both on free and agricultural lands, their impact is expressed in flora and fauna, respectively, since there is the total or partial elimination of plant life	[41]
Acidification and deforestation of the area due to the production of waste during the manufacture, installation, and use of photovoltaic systems	[42]

## 4 Discussion

Despite the benefits offered by the implementation of wave/tidal energy production systems, the implementation equipment of this technology invades the marine ecosystems [19], triggering a progressive degradation of the environment due to the loss or displacement of marine species that regulate the ecosystem. Additionally, equipment cable and devices installed along the seabed can trap marine animals and collide with large organisms.

Other potential risks identified for marine biodiversity are the formation of electromagnetic fields, the generation of noise, and water column disturbances [43], which alter the behavior of benthic marine animals such as flounder fish and stingrays, as well as disruptive displacement patterns of plankton and phytoplankton distribution due to changes in the circulation of the surface layer of the water column, thus affecting their supply in the spaces where they are captured by organisms that have to this group of microscopic organisms as the basis of their diet [44].

Among the ecological and environmental impacts caused by wind turbines, the transformation of the three-dimensional visual elements of the landscape stands out, due to the height they reach (between 50 and 80 m), which in turn causes discomfort in the human populations living nearby wind farms, which are manifested through sleep disturbance, psychological stress, anxiety, and memory and concentration problems; these effects are inversely related to the distance humans to wind farms [45]. Other important effects are related to the ecological and environmental component, which include increased mortality of birds and bats caused by direct collision with the blades or airscrews, as well as changes in the migration and reproduction

pattern of these groups of flying animals and disruption of behavior and food chains due to the displacement to other places in search of food, directly related to the loss of the vegetation cover that previously served as a source of food and permanent or temporary shelter [46–49].

According to [6, 50], the negative impacts generated during the implementation of photovoltaic systems are mainly related to conflicts in land use, soil compaction, and the alteration of its physical and chemical properties, the erosion of its surface layer, the increased sediment load or turbidity in local aquatic ecosystems, reduced infiltration of air pollutants and rainwater, reduced groundwater recharge, and loss of soil organic carbon. The same authors state that there may also be a deficiency in the availability of water in the communities near the sites where these projects are implemented, as well as ecological effects associated with habitat fragmentation, loss of native vegetation cover, and animals and microbiota associated with this type of formation.

Photovoltaic system is important to highlight that these systems produce chemical contamination due to the use of heavy metals such as cadmium, selenium, lead, aluminum, tin, copper, chromium, and silver, during the manufacturing and final disposal after the panels have completed their life cycle [36, 51–53], which results worrying because some estimates suggest that in the year 2050 the hazardous solid waste generated by this type of energy system will be 80 million tons [54].

Strategic planning is an important factor to take into account when reducing the negative ecotoxicological and environmental impact of alternative energies implementation (Fig. 3), by avoiding the development and start up of these technologies within highly relevant and sensitive areas where biodiversity conservation are essential for supporting life in earth [55], as occurs in many areas of Latin America where some biodiversity hotspots are still conserved [56]. Likewise, the

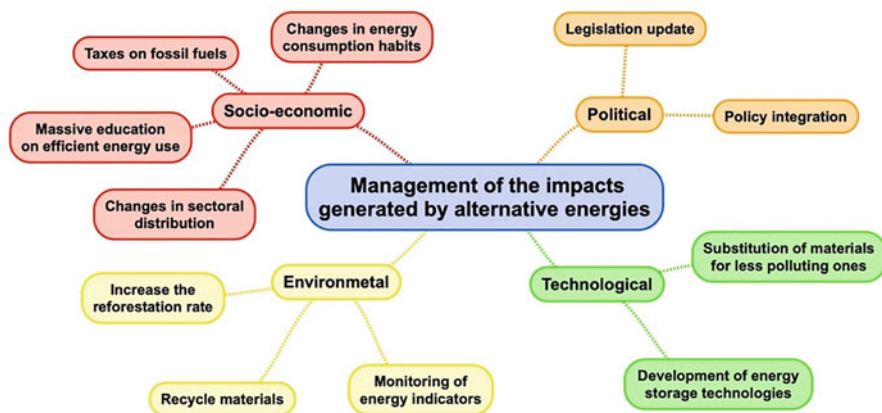


Fig. 3 Considerations on the management of the impacts generated by alternative energies



environmental education component must be strengthened, and the culture of change in energy consumption habits must be promoted, to reduce unnecessary energy demand and thus the carbon footprint.

Other aspects that authors such as Nazir et al. [5] propose to reduce the environmental impact of alternative energies include the use of energy management indicators and the integration of policies and regulations that regulate the use of hazardous materials or their replacement by others that are not during the construction of the devices energy production or at the time of final disposal.

## 5 Conclusions

Alternative energies contribute significantly to reducing the environmental impact of traditional energy production systems. However, these production methods also exert less weighting, but not insignificant, environmental, and ecotoxicological impacts, which is why it is necessary to improve knowledge in this regard, especially in areas with high ecological vulnerability such as tropical areas of Latin America.

Knowing the experiences of the effects associated with the implementation of alternative energy production projects is essential for their prevention in future projects of the same nature in Latin America.

Research is required to assess the true impact on different ecosystems, and knowing and prioritizing natural migration patterns of the species would likely help to plan and implement the alternative energy production technologies. A chain of events harmful to habitats, especially marine habitats, can be unleashed by just changing the energy contained in a wave. Moreover, underwater electromagnetic devices significantly affect marine species highly sensitive to changes in electromagnetic patterns.

## References

1. Luderer, G., Pehl, M., Arvesen, A., Gibon, T., Bodirsky, B., de Boer, H., Fricko, O., Hejazi, M., Humpenöder, F., Lyer, G., Mima, S., Mouratiadou, L., Pietzcker, R., Popp, A., van den Berg, M., van Vuuren, D., & Hertwich, E. (2019). Environmental co-benefits and adverse side-effects of alternative power sector decarbonization strategies. *Nature Communications*, 10(1), 1–13.
2. Kerr, D. (2007). Marine energy. *Philosophical Transactions. Series A, Mathematical, Physical, and Engineering Sciences*, 365(1853), 971–992. <https://doi.org/10.1098/rsta.2006.1959>
3. Dyatlov, S., Didenko, N., Ivanova, E., Soshneva, E., & Kulik, S. (2020). Prospects for alternative energy sources in global energy sector. In *IOP conference series: Earth and environmental science* (Vol. 434, No. 1, p. 012014). IOP Publishing.
4. Gibson, L., Wilman, E., & Laurance, W. (2017). How green is ‘green’ energy? *Trends in Ecology & Evolution*, 32(12), 922–935.
5. Nazir, M. S., Mahdi, A. J., Bilal, M., Sohail, H. M., Ali, N., & Iqbal, H. M. (2019). Environmental impact and pollution-related challenges of renewable wind energy paradigm – A review. *Science of the Total Environment*, 683, 436–444.







6. Dhar, A., Anne, M., Jennings, P., & Gamal, M. E. (2019). Perspectives on environmental impacts and A land reclamation strategy for solar and wind energy systems. *Science of the Total Environment*. <https://doi.org/10.1016/j.scitotenv.2019.134602>
7. Nazir, M., Ali, Z., Bilal, M., Sohail, H., & Iqbal, H. (2020). Environmental impacts and risk factors of renewable energy paradigm—A review. *Environmental Science and Pollution Research*, 27(27), 33516–33526.
8. Barbosa, L., Bogdanov, D., Vainikka, P., & Breyer, C. (2017). Hydro, wind and solar power as a base for a 100% renewable energy supply for South and Central America. *PLoS One*, 12(3), e0173820. <https://doi.org/10.1371/journal.pone.0173820>
9. Delmonte, N., Barater, D., Giuliani, F., Cova, P., & Buticchi, G. (2016). Review of oscillating water column converters. *IEEE Transactions on Industry Applications*, 52(2), 1698–1710. <https://doi.org/10.1109/TIA.2015.2490629>
10. Mustapa, M., Yaakob, O., Ahmed, Y., Rheem, C., Koh, K., & Adnan, F. (2017). Wave energy device and breakwater integration: A review. *Renewable and Sustainable Energy Reviews*, 77, 43–58.
11. López, I., Andreu, J., Ceballos, S., De Alegría, I. M., & Kortabarria, I. (2013). Review of wave energy technologies and the necessary power-equipment. *Renewable and Sustainable Energy Reviews*, 27, 413–434.
12. Wave Power. Available in: <https://inhabitat.com/portugal-wavepower-plant-goes-live/diagram-of-pelamis-wec/>
13. Hasan, M., & Manasseh, R. (2014). Dissipation in oscillating water columns. In *19th Australasian fluid mechanics conference*, Melbourne, Australia, pp. 8–11.
14. Inhabitat. Available in: <https://inhabitat.com/ocean-power-technologies-receives-federal-approval-for-the-first-commercial-wave-farm-in-the-us/opt-wave-farm-powerbuoy-150-ocean-power-visual-impact/>
15. Nuuttila, H. K., Bertelli, C. M., Mendzil, A., & Dearle, N. (2018). Seasonal and diel patterns in cetacean use and foraging at a potential marine renewable energy site. *Marine Pollution Bulletin*, 129(2), 633–644.
16. Greaves, D., Conley, D., Magagna, D., Aires, E., Leitão, J. C., Witt, M., Embling, C., Godley, B., Bicenell, A., Saulnier, J. B., Simas, T., O'Hagan, A., O'Callaghan, J., Holmes, B., Sundberg, J., Torre-Enciso, Y., & Marina, D. (2016). Environmental impact assessment: Gathering experiences from wave energy test centres in Europe. *International Journal of Marine Energy*, 14, 68–79.
17. Lin, L., & Yu, H. (2012). Offshore wave energy generation devices: Impacts on ocean bio-environment. *Acta Ecologica Sinica*, 32(3), 117–122.
18. Langhamer, O. (2010). Effects of wave energy converters on the surrounding soft-bottom macrofauna (west coast of Sweden). *Marine Environmental Research*, 69(5), 374–381.
19. Mendoza, E., Lithgow, D., Flores, P., Felix, A., Simas, T., & Silva, R. (2019). A framework to evaluate the environmental impact of ocean energy devices. *Renewable and Sustainable Energy Reviews*, 112, 440–449.
20. Klimley, A., Putman, N., Keller, B., & Noakes, D. (2021). A call to assess the impacts of electromagnetic fields from subsea cables on the movement ecology of marine migrants. *Conservation Science and Practice*, 3, e436.
21. Fisher, C., & Slater, M. (2010). *Effects of electromagnetic fields on marine species: A literature review*. Report by Oregon Innovation Council, 26p.
22. Buscaino, G., Mattiazzo, G., Sannino, G., Papale, E., Bracco, G., Grammata, R., Carillo, A., Kenny, J., De Cristofaro, N., & Mazzola, S. (2019). Acoustic impact of a wave energy converter in Mediterranean shallow waters. *Scientific Reports*, 9(1), 1–16.
23. Bergström, L., Kautsky, L., Malm, T., Rosenberg, R., Wahlberg, M., Capetillo, N. Å., & Wilhelmsson, D. (2014). Effects of offshore wind farms on marine wildlife—A generalized impact assessment. *Environmental Research Letters*, 9(3), 034012.
24. Willis, D., Niezrecki, C., Kuchma, D., Hines, E., Arwade, S., Barthelmie, R., Dipaola, M., Drane, P., Hansen, C., Inalpolat, M., Mack, J., Myers, A., & Rotea, M. (2018). Wind energy research: State-of-the-art and future research directions. *Renewable Energy*, 125, 133–154.

25. Mann, J., & Teilmann, J. (2013). Environmental impact of wind energy. *Environmental Research Letters*, 8(3), 035001.
26. Leung, D., & Yang, Y. (2012). Wind energy development and its environmental impact: A review. *Renewable and Sustainable Energy Reviews*, 16(1), 1031–1039.
27. Platteuw, M., Bakker, J., van den Bosch, I., Erkmann, A., Graafland, M., Lubbe, S., & Warnas, M. (2017). A framework for assessing ecological and cumulative effects (FAECE) of offshore wind farms on birds, bats and marine mammals in the southern North Sea. In *Wind energy and wildlife interactions* (pp. 219–237). Springer.
28. Jaber, S. (2013). Environmental impacts of wind energy. *Journal of Clean Energy Technologies*, 1(3), 251–254.
29. Scheidat, M., Tougaard, J., Brasseur, S., Carstensen, J., van Polanen Petel, T., Teilmann, J., & Reijnders, P. (2011). Harbour porpoises (*Phocoena phocoena*) and wind farms: A case study in the Dutch North Sea. *Environmental Research Letters*, 6(2), 025102.
30. Thomsen, F., Lüdemann, K., Kafemann, R., & Piper, W. (2006). *Effects of offshore wind farm noise on marine mammals and fish* (Vol. 62, pp. 1–62). Biola on behalf of COWRIE Ltd.
31. Rabaia, M., Abdelkareem, M., Sayed, E., Elsaid, K., Chae, K., Wilberforce, T., & Olabi, A. (2021). Environmental impacts of solar energy systems: A review. *Science of the Total Environment*, 754, 141989.
32. Kikuchi, R. (2008). Adverse impacts of wind power generation on collision behaviour of birds and anti-predator behaviour of squirrels. *Journal for Nature Conservation*, 16(1), 44–55.
33. Xu, Y., Li, J., Tan, Q., Peters, A., & Yang, C. (2018). Global status of recycling waste solar panels: A review. *Waste Management*, 75, 450–458.
34. Agathokleous, R., & Kalogirou, S. (2020). Status, barriers and perspectives of building integrated photovoltaic systems. *Energy*, 191, 116471.
35. Yin, W., Ming, Z., Wen, T., & Zhang, C. (2021). Photovoltaic curve management using demand response with long and short-term memory. *Energy*, 238, 121729.
36. Padmanathan, K., Govindarajan, U., Ramachandaramurthy, V. K., & Jeevarathnam, B. (2018). Integrating solar photovoltaic energy conversion systems into industrial and commercial electrical energy utilization—A survey. *Journal of Industrial Information Integration*, 10, 39–54.
37. Martinopoulos, G. (2018). Life cycle assessment of solar energy conversion systems in energetic retrofitted buildings. *Journal of Building Engineering*, 20, 256–263.
38. Pasqualino, J., Cabrera, C., & Vanegas Chamorro, M. (2015). The environmental impacts of folic and solar energy implementation in the Colombian Caribe. *PRO*, 13(1), 68–75.
39. Sahu, A., Yadav, N., & Sudhakar, K. (2016). Floating photovoltaic power plant: A review. *Renewable and Sustainable Energy Reviews*, 66, 815–824.
40. Vezmar, S., Spajić, A., Topić, D., Šljivac, D., & Jozsa, L. (2014). Positive and negative impacts of renewable energy sources. *International Journal of Electrical and Computer Engineering Systems*, 5(2), 47–55.
41. Varho, V. (2002). Environmental impact of photovoltaic electrification in rural areas. *Energy & Environment*, 13(1), 81–104.
42. Lepper, P., & Robinson, S. (2016). Measurement of underwater operational noise emitted by wave and tidal stream energy devices. In *The effects of noise on aquatic life II* (pp. 615–622). Springer.
43. Witt, M., Sheehan, E., Bearhop, S., Broderick, A., Conley, D., Cotterell, S., Crow, E., Grecian, J., Halsband, C., Hodgson, D., Hosegood, P., Inger, R., Miller, P., Sims, D., Thompson, R., Vanstaen, K., Votier, S., Attrill, M., & Godley, B. (2012). Assessing wave energy effects on biodiversity: The wave hub experience. *Philosophical Transactions of the Royal Society A: Mathematical, Physical and Engineering Sciences*, 370(1959), 502–529.
44. Schmidt, J., & Klokner, M. (2014). Health effects related to wind turbine noise exposure: A systematic review. *PLoS One*, 9(12), e114183.
45. Drewitt, A., & Langston, R. (2008). Collision effects of wind-power generators and other obstacles on birds. *Annals of the New York Academy of Sciences*, 1134(1), 233–266.

46. Desholm, M. (2009). Avian sensitivity to mortality: Prioritising migratory bird species for assessment at proposed wind farms. *Journal of Environmental Management*, *90*(8), 2672–2679.
47. Gaultier, S., Blomberg, A., Ijäs, A., Vasko, V., Vesterinen, E., Brommer, J., & Lilley, T. (2020). Bats and wind farms: The role and importance of the Baltic Sea countries in the European context of power transition and biodiversity conservation. *Environmental Science & Technology*, *54*(17), 10385–10398.
48. Román, P., Salinas, C., & Araújo, B. M. (2020). Assessing the effect of wind farms in fauna with a mathematical model. *Scientific Reports*, *10*(1), 1–11.
49. Celik, I., Mason, B. E., Phillips, A. B., Heben, M. J., & Apul, D. (2017). Environmental impacts from photovoltaic solar cells made with single walled carbon nanotubes. *Environmental Science & Technology*, *51*(8), 4722–4732.
50. Tammamaro, M., Salluzzo, A., Rimauro, J., Schiavo, S., & Manzo, S. (2016). Experimental investigation to evaluate the potential environmental hazards of photovoltaic panels. *Journal of Hazardous Materials*, *306*, 395–405.
51. Üçtuğ, F., & Azapagic, A. (2018). Environmental impacts of small-scale hybrid energy systems: Coupling solar photovoltaics and lithium-ion batteries. *Science of the Total Environment*, *643*, 1579–1589.
52. Yousef, S., Tatariants, M., Tichonovas, M., & Makarevicius, V. (2019). Sustainable technology for mass production of Ag nanoparticles and Al microparticles from damaged solar cell wafers. *Waste Management*, *98*, 126–134.
53. Chowdhury, M., Rahman, K., Chowdhury, T., Nuthammachot, N., Techato, K., Akhtaruzzaman, M., Kion, S., Sopian, K., & Amin, N. (2020). An overview of solar photovoltaic panels' end-of-life material recycling. *Energy Strategy Reviews*, *27*, 100431.
54. Kreidler, J., Schloss, C., Soong, O., Hannah, L., & Davis, F. (2015). Conservation planning for offsetting the impacts of development: A case study of biodiversity and renewable energy in the Mojave Desert. *PLoS One*, *10*(11), e0140226. <https://doi.org/10.1371/journal.pone.0140226>
55. Mittermeir, R., & Rylands, A. (2018). Biodiversity hotspots. In *Encyclopedia of the anthropocene* (pp. 67–75). Elsevier.
56. Kong, X., Zhou, Z., & Jiao, L. (2021). Hotspots of land-use change in global biodiversity hotspots. *Resources, Conservation and Recycling*, *174*, 105770.

# Design and Implementation of a Web-Based Residential Energy Assessment Platform: A Case Study in Cuenca, Ecuador



Willian Carrión-Chamba , Wilson Murillo-Torres ,  
Christian Naranjo-Ulloa , Katy Valdivieso-García ,  
Andrés Montero-Izquierdo , and Iván Acosta-Pazmiño 

## 1 Introduction

COVID-19 pandemic had a significant impact on energy consumption dynamics. Population confinement and the government's restrictive measures to control virus spread generated changes in electricity power-consuming patterns. Globally there was a 38% decrease in the short-term consumption trend during confinement and a 14.5% decrease during the reopening period, mainly caused by the shutdown and cessation of industrial and economic sectors [1, 2]. Nevertheless, in residential installations, energy demand increased by 30% during the isolation period [3]. The main factor is the increased use of energy-intensive systems during daylight hours, such as heating, air conditioning, lighting, and appliances. In confinement, the household electricity consumption increased by up to 30% in hours close to noon and 23% during typical working hours [4]. A study in New York City showed that total energy consumption in the industrial and commercial sectors decreased by approximately 7% during the pandemic period. However, household consumption increased by around 23% in March and 10% in April 2020 [5].

---

W. Carrión-Chamba · W. Murillo-Torres · C. Naranjo-Ulloa · K. Valdivieso-García ·  
A. Montero-Izquierdo (✉)

Grupo de Ingeniería de Reactores, Catálisis y Tecnologías del Medio Ambiente, Departamento  
de Biociencias, Universidad de Cuenca, Cuenca, Azuay, Ecuador  
e-mail: [willian.carrion@ucuenca.edu.ec](mailto:willian.carrion@ucuenca.edu.ec); [wilson.murillo@ucuenca.edu.ec](mailto:wilson.murillo@ucuenca.edu.ec);  
[christian.naranjo@ucuenca.edu.ec](mailto:christian.naranjo@ucuenca.edu.ec); [viviana.valdivieso@ucuenca.edu.ec](mailto:viviana.valdivieso@ucuenca.edu.ec);  
[andres.montero@ucuenca.edu.ec](mailto:andres.montero@ucuenca.edu.ec)

I. Acosta-Pazmiño

Tecnológico de Monterrey, Monterrey, Nuevo León, Mexico  
e-mail: [ivan.acosta.2015@ieee.org](mailto:ivan.acosta.2015@ieee.org)

Meanwhile, in Canada, the average daily electricity consumption in a residential household sample increased by 12% in 2020 compared to 2019 [6]. Similarly, research carried out in Huelva, Spain, showed that energy consumption from residential customers increased by around 15% during the total shutdown and 7.5% during the reopening period [1]. In Latin America and the Caribbean, final energy consumption decreased by approximately 9% due to containment measures between 2019 and 2020; however, energy consumption in the residential sector increased by 20% [7]. Ecuador also experienced an increment in electricity consumption in the residential area between March and August 2020; therefore, the consumption trend in this economic sector was the same for Cuenca [8]. According to data provided by the Empresa Eléctrica Regional Centro Sur C.A., for the year 2019, the electricity consumption in the residential sector in Cuenca was 265.9 GWh, from which 71.3% of energy consumption is represented by urban area. In 2020, energy consumption in Cuenca urban residential sector increased up to 193.8 GWh, unlike 2019 consumption, which was 189.4 GWh. In this context, on March 16th, there was a notable increase in average energy consumption per customer, where the maximum value throughout the year is recorded in May with 152 kWh; this is due to during the first 3 months of the sanitary emergency, the confinement measures were more restrictive [9] (Fig. 1). In May 2020, residential customers increased their electrical power consumption by 13%, taking the same month of the previous year [10]. Nevertheless, on the 25th of May, the city of Cuenca planned a flexible policy, going from red to yellow epidemiological traffic lights. In turn, the economy in the industrial and commercial sectors began to reactivate. It implied an increment in mobility and a reduction in household electricity consumption [11], in such a way that the average consumption per customer in August was 121 kWh. On September 13, the state of emergency ended [12], and in

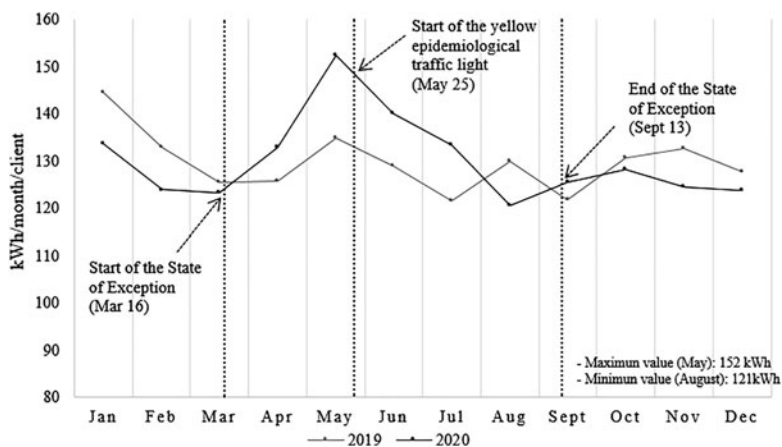


Fig. 1 Average monthly electricity consumption per customer in Cuenca

the urban area of Cuenca, electricity power consumption for the last 4 months of 2020 had a similar trend as in 2019.

Notably, during the time of confinement, the household electricity consumption profile had increased throughout the day. Nevertheless, no measures have been taken to ensure a sustainable energy supply to meet the required demand. Furthermore, the poor dissemination of energy-saving information and the high level of electricity subsidies are generally the leading causes of indifferent behavior toward the culture of reduction [13, 14]. To reduce energy intensity and absolute energy consumption, it is necessary to impose taxes or subsidize investment in more efficient technologies and propose incentives or even develop tools that contribute to generating changes in consumption habits [15]. Energy consumption in residential buildings can be reduced with energy-saving strategies such as energy sufficiency and efficiency. The first refers to the consumption of energy services at a level consistent with equity, welfare, and environmental limits [16, 17]. On the other hand, energy efficiency is a strategy consisting of using energy-efficient equipment without considering whether such equipment is used under sustainable consumption patterns [18]. Models have shown that the residential sector can achieve 48% savings in electricity consumption when efficient technology is implemented and consumption habits are improved [19]. Other research, such as Tonn's and Peretz's study, reports that energy efficiency practices in households reduce energy consumption by 20% [20]. In comparison, potential savings of 10–25% can be achieved when people adopt responsible consumption habits [21].

In this context, changes in energy consumption patterns in the residential sector resulting from the COVID-19 pandemic are a tipping point for accelerating environmental concern toward sustainable habits and behaviors in post-pandemic [22]. Therefore, energy assessment tools are alternatives that provide information, stimulate energy rationalization, and, with simplified language, allow quantifying electricity consumption in the residential sector. In Ecuador, there is no easy-to-use, easy-to-understand tools developed locally that enable consumers to counteract their lack of knowledge about electricity consumption regarding household appliances, which is one of the most important factors in total household consumption. The present work aims to evaluate energy savings and emission reduction in the residential sector of the city of Cuenca, Ecuador, through the design and implementation of an online platform to estimate electricity consumption and identify reduction opportunities. This tool can be further expanded to cover other cities inside Ecuador and other countries within the region.

## 2 Methods

The scope of the study covers urban residential areas of the city of Cuenca, which is located in the highlands at 2530 masl [23]. Cuenca is organized into 15 urban parishes with 99.64% electricity service coverage [24]. In Cuenca, single-family

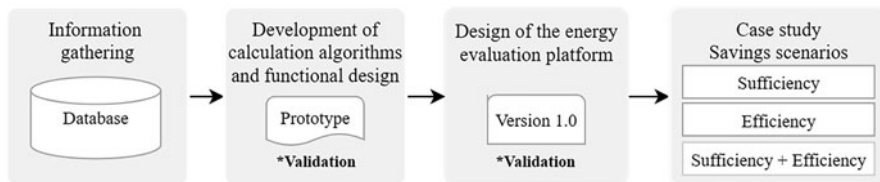


**Fig. 2** Methodology scheme

households represent 73.31% of residential construction with an average of 4.08 people per home [23, 25].

To design the online energy consumption platform, information related to main household appliances used in the residential sector of Cuenca, average electricity consumption, local cost of electricity, CO<sub>2</sub> emission factor, and electricity consumption reduction percentage is required. All the mentioned data, together with the energy sufficiency and efficiency measures, were collected. Based on these data, calculation algorithms, functional design of the prototype, and version 1.0 of the platform were developed. In Fig. 2, a general outline of the methodology applied in this research project is presented.

## 2.1 Data Collection

Electricity power savings and emission reduction assessment of Cuenca's residential sector began with a gathering of information on energy demand and technical specifications of commonly used household appliances. Different types of electronics and electric appliances that can be viewed and selected by platform users were obtained from digital surveys applied to 451 households in Cuenca. In this sense, the structure of the surveys based on semi-closed questions allowed access to quantitative data per household on electricity consumption, quantity, and time of daily use of household appliances. The specific sampling design applied is of the non-probabilistic opportunity sampling type, a sampling method considered due to the mobility difficulties and confinement measures generated by the COVID-19 pandemic. On the other hand, each appliance's model, power, and energy efficiency was obtained from a local household appliance retailer's database and different catalogs. In addition, the Technical Regulations of the Ecuadorian Institute of Standardization were reviewed to gain legal support and know which appliances comply with energy efficiency and labeling regulations.

To assess the energy reduction potential in housing, energy sufficiency and efficiency strategies were investigated. Saving percentages of these measures were extracted from academic sources and energy-saving and technical efficiency guides from certain organizations and countries. Saving strategies were organized according to household energy needs, taking into account six categories: heating,



**Table 1** Energy sufficiency measures

Categories	Energy sufficiency measures	Savings (%)	Sources
Water heating	Take regular showers for short periods (maximum 5 min)	20	[26]
Household appliances	Increase the freezer temperature by one degree Celsius	7.8	[27]
	Increase the temperature by one degree Celsius in the refrigeration compartment	2	
	Clean the back of the refrigerator	2	
	Place the refrigerator in a cool and ventilated place, away from possible heat sources: solar radiation, ovens, microwaves, stove, etc.	0.9	
	Do not open the refrigerator door unnecessarily	7	[28]
	Place the refrigerator at a distance of 15 cm between the back of the fridge and the wall	15	[29]
	Air dry clothes and do not tumble dry	100	
	Cook in containers with lids	25	[30]
Using the microwave instead of the conventional oven saves energy and time	60		
Technology and entertainment	Disconnect technological and entertainment equipment (TV, computers, consoles, etc.) when not in use	10	[31]

cooling, household appliances, lighting, sanitary water heating, and technology and entertainment. The application of energy sufficiency measures will depend on individual users' degree of interest, knowledge, and commitment to energy saving. Table 1 shows that sufficiency measures found have application in household appliances, water heating, and technology and entertainment categories.

In terms of energy efficiency, 14 strategies were considered, distributed in all categories. Applying these strategies has an investment cost that depends on the type of technology to be implemented. In general, the return on investment is only recognized after some time. Table 2 presents each of the considered energy efficiency measures and their respective savings percentages.

## 2.2 Calculation Algorithms

Before developing the platform, it was initially considered to integrate and test the calculation algorithms in a prototype developed in an Excel spreadsheet to test method functionality and effectiveness. Electricity consumption in homes is generated by lights, washing machines, refrigerators, showers, electric heaters, televisions, and computers. Calculation of monthly energy consumption derived from each appliance,  $E$ , is defined by Eq. 1:

**Table 2** Energy efficiency measures

Categories	Energy efficiency measures	Saving (%)	Sources
Space heating	Switch to an efficient portable electric heater	10	[29]
	If possible, install double-glazed windows	15	[32]
Water heating	Change the electric shower to a more efficient one (save water and energy)	15	[29]
Household appliances	Replace with a low energy consumption refrigerator (class A)	60	[27]
	Replace with a low energy consumption washing machine (class A)	30	[33]
	Buy cookers with induction plates because they consume less electricity than conventional glass-ceramics	20	[30]
	Replace the electric oven with one with low energy consumption (class A)	30	[29]
	Replace the microwave with a low-energy one (class A)	54	[34]
Space cooling	Switch to an air conditioner with inverter technology	60	[33]
	Install awnings on the windows where the sun shines the most, avoiding the entry of hot air into the house's interior and adequately insulating walls and ceilings	30	[30]
Lighting	Replace incandescent lamps with LEDs	85	[35]
	Replace fluorescent lamps with LEDs	60	[36]
	Incorporate lighting controllers (timers, occupancy sensors, dimmers)	20	[37]
Technology and entertainment	Replace the LCD TV with LED technology	40	[38]

$$E = P \cdot Q \cdot t \cdot f_1 \cdot f_2 \quad (1)$$

where  $P$  is the power for each appliance (Watt),  $Q$  is quantity per appliance type (units),  $t$  is daily usage time (hours),  $f_1$  is an energy conversion factor (1 kW/1000 W), and  $f_2$  is a time conversion factor (30 days/1 month). However, to determine a household's total energy consumption ( $E_T$ ), Eq. 2 is used, where  $i$  is a type of appliance,  $n$  indicates the total number of appliance types,  $j$  is one of the rooms,  $m$  is the total number of rooms, and  $E_{i1} + E_{i2} + E_{i3} + \dots + E_{nm}$  represent the set of electrical consumption values of the appliances in each room (kWh/month). Equation 2 provides more accurate consumption values since the total consumption is calculated based on the energy consumption per room. It is easier for the user to remember what equipment they have in their home:

$$E_T = \sum_{i=1}^n \sum_{j=1}^m E_{ij} = E_{i1} + E_{i2} + E_{i3} \dots + E_{nm} \quad (2)$$

The monthly value to be paid for electricity consumption,  $V_p$ , is determined with Eq. 3, where  $c$  is the tariff in USD per kWh applied according to the level of

consumption and as established in the current tariff schedule [39]. The annual CO<sub>2</sub> emissions generated by electricity consumption,  $G_e$ , are calculated with Eq. 4, where  $f_3$  is the time conversion factor (12 months/year) and  $F_e$  is the emission factor (0.4897 kgCO<sub>2</sub>/kWh) used [40]:

$$V_p = E_T \cdot c \quad (3)$$

$$G_e = E_T \cdot F_e \cdot f_3 \quad (4)$$

Once electricity consumption has been estimated, saving strategies can be applied to improve energy consumption in the household. Equations 5 and 6 establish the improved consumption with energy sufficiency,  $E_{se}$ , and the enhanced consumption with energy efficiency,  $E_{ee}$ , for each appliance, respectively. In the equations below,  $se$  denotes savings percentage with sufficiency, and  $ee$  represents savings percentage with energy efficiency for each appliance:

$$E_{se} = E \cdot \left(1 - \frac{se}{100}\right) \quad (5)$$

$$E_{ee} = E \cdot \left(1 - \frac{ee}{100}\right) \quad (6)$$

However, Eq. 7 shows improved consumption in a household when energy sufficiency and efficiency,  $E_{see}$ , are simultaneously applied:

$$E_{see} = E_{ee} \left(1 - \frac{se}{100}\right) \quad (7)$$

The prototype's calculation structure was validated by performing different calculation exercises to verify that the energy consumption reported in the electricity consumption plan of a household is similar to the value provided by the prototype.

### 2.3 Energy Assessment Platform Design

Once the calculation methodology was validated in the base prototype, a visual design of the web platform (<https://redies.com.ec/calculadora/>) was developed. This tool has interactive features that ensure easy understanding by non-specialized users to guide them toward an energy-saving culture. Residential energy assessment platform functionality is divided into three sequential stages (Fig. 3). The first one consists of collecting input data such as the type, quantity, power, and hours of daily use of the appliances according to the number of rooms in the house to make it easier for the user to identify the appliances in each room. In this first step, users can use default appliance power values or modify them according to the power specified on the label of each appliance in their home. With this input data, the platform will show the monthly estimate of the home's total energy consumption, consumption

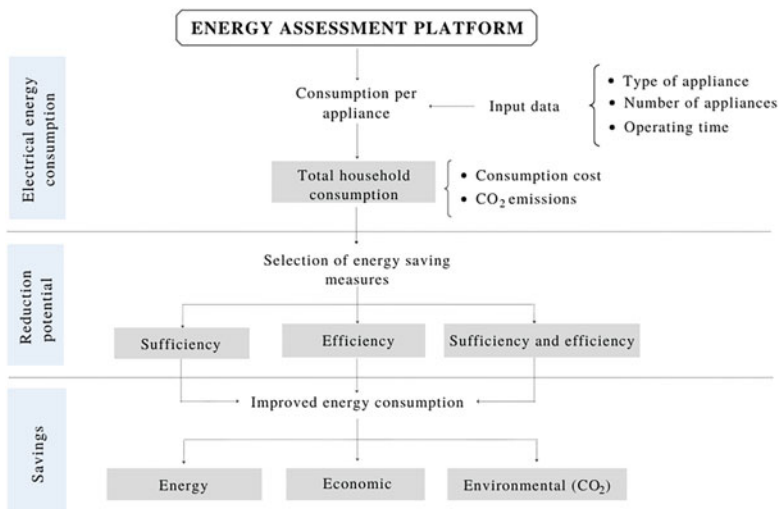


**Fig. 3** Energy assessment platform functional diagram

distributed by rooms and categories, the estimated cost for the electric service, and CO<sub>2</sub> emissions expressed as the annual equivalent that a vehicle can exhaust.

The second phase corresponds to the saving potential; here, the platform provides a series of energy efficiency and sufficiency measures to select and see the energy consumption reduction reflected. In the last stage, a detailed summary of the savings achieved in energy, economic, and environmental terms is presented on the platform. It also displays improved electricity consumption, percentage energy savings generated by the selected energy sufficiency and efficiency measures, and a pie chart showing improved consumption distribution by category (Fig. 4). Finally, to inform about the platform's existence and encourage a culture of energy saving in the population, in this last section, the user is given the option to share the findings of their energy evaluation experience through social networks.

To ensure the proper functioning of the platform, several test exercises were carried out until the results were congruent with the Excel prototype.

## 2.4 Case Study

The following is a case study based on data obtained from surveys conducted through digital media, so it should be noted that the results could be biased toward the upper-middle class stratum. The data show that 139 of the 451 respondents belong to families with four members, representing the average number of people in a household in Cuenca. Thus, the aim is to quantify the average consumption of a home and the reduction that can be achieved by applying the saving strategies available in the residential energy assessment platform.

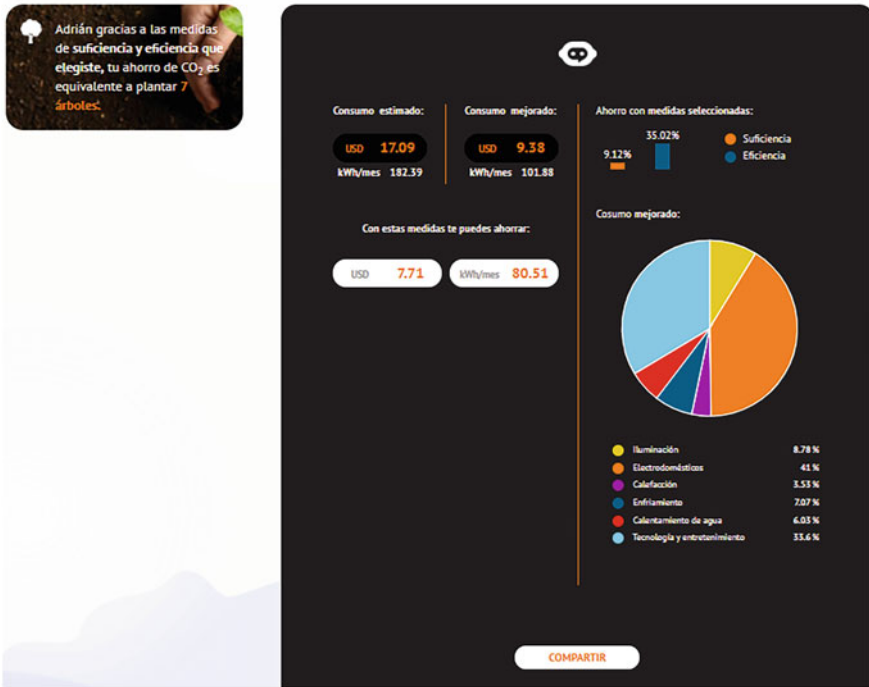


Fig. 4 Screenshot of platform results section (results in Spanish)

To determine energy-saving potential through the platform, it is necessary to know each appliance’s power and the daily number of usage hours. Most common equipment and time of use were obtained based on the surveys. To avoid using low or high power values in the appliances, an average power level was determined for each type of appliance using as reference the power of the efficient and non-efficient equipment available on the platform. Table 3 shows the power, quantity, and time of daily use of the appliances used to calculate the base consumption of a household in Cuenca.

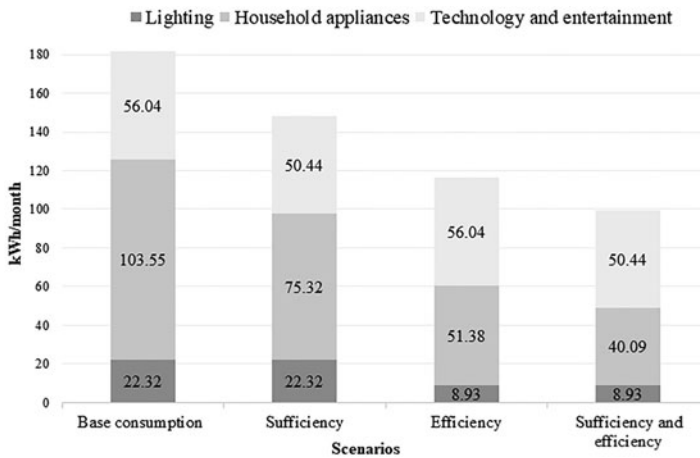
With the appliances’ technical information and using the energy platform, a typical or baseline consumption of a house in Cuenca was estimated. Once the average consumption of a household was estimated, sufficiency and efficiency scenarios and the integration of energy sufficiency and efficiency were evaluated to determine the reduction potential in energy, economic, and environmental terms.

**Table 3** Appliances used for the case study

Categories	Appliances	Power (Watt)	Quantity	Time of daily use
Household appliances	Refrigerator	339	1	8 h <sup>a</sup>
	Clothes washer	743	1	15 min <sup>b</sup>
	Vacuum cleaner	1800	1	15 min
	Microwave	1300	1	5 min
Technology and entertainment	LED TV	93	1	1 h
	Plasma TV	170	1	1 h
	Desktop PC	75	2	8 h
	Home audio system	135	1	3 h
Lighting	Luminaire	31	6	4 h

<sup>a</sup>Daily refrigerator run time is based on the proposal estimated by the United States Department of Energy (USDOE) [41]

<sup>b</sup>Daily usage time is based on washing machine usage twice a week with a 50–60 min wash cycle duration

**Fig. 5** Base consumption and energy consumption reduction scenarios

### 3 Results

Based on the information gathered, the results of this study show that the average electricity consumption in a typical upper-middle-class home in Cuenca is 182 kWh/month, which is equivalent to a cost for the service of 17.1 USD and an annual emission of 1068.9 kgCO<sub>2</sub>. Figure 5 shows that of the base consumption, the household appliances category represents 56.9% (103.55 kWh/month) of total electricity consumption, including the refrigerator, washing machine, microwave, and vacuum cleaner within this category. Technology and entertainment

**Table 4** Reduction potential analysis on base energy consumption in energy, economic, and environmental terms

Scenarios	Cost (USD)	CO <sub>2</sub> emissions (kg/year)	Energy-saving (%)	Monetary savings (USD)	CO <sub>2</sub> savings (kg/year)
Base consumption (BC)	17.1	1068.9	n.d.	n.d.	n.d.
BC + sufficiency	13.8	870.2	19	3.3	198.8
BC + efficiency	10.8	683.7	36	6.3	385.3
BC + sufficiency and efficiency	9.2	584.4	45	7.9	484.6

*Note:* The monetary values correspond only to the charge for electrical energy consumption and are based on the tariff schedule

(televisions, computers, and sound systems) occupies second place in the level of consumption with 30.8% (56.04 kWh/month), while luminaires contribute 12.3% of total energy consumption in the home. In addition, there is evidence of a gradual reduction in energy consumption as energy strategies are applied. At the same time, the household appliances category shows the highest percentage of savings in all scenarios comparatively because these appliances have the highest energy consumption, as is the case of refrigerators.

According to the above, applying energy sufficiency measures in a household in the city of Cuenca will have an improved consumption of 148 kWh/month, 116 kWh/month with energy efficiency measures, and 99 kWh/month applying the two measures, which in turn represent 19%, 36%, and 45% energy savings in the household, respectively (Table 4). In addition, with energy sufficiency, efficiency, and energy sufficiency-efficiency measures, the family can achieve monthly economic savings of about 3.3, 6.3, and 7.9 USD, respectively, and an annual reduction in emissions of up to 484.6 kg CO<sub>2</sub>/year could be achieved with energy sufficiency-efficiency measures.

In household appliances, energy sufficiency measures were targeted at the refrigerator as the appliance with the highest consumption. These strategies included increasing by one degree Celsius in the freezer and refrigeration compartment, cleaning the back, avoiding opening the door unnecessarily, placing the refrigerator away from potential heat sources, and placing it at a 15-centimeter distance from the wall. As for the technology and entertainment category, the measure applied was disconnecting these appliances on standby. On the other hand, replacing high-consumption appliances and devices with Class A labeling was proposed to evaluate savings with energy efficiency measures.

## 4 Discussion

The platform is a dynamic and easy-to-use web tool designed to be used by residential users in Cuenca's urban area to evaluate the electricity consumption in their homes. The particularity of this tool is that it orients the user toward a saving culture based not only on efficiency measures but also on energy sufficiency. It allows evaluating electricity consumption reduction according to family solvency. In addition, it reflects the results of energy savings in monetary and environmental terms, which can be very useful for users to understand the economic benefits and generate awareness within the family environment about the importance of reducing greenhouse gas emissions. These innovative features and advantages extend and improve the functionalities provided by other web tools such as "Planillita" developed by the Electricity Regulation and Control Agency in Ecuador [42], the "Edenor Simulator" of Argentina [43], and the "Energy Calculator" of the Ministry of Energy and Mines of Peru [44]. They only have functions that integrate the calculation of the monthly electricity consumption and the service cost without providing information to the user on the energy, economic, and environmental savings that can be achieved if consumption reduction strategies are applied.

Based on the proposed case study, the results show that the average consumption of a house in Cuenca is 182 kWh/month and that by using the platform to determine the potential for reduction according to energy sufficiency, efficiency, and sufficiency-efficiency scenarios, a reduction of 19%, 36% and 45% in electrical consumption can be achieved. These results are consistent with those reported by Baquero and Quesada [23]. They determined that by applying basic strategies such as replacing electrical appliances with efficient equipment, taking advantage of natural lighting, and replacing conventional lighting fixtures with LEDs, a 46% maximum electricity saving of total consumption is achieved. However, the average consumption for a home in Cuenca determined from this work is 10.66% higher than the value reflected in our study. Another research conducted in Bogotá, Colombia, showed that, by applying a model of demand management strategies, consumption reductions from 7% to 19% are achieved when residential users change their consumption habits. The reduction goes from 6% to 26% when replacing devices and 17% to 45% of total savings combined with energy sufficiency and efficiency strategies [45].

However, it should be noted that the platform calculates consumption reduction potential based on energy efficiency and sufficiency saving percentages extracted from academic sources. Although the values may be determined in different conditions and contexts, it can be considered that the first version of the electricity consumption calculator generates valuable insights to encourage electricity savings in residential customers. As for the source of the appliance list displayed on the platform, the database of a local retailer and various equipment catalogs were included. The advantage of having a first complete local inventory of electrical and electronic equipment is the possibility of showing to the user appropriate data according to the study area with relatively little specific information. However, this



data can be modified as new information becomes available until a sufficiently nourished database is consolidated.

Finally, the accuracy of electricity consumption calculation and the potential savings after using the residential energy assessment platform will depend on the accuracy level of the appliance usage time, power according to the efficiency level, and the number of strategies that the user applies to the equipment present in the household.

## 5 Conclusions

In this paper, we have presented the development of the first version of a residential energy assessment platform that allows a dynamic and simple way to estimate the electricity consumption of households in Cuenca. This tool has 11 sufficiency measures and 14 energy efficiency measures distributed in six consumption categories, so that the user can evaluate the potential energy, economic, and environmental savings. Concerning this case, which determined that the average consumption in a typical upper-middle-class house in Cuenca is 182 kWh/month and evaluating the reduction potential for this consumption with the scenario that integrates energy sufficiency and efficiency, it is possible to achieve 45% of energy savings. It represents a monthly saving of 7.9 USD in the payment of the electricity bill and a reduction in emissions of 484.6 kg CO<sub>2</sub>/year. However, when evaluating the energy sufficiency scenario where no investment is required, a 19% reduction in energy consumption can be achieved. A monetary saving of 3.3 USD and the annual emission of 198.8 kg CO<sub>2</sub> into the atmosphere can be avoided. These results demonstrate how energy sufficiency and efficiency contribute to managing electricity demand in the residential sector. Finally, as future work, it has been planned to carry out acceptance tests of the platform and a statistical analysis on the estimates of electricity consumption, electricity savings, and CO<sub>2</sub> emissions using the record of information provided by the users through the platform. In addition, we intend to conduct pilot tests with distribution and commercialization agents (electricity companies) to extend the application to other cities in Ecuador.

**Acknowledgments** The authors wish to thank to Senescyt and Deutsche Gesellschaft für Internationale Zusammenarbeit (GIZ) for funding the Project “Plataforma de evaluación energética residencial.” Also, this project was co-financed by the Dirección de Investigación (DIUC) of Universidad de Cuenca, Cuenca-Ecuador.

## References

1. García, S., Parejo, A., Personal, E., Guerrero, J. I., Biscarri, F., & León, C. (2021). A retrospective analysis of the impact of the COVID-19 restrictions on energy consumption at a disaggregated level. *Applied Energy*, 287, 116547. <https://doi.org/10.1016/j.apenergy.2021.116547>

2. Kang, H., An, J., Kim, H., Ji, C., Hong, T., & Lee, S. (2021). Changes in energy consumption according to building use type under COVID-19 pandemic in South Korea. *Renewable and Sustainable Energy Reviews*, 148, 111294. <https://doi.org/10.1016/j.rser.2021.111294>
3. Krarti, M., & Aldubyan, M. (2021). Review analysis of COVID-19 impact on electricity demand for residential buildings. *Renewable and Sustainable Energy Reviews*, 143, 110888. <https://doi.org/10.1016/j.rser.2021.110888>
4. Chen, C., Zarazua de Rubens, G., Xu, X., & Li, J. (2020). Coronavirus comes home? Energy use, home energy management, and the social-psychological factors of COVID-19. *Energy Research & Social Science*, 68, 101688. <https://doi.org/10.1016/j.erss.2020.101688>
5. The Earth Institute, Columbia University. *New data suggest COVID-19 is shifting the burden of energy costs to households*. <https://news.climate.columbia.edu/2020/04/21/covid-19-energy-costs-households/>. Last accessed 29 July 2021.
6. Abdeen, A., Kharvari, F., O'Brien, W., & Gunay, B. (2021). The impact of the COVID-19 on households' hourly electricity consumption in Canada. *Energy and Buildings*, 250, 111280. <https://doi.org/10.1016/j.enbuild.2021.111280>
7. García, F., Moreno, A., & Schuschny, A. (2020). *Análisis de los impactos de la pandemia del COVID-19 sobre el Sector Energético de América Latina y el Caribe*. OLADE.
8. Gobierno de la República del Ecuador.: *El Gobierno asumirá el valor del consumo extra de energía eléctrica generado durante la emergencia sanitaria*. <https://www.comunicacion.gob.ec/el-gobierno-asumira-el-valor-del-consumo-extra-de-energia-electrica-generado-durante-la-emergencia-sanitaria/>. Last accessed 4 June 2021.
9. Gobierno de la República del Ecuador. (2020). Decreto Ejecutivo 1017 Declaración del estado de excepción por calamidad pública en todo el territorio nacional. [https://www.defensa.gob.ec/wp-content/uploads/downloads/2020/03/Decreto\\_presidencial\\_No\\_1017\\_17-Marzo-2020.pdf](https://www.defensa.gob.ec/wp-content/uploads/downloads/2020/03/Decreto_presidencial_No_1017_17-Marzo-2020.pdf)
10. Neira, M. (2021). Consumo de energía eléctrica del cantón Cuenca de los años 2018, 2019 y 2020. Interview with Marcelo Neira. April 30, 2020.
11. Gobierno Autónomo Descentralizado Municipal del Cantón Cuenca. *Con semáforo amarillo, mercados y plazas de Cuenca incorporan plan de retorno progresivo*. <http://www.cuenca.gob.ec/?q=content/con-sem%C3%A1foro-amarillo-mercados-y-plazas-de-cuenca-incorporan-plan-de-retorno-progresivo>.
12. Gobierno de la República del Ecuador. (2020). Decreto Ejecutivo 1026 Renovar el estado de excepción por calamidad pública en todo el territorio nacional. <https://asobanca.org.ec/wp-content/uploads/2021/07/DECRETO-1127-Renovacion-estado-de-excepcion-por-30-dias-1.pdf>
13. Shimoda, Y., Yamaguchi, Y., Iwafune, Y., Hidaka, K., Meier, A., Yagita, Y., Kawamoto, H., & Nishikiori, S. (2020). Energy demand science for a decarbonized society in the context of the residential sector. *Renewable and Sustainable Energy Reviews*, 132, 110051. <https://doi.org/10.1016/j.rser.2020.110051>
14. Suástegui Macías, J. A., Pérez Tello, C., Acuña Ramírez, A., Lambert Arista, A. A., Magaña Almaguer, H. D., Rosales Escobedo, P. F., & Ruelas Puente, A. H. (2018). Assessment of electrical saving from energy efficiency programs in the residential sector in Mexicali, Mexico. *Sustainable Cities and Society*, 38, 795–805. <https://doi.org/10.1016/j.scs.2018.01.031>
15. Santiago, I., Moreno-Munoz, A., Quintero-Jiménez, P., García-Torres, F., & Gonzalez-Redondo, M. J. (2021). Electricity demand during pandemic times: The case of the COVID-19 in Spain. *Energy Policy*, 148, 111964. <https://doi.org/10.1016/j.enpol.2020.111964>
16. Sorrell, S., Gatersleben, B., & Druckman, A. (2020). The limits of energy sufficiency: A review of the evidence for rebound effects and negative spillovers from behavioural change. *Energy Research & Social Science*, 64, 101439. <https://doi.org/10.1016/j.erss.2020.101439>
17. Darby, S., & Fawcett, T. (2018). *Energy sufficiency: An introduction*. Environmental Change Institute.
18. Lorek, S., & Spangenberg, J. H. (2019). Energy sufficiency through social innovation in housing. *Energy Policy*, 126, 287–294. <https://doi.org/10.1016/j.enpol.2018.11.026>

19. Escobar, P., Martínez, E., Saenz-Díez, J. C., Jiménez, E., & Blanco, J. (2020). Modeling and analysis of the electricity consumption profile of the residential sector in Spain. *Energy and Buildings*, 207, 109629. <https://doi.org/10.1016/j.enbuild.2019.109629>
20. Tonn, B., & Peretz, J. H. (2007). State-level benefits of energy efficiency. *Energy Policy*, 35, 3665–3674. <https://doi.org/10.1016/j.enpol.2007.01.009>
21. Zhang, Y., Bai, X., Mills, F. P., & Pezzey, J. C. V. (2018). Rethinking the role of occupant behavior in building energy performance: A review. *Energy and Buildings*, 172, 279–294. <https://doi.org/10.1016/j.enbuild.2018.05.017>
22. Severo, E. A., De Guimarães, J. C. F., & Dellarmelin, M. L. (2021). Impact of the COVID-19 pandemic on environmental awareness, sustainable consumption and social responsibility: Evidence from generations in Brazil and Portugal. *Journal of Cleaner Production*, 286, 124947. <https://doi.org/10.1016/j.jclepro.2020.124947>
23. Baquero, M., & Quesada, F. (2016). Eficiencia energética en el sector residencial de la Ciudad de Cuenca, Ecuador. *MSKN*, 7, 147–165. <https://doi.org/10.18537/mskn.07.02.11>
24. Gobierno Autónomo Descentralizado Municipal del Cantón Cuenca. (2015). *Plan de Desarrollo y Ordenamiento Territorial del cantón Cuenca*. [http://app.sni.gob.ec/sni-link/sni/PORTAL\\_SNI/data\\_sigad\\_plus/sigadplusdocumentofinal/0160000270001\\_documento%20completo\\_13-03-2015\\_10-31-46.pdf](http://app.sni.gob.ec/sni-link/sni/PORTAL_SNI/data_sigad_plus/sigadplusdocumentofinal/0160000270001_documento%20completo_13-03-2015_10-31-46.pdf)
25. Guillén-Mena, V., & Quesada, F. (2019). Assessment model of energy performance in housing of Cuenca, Ecuador. *Ain Shams Engineering Journal*, 10, 897–905. <https://doi.org/10.1016/j.asej.2019.03.010>
26. Codema: *Guide to home energy savings. Simple tips to get you saving today*. (2020). [https://www.codema.ie/images/uploads/docs/2020\\_Guide\\_to\\_Home\\_Energy\\_Savings.pdf?fbclid=IwARILxmPYftriiQiqzwaAPK8nMHH1ouGEWtEOSnVIPVcdROloH5fbWjy92Jlk](https://www.codema.ie/images/uploads/docs/2020_Guide_to_Home_Energy_Savings.pdf?fbclid=IwARILxmPYftriiQiqzwaAPK8nMHH1ouGEWtEOSnVIPVcdROloH5fbWjy92Jlk)
27. Belman-Flores, J. M., Pardo-Cely, D., Elizalde-Blancas, F., Gallegos-Muñoz, A., Pérez-García, V., & Gómez-Martínez, M. A. (2019). Perspectives on consumer habits with domestic refrigerators and its consequences for energy consumption: Case of study in Guanajuato, Mexico. *Energies*, 12, 860. <https://doi.org/10.3390/en12050860>
28. Khan, M. I. H., & Afroz, H. M. M. (2014). An experimental investigation of door opening effect on household refrigerator: The perspective in Bangladesh. *Asian Journal of Applied Sciences*, 7, 79–87. <https://doi.org/10.3923/ajaps.2014.79.87>
29. Ulloa Arízaga, E. (2015). *Eficiencia del Consumo Eléctrico en el Sector Residencial Urbano de Cuenca*. <http://dspace.ucuenca.edu.ec/handle/123456789/22992>
30. IDAE. (2010). *Guía Práctica de la Energía Consumo eficiente y responsable*. [https://www.idae.es/uploads/documentos/documentos\\_11406\\_Guia\\_Practica\\_Energia\\_3ed\\_A2010\\_509f8287.pdf](https://www.idae.es/uploads/documentos/documentos_11406_Guia_Practica_Energia_3ed_A2010_509f8287.pdf)
31. CONUEE, PROFECO. (2014). *Revista del consumidor*. [https://issuu.com/profeco/docs/revista\\_del\\_consumidor\\_conuee\\_151](https://issuu.com/profeco/docs/revista_del_consumidor_conuee_151)
32. Ríos, A., Guamán, J., & Vargas, C. (2018). Análisis de la Implementación de una Estrategia de Reducción del Consumo Energético en el Sector Residencial del Ecuador: Evaluación del Impacto en la Matriz Energética. *Revista Técnica “energía”*, 15, 98–109. <https://doi.org/10.37116/revistaenergia.v15.n1.2018.328>
33. Galarza-Chacón, L., & Mera-Gencón, C. (2012). *Ahorro y Eficiencia de Energía en el Sector Residencial de Guayaquil*. <https://www.dspace.espol.edu.ec/handle/123456789/24296?mode=full>
34. Servicio Ecuatoriano de Normalización INEN. (2014). RTE INEN 123 Eficiencia energética para hornos microondas. <https://www.normalizacion.gob.ec/buzon/reglamentos/RTE-123.pdf>
35. OCDE, AIE, BID. (2016). *25 Ideas brillantes para eficiencia energética en América Latina y el Caribe*. <https://publications.iadb.org/publications/spanish/document/25-ideas-brillantes-para-eficiencia-energ%C3%A9tica-en-Am%C3%A9rica-Latina-y-el-Caribe.pdf>
36. Avella, J., Souza, T., & Silveira, J. (2015). A comparative analysis between fluorescent and LED illumination for improve energy efficiency at IPBEN building. In *Efficient use of energy/ power quality*. Ministério da Cultura.

37. ONU. (2018). *Aceleración de la adopción mundial de la iluminación energéticamente eficiente. Organización de las Naciones Unidas*. <https://united4efficiency.org/wp-content/uploads/2017/04/Lighting-Policy-Guide-Spanish-20180201.pdf>
38. García, J. C. S., & Rodrigo, J. S. (2021). Química Computacional al servicio de la innovación y el desarrollo sostenible: Investigando nuevos mecanismos de emisión de luz con aplicaciones en OLEDs. *Anales de Química de la RSEQ*, 117, 29–29.
39. Agencia de Regulación y Control de Electricidad. (2020). *Pliego Tarifario para las Empresas Eléctricas de Distribución Servicio Público de Energía Eléctrica*. <https://www.regulacionelectrica.gob.ec/resoluciones-pliegos-tarifarios/>
40. Comisión Técnica de determinación de Factores de Emisión de Gases de efecto invernadero. (2019). Factor de Emisión de CO2 del Sistema Nacional Interconectado de Ecuador, Ecuador.
41. United States Department of the Energy. *Estimating appliance and home electronic energy use*. <https://www.energy.gov/energysaver/estimating-appliance-and-home-electronic-energy-use>. Last accessed 4 Oct 2021.
42. Agencia de Regulación y Control de Electricidad. *Planillita Calcula y Ahorra*. <https://planilla-electrica.herokuapp.com/#/calculo-factura>. Last accessed 18 Aug 2021.
43. Edenor. *Simulador de consumo Edenor*. <https://simulador.edenor.com>. Last accessed 5 Feb 2021.
44. Ministerio de Energía y Minas del Perú. *Calculadora energética*. <http://eficienciaenergetica.minem.gob.pe/calculadora/>. Last accessed 18 Aug 2021.
45. Pavas Martínez, F. A., Gonzalez Vivas, O. A., & Sanchez Rosas, Y. S. (2017). Cuantificación del ahorro de energía eléctrica en clientes residenciales mediante acciones de gestión de demanda. *Revista UIS Ingenierías*, 16, 217–226. <https://doi.org/10.18273/revuin.v16n2-2017020>

# Analysis and Evaluation of Energy Efficiency in Buildings Based on Building Information Modeling



Vicente Macas-Espinosa , Landie Vera-Rodríguez ,  
and Julio Barzola-Monteses 

## 1 Introduction

The increment in the concentration of carbon dioxide in the atmosphere and its effects on change of temperature of earth is a worldwide topic of great interest. The CO<sub>2</sub> emissions related to energy consumption in buildings have increased in the last years after having remained constant between 2013 and 2016. Direct and indirect emissions from the use of electricity and heat were close to 10.1 GtCO<sub>2</sub> in 2019, an 8.6% of increment in relation to 2010 and a 31.16% of increment in relation to 2000 according to reference [1].

Some of the main factors that have contributed to this increase are the energy demand amplification for heating and cooling, the increment in the purchase of air conditioning equipment, and the extreme climatic conditions [1]. In 2018, worldwide, the residential sector registered 21% of the total energy consumed, while the commercial and public services sector registered 8%. These two sectors together represented energy consumption in buildings at 29%, after the industrial sector (38%) and transport (29%) [2]. In Ecuador, in terms of final energy consumption, the residential sector registers a consumption of 13.43% and the commercial and public services sector 7.91%, and as a result 21.34% is the final energy use for buildings [3].

---

V. Macas-Espinosa (✉) · L. Vera-Rodríguez  
Facultad de Arquitectura y Urbanismo, University of Guayaquil, Guayaquil, Ecuador  
e-mail: [vicente.macase@ug.edu.ec](mailto:vicente.macase@ug.edu.ec)

J. Barzola-Monteses  
Artificial Intelligence and Information Technology Group, University of Guayaquil, Guayaquil,  
Ecuador

Department of Computer Science and Artificial Intelligence, Escuela Técnica Superior de Ingenierías Informática y de Telecomunicación, Universidad de Granada, Granada, Spain

Considering what was stated in the previous paragraphs, the Ecuadorian government approved an energy efficiency law in March 2019. Among the sectors regulated by this law, energy efficiency in buildings (EEB) is considered part of the regulation [4]. In the last 5 years, EEB has been a research field highly driven by interdisciplinary research groups [5–13]. Energy use intensity (EUI) is a quantification approach to compare the energy performance of similar buildings and evaluate their design against standard benchmarks [14]. The energy intensity in the building sector (the final energy per square meter) has been decreasing up to 1% annually since 2010, being considered insufficient, since the average growth in the area of buildings borders 2.5%.

The EUI is a widely used indicator in energy efficiency studies in buildings. One way to calculate the EUI is through computational tools based on building information modeling (BIM). BIM is a process of development of a digital model that includes information associated with the physical and functional characteristics of the building and in which architects, engineers, and the construction industry participate, providing efficiency design, construction, and operability in the three phases: pre-construction, construction, and post-construction [15].

In the case of existing buildings, the modernization strategy is considered as an opportunity to reduce global energy consumption and greenhouse gas emissions. This rehabilitation must be technically and economically feasible. BIM plays an important role for these feasibility analyses [16]. The objective of this research is to model the building of the Faculty of Mathematical and Physical Sciences through BIM-type software, to parameterize the construction materials and their envelope, in order to carry out the energy evaluation creating different scenarios according to the materials used.

## 2 Methodology

### 2.1 Description of the Building to Be Analyzed

The studied building is the one for the Faculty of Physical and Mathematical Sciences of the University of Guayaquil that was built between 1949 and 1952 [17] and which has the classrooms, laboratories, and administrative offices.

The three-story building is located in a scattered urban plot with characteristics of an isolated plot of land, without a courtyard, with galleries in one section, a central hallway, stairs in the middle on the left and on the right side, and green areas in the surrounding area. With some measurements made with an electrical energy analyzer, it was determined that the building consumes approximately in a range from 1.383 to 1935 kWh of electrical energy in an average working day [10].

Considering the study of this building, Fig. 1b shows the phases and processes developed for the elaboration of geometric model and the energy simulations.

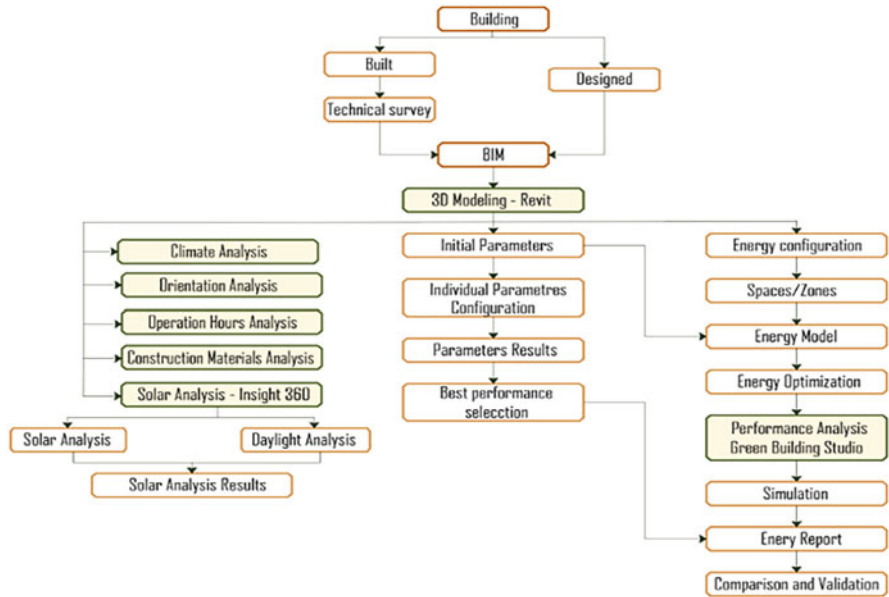


Fig. 1 Process flow diagram for FCMF building 3D modeling

The design of the building corresponds to its current construction, as well as the spaces and their respective distribution. The building has two blocks, the first block with three levels and a mezzanine, while the second block has five levels.

First floor: distributed by hall; lobby; classrooms of 78.21 m<sup>2</sup>, 58.58 m<sup>2</sup>, 22.04 m<sup>2</sup>, and 28.85 m<sup>2</sup>; a multiple classroom of 72.60 m<sup>2</sup>; administrative office; sanitary facilities; laboratories; library; conference room; reading rooms; and storage room.

## 2.2 Development Phases

The process in Fig. 1 begins by making a difference between a constructed building (in operation) and one in the design stage; this study case will be the first. For this reason, it begins with the review of the available two-dimensional architectural drawings and carrying out the information site survey, this with the aim of constructing the three-dimensional building model in the Revit BIM software. Then the initial configuration of the model in BIM will be performed, the project information is entered, the construction parameters and materials used are being configured, and finally the spaces configuration and areas of the building are carried out.

Once the model is finished, the first analysis begins, which is the climate analysis is carried out, where the sun’s path is considered through the solar diagram, the elevation in meters above sea level, the average incident solar energy, the perceived

and relative humidity, the minimum, maximum and average temperature, through [18], and the graphics of the wind rose showing direction and speed unit.

The orientation analysis and its influence on energy consumption are then carried out, since it examines the solar incidence on the envelope and the effect on the facade heating, as well as the use of the entrance of natural light and the incident winds.

Based on the measurement of the electrical parameters carried out with an energy analyzer, power will be taken as a starting point to examine how the hours of current operation of the building contributes directly to the energy consumption. In addition, another operating scenario will be simulated by varying the hours and days as 12/7, 24/7, 12/6, and 12/5 (h/day).

The materials of the construction elements play a very important role in the energy evaluation, which is why a survey is carried out to know the construction materials of the building such as walls, floors, roofs, windows, and doors.

These elements are decomposed into sub-elements in order to determine their conductivity and thermal resistance, which will be parameterized in the Revit software for energy simulation.

Details of possible materials are elaborated for the set of elements that make up the building, these materials are taken according to the range of local use, and the physical characteristics of the materials are indicated such as thermal conductivity, specific heat, density, thickness, and heat transfer.

Finally, in the analysis of solar incidence, the study of cumulative insolation is carried out to determine the suitability of the location of the current main facade; likewise, the analysis of daylight analyzes the percentage of natural light entry per floor, taking as a reference the international LEED regulation.

### ***2.3 3D Building Modeling and Revit Energy Analysis Simulation Tool***

The construction modeling of this project is made of an already built edification, currently a heritage building, in which was obtained two-dimensional plans, measurements, and spaces through an on-site survey, in which it is considered to add the characteristics of existing materials in the building, which were provided by the Ministry of Heritage and Culture through the building's heritage file [14].

Energy simulation helps to analyze the movement of energy in, out, and through the rooms and volumes in a building model. Whole building energy simulation measures expected energy use (fuel and electricity) based on the building's geometry, climate, building type, envelope properties, and active systems (HVAC & Lighting). Revit uses Green Building Studio Software, which is a flexible cloud-based service that uses the DOE2 simulation engine, a widely used and accepted freeware building energy analysis program that can predict the energy use and cost for all types of buildings.



## 2.4 Initial Settings

The Revit program considers several conditions when performing the energy analysis, such as the type of building being modeled, in which it defines parameters according to the category of building that is established. As the faculty is a university building, “Educational Center” is chosen as the type of building in which the general parameters are the number of people per 100 m<sup>2</sup>, in this case 25 people, as well as an increase in latent heat, load density of equipment or internal infrastructure of the building, among others. Using these parameters in spaces that have not been previously defined is considered as limit values.

In order to know which materials were used for the building’s construction, we accessed to the heritage file that is provided by the heritage institute in Guayaquil, whose file indicates each of the materials that the building is made of in both floors, slabs, roofs, walls, windows, doors, stairs, and others. This asset file can be reviewed in the annexes attached to this document. The values of heat transfer coefficient (U) and thermal resistance (R) are determined according to the thermal characteristics of each material and also considering its thickness.

Table 1 shows the configuration in the Revit software of the existing building components.

In general, in terms of floor space occupied, there are 155 spaces, which are grouped into areas by common spaces and total on each floor, Zone 1: auditorium, Zone 2: classrooms, Zone 3: library, Zone 4: circulation, Zone 5: offices, Zone 6: auxiliary room, Zone 7: technical room, and Zone 8: services.

**Table 1** Building type information entered into Revit

Parameter	Default value
Occupancy planning table	Educational center – 8 AM to 9 PM
Lighting/equipment planning char	Educational center – 7 AM to 9 PM
People/100 m <sup>2</sup>	25
Human activity level	Standing, light work, walking
Increase in heat due to the presence of people (W/person)	73
Latent heat increase due to the presence of people (W/person)	59
Lighting load density (W/m <sup>2</sup> )	12.92
Equipment load density (W/m <sup>2</sup> )	16.15
Radiant percentage of electrical equipment	0.5
Carpet (S/N)	N
Type of conditioning	Cooling
L/s of outside air per person	8
Outdoor air flow per area (m <sup>3</sup> /h/m <sup>2</sup> )	3.7
Unoccupied cooling setting position (F)	85

## 2.5 Climate Analysis

Guayaquil has a latitude of  $2^{\circ}12'36''$  South and longitude  $79^{\circ}54'00''$  West; in Fig. 2, two seasons per year are shown—the hottest season is considered from March 7 to May 8 which lasts approximately 2 months, with an average daily temperature greater than  $30^{\circ}\text{C}$  determining the hottest day of the year on April 3 with an average maximum temperature of  $3^{\circ}\text{C}$  and minimum of  $24^{\circ}\text{C}$  average and the coolest season is considered from June 17 to August 20 which lasts more than 2 months approximately, with an average daily temperature lower than  $29^{\circ}\text{C}$  determining the coldest day of the year on August 20 with an maximum average temperature of  $29^{\circ}\text{C}$  and average minimum of  $21^{\circ}\text{C}$ .

## 3 Results

### 3.1 Solar Analysis

The solar analysis is carried out on the winter and summer solstice dates; one was the accumulative insolation on all the facades of the envelope, considering the climatic seasons and the facades with the highest solar incidence, while the other was the final performance, which consists of the amount of natural light that enters into the building per floor through openings, doors, or windows.

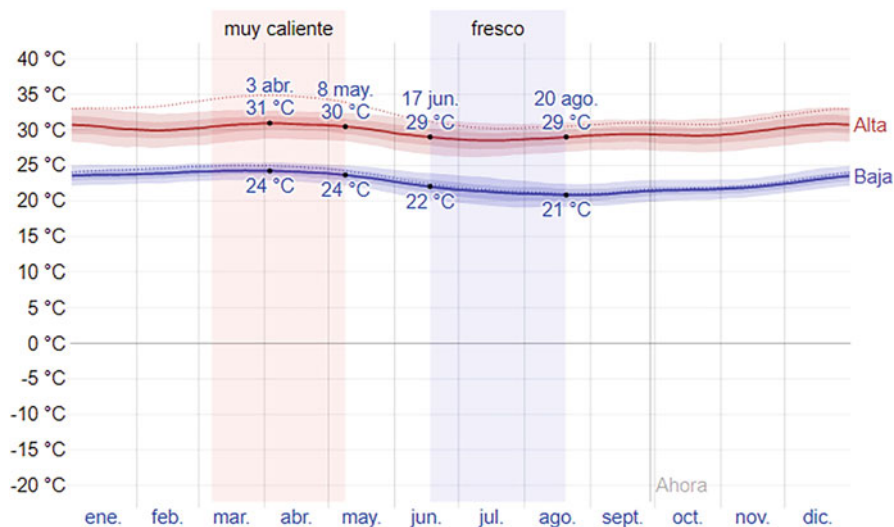
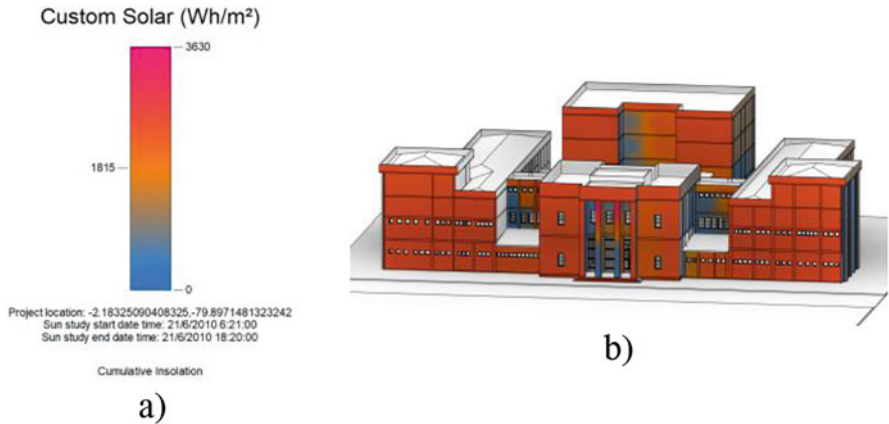


Fig. 2 Maximum and minimum average temperature



**Fig. 3** (a) Energy received at summer solstice and (b) summer accumulated insolation—west facade

**Insolation**

The analysis of the amount of energy received by each of the facades is carried out; in Fig. 3 the solar scale is observed from a cold heat (blue) to a warm color (red) to show the amount of energy per unit of surface Wh/m<sup>2</sup>.

During the summer solstice, which occurs on June 21, it was obtained that the maximum amount of energy that the building receives is 3134 Wh/m<sup>2</sup>, while on the winter solstice it received an amount of 3028 Wh/m<sup>2</sup>.

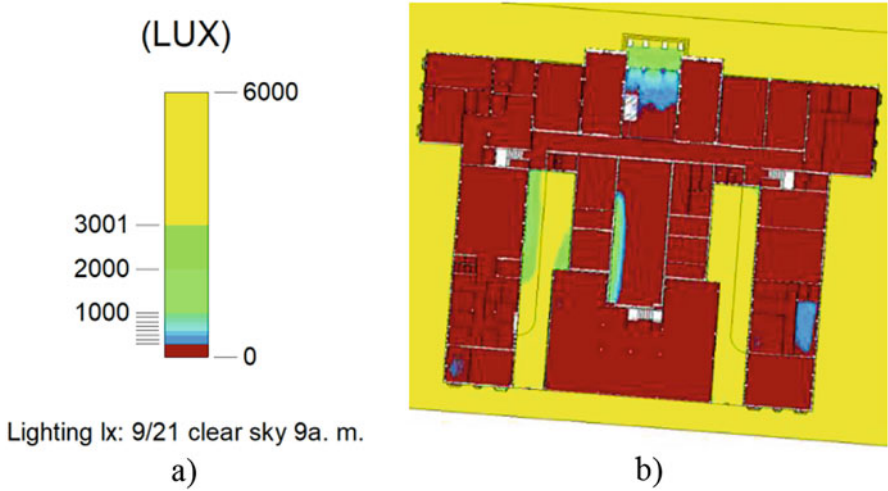
**Day Light**

This section is to analyze which surfaces or areas have solar overexposure due to the areas of natural light entry. For the analysis, we used data referring to the average of the equinoxes in Guayaquil on September 21 and March 21, from 9 am to 3 pm, performed in LEED v4 EQc 7 opt 2 standards with light threshold from 300 to 3000 lx (Fig. 4).

Due to the fact that in the building the types of windows, doors, openings, or any other element that allows the entry of natural light are small compared to the volume of the building, it can be observed in the graphs that at least up to the third and fourth floor, artificial lighting must be used, and small areas near the corridors that connect to the building receive direct natural light, but the percentage that does not receive is much higher.

**3.2 Orientation Analysis**

From the 3D building model, there are five possible orientation scenarios that have been studied: current orientation of 2.88° and then +45°, + 90°, + 180°, -45°, and -90° according to the current orientation. The orientations studied are scenarios



Lighting lx: 9/21 clear sky 9a. m.

**Fig. 4** (a) Lighting scale and (b) ground floor daylight illuminance

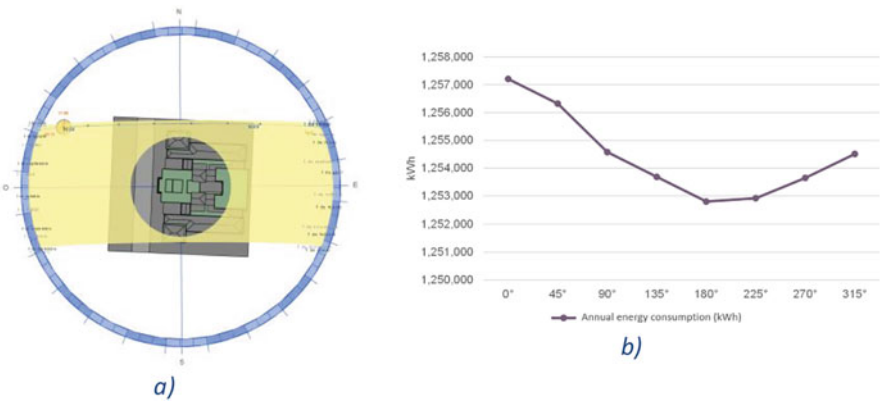


**Fig. 5** (a) FCMF building orientation simulation and (b) orientation scenarios energy consumption

that could not be implemented now due to the fact that the building is already constructed. Figure 5a shows the path of the sun in the current orientation of the building.

The software used simulates the amount of electrical energy that would be consumed inside the building. Figure 5b shows the amount of electrical energy consumed for each orientation scenario.

### 3.3 Analysis of Operational Hours

The operational hours of the building have been determined in relation to the real use of electrical energy, which was measured by the research group of the building under study, and the measurement defines the use that the building has with respect to the measured energy in 24 h starting at 0:00 and finishing at 11:59 p.m.; as a result, from 06:00 the power varies until 23:06, while for the rest of the time (early morning) from 23:06 to 05:59, the base electricity power did not change. This data is used to establish approximately what hours there is occupancy per person in the building and energy occupancy in it.

Through the energy consumption information, it is possible to enter occupation data per person in the software for the energy model future simulation.

According to the input data, the times in which the building reaches its maximum number of occupancies are determined by average of percentages and at what time of the day the most energy is consumed.

In Fig. 6b, it can be seen that the energy consumption of 2 hours 12/6 and 12/5 with respect to the initial day 12/7.

### 3.4 Analysis of Construction Elements According to the Material

Each element together with the possible materials shows that through the Revit software used, one can obtain references of the thermal properties of the materials such as thermal resistance (R), heat transfer coefficient (U), the coefficient of heat increase, and visual light transmittance. Each element has a different interior configuration and variables such as combination of sub-elements, number of sub-elements, thickness of each sub-element, and types of materials of the sub-elements are handled. The construction elements to be developed are walls, floors, roofs, windows, and doors.

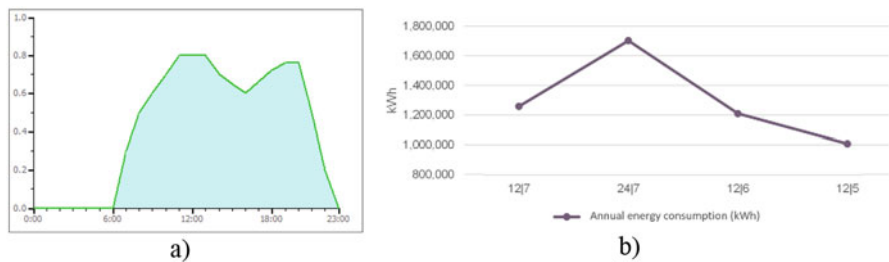


**Fig. 6** (a) Educational center occupation planning and (b) occupation scenario energy consumption

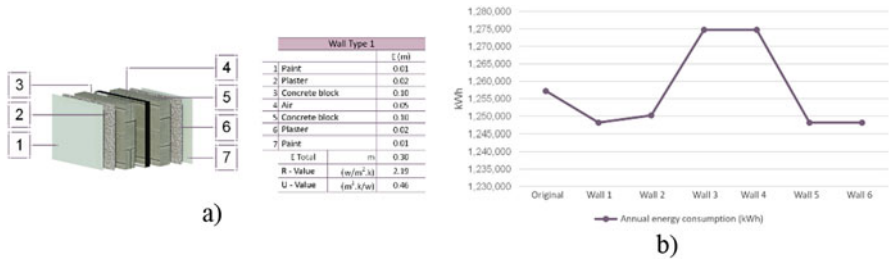


Fig. 7 (a) Type 1 wall configuration 1 and (b) wall type scenario energy consumption

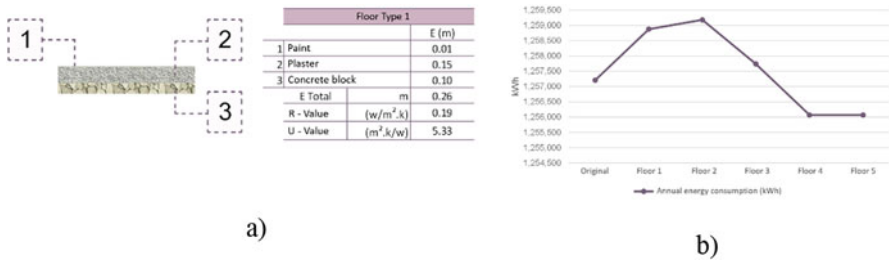


Fig. 8 (a) Type 1 floor configuration 1 and (b) floor type scenario energy consumption

In Figs. 7a and 8a, the configuration of the type 1 wall and floor 1, respectively, is shown, in the same way the other construction elements have been configured; for each of them the construction materials used are specified including their individual thickness, its total thickness, the thermal resistivity value, and the thermal conductivity value.

In Figs. 7b and 8b, the simulation of electrical energy type 1 wall and floor 1, respectively, is shown. All types of construction elements were created considering standard configurations and representative materials used in construction at the local level.

Once the constructive elements have been analyzed individually, creating scenarios in them; in Fig. 9 the best scenarios in the elements have been selected in such a way as to create the best possible scenario in the present research.

## 4 Discussion

The modeling of the building was carried out through an analysis of the existing documentation and the on-site survey of the construction materials. The material configuration was carried out in the BIM software taking into consideration the heat transfer coefficients of each material and the thickness used.

In the climatic analysis, it can be indicated that thermal comfort depends on many factors, of which one of them is humidity, which greatly influences whether an environment is fully conditioned for the activity to be carried out. The perceived

Tested parameters		Variables							
1	Orientation from original implantation	(x) 0°	(x) 45°	(x) 90°	(x) 135°	(✓) 180°	(x) 225°	(x) 270°	(x) 315°
2	Wall Type	(x) Original	(x) Type 1	(x) Type 2	(x) Type 3	(x) Type 4	(✓) Type 5	(x) Type 6	
3	Floor type	(x) Original	(x) Type 1	(x) Type 2	(x) Type 3	(✓) Type 4	(x) Type 5		
4	Roof type	(x) Original	(x) Type 1	(x) Type 2	(✓) Type 3	(x) Type 4	(x) Type 5		
5	Windows type	(x) Original 1	(x) Original 2	(x) Type 1	(✓) Type 2				
6	Door Type	(x) Original 1	(x) Original 2	(✓) Type 1					
7	Operating hours	(x) 24/7	(x) 12/7	(✓) 12/6	(x) 12/5				

Fig. 9 Selection of best individual scenarios

humidity in Guayaquil varies extremely, having a longer period of the year more humid for approximately 8 months from November 18 to July 24 in which the comfort level according to Cedar Lake Ventures, Inc. is considered muggy, oppressive, or unbearable at least 59% of the time.

The orientation analysis shows the energy performance with the current orientation of the building (+2.88 degrees from the north) and the performance with six different orientation scenarios proposed in Fig. 5b, being the 180-degree scenario with 0.32% of better performance, considering that this scenario is indicative for new constructions because the building under study is built and in operation.

The analysis of the operating hours was developed based on the measurement of the electrical energy of the building and parameterized in Revit. From the four scenarios proposed, the 12/5 scenario has the best energy performance, exceeding by 22.50% to scenario 12/7 which is considered the operative one.

The configuration of the physical parameters of the constructive elements under study and their simulation has been able to show that the type of wall T1 with 0.40% savings is the best scenario compared to the existing one, as well as scenarios T4 and T5 show a higher energy consumption around -1.59%, placing the concrete and air block as the best combination over the common brick. Regarding to the floors, scenarios T4 and T5 show a better and similar result with a 0.08% saving over the existing one, focusing on the use of additional layers of air and insulation. The T3 roof scenario shows an insignificant improvement in relation to the existing scenario, for which it was tested with the T4 and T5 scenarios, which use vegetation and soil in different proportions, but these reduced savings by -0.36% and -0.99%, respectively. The T2 window scenario has been the one with the best performance with 4.76%, emphasizing the use of triple glass over single-layer glass. The last element analyzed is the gate, in which an additional T1 scenario has been simulated, which shows an improvement in performance of 0.06%.

Finally, the global scenario, that of the best element options, results in a consumption of 1,177,474 kWh of annual electrical energy compared to the existing 1,257,207 kWh, which represents a 6.34% saving, helping to avoid 834,455 kg of greenhouse gases effect and an economic saving in energy costs of \$ 7175.00. Compared with the study [19], which indicates that the range of energy savings would be between 6% and 22%, this study would be at the lower limit of this range, which is convenient to deeply investigate the choice of materials simulations to find scenarios that can further improve the overall energy efficiency of the building.

## 5 Conclusions

This research has developed a methodology to evaluate the energy efficiency of an operational educational building, from obtaining all the necessary information for the elaboration of the 3D model, which allowed to carry out simulations and scenarios of orientation, solar irradiation, hours of operation, and constructive elements. This development made it possible to choose the best scenarios: 180° orientation, common brick walls, tile floors, membrane and plywood covers, aluminum-triple glass windows, and 12/6 operation hours.

It is important to indicate that the present work has presented an energy efficiency close to 6%, which is considered low; therefore, it is necessary to look for other ways to increase this indicator and for future work consider being able to simulate the installation of photovoltaic panels in the covers available, using the same evaluation methodology considering the increase of the solar system.

## References

1. IEA. (2020). Tracking buildings 2020. IEA. [Online]. Available: <https://www.iea.org/reports/tracking-buildings-2020>
2. IEA. (2020). *World energy balances*. Francia.
3. IIGE. (2019). *Balance Energético Nacional*. IIGE.
4. Asamblea Nacional República del Ecuador. (2019). *Ley orgánica de eficiencia energética* (p. 8). Asamblea Nacional República del Ecuador.
5. Chandel, S. S., Sharma, A., & Marwaha, B. M. (2016). Review of energy efficiency initiatives and regulations for residential buildings in India. *Renewable and Sustainable Energy Reviews*, 54, 1443–1458.
6. Martínez-Molina, A., Tort-Ausina, I., Cho, S., & Vivancos, J. L. (2016). Energy efficiency and thermal comfort in historic buildings: A review. *Renewable and Sustainable Energy Reviews*, 61, 70–85.
7. D’Agostino, D., Cuniberti, B., & Bertoldi, P. (2017). Energy consumption and efficiency technology measures in European non-residential buildings. *Energy and Buildings*, 153, 72–86.
8. de la Cruz-Lovera, C., Perea-Moreno, A. J., de la Cruz-Fernández, J. L., Alvarez-Bermejo, J. A., & Manzano-Agugliaro, F. (2017). Worldwide research on energy efficiency and sustainability in public buildings. *Sustainability*, 9(8), 1294.



9. Fan, C., Xiao, F., Li, Z., & Wang, J. (2018). Unsupervised data analytics in mining big building operational data for energy efficiency enhancement: A review. *Energy and Buildings*, 159, 296–308.
10. Barzola-Monteses, J., Espinoza-Andaluz, M., Mite-Leon, M., & Flores-Moran, M. (2020, November). Energy consumption of a building by using long short-term memory network: A forecasting study. In *Proceedings – International conference of the Chilean Computer Science Society, SCCC*, Vol. 2020, pp. 1–6.
11. Barzola-Monteses, J., Guerrero, M., Parrales-Bravo, F., & Espinoza-Andaluz, M. (2021). Forecasting energy consumption in residential department using convolutional neural networks. In *Conference of information and communication technologies – TICEC2021*, pp. 1–12.
12. Segura, G., Guamán, J., Mite-león, M., Macas-Espinosa, V., & Barzola-Monteses, J. (2021). Applied LSTM neural network time series to forecast household energy consumption. In *19th LACCEI International Multi-Conference for Engineering, Education, and Technology: “Prospective and trends in technology and skills for sustainable social development” “Leveraging emerging technologies to construct the future”*, pp. 1–6.
13. Litardo, J., et al. (2020). Urban Heat Island intensity and buildings’ energy needs in Duran, Ecuador: Simulation studies and proposal of mitigation strategies. *Sustainable Cities and Society*, 62(February), 102387.
14. Samadi, M., & Fattahi, J. (2021, March). Energy use intensity disaggregation in institutional buildings – A data analytics approach. *Energy and Buildings*, 235, 110730.
15. Panteli, C., Kylili, A., & Fokaides, P. A. (2020). Building information modelling applications in smart buildings: From design to commissioning and beyond a critical review. *Journal of Cleaner Production*, 265, 121766.
16. Habibi, S. (2017). The promise of BIM for improving building performance. *Energy and Buildings*, 153, 525–548.
17. INPC. (2016). *Ficha de Inventario Edificio FCFM*. INPC.
18. Cedar Lake Ventures Inc. (2021). *Weather spark*. [Online]. Available: <https://es.weatherspark.com/y/19346/Clima-promedio-en-Guayaquil-Ecuador-durante-todo-el-año>. Accessed: 19 Feb 2021.
19. Litardo, J., Hidalgo-Leon, R., Macías, J., Delgado, K., & Soriano, G. (2019, November). Estimating energy consumption and conservation measures for ESPOL Campus main building model using EnergyPlus. In *2019 IEEE 39th Central America and Panama Convention CONCAPAN 2019*, Vol. 2019.

# Strategies to Reduce Energy Curtailment in a Power System with High Penetration of Renewable Energy: Case Study of San Cristobal, Galapagos



Jimmy Cordova, Manuel S. Alvarez-Alvarado, Ivan Endara, Edison Azuero, and Jose Diaz

## 1 Introduction

Nowadays, the production of energy from thermal power plants drive to the emission of greenhouse gases and the use of fossil fuels, which leads to an increase in the cost of electricity [1]. For San Cristóbal Island, thermal generation involves a sub-process of supplying fuel by marine transportation from continental Ecuador to Galapagos. This activity represents a danger for the marine flora and fauna of the Galapagos, existing the possibility of a fuel spill as reported in 2000, when the Jessica tanker spilled 180,000 gallons of fossil fuel in front of the coast of Puerto Baquerizo Moreno [1]. Additionally, the existing thermal generation systems on the island depend on the availability of fuels (e.g., petroleum); therefore, it is necessary for renewable systems to be able to supply the energy when oil reserves run out. From an economic point of view, the waste of energy implies the reduction of economic income for the owners of the generating plants during the renewable generation peaks. Under this context, the Galapagos Island is migrating to the use of renewable energies. For instance, San Cristobal Island presents a wind farm with a 2.4 MW total capacity installed, with a penetration around 33% [2]. Photovoltaic power plants are also included in the mix of generation in Galapagos. Nowadays, low-capacity renewable power plants are installed, but country policies are changing, and it is planned to expand the capacity to increase the penetration of renewable energy in Galapagos and reduce the use of fossil fuels [3].

Focusing on photovoltaic and wind generation, they present intermittent behaviors that depend on solar radiation and wind speed, respectively. Such fact restricts

---

J. Cordova (✉) · M. S. Alvarez-Alvarado · I. Endara · E. Azuero · J. Diaz  
Escuela Superior Politécnica del Litoral (ESPOL), Guayaquil, Ecuador  
e-mail: [jjcordov@espol.edu.ec](mailto:jjcordov@espol.edu.ec)

the continuous operation and produces wasted energy, in periods when the capacity is not required. For instance, when there is a high incidence of this type of plant in an isolated system, there are periods of time in which the energy available from RE plants exceeds the energy demand of the power system; therefore, the electric system operator must limit the RE generation to preserve the balance between generation and load and in that way maintain the stability of the electrical system [4]. To face this problem, energy storage emerges as a potential solution. These systems store electrical energy that can be dispatched to supply the electrical demand. Currently, the most used technologies for energy storage are storage by hydraulic pumping, compressed air, flywheels, batteries, among others [5]. This research focuses on the incorporation of cryogenic energy storage, lithium-ion batteries, and flow batteries.

Cryogenic energy storage is characterized by its large amounts of energy than can storage. The storage process starts when the excess electrical energy from the network is used to capture and purify air and then cool it down to  $-196\text{ }^{\circ}\text{C}$ , transforming it into a liquid to be stored in thermally insulated tanks. When it is required, the liquid is pumped and heated to ambient temperature producing its expansion and reaching up to 700 times the volume that it had initially in liquid state, and the pressure resulting is used to move the turbine coupled to an electric generator which delivers energy back to the electrical grid. One of the limitations of this system is its low efficiency that reaches up to 50% [6]. On the other hand, lithium-ion batteries are made up by positive electrode (anode) made of lithium cobalt oxide  $\text{LiCoO}_2$ , negative electrode made of carbon, and a separator that is a micro-perforated sheet that separates the two electrodes but allows ions to travel between both electrodes [7]. During battery charging, lithium ions move through an electrolyte from the cathode to fixate on the carbon at the anode, and in the discharge process, the lithium ions return to the cathode. This process degrades the battery electrodes, so these batteries have a short lifetime compared to other storage systems. Additionally, this type of battery has the disadvantage of being very expensive [7]. Similarly, energy storage in flow batteries operates with same components. The main difference between such technologies lies in the storage energy process. The most developed type of flow batteries are redox batteries [8], and the name comes from the internal process that is followed in charging and discharging processes (oxidation and reduction). This type of battery uses two tanks to separate the same electrolyte but with different oxidation states, that is, in one tank the electrolyte is positively charged and in the other negatively charged. The operating principle during battery discharge is based on the oxidation of the electrolyte at the anode and reduction of the electrolyte at the cathode; this allows an electric current to be generated from cathode to anode which is established by a membrane that avoids the mixing of the anode and cathode electrolytes but allows the passage of ions in the oxidation and reduction processes [8]. The advantage of this system is that the oxidation and reduction processes are carried out between the electrolytes and no between the electrodes, avoiding their accelerated degradation and increasing the life span of the batteries.

Another innovative way to store energy is the use of electric vehicles (EV); the surplus energy is stored in the batteries of EVs and used when it runs. The key factor

is the method to store the energy, in other words the EV charge system, and it is possible to classify the charging process into three categories. Slow charge of EVs has been widely used, and this system charges the batteries of the vehicles for five to 8 h; generally the users charge the EV during the night by connecting the vehicles to charging modules located in their residence. This charging method requires low power from the network and avoids the problems associated to fast charging [9]. Fast charge is used to eliminate the discomforts perceived by EV users, when they must wait long periods of time to charge the batteries. A fast charge implies that in a time that goes from 20 to 40 min, 80% of the battery capacity is charged. While this method avoids the stress of waiting several hours for a full battery charge, it can end up shortening battery life [10]. A battery exchange station operates in a similar way to a gas station. In this context, the discharged batteries are removed (either manually or automatically) from the electric vehicle and replaced by fully charged batteries that are available at the station. In this manner, the electric vehicle is available to operate within a few minutes [11].

This paper aims to take as a case study the electrical system of the island of San Cristóbal in Galapagos and examine the feasibility to incorporate two strategies to reduce energy wasted. Both strategies are based on the reduction of load curtailment by (1) inclusion of liquid air energy storage (family of cryogenic energy storage technology), lithium-ion batteries, and energy storage in flow batteries and (2) using electric vehicles.

## 2 Methods

The energy curtailment is produced when energy demand is low in comparison with energy production, especially in high penetration hybrid systems. The stochastic behavior of RE leads to have periods in which the energy production is higher than the demand. To analyze the operation of the electrical system of San Cristóbal, it should be performed in a point when the operation could be compromised for the introduction of RE sources. According to the PME the entry of nonconventional renewable power plants is planned until year 2024 for San Cristóbal Island.

For modeling the island's load, data from the electrical demand of San Cristóbal island provided by the Galápagos Provincial Electric Company (EEPG) is used, and the demand records are active and reactive power; they are recorded every 15 min for the three feeders of San Cristóbal Island during year 2018. With these data and considering a load growth rate of 7% based on EEGP statistics [12], the load for the island by the year 2024 is estimated.

To model the generation installed on the Island, the power plants that are installed and operating until 2019 are considered, and the information for these power plants is shown in Table 1. The load profile and installed generation data for the year 2024 were loaded in the Homer Energy Software (evaluation version), using the location of site; the software determines the renewable resources available. Homer Energy was used to obtain net values of renewable generation, load, and the contribution of

**Table 1** Installed power on San Cristóbal Island until 2019 [13]

Power plant	Type of power plant	Nominal power [MW]	Effective power [MW]
San Cristóbal	Thermal ICE	7.41	5.91
San Cristóbal Eolic	Eolic	2.4	2.4
San Cristóbal PV	Photovoltaic	0.013	0.013
Total			5.91

**Table 2** Generation expansion for San Cristóbal Island until 2024

Project	Characteristics
Photovoltaic power plant	3.5 MWp
Energy storage system	3.6 MWh
Wind power plant	5.6 MW

the BESS to San Cristóbal hybrid system by the year 2024. The net values of renewable generation, load, and input and output power to the BESS were saved in an Excel file to be imported into MATLAB for analysis of the different alternatives to reduce the energy curtailment. A schedule for the adding RE power plants is shown in Table 2.

## 2.1 Local Site, Profiles, and Proposed Solutions

The simulations performed in Homer Energy show two seasons for Galapagos Islands, the hot season from January to June and the cold season from July to December (Fig. 1). In the hot season the wind speed is low, but the solar resource is high; in contrary, in cold season the wind speed is high, and the solar radiation is low. The load profile also shows a behavior related with ambient temperature, and in the hot season the system has its peak load; this behavior is due to refrigeration loads [14, 15].

The energy curtailment is higher in the cold season because of the low demand and the high values for wind speeds. The higher values for wind speed are shown from 12:00 to 15:00, and this matches with higher values of solar radiation, and this produces a greater energy curtailment. To reduce the energy curtailment two main strategies are analyzed: the first strategy is to increase the capacity of BESS, proposing three technologies: liquid air energy storage (LAES), flow batteries, and Li-ion batteries. The second strategy is to store energy in batteries of EV, proposing a swap battery station.

To establish the baseline of energy curtailed, it was necessary to determine a daily profile of excess in energy production. Figure 1 shows the daily profile of energy curtailed; months from January to May show a low excess in energy production due to high demand and low availability of renewable resource, and on the other hand,

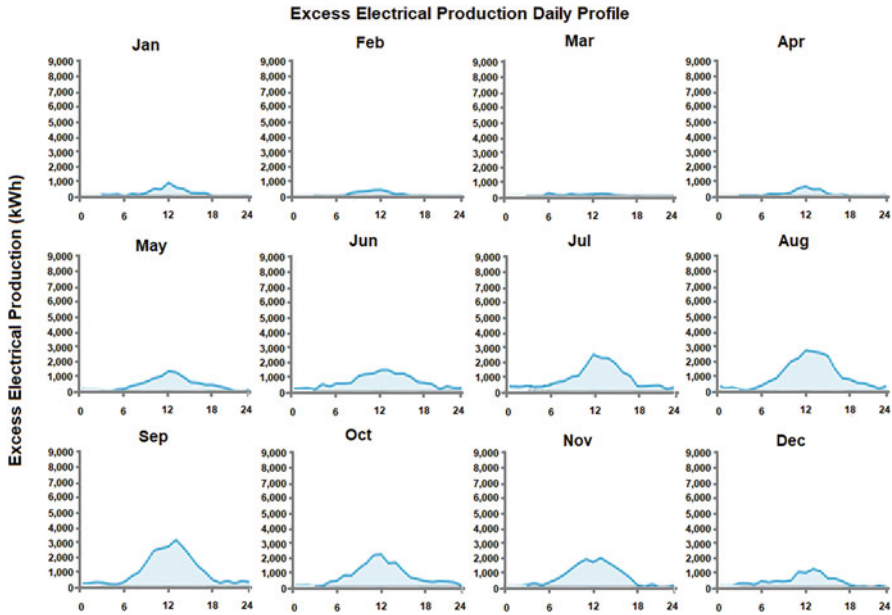


Fig. 1 Daily energy curtailment profile per month

months from June to December show a high excess in energy production due to reduction in cooling loads such as air conditioners.

**2.1.1 BESS Operational Parameters for Simulations**

For the first stage of simulations, the operation of three types of BESS is analyzed, and the simulations are performed to determine how the BESS parameters affect the energy curtailment. The main parameters to analyze are the minimum power to operate the storing process (input power), the storage system, and the turbine-generator/inverter system (output power). To optimize these parameters an algorithm was developed in MATLAB, using the results from Homer Energy, and several combinations of input power, storage capacity, and output power were analyzed determining the reduction in energy curtailment; the ranges for the optimized parameters are shown in Table 3.

**2.1.2 Energy Storage in EV’s Batteries**

EV batteries store energy until the moment the user needs the EV; this process has some drawback, for instance, the time to complete the full charge, which can be unpleasant for customers. Even though some advances in fast battery charging systems have been achieved, this type of charging reduces the useful life of the battery. For this reason, the introduction of a battery swap system is proposed; in this

**Table 3** ESS operational and economic parameters.

Parameter	LAES	Li-ion battery	Flow battery
Input power	0–10 MW	0–10 MW	0–10 MW
Output power	0–10 MW	0–10 MW	0–10 MW
Store capacity	0–100MWh	0–200MWh	0–200MWh
Life span	30 years	20 years	30 years
Efficiency	50%	88%	88%
Energy cost for sale	108.7 \$/MWh	108.7 \$/MWh	108.7 \$/MWh
Liquefaction system cost	1450 \$/kW		
Investment storage system	25 \$/kWh	362 \$/kWh	108 \$/kWh
Investment conversion system	354 \$/KW	1446 \$/kW	862 \$/kWh
Maintenance and operation costs	3 \$/kW	12 \$/kW	10 \$/kW
O&M variable costs	3 \$/MWh	0,3 \$/MWh	0,3 \$/MWh
Discount rate	6%	6%	6%

**Table 4** Parameter for a battery swap station

Parameter	Value
Station life span	15 years
Subscription	20 \$/monthly
Energy cost 22:00–08:00	0.05 \$/kWh
Curtailed energy cost	0.02 \$/kWh
Batteries investment	100 \$/kWh
Power transformer investment	120 \$/kWh
Power converter investment	715 \$/kW
Operation and maintenance	50000 \$/year
Discount rate	6%

way a certain amount of fully charged batteries are kept in stock. A fully charged battery will be used to replace the discharged battery in an EV, reducing the waiting time for the user. Another advantage is the side energy demand achieved because the batteries are charged when there is a surplus of energy from the renewable sources.

The analysis of this alternative determined the optimal number of users that can subscribe to this service. This number of users will depend on the number of batteries to be kept in stock, the capacity of the battery charger, the number of vehicles that will be served per day, thereby determining the investment costs and economic income of the project. To determine the optimal number of batteries, a user profile was considered that fits the needs of the residents of San Cristóbal Island, an autonomy of 80 Km, and a charging time of 4 h. The algorithm explores different scenarios considering the following: the number of subscribed customers, the capacity of the charging system, and the number of batteries in the station. Then, every scenario is evaluated and the best scenario with the lowest investment costs and the most affordable income is determined (Table 4).

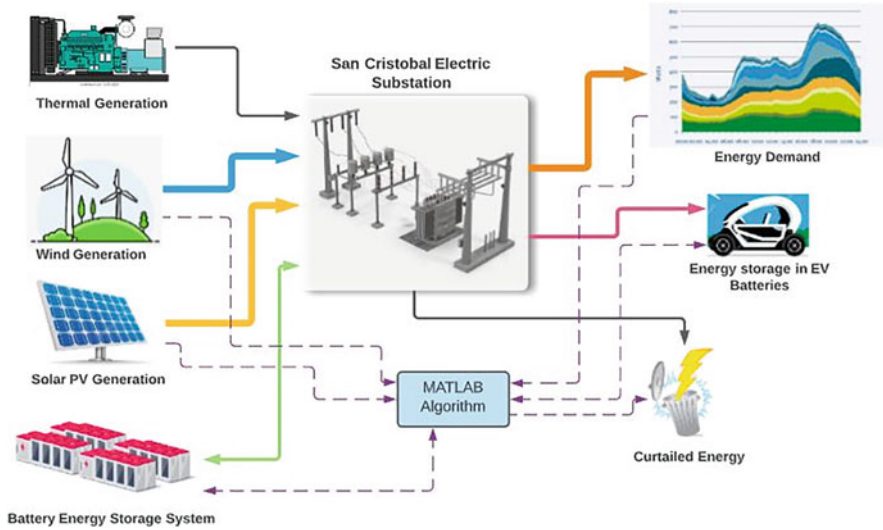


**Fig. 2** Diagram of energy and control flow

The energy flow and the schematic control for the optimization algorithm is shown in Fig. 2. The thermal and renewable energy plants operate in coordination to supply the local demand and EV batteries and the surplus energy is stored in external batteries. If the external batteries are fully charged, the energy is curtailed. The MATLAB algorithm calculates the energy curtailment and perform several simulations to find the parameters for each type of energy storage reducing the energy curtailment.

### 3 Results

#### 3.1 Battery Energy Storage System Simulations

The projects state three technologies to be analyzed, LAES, flow batteries, and Li-ion batteries. To determine the optimal characteristics of the energy storage system applicable to San Cristóbal electrical system, a scan of combination of parameters was performed, input power, output power, and storage capacity, obtaining the reduction of energy curtailment associated with each combination of parameters.

Every combination of parameter combined with the energy production and energy demand produce a value of energy curtailment. The algorithm optimized the system characteristic when it found a minimum value of energy curtailment. Due to the variation on the renewable resource and the low demand (high penetration of RE), it is not possible to eliminate completely the energy curtailment. Nevertheless, any reduction in the use of fossil fuel to produce power in Galapagos is an especial achievement to preserve this endangered ecosystem.



The optimized parameter for each technology has a net present value (NPV) associated, and this value directly affects the project feasibility by increasing the levelized cost of energy (LCOE). For each optimized system, the total energy produced is calculated to estimate its energy production and estimate the levelized cost of energy (LCOE). The total investment in for any kind of project is higher in comparison with other places in Ecuador; therefore, in many cases the projects are not attractive for investors. However, the environmental impacts make any project important for conservation of this natural reserve.

Figure 3 shows the total energy required to meet the demand of San Cristobal Island. It is relevant to highlight that during the months from June to November, the demand is low, hence, energy storage increases. Notice that in some cases, the energy is curtailed, as the batteries are fully charged.

### 3.2 *EV Battery Swap Station Simulations*

The implementation of a battery swap station for EV is a strategy to use the curtailed energy on San Cristóbal hybrid system, and it was possible to determine that the characteristics that allow the maximum profitability for the battery swap station are detailed in Table 7. For a battery swap station, there is no energy produced by this system, but a big amount of energy that was curtailed before; now it is recovered and used to recharge the EV batteries (Table 5).

Figure 4 shows in blue the energy that would be curtailed, but was used to charge the batteries, and the yellow band corresponds to the additional thermal generation, which is added to the normal generation to cover the demand, because of the operation of the battery swap station (Table 6). This involves more fuel transport to San Cristóbal Island for thermal generation and an increase in CO<sub>2</sub> emissions, but this negative effect is minimized by the amount of fuel that will not be transported to the island for transportation. The main benefits obtained due to the incorporation of a battery swap station for EVs are detailed in Table 7.

## 4 Discussion

Energy curtailment is a serious problem in high-penetration hybrid systems; the mismatch between the peak demand and the fluctuating renewable resource leads to curtail some energy that could be stored. The performance of each energy storage systems relays on the capacity and the input power; the higher the input power, the higher the storage of energy. The storage capacity increases the penetration of renewable energy, but at some operational points, the output power capacity is more important to support the network in case of a fault which needs high power; the storage system could maintain the system stability.

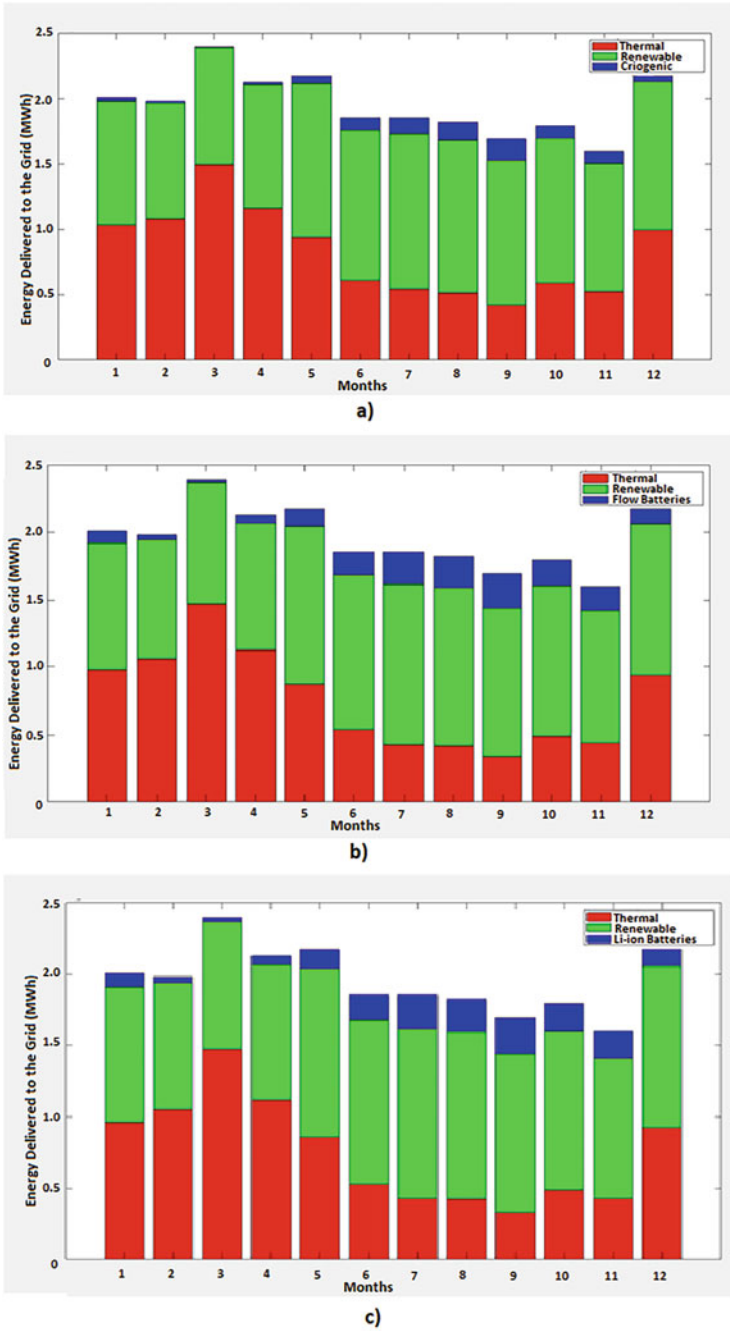
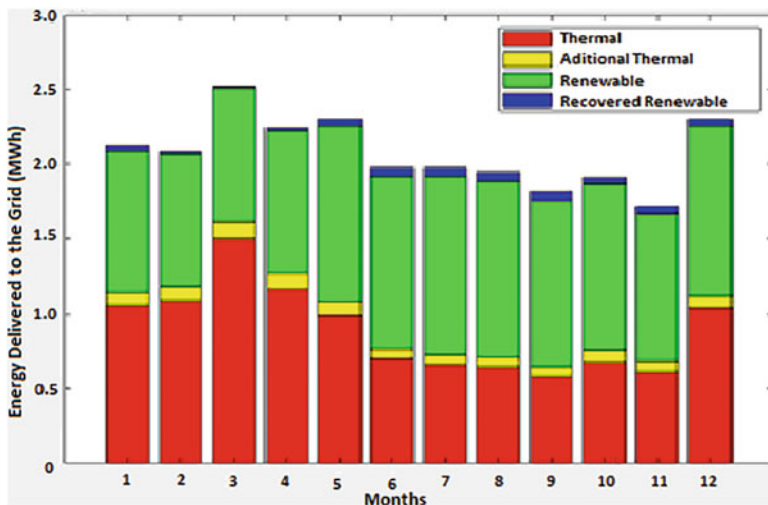


Fig. 3 Annual energy production using (a) LAES, (b) flow batteries, and (c) Li-ion batteries

**Table 5** Optimized BESS parameters

Parameter	LAES	Flow batteries	Li-ion batteries
Input power (kW)	2900	2400	2500
Output power (kW)	400	2000	2500
Storage capacity (kWh)	58,000	20,000	18,000
Efficiency (%)	50	82	88
NPV (M\$)	-5536	-1996	-8292
Energy curtailment (%)	17.28	12.10	11.88



**Fig. 4** Energy production and use in a battery swap station

**Table 6** Optimized operational parameter for an EV swap battery station

EV number	1254
Monthly payment for service (\$)	\$20
Battery capacity (kWh)	16
Range (km)	80
Power converter (kW)	650
Stock of batteries	376

**Table 7** Operation results for an EV swap battery station

Recovered energy (kWh/year)	464,452.60
Annual incomes (\$)	\$300,960.00
CO2 reduction (tons)	707,659.24
Energy curtailment	19.70%
NPV (\$)	\$873,218.66

In an endangered place such as Galapagos Islands, the implementation of a LAES system will not only increase the penetration of renewable energy but also reduce the use of fossil fuel and avoid the use of batteries with dangerous chemical components. However, the higher reduction in energy curtailment is achieved with flow batteries, at a lower cost. Other important advantage of flow batteries is the system scalability, the power converter could be kept, and only the storage system is increased, reducing the total investment.

A battery swap station will increase the penetration of renewable energy and reduce the energy curtailment, but as this energy is not reinjected to the grid, it is not possible to achieve an increase in system stability. This type of technology will improve the total energy efficiency of the island and reduce the dependency on fossil fuels transported from continental Ecuador.

A major issue with the current operation of hybrid systems in Galapagos is the spinning reserve kept in normal conditions. Now, when the renewable resource is high, the generation from thermal plants is reduce to a minimum, reducing in this way the system inertia in case of a fault. Further research on this topic is necessary, to state the best operational setpoints, assuring the system stability and allowing a higher penetration of renewable energy.

## 5 Conclusions

In hybrid systems with high penetration of renewable resources, the inevitable energy curtailment is mainly produced by the intermittence of the renewable resource. To reduce the energy curtailed due to the mismatch between demand and fluctuating generation, it is important to correctly design the power plant capacity.

Flow batteries probe to be one of the best options to reduce the energy curtailment with low investment. The cost of energy storage systems for flow batteries is lower than Li-ion batteries, demonstrating that flow batteries are likely to replace the use of Li-ion batteries in large-scale energy storage applications. This is because the operating mechanism of the flow batteries does not degrade the electrodes in an accelerated way, allowing a longer useful life.



The implementation of a battery swap station as a strategy to reduce energy curtailment did not generate such a significant impact in reducing the curtailment. However, it is the alternative that has the highest profit, and the environmental impact associated to the reduction in fossil fuels consumption is promising alternative for Galapagos.

## References

1. PNUD, GEF y MEER. (2016). *Energía Verde para Galápagos Inagotable, Limpia y Segura*. PNUD.
2. Kornbluth, K., Hinokuma, R., Johnson, E., & McCaffrey, Z. (2009). *Optimizing wind energy for a small hybrid wind/diesel grid in the Galapagos islands*. University of California, Davis Energy Efficiency Centre.
3. Villagómez, J. C. (2013). Energy demand analysis and management according to availability of renewable energy sources in Galapagos Islands. In *The first LACCEI international symposium on mega and micro sustainable energy projects, Mexico*, Vol. 298.
4. Kroposki, B., Johnson, B., Zhang, Y., Gevorgian, V., Denholm, P., Hodge, B. M., & Hannegan, B. (2017). Achieving a 100% renewable grid: Operating electric power systems with extremely high levels of variable renewable energy. *IEEE Power and Energy Magazine*, 15(2), 61–73.
5. Huang, X., Xu, Z., Sun, Y., Xue, Y., Wang, Z., Liu, Z., Li, Z., & Ni, W. (2018). Heat and power load dispatching considering energy storage of district heating system and electric boilers. *Journal of Modern Power Systems and Clean Energy*, 6(5), 992–1003.
6. He, T., Lv, H., Shao, Z., Zhang, J., Xing, X., & Ma, H. (2020). Cascade utilization of LNG cold energy by integrating cryogenic energy storage, organic Rankine cycle and direct cooling. *Applied Energy*, 277, 115570.
7. Kim, T., Song, W., Son, D. Y., Ono, L. K., & Qi, Y. (2019). Lithium-ion batteries: Outlook on present, future, and hybridized technologies. *Journal of Materials Chemistry A*, 7(7), 2942–2964.
8. Luo, J., Hu, B., Hu, M., Zhao, Y., & Liu, T. L. (2019). Status and prospects of organic redox flow batteries toward sustainable energy storage. *ACS Energy Letters*, 4(9), 2220–2240.
9. Meza, J., & García, E. (2018). Asignación de recursos para la recarga de vehículos eléctricos en estaciones de servicios basado en la respuesta a la demanda. *I+D Tecnológico*, 14(2), 66–73.
10. Dimitrov, B., Hayatleh, K., Barker, S., Collier, G., Sharkh, S., & Cruden, A. (2020). A buck-boost transformerless DC–DC converter based on IGBT modules for fast charge of electric vehicles. *Electronics*, 9, 397.
11. Zhong, L., & Pei, M. (2020). Optimal design for a shared swap charging system considering the electric vehicle battery charging rate. *Energies*, 13(5), 1213.
12. ELECGALÁPAGOS, Programa De eficiencia energética para cocción por inducción y calentamiento de agua con electricidad en la Isla San Cristóbal, Puerto Baquerizo Moreno (2013).
13. Ministerio de Energía y Recursos Naturales no Renovables, Plan Maestro de Electricidad (2019).
14. Rosiek, S., Romero-Cano, M. S., Puertas, A. M., & Batlles, F. J. (2019). Industrial food chamber cooling and power system integrated with renewable energy as an example of power grid sustainability improvement. *Renewable Energy*, 138, 697–708.
15. Lu, Y., Khan, Z. A., Alvarez-Alvarado, M. S., Zhang, Y., Huang, Z., & Imran, M. (2020). A critical review of sustainable energy policies for the promotion of renewable energy sources. *Sustainability*, 12(12), 5078.

# Energy and Economical Study of Different Renewable Energy Technologies for Domestic Hot Water Production Under the Climatic Conditions of the Main Cities in Ecuador



Carlos Naranjo-Mendoza , Jesús López-Villada, Patricia Otero , and Sebastián Casco

## 1 Introduction

It is known that approximately 40% of energy consumption in the world comes from the building sector. Thus, one of the Sustainable Development Goals worldwide is to mitigate the effects of global warming through renewable energy sources and efficient technologies to reduce CO<sub>2</sub> emissions from the building sector [1].

In recent decades, this sector has focused its efforts on reducing energy consumption on heating, ventilation, air conditioning (HVAC) systems, and lighting [2]. This has generated that the energy used to produce domestic hot water (DHW) increases in buildings, reaching up to 32% of the annual energy balance consumption [3].

The goal is to replace conventional systems for DHW production (gas boilers, electric boilers, tanks with electric heating, electric showers, etc.) [4] for more efficient technologies and the use of renewable energy resources [5]. Thus, the proper selection of DHW systems can significantly help reduce energy consumption, CO<sub>2</sub> emissions, and operating costs.

At a global level, different, more efficient, and environmentally friendly technologies have been developed for DHW production; for example, heat pumps that are optimal for their high operating coefficient (COP), on average, has values close to

---

C. Naranjo-Mendoza (✉) · S. Casco

Escuela Politécnica Nacional, Departamento de Ingeniería Mecánica, Quito, Ecuador

e-mail: [carlos.naranjo@epn.edu.ec](mailto:carlos.naranjo@epn.edu.ec)

J. López-Villada

Universidad Internacional SEK, Facultad de Ingenierías y Ciencias Aplicadas, Quito, Ecuador

P. Otero

Escuela Politécnica Nacional, Departamento de Energía Eléctrica, Quito, Ecuador

© The Author(s), under exclusive license to Springer Nature Switzerland AG 2022

M. Espinoza-Andaluz et al. (eds.), *Congress on Research, Development*

*and Innovation in Renewable Energies*, Green Energy and Technology,

[https://doi.org/10.1007/978-3-030-97862-4\\_12](https://doi.org/10.1007/978-3-030-97862-4_12)

3. Hence, for each unit of electricity consumption, there are three units of heat production [6]. This type of system has been developed in the last decade and has a lot of potential for hot water production at low operating costs.

Other technologies use a renewable energy source like the sun. Solar thermal systems (ST) transform solar radiation into heat using solar collectors like flat plates, vacuum tubes, or concentration collectors [7]. Solar photovoltaic (PV) technologies transform solar energy into electrical energy, which is used for water heating [8]. While this system is not energetically efficient, the production costs of PV panels make it very economically competitive. There is also thermophotovoltaic (PV/T) technology, which combines the two systems mentioned above, and heat can be used directly to produce DHW. In contrast, electricity can be used for direct water heating with a heat pump or the immediate electricity consumption of the building [9].

In recent years in Ecuador, greater importance has been given to reducing energy consumption since it represents a high public cost due to the subsidies. The Organic Law of Energy Efficiency regulates the rational use of energy and favors research and technological development in this field [10]. In the building sector, the primary energy demand is due to the lighting, office equipment, and in the residential sector to produce DHW [11]. As far as the production of DHW is concerned, the most used systems are electric (electric shower or boiler) and gas boilers. Considering that both energy sources are subsidized, there is a potential for economic savings if the country changes to more efficient systems. It is essential to mention that Ecuador has a high and constant solar potential throughout the year and the territory [12], making it necessary to investigate technologies such as solar thermal and photovoltaic for application in DHW production.

In this context, this article shows energy and economic research on using different systems for DHW production in the residential sector in different cities of Ecuador. This is done to identify which technologies are more efficient according to the weather and the electricity consumption rate in different country cities.

## 2 Methods

To reach the objective of this study, a methodology divided mainly into an energy analysis, and an economic analysis is proposed. The energy analysis will estimate the electricity demand of the different DHW production systems at a monthly and annual level. The economic analysis will use the system yearly energy consumption data to evaluate, in the long term, which of the alternatives is more economically feasible in the different cities. The following section describes the details of the case study and the methodology used for energy and economic analysis.

## 2.1 Case Study

In this field, the use of different systems to prepare DHW in a typical house in Ecuador located in different places with markedly different climates has been analyzed. The house is inhabited by four people and has a consumption of DHW of 120 L/day. The consumption profile presents a peak of 60 L from 7 to 9 h, 30 L at 14 h, and 30 L at 19 h.

## 2.2 Weather Data

To consider different climatic conditions, the study has been carried out in the following cities of Ecuador: Quito, Guayaquil, Esmeraldas, Tena, Santo Domingo de los Tsáchilas, and Puerto Baquerizo Moreno. Table 1 shows the annual values of global irradiation, diffuse irradiation, and annual ambient temperature mean for each location. This data has been obtained from the NSRDB database managed by the *Systema Advisor Model* (SAM) simulation software.

## 2.3 Systems Description

In the present study, six different ACS production systems are evaluated:

- *Heating system with electrical resistance*: This system is considered as the reference system or conventional system. It consists of a water storage tank of 150 liters of water volume that is heated by a 700 W electrical resistance. This resistance is powered by energy from the entire electrical network (Fig. 1a).
- *Heating system with heat pump*: This system consists of a heat pump of 750 W thermal power and a nominal COP of 3 that is connected to the storage tank (150 liters) through a heat exchanger. The heat pump is powered by energy from the entire power grid (Fig. 1b).

**Table 1** Locations annual global and diffuse solar irradiation and ambient temperature mean

City	Temperature	Solar radiation	Diffuse solar radiation
	°C	kWh/m <sup>2</sup>	kWh/m <sup>2</sup>
Quito	11.1	1908	863
Guayaquil	25.7	1767	870
Esmeraldas	25.4	1804	920
Tena	23.2	1569	897
Santo Domingo	22.7	1307	912
Puerto B. Moreno	23.7	2100	731



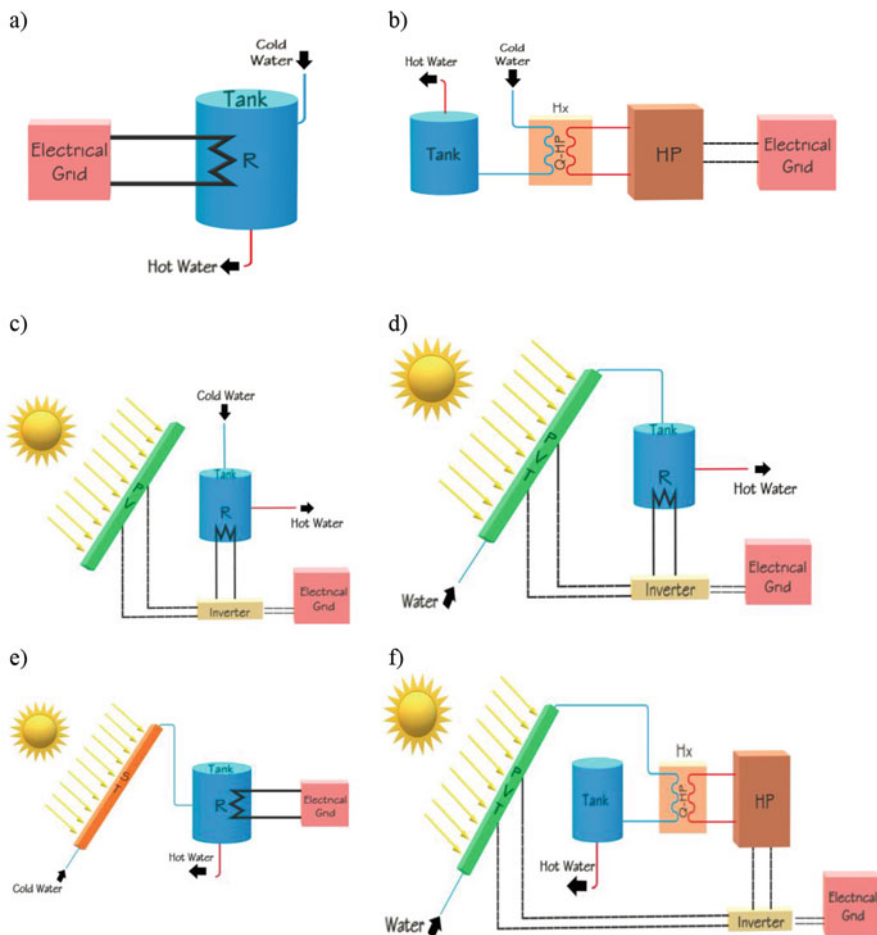


**Fig. 1** Systems analyzed for DHW production: (a) electrical resistance, (b) heat pump, (c) electrical resistance + PV, (d) electrical resistance plus PV/T, (e) electrical + solar thermal resistance, and (f) PV/T + heat pump

- *Water heating system with electrical resistance assisted by a photovoltaic panel (PV):* The difference with the reference system is that the electrical resistance is assisted by the energy produced in a  $2 \text{ m}^2$ , 330 Wp photovoltaic panel, which is connected to the electricity grid to inject the surplus energy (when it exists). Likewise, the resistor is connected to the electrical network in case the energy produced in the PV panel is not enough or null (Fig. 1c).
- *Water heating system with electrical resistance assisted by a thermophotovoltaic panel (PV/T):* In this system, the water heating is assisted by solar thermal energy from the thermal side of the PV/T panel that serves to heat or preheat the water. If the thermal energy is not enough to reach the desired temperature, an electrical resistance (700 W) is used as an auxiliary system. The electrical resistance uses

the electrical energy produced by the PV/T. The PV/T is connected to the grid to inject any energy (if needed). Likewise, the resistance can use 100% of the electrical network energy in case the solar resource is null (Fig. 1d). The PV/T panel has a peak electrical power of 300 W, a maximum optical performance of 90%, and a surface area of 2 m<sup>2</sup>.

- *Water heating system by solar thermal collector:* This is a heating system assisted by solar thermal energy from flat plate solar collectors with maximum optimal performance of 80% and a surface area of 2 m<sup>2</sup>. If the solar resource is not sufficient to reach the desired temperature in the storage tank, an electrical resistance (700 W) connected to the grid heats the water (Fig. 1e).
- *Water heating system with heat pump assisted by a thermophotovoltaic panel (PV/T):* This system has a water storage tank (150 liters), and the water heating is assisted by solar thermal energy from the PV/T panel. When the solar thermal energy is not enough to reach the desired temperature in the tank, a heat pump is activated that is assisted by the electrical energy coming from the PV/T. The PV/T is connected to the mains for the injection of any surplus energy. Likewise, the heat pump is connected to the electrical network to be fed in case the electrical energy of the PV/T is not enough or is null (Fig. 1f).

## 2.4 Energy Analysis

To perform the energy analysis, TRNSYS dynamic simulation tool for energy systems will be used. This tool has different libraries of systems such as solar thermal collectors, photovoltaics, water tanks, solar irradiation processors, pumps, etc. Fig. 2 shows the Graphical Programming Environment Simulation Studio of TRNSYS for the system in Fig. 1f. It is important to mention that TRNSYS simulates the performance of the different thermal systems considering the dynamic behavior. TRNSYS performs a yearly simulation in 1-hour timestep. That is, it performs 8760 simulations considering the weather variations from a typical meteorological year (TMY) file.

## 2.5 Economic Analysis

The public electricity service in Ecuador is characterized by being highly subsidized, with a complex tariff schedule, which divides consumers into different types and categories according to the range of consumption [13]. The residential consumers' categorization implies that a different rate may apply depending on the region of Ecuador, given the geographical location.

Likewise, the economic development of a province determines the demand for electricity in each household. Hence to establish the rate applicable to each city, the per capita consumption according to the province is taken as a reference [14], and a

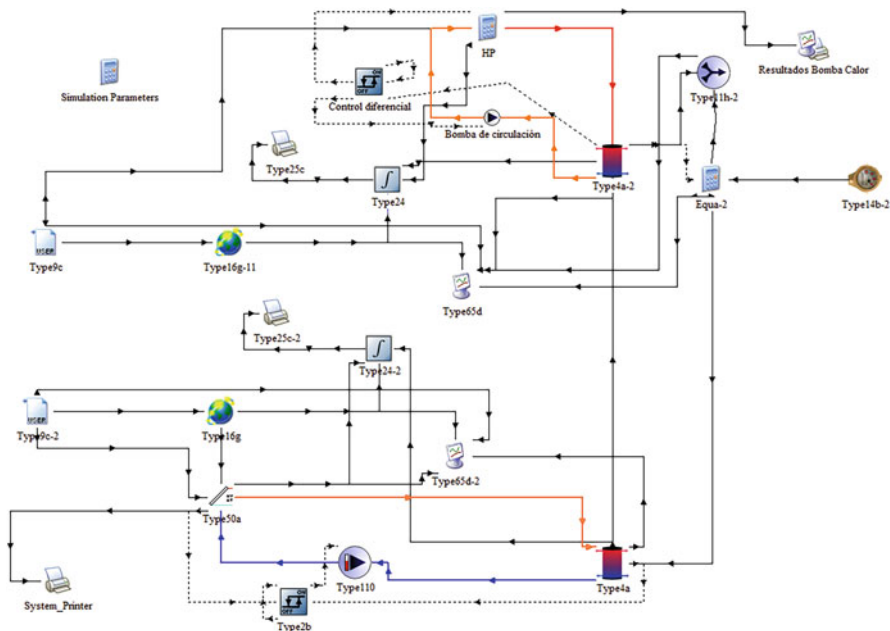


Fig. 2 Schematic of TRNSYS Simulation Studio for the system in shown in Fig. 1f

Table 2 Electricity rate according to the city

City	Per capita consumption kWh/year	Category consumption	Fare USD/kWh
Quito	1261	351–500	0. 105
Emeralds	822	351–500	0. 105
Puerto Baquerizo Moreno	1729	501–700	0. 1285
Guayaquil	1681	501–700	0,1285
Loja	562	151–200	0. 097
Tena	655	201–250	0. 099
Santo Domingo	974	301–350	0. 103
Zamora	1234	351–500	0. 105
Macas	562	151–200	0. 097

family nucleus of four people is considered. The average kWh consumed monthly is being set and as a result of the tariff range in which this consumption falls. Table 2 shows the electricity tariff data for the cities under study.

The rate per kWh is used to determine the operating cost of each of the systems under study and to calculate the savings produced by replacing the heating of water with electrical resistance with other alternatives.

The calculation of the annual costs includes the cost of operation and maintenance of the systems, as reflected in the estimation is 1 and 2 respectively:

$$C_{op} = E_c \times T_e \quad (1)$$

$$C_{om} = C_{op} + C_m \quad (2)$$

where  $C_{op}$  is the annual operating cost in USD,  $E_c$  is the annual energy consumed by the system in kWh,  $T_e$  is the electricity tariff in USD/kWh,  $C_m$  is the annual maintenance cost in USD, and  $C_{om}$  is the annual operation and maintenance cost in USD.

The maintenance period is every ten years for the electrical resistance system and every five years for the other systems. Maintenance includes labor costs and component replacement. To establish energy savings, the difference between consumption with the use of electrical resistance and the alternative system is considered, according to Eq. 3:

$$Savings = (E_{cr} - E_c) \times T_e \quad (3)$$

where  $Saving$  is in USD and  $E_{cr}$  is the energy consumed by the system with electrical resistance in kWh.

It is important to mention that being a service that uses a residence, water heating becomes an expense. Therefore, the analysis is oriented to determine which of the systems represents a lower cost throughout the useful life of the equipment. A time of 20 years is used for the analysis, which refers to the duration of the photovoltaic panel.

In this way, the energy savings represent economic risk or absence of expense, which could compensate for the initial investment in the installation of the system.

In this context, a cash flow, with the discount rate equal to the reference passive rate of the Central Bank of Ecuador, is used to calculate the net present value of the total expenditure over the life of the equipment. A lower cost will be beneficial for the user since it represents a saving in the expense from the use of solar energy instead of the electrical energy coming from the distribution network. If the result gives a positive value, this will imply that there is a recovery of the capital initially invested in the installation of the system caused by the savings in operation.

### 3 Results

This section shows the relevant and summarized results of the energy and economic analysis carried out for the six heating systems studied in the nine defined cities.

### 3.1 Energy Analysis: Electricity Demand

Figure 3 shows the results obtained from the energy analysis for the city of Quito with the monthly electricity demand of each of the systems studied. The reference system (electrical resistance) is the one with the highest electricity consumption followed by the photovoltaic (PV) panel-assisted electrical resistance system.

The latter has a high electricity consumption due to the photovoltaic panels having a low efficiency (less than 15%), so the electrical resistance would work constantly. On the other hand, it can be seen in Fig. 3 that the PV/T system assisted by heat pump presents a negative electricity consumption in all months. This is because the heat pump can provide hot water without having a high electricity consumption. In this way, the electricity demand of the heat pump is assisted in total (at a monthly level) by the electrical energy gained in the PV/T panel. The negative value indicates that a surplus of electricity is injected into the electricity grid, thus generating an electricity credit on the monthly payroll that can be compensated with the electricity consumption of the house (for lighting and equipment).

A more favorable case is that of the Puerto Baquerizo Moreno city, shown in Fig. 4, with better values of extra energy injected to the grid.

Table 3 shows the summary of the results of the energy analysis for all the cities part of this study. As can be seen in the table, for all the cities of study, the PV/T system with heat pump is the one that energetically has a better behavior. This was to be expected since the heat pump has a low energy consumption (compared to an electrical resistance) that is supplied entirely by the electrical energy generated in the PV/T panels.

It can also be observed that although the demand for electricity for water heating is similar in all cities, electricity consumption varies in each system. In the case of the heat pump system, it is expected that warmer cities will have lower energy consumption compared to colder cities. This is because the performance (COP) of the

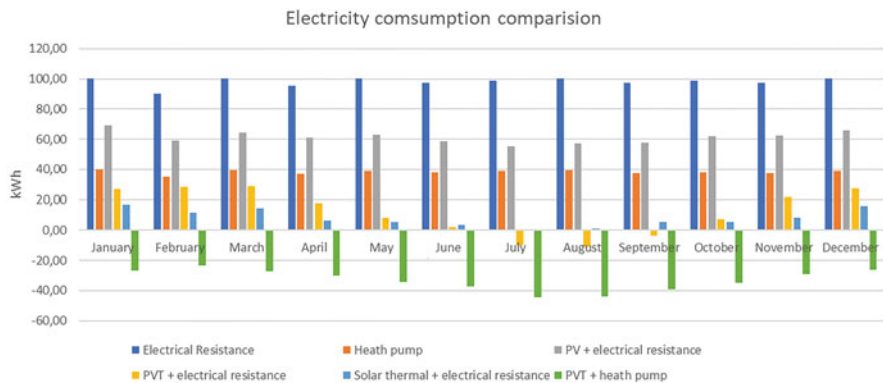
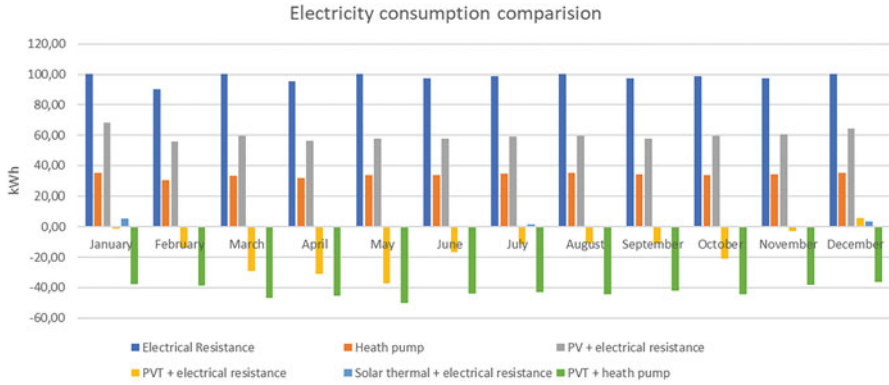


Fig. 3 Comparison of electricity consumption for the different systems studied for the city of Quito



**Fig. 4** Comparison of electricity consumption for the different systems studied for the Puerto Baquerizo Moreno City

heat pump is influenced by the environmental conditions of the heat source (ambient temperature). Thus, where the ambient temperature is higher, a heat pump for heating will operate with a higher COP.

### 3.2 Economic Analysis

The energy analysis is combined with the costs established in the electricity tariff for each city and is used for the calculation of the net present value that allows to compare the cost of the systems for the user, considering a useful lifetime of 20 years. The heating system with electrical resistance, used as the reference case, produces the installation, operation, and maintenance costs, for the studied places indicated in Table 4.

By performing the same analysis for the rest of the cities and systems, the least expensive system for each city can be determined. These results are shown in Table 5.

It is evident that the cost of installation, operation, and maintenance depend on both the electricity tariff and the solar resource present in the place. All cases have in common that the alternatives to the reference system are less expensive, and even in the case of Puerto Baquerizo Moreno, it is possible to recover the investment during the analysis period.

**Table 3** Annual electricity consumption for all the systems studied for each city

City	Electrical resistance	Heat pump	PV + resistance	PV/T + resistance	ST + resistance	PV/T + heat pump
Quito	1176.36	458.31	735.5	144.78	95.32	-395.94
Emeralds	1176.36	397.80	779.74	-27.16	51.96	-424.36
P.B. Moreno	1176.36	404.25	715.49	-179.23	13.16	-510.00
Guayaquil	1176.36	395.78	790.74	-89.18	43.62	-426.18
Loja	1176.36	432.06	795.66	219.35	144.57	-144.57
Tena	1176.36	438.63	814.64	361.64	229.35	-274.84
Sto. Domingo	1176.36	417.41	884.89	497.9	367.72	-197.68
Zamora	1176.36	428.07	845.77	396.21	317.38	-240.82
Macas	1176.36	427.26	818.1	300.01	190.86	-296.62

**Table 4** VAN of the total cost of the electrically resisted system

City	VAN USD
Quito	-2115. 28
Emeralds	-2115. 28
Fr.B. Moreno	-2466. 78
Guayaquil	-2466. 78
Loja	-1995. 62
Tena	-2025. 53
Sto. Sunday	-2085. 36
Zamora	-2115. 28
Macas	-1995. 62

**Table 5** NPV results for the least expensive system by the city

City	Major VAN system	VAN USD
Quito	Solar thermal with electrical resistance	-1003. 22
Emeralds	PV/T with electrical resistance	-846. 87
Fr.B. Moreno	PV/T with electrical resistance	17. 80
Guayaquil	PV/T with electrical resistance	-276. 47
Loja	Solar thermal with electrical resistance	-1224. 98
Tena	Solar thermal with electrical resistance	-1415. 86
Sto. Sunday	PV/T with heat pump	-1678. 17
Zamora	PV/T with heat pump	-1523. 02
Macas	Solar thermal with electrical resistance	-1339. 16

## 4 Conclusions

The present study aimed to analyze energetically and economically different systems of production of domestic hot water (DHW). Through the results it was possible to show that for all the cities studied there is a more efficient DHW production system than the reference system (heating with electrical resistance). However, it was shown that, depending on the electricity tariff and the solar radiation potential of each city, not always the same DHW production system is the most feasible.

For example, for the cities of Quito, Loja, Tena, and Macas, due to their relatively high solar radiation and no lower electricity cost than in other cities, the most economically feasible system is the solar thermal system with flat plate solar collectors and an electrical resistance as an auxiliary system. On the other hand, for cities with high solar radiation and high cost of electrical energy such as Esmeraldas, Puerto Baquerizo Moreno, and Guayaquil, the DHW production system with PV/T and electrical resistance as an auxiliary system is the most profitable. This is due to the electricity savings that are produced by the electrical production of PV/T panels.

Finally, for the cities of Santo Domingo and Zamora, due to their lower solar radiation and high electricity cost, it was evident that the DHW production system with PV/T-assisted heat pump is the most profitable in the 20-year horizon. Although this system is the one with the highest initial investment cost, the electricity savings from the use of a heat pump justify this investment in the long term.






This work opens the door for future research on the technical feasibility of local development of technologies such as solar panels, PV/T, and heat pumps in the country. Due to the unique weather conditions in Ecuador, a low-power heat pump would work efficiently and without representing a high investment. Likewise, different electric energy cost scenarios can be studied to determine minimum electric energy costs so that each of these systems are profitable throughout their useful life. Finally, it is worth mentioning that nowadays the use of artificial intelligence tools such as machine learning could be used to predict the performance of DHW systems considering the variability of the weather conditions in a place like Ecuador. This could open the door for further interdisciplinary investigation in this field.

## References

1. International Energy Agency (IEA). (2019). *World Energy Outlook 2019 – Analysis - IEA*. World Energy Outlook.
2. Pomianowski, M. Z., Johra, H., Marszal-Pomianowska, A., & Zhang, C. (2020). Sustainable and energy-efficient domestic hot water systems: A review. *Renewable and Sustainable Energy Reviews*, 128, 109900. Elsevier Ltd. <https://doi.org/10.1016/j.rser.2020.109900>
3. O. Ibrahim, F. Fardoun, R. Younes, and H. Louahlia-Gualous, "Review of water-heating systems: General selection approach based on energy and environmental aspects," *Building and Environment*, vol. 72. pp. 259–286, Feb. 2014, <https://doi.org/10.1016/j.buildenv.2013.09.006>.
4. Li, X., Wu, W., & Yu, C. W. F. (2015). Energy demand for hot water supply for indoor environments: Problems and perspectives. *Indoor and Built Environment*, 24(1), 5–10. SAGE Publications Ltd. <https://doi.org/10.1177/1420326X14564285>
5. Fuentes, E., Arce, L., & Salom, J. (2018). A review of domestic hot water consumption profiles for application in systems and buildings energy performance analysis. *Renewable and Sustainable Energy Reviews*, 81, 1530–1547. <https://doi.org/10.1016/j.rser.2017.05.229>
6. F. J. Aguilar, S. Aledo, and P. V. Quiles, "Experimental study of the solar photovoltaic contribution for the domestic hot water production with heat pumps in dwellings," *Applied Thermal Engineering*, vol. 101, pp. 379–389, May 2016, <https://doi.org/10.1016/j.applthermaleng.2016.01.127>.
7. British Standards Institution. (2006). *Thermal solar systems and components: Solar collectors. Part 2, Test methods*. BSI British Standards Institution.
8. Aguilar, F. J., Crespi, D., & Quiles, P. V. (2019). Experimental and numerical study of the domestic hot water production with PV panels and a heat pump. *E3S Web of Conferences*, 111, 01066. <https://doi.org/10.1051/e3sconf/201911101066>
9. Chow, T. T. (2010). A review on photovoltaic/thermal hybrid solar technology. *Applied Energy*, 87(2), 365–379. <https://doi.org/10.1016/j.apenergy.2009.06.037>
10. ASAMBLEA NACIONAL. (2019). Ley Orgánica de Eficiencia Energética. *Registro Oficial*, 449.
11. Ministerio Coordinador de Sectores Estratégicos, Balance Energético Nacional. 2015.
12. Ordóñez, F., Morales, C., López-Villada, J., & Vaca, S. (2018). Assessment of the energy gain of photovoltaic systems by using solar tracking in equatorial regions. *Journal of Solar Energy Engineering*, 140(3). <https://doi.org/10.1115/1.4039095>
13. ARCONEL. (2019). Pliego Tarifario para las Empresas Eléctricas de Distribución.
14. ARCONEL. (2019). Estadística Anual y Multianual del Sector Eléctrico Ecuatoriano.

# Impact of the Biodiesel Blend (B20) Strategy “Club de Biotanqueo” (Biofueling Club) on the Socioeconomic and Environmental Aspects in Medellín, Colombia



Mónica Andrea Sánchez Anchiraico , Lily Margarita León Sánchez ,  
Jhojan Stiven Zea Fernández , Mario Luna-delRisco ,  
Carlos Arrieta Gonzalez , Erika Viviana Díaz Becerra,  
and Liliana González Palacio 

## 1 Introduction

Colombia is the fourth largest producer of palm oil in the world and the first in America. The Colombian palm cultivation has been leading in the national agricultural sector due to its productive dynamics, versatility, and mainly, its commitment to social sustainability. In addition, it has been positioned as the main raw material to produce biodiesel [1]. Currently, palm cultivation is in 21 departments and 162 municipalities with 590,189 hectares. Oil palm is the most productive oilseed on the planet since one hectare produces between six and ten times more than any other [2].

In Colombia, palm oil is an agrobusiness established based on social and economic policies, where industrial growth has been encouraged through products such as food, energy, and cosmetics, in which the latter are considered complementary products to the production of vegetable oil for food use. This industry was firstly supported by Fedepalma as a trade union organization in Colombia. This government agency supported farmers in the development and expansion of the crop production. In addition, it also regulates business alternatives for the diversification of the palm oil industry [3].

---

M. A. Sánchez Anchiraico · L. M. León Sánchez · J. S. Zea Fernández · M. Luna-delRisco (✉) ·  
C. Arrieta Gonzalez  
Universidad de Medellín, Medellín, Colombia  
e-mail: [mluna@udemedellin.edu.co](mailto:mluna@udemedellin.edu.co)

E. V. Díaz Becerra  
Bio D S.A, Terminal de combustibles Sabana Mancilla – Facatativa, Facatativa, Colombia

L. González Palacio  
Universidad EAFIT, Medellín, Colombia

Production and use of biodiesel in the first semester of 2019 presented a growth in the national demand of 6.6% compared to the first semester of 2018; this is due to the demand for diesel and the current biofuel blend mandate of B10 [4]. In 2020, B10 demand was affected due to mobility restrictions as a result of the Covid-19 pandemic. This phenomenon caused a decrease in sales of approximately 3.8% in relation to 2019. There were reported a total sale of 391,000 tons of biodiesel in 2020, representing 25% of the total for the sector and 7.1% below the volume of 2019 [1]. On the other hand, production of biodiesel brings workers in the palm sector benefits such as higher incomes leading to good quality of life and consolidate in the local market [5].

Environmental impacts of biodiesel have been widely studied for decades from raw materials like palm oil and other oils in the world. Manufacturers and producers of biodiesel have made efforts in countries such as the United States, Brazil, and Argentina to study the behavior of different types of vehicles as the proportion of biodiesel in fossil diesel increases, and in some cases, they have even used B100 on their engines. Colombia has successfully made a mixture of B20, going from the regulated B10 to B20 with 180 light-duty vehicles with a traveled distance of more than three million kilometers and a vehicle with B100 that has traveled more than 35,000 kilometers. Studies conducted by the University of Antioquia together with the company Bio D S.A. have evaluated the emissions of particulate matter PM<sub>2.5</sub> in dynamic tests, finding lower particle emissions reaching a reduction of up to 37% and 65%, respectively [6]. These results were observed and validated after approximately an hour later of travel when biofuel was mixed on tested vehicles. However, heavy-duty vehicles are expected to obtain even greater reductions in normal operating conditions. The main objective of this research is to present the evidence of the successful pilot test of heavy-duty vehicles during normal periods of operation on the road and their reduction in emissions of particulate matter.

## **2 Land Use Background and National Overview of Biodiesel Production in Colombia**

### ***2.1 Agricultural Development Toward Biomass Production***

Agriculture in Colombia has been affected in the past three decades by changes in public policies. In the 1990s, a reform was made that favored imports of various food goods, thus subjecting national farmers to competition from the external market resulting in a slowed down of the agriculture market growth [7]. This situation caused a decrease of planted area of temporary crops, thus increasing permanent crops. In this way, temporary crops went from representing more than half of the area planted in the 1990s to occupying between 30% and 40% in the last decade.

Permanent crops in Colombia have shown a significant growth of the sowing areas as well as a strong promotion toward the main traditional crops. Between 2007 and 2020, the participation of permanent crops has increased by almost one million hectares, in which the oil palm stands as the one with the highest market participation with an increase of 102%.

## ***2.2 Potential Energy Use of Residual Biomass***

Demographic increase in Colombia during the past few decades has increased pressure on agricultural fields, agroindustry processes, and especially on natural resources. In this matter, the Food Loss Index (FLI) of the Food and Agriculture Organization of the United Nations (FAO) estimated that around 14% of all crops are lost worldwide. The study included biomass from its post-harvest state to retail sale [8]. On the other hand, it is estimated that in Colombia approximately 11.6 million tons of solid waste are generated per year, of which only 17% is used [9]. The use of residual biomass could lead to a solid strategy that promotes food security as well as the development of new business models that encourage circular economy, including bioenergy production [10].

Currently, these energy sources do not represent a large share in the Colombian energy basket; only 5% of the energy used by the transport system comes from biofuels. By 2030, it is planned to decarbonize the energy source of transport by 20% using renewable energy sources such as biomass [11].

## ***2.3 Share of Biofuels in the Colombian Energy Market***

Main biofuels used in Colombia are bioethanol and biodiesel. Regulation and promotion of biogas has recently gained interest, but its promotion lacks governmental support. By 2021, data gathered from different countries showed that world biofuels produced comes from about 64% of ethanol that is produced from corn, 26% from sugar cane, 3% from molasses, 3% from wheat, and the rest from other cereals such as cassava or sugar beets. For biodiesel, production is based on 77% vegetable oils (37% canola oil, 27% soybean oil, and 9% palm oil) and 23% from residual cooking oils. Biofuel production sectors are strongly regulated by national policies with three main objectives: to provide support to the producer, to reduce greenhouse gas (GHG) emissions, and to reduce energy dependence on fossil fuels [12].

In 2005, Colombia began to implement a biofuel blend strategy in the transport sector with the aim of reducing polluting emissions from gasoline and motor fuel oil (ACPM) using bioethanol and biodiesel, respectively. For this, the government began to give incentives to the agricultural sector to promote the cultivation of the necessary inputs such as sugarcane and palm oil [13].

Biodiesel was implemented in Colombia in 2008 by using palm oil as raw material. This decision was argued given that the country was the first producer in Latin America and the fifth in the world for that year. By 2021, Colombia has implemented 11 biodiesel production plants distributed in various areas of the country, with a production of about 770,000 tons per year of biodiesel [14].

## 2.4 Geographical Distribution of Biodiesel Production Industrial Facilities

In 2008, production of biodiesel began its operations in Colombia with the use of palm oil as a raw material. By 2013, Colombia reached an approximate production of 1 million tons of palm oil. Later in 2017, production reached more than 1.6 million tons of palm oil, production that has remained stable until 2021. Colombia has 11 biodiesel production plants with a total capacity of biofuel production of 767,000 tons per year [15]. The spatial location of these biorefineries is presented in Fig. 1.

Among the 11 facilities that are currently operating in Colombia, Bio D stands as the company with the highest production of biodiesel with a 26% share of the total market. Biodiesel produced and blended to B20 is supplied by the Bio D company as a voluntary blending strategy for dump trucks and trucks sector.

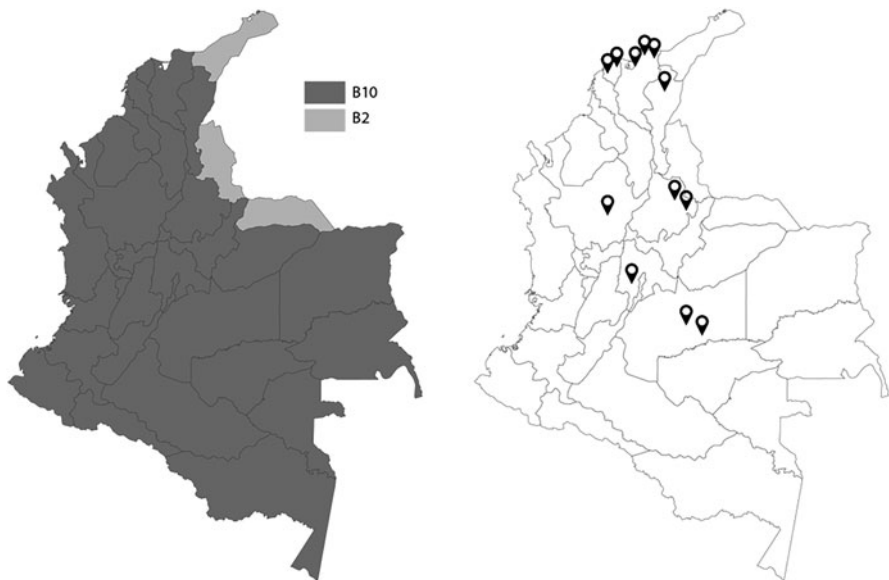


**Fig. 1** Biodiesel geographical blend distribution and location of facilities

### 3 Results and Discussion

The palm oil industry in Colombia stands as a national development instrument that improves the living conditions of the rural population, through employment and poverty reduction [16]. The cultivation of palm oil generates more than 185,000 direct and indirect jobs that benefit thousands of Colombian families. This industrial sector has 133 Strategic Productive Alliances (SPA) and models of good business care. It is supported by the state and provides significant changes in the quality of life of rural residents and communities [2]. Through these alliances, the palm sector promotes legal formality, well-paid employment, and health coverage for its employees, among other benefits that other agricultural activities do not have [17]. In addition, it promotes exclusive businesses and associativity in the different palm tree areas [18].

By 2020, the unemployment rate in the agricultural sector in Colombia was 15.9%, 5.4 percentage points higher than the previous year (10.5%). This phenomenon originated from the combined effect of the digital transformation and the pandemic [1]. Despite this, the palm sector reported 82.4% of formal jobs generated, meaning 188,506 total jobs with an average salary of 1.5 times higher than the Colombian minimum wage [19].

In addition, palm oil cultivation has represented an important change in some regions of the Colombian armed conflict since it presents a viable substitute for illicit crops by providing a legal and stable employment opportunity for a group of rural workers [16].

#### 3.1 *Club de Biotanqueo Strategy Overview*

The Colombian government allows biodiesel blend up to 12% in the diesel fuel that is distributed in Colombia. With this strategy, the government aims at reducing approximately two million tons of CO<sub>2</sub> per year. In order to achieve a greater impact on the reduction of greenhouse gases generated by the automobile fleet, in 2020, resolution 40,177 established the criteria for pilots of superior biodiesel mixtures in which the Club de Biotanqueo with 180 vehicles was started [6]. This program is supported by the National Federation of Biofuels in Colombia, which is a union entity that groups entrepreneurs and institutions that are committed to the development and positioning of biofuels to contribute to energy autonomy, environmental sustainability, and employability in rural areas of the country [20].

The Club de Biotanqueo is a voluntary biodiesel blending program that consists of a group of Colombians who promote sustainable mobility. The objective of the program is to increase the percentage of diesel biofuel mixture (B20, B50, B100) to that established by the current biodiesel regulation (B10) [21].

One of the allies and beneficiaries of the strategy is the Association of Dump Truck Drivers from Antioquia (DTDA), a sector that has been widely criticized for its contribution to air pollution in the metropolitan area of Aburra Valley (Antioquia, Colombia). Consequently, the DTA demonstrated its commitment to the environment and decided to change the fuel mix they currently use (B10) and replace it with the voluntary biodiesel mix B20 [6]. By 2021, the Club de Biotanqueo has the participation of approximately 700 vehicles including dump trucks and other heavy-duty trucks in accordance with the agreements established in resolution 31,392 of September 15, 2020. In the same way, the company Coordinadora Mercantil is also operating its 200 vehicles with a B20 mix, approved by resolution 31,440 of December 11, 2020 [22].

### ***3.2 Club de Biotanqueo Vehicle Selection***

The pilot test was carried out under the supervision and support of the Metropolitan Area of Aburra Valley and the Colombian Ministry of Environment and Sustainable Development through agreement 686 of 2020 with the University of Antioquia. Heavy-duty vehicles such as trucks and dump trucks that operate with diesel fuel and that have a cylinder capacity greater than 2500 cubic centimeters participated in the study for free. Additionally, the participant vehicles had to comply with emissions lower than 1.5 million particles per cubic centimeter of PM 2.5. Selected vehicles were differentiated with a labeling that identified them with the traffic authorities of the Aburra Valley.

### ***3.3 Club de Biotanqueo Supply Chain***

There are six stages on the fuel supply chain to generate B20 biodiesel mixture. The chain starts from the diesel production at B2 in a petroleum refinery (ECOPETROL) that is later distributed via pipelines throughout the national territory. Subsequently, fossil diesel is mixed by the wholesaler with biodiesel at B100 and conditioned to B20. The whole process is mandatory complying with the quality certifications established by resolution 40,103 of 2021 [23]. Throughout the process, the custody of the quality of the B20 mixture is supervised by the B100 producing company (Bio D). The custody also guarantees the fuel mixture quality for the end user (Fig. 2).

Along the supply chain, the B100 producer periodically conducts pilot tests to verify the environmental benefits of the use of biofuel, presenting the carbon footprint associated with the use of B20 biofuel. Additionally, it promotes strategic alliances with engine manufacturers, biodiesel producers nationwide, and actors in the fuel supply chain. The aim of building strategic alliances allows strengthening the requirements for the use of biofuel B20 before the national authorities.

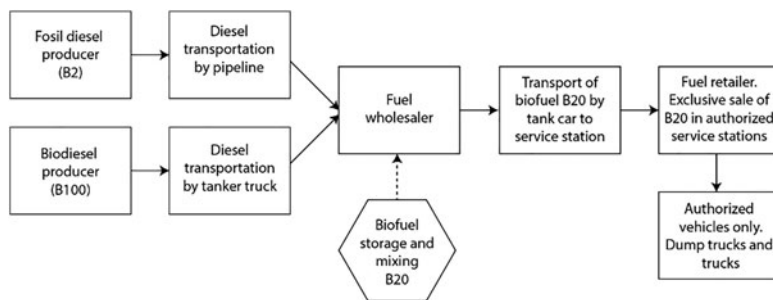


Fig. 2 B20 supply chain from producers to final consumer

Table 1 Comparison of PM2.5 emissions reduction for B10 and B20 blends

Vehicle Brand	Model	B10 (#/cm <sup>3</sup> )	B20 (#/cm <sup>3</sup> )	B20 emission reduction (%)
Renault	2013	2.54	2.19	14%
Kenworth	2015	4.91	1.65	66%
International	2013	2.05	0.92	55%
Freightliner	2013	1.58	1.15	27%
Ford	1963	10.19	2.67	74%

Source: BioD, 2021

### 3.4 Environmental and Social Impact of the Club de Biotanqueo Strategy

From an environmental perspective, the Club de Biotanqueo encourages the use of biofuel by promoting the reduction of up to 90% the opacity of the fumes, which would reduce the visual pollution generated by the exhausts of the vehicles. In addition, the use of the B20 mixture reduces SOx emissions and reduces soot emissions by up to 55%, eliminating black smoke and bad odors. With the proposed biofuel blend strategy, it is estimated a reduction of 4.3 million tons of CO<sub>2</sub>, which is a key factor for Colombia to reach the decarbonization goal established in the commitments of the Paris agreement to mitigate climate change.

According to data reported on August 11, 2021, dump trucks that use the voluntary B20 blend reported an estimated emissions reduction of about 191 tons of CO<sub>2</sub> equivalent into the atmosphere, data obtained from sensors coupled to the fuel system of the vehicles (Table 1).

Likewise, the production of biodiesel in Colombia leads to changes in the social and economic environment of the country. From the oil extraction process in the cultivation fields, its transformation, and commercialization, biodiesel encourages the development and growth of the production chain by impacting positively raw material suppliers, biodiesel producers, and biodiesel distributors.



### 3.5 Regulations and Incentives

The Colombian government seeks to promote the production of biofuels through regulatory instruments and economic incentives in order to take advantage of opportunities for economic and social development in the market [24]. Table 2 presents some of the main laws, decrees, and resolutions to produce biodiesel.

### 3.6 Scalability Potential of the Club de Biotanqueo Strategy

Fedepalma followed the initiative of the Club de Biotanqueo to promote the use of superior biodiesel blends. In the pilot test, two vehicles with B50 blend were analyzed on route. The test was carried out with Cenipalma and Bio D S.A. in the second semester of 2019 in Bogotá without presenting any issues. The strategy was also extended to Transmilenio (mass transportation system in Bogota), Terpel, Conexión Móvil, Bio D S.A., National University (Universidad Nacional) and Gesoltec in a project for the use of B50 in Transmilenio. The trial presented

**Table 2** Regulatory framework of biodiesel in Colombia

Legislation	Description
Law 693 of 2001	Authorization of biodiesel blends
Resolution 910 of 2008	It establishes the permissible levels of pollutant emission that land mobile sources must comply with are regulated
CONPES (National Council for economic and social policy) 3510 of 2008	Policy guidelines to promote sustainable biofuel production in Colombia
Law 1715 of 2014	Regulates the integration of nonconventional renewable energies to the National Energy System
Law 1819 of 2017	Fixed income tax for late-yield crops with a preferential rate of 9% for 10 years
Resolution 40,666/2019	It establishes a maximum biofuel content for use in diesel engines of 12% in the mixture with fossil diesel fuel in some areas of the country
Resolution 1972 of 2019	It establishes the protection of the rights to health and a healthy environment, establishing measures aimed at reducing polluting emissions from mobile sources
Resolution 40,178/2020	It establishes provisions for conducting pilot programs for superior biofuel blends for exclusive use in motor vehicles or land mobile sources
Resolution 40,177 of 2020	It defines energy sources with low or zero emissions having as a fundamental criterion their content of components that are harmful to health and the environment
Resolution 40,103/2021	It establishes diesel fuel quality parameters and requirements for use in ignition engines

Source: The authors. Adapted from [25–27]

promising results in which a reduction of 62.5% of the particulate matter compared to mixture B10 was obtained. These data confirm that blends with biodiesel B20 or higher are an alternative to reduce pollution in urban centers [28]. Similarly, regarding the dump trucks and trucks sector, studies carried out during the pilot tests showed an increase in the performance of engines that increases the life of the engines because it has a greater lubricating power and it also decreases the noise of the engines due to its detergent power, keeping the fuel circuit driving and injection systems of the engines clean. Although the selling price of B20 biodiesel is higher than the B10 mix price available at service stations nationwide, benefits such as savings in engine oil change due to lubrication benefits and environmental certification for free movement in the urban centers have generated great interest toward adoption in the Aburra Valley. The results obtained until 2021 of this pilot tests encourage the implementation of the strategy in other urban centers with high levels of air pollution, guaranteeing the mobilization of dump trucks and trucks, vehicles required for the development of the construction sectors, the final disposal debris, among others.

## 4 Conclusions

Production of biodiesel from palm oil in Colombia and its blending into the fossil fuel matrix for the public and private transportation system is proposed as a strategy that aims to reduce the environmental impacts generated by mobile sources. The continuous improvements in the production processes of biodiesel production plants, complying with quality standards, and a regulatory framework that incorporates incentives for companies, brings benefits in air quality and encourages the generation of employment and the diversification of fuels in the Colombian territory.

The results obtained, in terms of air quality, by the dump trucks and trucks sector, open the door to the implementation of new fuel stations with biodiesel blends higher than those regulated by the actual Colombian regulation (B10). However, the commitment of government entities is required for the more inclusive promotion of these strategies so that they can be replicated in other cities in Colombia.

Similarly, biodiesel quality certifications, environmental commitment along the production chain, and the corresponding permits for the use of these fuels in the vehicle fleet of dump trucks and trucks are consolidated as good practices that support the relevance of biodiesel blends regarding the benefits on air quality.

The Club de Biotanqueo strategy presents results that allow improving the quality of life of the population by reducing the emission of particulate matter (PM), mainly PM 2.5, which is the main cause of respiratory diseases and early deaths. In addition, biodiesel does not contain sulfur dioxide (SO<sub>2</sub>), which is a gaseous pollutant that directly affects health. In recent years, according to the National Planning Department (DNP), nearly 67 million illnesses and respiratory symptoms have been seen, due to poor air quality; therefore, the use of biodiesel in the diesel fuel mixture would contribute to avoid about 6000 deaths annually and a great reduction in cases of respiratory diseases.

**Acknowledgments** The authors would like to thank the University of Medellín, especially the Faculty of Engineering and its Research Center (CEIN), for the economic and strategic support to carry out this research. We also want to highlight the contributions made by the Dump Truck Community of Antioquia for all the meetings held that allowed us to deepen into this research. Likewise, we express our greatest gratitude to the Bio D company for all the support, information, and management carried out during this investigation.

## References

1. Fedepalma. (2020). Informe de gestión de Fedepalma.
2. Fedepalma. (2021). La palma de aceite en Colombia.
3. Yusoff, M. N. A. M., et al. (2021). Sustainability of palm biodiesel in transportation: A review on biofuel standard, policy and international collaboration between Malaysia and Colombia. *Bioenergy Research*, 14(1), 43–60. <https://doi.org/10.1007/s12155-020-10165-0>
4. Fedebiocombustibles. (2019). Biocombustibles: Boletín N° 198. <http://www.fedebiocombustibles.com/v3/nota-web-id-3163.htm>. Accessed 26 Aug 2021.
5. Ramírez Camacho, J. A., & Rodríguez Pava, S. C. (2019). Conveniencia de la Producción de Biodiesel en Colombia desde la Perspectiva del Desarrollo Sostenible. *Univ. Catol. Colomb.*, 1(1): 1–40, [Online]. Available: [https://repository.ucatolica.edu.co/bitstream/10983/23602/1/Conveniencia de la producción de biodiesel en Colombia desde la perspectiva del desarrollo sostenible.pdf](https://repository.ucatolica.edu.co/bitstream/10983/23602/1/Conveniencia%20de%20la%20producci3n%20de%20biodiesel%20en%20Colombia%20desde%20la%20perspectiva%20del%20desarrollo%20sostenible.pdf).
6. Agudelo, J., Gutierrez, E. & Benjumea, P. (2019). Análisis experimental de la combustión de un motor diésel de automoción operando con mezclas diésel-biodiésel de palma. *Revista Dyna*, vol. 76, pp. 103–113.
7. Perfetti, J. J., & Hernández, A.. (2016). Nota de lineamientos estratégicos para la agricultura en Colombia, pp. 2–247.
8. P. y U. FAO, FIDA, OMS, *El estado de la seguridad alimentaria y la nutrición en el mundo 2019*. 2019.
9. Daza Serna, L. V., Solarte Toro, J. C., Serna Loaiza, S., Chacón Perez, Y., & Cardona Alzate, C. A. (2016). Agricultural waste management through energy producing biorefineries: The Colombian case. *Waste Biomass Valorization*, 7(4), 789–798. <https://doi.org/10.1007/S12649-016-9576-3>
10. MADS. (2021). Colombia inicia acciones para la gestión sostenible de la biomasa residual | Ministerio de Ambiente y Desarrollo Sostenible. <https://www.minambiente.gov.co/index.php/noticias/5170-colombia-inicia-acciones-para-la-gestion-sostenible-de-la-biomasa-residual>. Accessed 17 Aug 2021.
11. Fedebiocombustibles. (2020). Menosprecio por los biocombustibles. <https://www.fedebiocombustibles.com/nota-web-id-3259.htm>. Accessed 18 Aug 2021.
12. F. OCED. (2020, October). OCDE-FAO Perspectivas Agrícolas 2020–2029. <https://doi.org/10.1787/A0848AC0-ES>.
13. Triana, J. M., & Econ, C.. (2020). Desempeño del fondo de estabilización de precios del aceite crudo de palma en la mantención del ingreso del palmicultor colombiano: 2005–2015, pp. 2005–2015.
14. Fedebiocombustibles. (2020). Biodiésel de palma de aceite. [http://www.fedebiocombustibles.com/v3/estadistica-mostrar\\_info-titulo-Biodiesel.htm](http://www.fedebiocombustibles.com/v3/estadistica-mostrar_info-titulo-Biodiesel.htm). Accessed 18 Aug 2021.
15. Bautista, S., Espinoza, A., Narvaez, P., Camargo, M., & Morel, L. (2019). A system dynamics approach for sustainability assessment of biodiesel production in Colombia. Baseline simulation. *Journal of Cleaner Production*, 213, 1–20. <https://doi.org/10.1016/J.JCLEPRO.2018.12.111>

16. Mesa, J., et al. (2016). La palma de aceite una agroindustria eficiente, sostenible y mundialmente competitiva. *Rev. Palmas Espec. Tomo I*, 37, 121–2923.
17. Departamento Administrativo Nacional de Estadística [DANE]. (2018). Boletín técnico Encuesta de Empleo Directo Sector Palmero 2016. *Dane*, 1–22.
18. Garc, F., & Bogot, D. S. (2019). Contexto y perspectivas económicas de la agroindustria de la palma de aceite en Colombia 1. Contexto global de la palmiticultura.
19. Mesa Dishington, J., & Azuero García, A. F. (2021). Balance 2020 y perspectivas 2021 de la agroindustria de la palma de aceite. *Fedepalma*: 41, [Online]. Available: [http://web.fedepalma.org/sites/default/files/files/Fedepalma/03032021\\_Balance\\_y\\_perspectivas\\_de\\_la\\_agroindustria\\_de\\_la\\_palma\\_de\\_aceite\\_2020-2021\\_CMG\\_ASM.pdf](http://web.fedepalma.org/sites/default/files/files/Fedepalma/03032021_Balance_y_perspectivas_de_la_agroindustria_de_la_palma_de_aceite_2020-2021_CMG_ASM.pdf)
20. Heckman, J. J., Pinto, R., & Savelyev, P. A. (2017). Informe COE 2016–2017. *Angew. Chemie Int. Ed.*, 6(11), 951–952.
21. Fedebiocombustibles. El club de biotanqueo. <http://www.fedebiocombustibles.com/main-pagina-id-36.htm>. Accessed 25 Aug 2021.
22. Fedebiocombustibles. (2021). Lo que nos dejó el 2020 y lo que promete el 2021. <https://www.fedebiocombustibles.com/nota-web-id-3300.htm>. Accessed 25 Aug 2021.
23. Orjuela-Castro, J. A., Aranda-Pinilla, J. A., & Moreno-Mantilla, C. E. (2019). Identifying trade-offs between sustainability dimensions in the supply chain of biodiesel in Colombia. *Computers and Electronics in Agriculture*, 161, 162–169. <https://doi.org/10.1016/J.COMPAG.2018.03.009>
24. Conpes 350, *Lineamientos de políticas para promover la producción sostenible de biocombustibles en Colombia*. 2008.
25. Vásquez Quintero, A. (2016). El sector de la agroindustria: condiciones laborales y problemáticas en la producción de aceite de palma y azúcar El Sector de la Agroindustria. *Esc. Nac. Sindica*, 172.
26. Heber Segura, S. (2019). Incentivos a actividades económicas consolidadas en Colombia: El caso de los biocombustibles como el Etanol y el Biodiesel.
27. Fedebiocombustibles. (2021). Normatividad de la Agroindustria de los biocombustibles. <https://www.fedebiocombustibles.com/main-pagina-id-2-titulo-normatividad.htm>. Accessed 18 Aug 2021.
28. Fedepalma. (2019). Optimizar la Rentabilidad Palmera.

# Index

## A

- Adaptive neuro-fuzzy inference system (ANFIS), 15
- Airfoils
  - computers, 104
  - efficiency, 94, 95
  - Eulerian frame of reference, 92
  - flow chart, 99, 100
  - geometrical model, 95
  - mapping of efficiency, 92
  - movements, 93
  - NACA 0020 vs. NACA 1412, 99, 100, 102, 103
  - numerical model
    - boundary conditions and loads, 98
    - dynamic mesh, 98
    - mesh types, 96
    - meshing and mesh independence analysis, 96
    - solver and residuals, 99
    - UDF, 98
  - optimal parameters, 92
  - oscillatory, 91
  - power, 94, 95
  - power extraction regime, 94
  - recommendations, 105
  - results
    - energy and efficiency, 100, 102, 103
    - forces, 99
    - observation, 104
    - validation, 104
    - types, 91
- Alternative energy sources
  - altruistic philosophy, 110
  - benefits, 115
  - development and implementation, 109, 117
  - ecotoxicological and environmental effects, 110
  - habitats, 117
  - impacts, 111
  - management, 116
  - methods, 110, 117
  - photovoltaic energy, 114, 115
  - photovoltaic systems, 116
  - potential risks, 115
  - production systems, 109
  - selected articles, 111
  - technologies, 110
  - wave power, 112, 113
  - wind power, 113
  - wind turbines, 115
- Altruistic philosophy, 110
- Ansys fluent, 96
- Articulated semi-submerged cylindrical equipment (AsSCE), 112
- Artificial neural networks (ANN), 15
- Association of Dump Truck Drivers from Antioquia (DTDA), 180
- Au-PSC, 39
- Autoregressive integrated moving average (ARIMA) model, 15, 18
- Autoregressive moving average (ARMA), 15

**B**

Battery energy storage systems (BESS), 154, 155, 157, 158

Biodiesel blend (B20) strategy

agricultural development, 176

agricultural sector, 179

agrobusiness, 175

air quality, 183

biofuels, 177, 178

Club de Biotanqueo

environmental and social impact, 181

regulations and incentives, 182

scalability, 182, 183

strategy, 179, 180

supply chain, 180

vehicle selection, 180

Colombia, 175

environmental impacts, 176

FedePalma, 175

geographical distribution, 178

heavy-duty vehicles, 176

industrial facilities, 178

oil palm, 175

palm cultivation, 175

palm oil industry, 179

PM, 183

production, 176

Biofuels, 177, 178

Biogas, 47, 48, 53

Bioreactor

biogas production, 53, 55

characteristics, 51, 53

design, 49, 58

geometry, 48

Gompertz model application, 56–58

implementation, 58

instrumentation, 50, 51

materials, 49

monitoring, 53

organic fraction, 48, 51, 58

preparation, 53

prototype, 57

size, 57

Box-Jenkins methodology, 18

Building information modeling (BIM), 138

**C**

Carbon, 35

Carbon-based perovskite solar cells (C-PSC)

characteristic values, 36

commercialization, 40

fabrication method, 39

FTO, 37

fully printable, 37, 38

HTM-free printable, 37

interfacial engineering, 38

manufacturing methods, 40

materials, 35

modular design, 39

multidimensional interface, 38

Ni-doped rutile TiO<sub>2</sub>, 38

PCE, 41

perovskite layer deposition, 41

post-treatment, 39

production cost, 35

research, 37

schemes, 35, 37

TDPI, 37

Carbon film preparation, 39

Carbon nanotubes (CN), 39

Colombian Ministry of Environment, 180

Colombian Refrigeration Potential Map

absorption cooling cycles, 4

cooling potential, 10

fuel supply, 11

modeling/methodology

absorption cooling system, 8

MATLAB script, 8

subscripts, 6

symbols, 5, 6

thermodynamic model, 6, 8

national territory, 4, 9

nonrenewable energy sources, 3

renewable energy, 3

results, 8, 10, 11

system description, 4

uses, 12

Commercial silicon photovoltaic cells, 36

Computational fluid dynamics (CFD), 70

Copper phthalocyanine (CuPc), 38

COVID-19 pandemic, 121

**D**

Deep recurrent neural networks (DRNN), 15

Domestic hot water (DHW)

auxiliary system, 173

building sector, 163

case study, 165

economic analysis, 164, 167–169, 171

electric and gas boilers, 164

electricity demand, 170, 172

electricity tariff, 173

energy analysis, 164, 167

machine learning, 174

- renewable energy resources, 163
  - results, 169
  - solar radiation, 173
  - systems description, 165, 167
  - weather data, 165
- E**
- Educational building, 148
  - Electrical resistance, 165
  - Electricity power, 124
  - Electric vehicles (EV), 152
  - Electrodes, 41
  - Electron transport material (ETM), 34
  - Energy assessment platform
    - accuracy, 133
    - algorithms calculation, 125
    - case study, 128, 129
    - CO<sub>2</sub> emissions, 127, 128, 133
    - consumption reduction potential, 132
    - data collection, 124–126
    - design, 127, 128
    - development, 133
    - energy consumption, 132
    - methodology scheme, 124
    - residential sector, 122–124, 133
    - results, 130, 131
    - savings potential, 133
    - uses, 132
  - Energy calculator, 132
  - Energy curtailment, 153–155, 157, 158
  - Energy efficiency
    - carbon dioxide, 137
    - climate analysis, 142, 146
    - construction elements, 145–147
    - description, building, 138, 139
    - development phases, 139, 140
    - direct and indirect emissions, 137
    - economic saving, 148
    - educational center, 141
    - energy demand amplification, 137
    - energy simulation, 140
    - greenhouse gases effect, 148
    - heat transfer coefficient, 141
    - operational hours, 145
    - orientation analysis, 143, 147
    - photovoltaic panels, 148
    - Revit program, 141
    - Revit software, 141
    - thermal resistance, 141
    - 3D building modeling, 140
    - 3D model, 148
  - Energy efficiency in buildings (EEB), 138
  - Energy management systems, 13
  - Energy use intensity (EUI), 138
  - Error, trend, and seasonality (ETS), 17
  - Exponential smoothing, 18
- F**
- Fabrication process, 35
  - Final prediction error (FPE), 15
  - 5-ammonium valeric acid iodide (5-AVA), 37
  - Flexible manufacturing technologies, 41
  - Fluorine-doped tin oxide (FTO), 37
  - Fuzzy prediction interval (FPI) models, 14
- G**
- Gated recurrent units (GRU), 14
  - Global warming, 3
  - Gompertz model application, 56, 57
  - Graphene-based PSC (G-PSC), 39
  - Greenhouse gas (GHG) emissions, 109, 177
  - Green hydrogen, 77, 86
  - Guadalajara Metropolitan Zone (GMZ), 48
- H**
- Heating system, 165
  - Heating, ventilation, air conditioning (HVAC)
    - systems, 163
  - Heat pump, 165
  - Hole transport material (HTM), 34
  - Holt-Winters model
    - PV power forecasting, 25, 26
    - solar irradiance forecasting, 22, 24
  - Homer Energy Software, 153
  - HTM-free printable C-PSC, 37, 39
  - Hydrogen economy, 77
    - calculation method, 78
    - firewood, 78
    - fossil fuels, 86
    - H<sub>2</sub> consumption
      - firewood and LPG, 80–82
      - gasoline and diesel, 79
    - renewable energy resources, 78, 86
    - renewable hydrogen potential
      - firewood and LPG, 83
      - gasoline and diesel, 82
- I**
- Institute of Hydrology, Meteorology and Environmental Studies (IDEAM), 8
  - Interfacial engineering, 40

**L**

Levelized cost of energy (LCOE), 158  
 Li-ion batteries, 154  
 Liquefied petroleum gas (LPG), 78, 83  
 Liquid air energy storage (LAES), 154  
 Liquid electrolyte-based dye-sensitized solar cell configuration, 34  
 Long short-term memory (LSTM), 14  
 Lower heating value (LHV), 79

**M**

MAPbI<sub>3</sub>/carbon interface, 37  
 Mean absolute error (MAE), 15  
 Mean absolute percentage error (MAPE), 15  
 Mean square error (MSE), 19  
 Medium-scale industry, 62  
 Metal electrode-based PSC, 41  
 Methylammonium iodide (MA), 37  
 Microgrids, 14, 16  
 Ministry of Industry and Commerce (MIC), 79  
 Monolithic liquid electrolyte-sensitized solar cell, 36  
 Multilayer perceptron (MLP), 16  
 Municipal solid waste (MSW), 47

**N**

National Planning Department (DNP), 183  
 Navier–Stokes equation, 99  
 Net present value (NPV), 158  
 Non-interconnected zones, 11  
 Nonlinear autoregressive (NAR), 15  
 Numerical weather prediction (NWP), 16

**O**

Organic fraction of MSW (OFMSW), 47  
 Organic Law of Energy Efficiency, 164  
 Oscillating water column equipment (OWCE), 112

**P**

Paraguay, *see* Hydrogen economy  
 Paris Agreement, 13  
 Particle swarm optimization (PSO), 15  
 Peak sun hours (PSH), 8  
 Perovskite solar cells (PSC)  
   application, 34  
   configurations, 34  
   C-PSC (*see* Carbon-based perovskite solar cells (C-PSC))

  intrinsic properties, 34  
   light-absorbing layer, 34  
   sequence of reactions, 34  
 Petroleum products, 86  
 Photovoltaic (PV) energy, 114, 115  
 Photovoltaic (PV) panel, 166  
 Photovoltaic (PV) power forecasting  
   Holt-Winters model, 25, 26  
   power test data and predicted data, 25, 27  
   results, 28  
   SARIMA model, 24–26  
 Planillita, 132  
 Proton exchange membrane fuel cell (PEMFC), 85  
 PSC configurations schemes, 35

**R**

Recurrent neural networks, 14  
 Renewable energy  
   air conditioners, 155  
   BESS operational parameters, 155  
   BESS simulations, 157, 158  
   cost of electricity, 151  
   cryogenic energy storage, 152  
   demand, 153  
   electric vehicles (EV), 152  
   electrical system, 152, 153  
   electrodes, 152  
   energy demand, 152  
   EV batteries, 155  
   EV battery swap station simulations, 158, 160  
   flow batteries, 154, 161  
   Homer Energy, 154  
   hybrid systems, 161  
   hydraulic pumping, 152  
   implementation, 161  
   marine flora and fauna, 151  
   oxidation and reduction processes, 152  
   photovoltaic and wind generation, 151  
   photovoltaic power plants, 151  
   production, 154  
   redox batteries, 152  
   thermal generation systems, 151  
 Residual biomass  
   biomass furnace, 62  
   combustion chamber, 73  
   combustion furnace, 64, 69, 71  
   design selection  
     heat transfer, 63, 64  
     oven type, 63, 64  
   energy, 62, 73



- heat exchanger design analysis, 67
- laboratory equipment, 62, 71
- mathematical analysis
  - air-fuel ratio, 65, 66
  - combustion, 65
  - flue gas flow, 66
  - rice husk flow, 66
- result
  - combustion chamber, 68
  - combustion furnace design, 69
  - heat exchanger analysis, 69
- rice husk, 73
- simulation, 69, 71
- STM A36 Steel, 73
- tests, 72
- thermal analysis, 66, 67
- Rice husk, 61
- Rice mill plants, 61

## S

- Screen-printing techniques, 41
- Self-adhesive macroporous carbon film, 38
- Slot-die coating technology, 40
- Solar analysis
  - day light, 143
  - insolation, 143
- Solar collectors, 164, 167, 173
- Solar energy forecasting, 14, 16
- Solar irradiance forecasting
  - Holt-Winters model, 22, 24
  - results, 24
  - SARIMA model, 23
- Solar photovoltaic (PV) technologies, 164
- Solar powered absorption systems, 11
- Solar thermal collector, 167
- Solar thermal systems (ST), 164
- Solid biomass, 73
- Solid-state anaerobic digestion (SSAD), 48
- Spiro-OMeTAD, 34, 40
- Stational-autoregressive integrated moving average (SARIMA) model
  - PV power forecasting, 24–26

- solar irradiance forecasting, 23
- Strategic Productive Alliances (SPA), 179
- Sulfur dioxide (SO<sub>2</sub>), 183
- Support vector machine (SVM), 15
- Support vector regression (SVR), 15
- Sustainable development, 180
- Sustainable Development Goals, 13, 163
- Sustainable waste management, 47
- Systema Advisor Model* (SAM), 165

## T

- Thermophotovoltaic panel (PV/T) technology, 164, 166, 167
- 5,10,15-Triphenyl-5Hdiindolo[3,2-a:30,20-c]carbazole (TDPI), 37
- Triple cation perovskite, 38
- Typical meteorological year (TMY), 167

## U

- Univariate time-series models
  - ARIMA forecasting models, 29
  - Box-Jenkins methodology, 18
  - datasets, 21
  - experimental design, 21
  - exponential smoothing, 17
  - forecasting errors, 19
  - Holt-Winters model, 28, 29
  - proposed forecasting approach, 19, 21
  - renewable energies, 13
  - SARIMA model, 29
  - solar energy forecasting, 14, 16
  - time-series decomposition, 17
- Urban solid waste, 48, 51
- User-defined function (UDF), 92, 98

## W

- Water heating system, 167
- Wave collectors (WC), 112
- Wave power, 112, 113
- Wind power, 113